UNIVERSITY OF CALIFORNIA, SAN DIEGO

Screening and Characterizing Amino Acid Metabolic Proteins for Functions in Chromatin Regulation

A dissertation submitted in partial satisfaction
of the requirements for the degree Doctor of Philosophy

in

Biology

by

Xue Su

Committee in charge:

Professor Lorraine Pillus, Chair
Professor Michael Burkart
Professor Beverly Emerson
Professor Douglass Forbes
Professor Amy Pasquinelli

2014

The Dissertation of Xue Su is approved, and it is acceptable in quality and form for publication on microfilm and electronically:

_____

_____

_____

_____

_____

Chair

University of California, San Diego

2014

DEDICATION

This thesis is dedicated to my grandmother, Shulan Shi, who would have been proud to see its completion.

TABLE OF CONTENTS

LIST OF ABBREVIATIONS

5-FOA	5-fluoroorotic acid
Ade	Adenine
Arg	Arginine
Can	Canavanine
CEN	Centromeric
ChIP	Chromatin immunoprecipitation
CPT	Camptothecin
IP	Inositol polyphosphate
DNA	Deoxyribonucleotide
GFP	Green fluorescent protein
HAT	Histone acetyltransferase
HDAC	Histone deacetylase
His	Histidine
HU	Hydroxyurea
LB	Luria broth
Leu	Leucine
Met	Methionine
MMS	Methyl methanesulfonate
NAD^+	Nicotinamide adenine dinucleotide
NES	Nuclear export sequence

PP-IP	Inositol pyrophosphate
PEV	Postion effect variegation
rDNA	Ribosomal DNA
SAM	S-adenosyl methionine
SC	Synthetic complete
TPE	Telomere position effect
Trp	Tryptophan
Ura	Uracil
WT	Wild type
YPAD	Yeast peptone dextrose supplemented with adenine

LIST OF FIGURES

LIST OF TABLES

ACKNOWLEDGEMENTS

I would first like to thank my advisor Lorraine Pillus for welcoming me into the lab in Dec 2010. Since then she has been a great mentor. I particularly appreciate her emphasis on the importance of being a good colleague to the scientific community.

I thank my committee for their unreserved support and for their critical evaluations of my work.

I thank Ana Lilia Torres Machorro, for teaching me the lab techniques and for helping me with the early set-up of the work. I am especially grateful for her optimism and friendship, which helped me through the ups and downs of research.

I thank the Pillus lab, past and present, for creating a positive and supportive work environment. Their unreserved help and insightful comments have been instrumental to the completion of this work. In particular, I would like to thank Naomi Frank, Ana Lilia Torres Machorro and Emily Petty for proofreading my manuscript and my thesis.

I thank my collaborator Harihar Basnet, for the opportunity to work on an inspiring cross-species project.

I thank my classmates in the UCSD biology program for making my time in San Diego an enjoyable one. In particular, I want to thank Yangbin Gao and Helena Sun for always reaching out to me when I needed help. Also, I want to thank my friends back in China and Europe: Feng Feng, Lingfei Gao, Fuyao Geng, Zhennan Huan and Chang Lian. I owe much of the completion of this work to your love, understanding and emotional support. I thank my grandmother, Shulan Shi, for inspiring me to be a courageous individual and for leaving me fond memories. Last but not least, I thank my husband for having faith in me and supporting my scientific career.

Chapter 2, in full, is currently under review for publication in *Genes and Development*, and may appear as Su XB and Pillus L 2014. The Gdh1 Glutamate Dehydrogenase Regulates Telomeric Silencing Through Modulating α-ketoglutarate, Recruitment of the SIR Complex and Histone H3 clipping. The dissertation author was the primary investigator and author of this paper.

Chapter 4 includes collaborative work with Ana Lilia Torres Machorro.

Chapter 5, in full, contains material published in *Nature* 2014. Basnet H, Su XB, Tan Y, Meisenhelder J, Merkurjev D, Ohgi KA, Hunter T, Pillus L and Rosenfeld MG. Tyrosine phosphorylation of histone H2A by CK2 regulates transcriptional elongation. The dissertation author was a contributing author to this material.

VITA

2006 Bachelor of Arts Honors, University of Cambridge

Major: Natural Sciences

2008 Master of Science, Stanford University

Field of study: Biological Sciences

2014 Doctor of Philosophy, University of California San Diego

Field of study: Biology

PUBLICATIONS

Su XB and Pillus L. The Gdh1 Glutamate Dehydrogenase Regulates Telomeric Silencing Through Modulating α-ketoglutarate, Recruitment of the SIR Complex and Histone H3 clipping. *In review.*

Basnet H, Su XB, Tan Y, Meisenhelder J, Merkurjev D, Ohgi KA, Hunter T, Pillus L and Rosenfeld MG. Tyrosine phosphorylation of histone H2A by CK2 regulates transcriptional elongation. *Nature.* doi: 10.1038/nature13736.

Taylor KW, Kim JG, Su XB, Aakre CD, Roden JA, Adams CM, Mudgett MB. 2012. Tomato TFT1 is required for PAMP-triggered immunity and mutations that prevent T3S effector XopN from binding to TFT1 attenuate *Xanthomonas* virulence. *PLoS Pathog* 8: e1002768.

Wang D, Garcia-Bassets I, Benner C, Li W, Su X, Zhou Y, Qiu J, Liu W, Kaikkonen MU, Ohgi KA *et al.* 2011. Reprogramming transcription by distinct classes of enhancers functionally defined by eRNA. *Nature* 474: 390-394.

Kim JG, Li X, Roden JA, Taylor KW, Aakre CD, Su B, Lalonde S, Kirik A, Chen Y, Baranage G *et al.* 2009. *Xanthomonas* T3S effector XopN suppresses PAMP-triggered immunity and interacts with a tomato atypical receptor-like kinase and TFT1. *Plant Cell* 21: 1305-1323.

ABSTRACT OF THE DISSERTATION

Screening and Characterizing Amino Acid Metabolic Proteins for Functions in Chromatin Regulation

by

Xue Su

Doctor of Philosophy in Biology

University of California, San Diego, 2014

Professor Lorraine Pillus, Chair

The eukaryotic DNA is packaged into chromatin that is compartmentalized in the nucleus. Enzymatic activities directed towards chromatin and chromatin-associated

proteins thus directly determine the accessibility of the DNA to various cellular machineries. A growing field in the study of chromatin is the interplay between metabolic proteins and chromatin regulation. Previous work on the yeast homocitrate synthase Lys20 demonstrated that this lysine biosynthetic enzyme has a moonlighting function in DNA damage repair. This raised the question of whether other amino acid metabolic proteins participate in chromatin regulation. In this work, an *in silico* screen was conducted to search for candidate proteins that potentially function in chromatin regulation. Silencing reporter assays revealed that four new candidate proteins, Gdh1, Arg82, Hom2 and Hom6 are involved in chromatin silencing. Work focused on Gdh1, the broadly conserved glutamate dehydrogenase enzyme, demonstrated a positive regulatory role of this protein in telomeric silencing. Its silencing function is dependent on a catalytic residue required for its metabolic function, suggesting that Gdh1 regulates silencing in a metabolism- dependent manner. Further analyses showed that high α-ketoglutarate levels, such as that associated with the deletion of *GDH1* are in general detrimental to telomeric silencing. Moreover, deletion of *GDH1* results in decreased binding of the silent information regulator (SIR complex) and increased H3 N-terminal clipping at the telomeres. A histone mutant with reduced clipping improved silencing at some telomeres in the *gdh1Δ* mutant, indicating that Gdh1 at least partially regulates telomeric silencing by controlling H3 clipping. Further analysis was also undertaken for Hom2 and Hom6, which suggested a role of threonine metabolism in the regulation of rDNA silencing. Also, works on Hom6 and Arg82 revealed possible moonlighting functions of these proteins in chromatin silencing. Another work related to the general theme of chromatin regulation is the characterization of a new tyrosine phosphorylation

site on histone H2A and its role in transcriptional elongation. The results presented in this thesis add to the growing recognition that chromatin function is tightly regulated by metabolism and metabolic proteins, and that histone tyrosine phosphorylation has important roles in chromatin regulation.

Chapter 1. Introduction

During the course of evolution, the eukaryotic genome evolved two important features. First, the eukaryotic genomic DNA became packaged into a higher order structure known as chromatin, and second, the eukaryotic genome was compartmentalized into the nucleus by the formation of the nuclear membranes.

The basic subunit of chromatin is the nucleosome. The core nucleosome consists of 147 base pairs of DNA wrapped around a histone octamer, which contains two copies of each of the four canonical histones H2A, H2B, H3 and H4 (Fig. 1-1). Importantly, the interaction between DNA and histones is not static, but is dynamically regulated by two types of activities: post-translational modifications on histones, and chromatin remodeling activities on nucleosomes. These two types of chromatin regulatory mechanisms thus directly influence the accessibility of genomic DNA to cellular machineries such as those involved in DNA replication, transcription and DNA damage repair (Reviewed in Kouzarides 2007).

In addition, eukaryotic chromatin is separated from the cytoplasm through the formation of double nuclear membranes. The nuclear membranes are perforated by macromolecular structures known as nuclear pores, which permit free diffusion of small molecules and proteins less than 20-40 kDa, while tightly regulating transport of large proteins and RNAs (reviewed in Adams and Wente 2013). The physical separation of the chromatin from the cytosol allows the genome to be protected from potential sources of damage and to be more efficiently regulated by nuclear-localized chromatin modifiers.

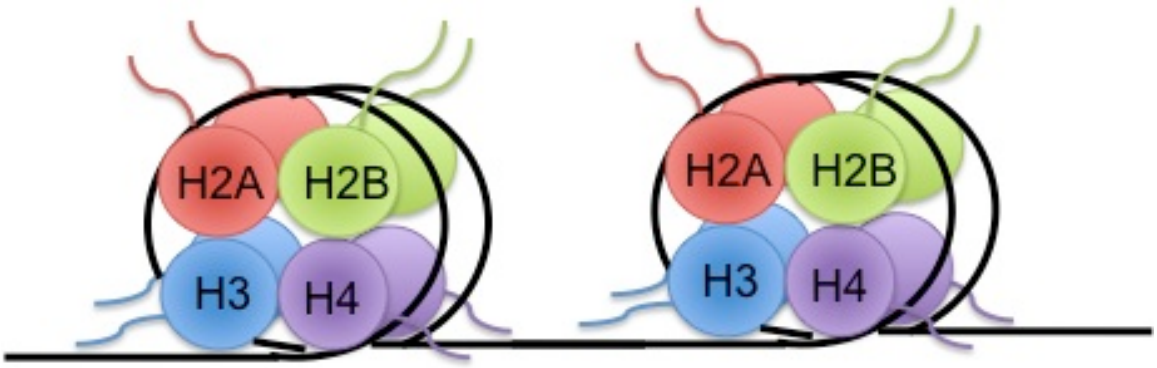

Figure 1-1. Composition of the core nucleosomes. DNA is wrapped around histone octamers to form the core nucleosome. The globular domain of each histone is embedded at the center of the nucleosome, while the tails protrude towards the surface of the nucleosome.

In this chapter, three main topics pertinent to the thesis are presented: histone post-translational modifications, mechanisms regulating chromatin silencing and the crosstalks between metabolism and chromatin function.

Histone post-translational modifications

To date, a myriad of histone post-translational modifications have been identified, including acetylation of lysine residues, phosphorylation of serine/threonine/tyrosine residues, histone tail cleavage, methylation of lysine and arginine residues, ubiquitination and sumoylation of lysine residues and so forth (reviewed in Bannister and Kouzarides 2011).

A major class of histone modification is the dynamic acetylation and deacetyltion of lysine residues. Unmodified lysine residues are positively charged, thus neutralizing the negative charges on the phosphate groups of DNA and causing a condensed chromatin state (Fig. 1-2A and Figure 1-2C). Acetylated lysine residues, in contrast, are no longer able to neutralize the negative charges of DNA, thus enabling a more accessible chromatin state (Fig. 1-2B-C).

The enzymes catalyzing histone acetylation are known as histone acetyltransferases (HATs) or lysine acetyltransferases (KATs). In budding yeast, there are two major families of HATs: the GNAT (abbreviated for Gcn5 *N*-terminal acetyltransferases) family and the MYST (named after its founding members *MOZ*, *YBF2/SAS3*, *SAS2*, and *TIP60*) family. Both families of HATs function as multi-subunit protein complexes. Gcn5 is the founding member of the GNAT family of HATs, and it is

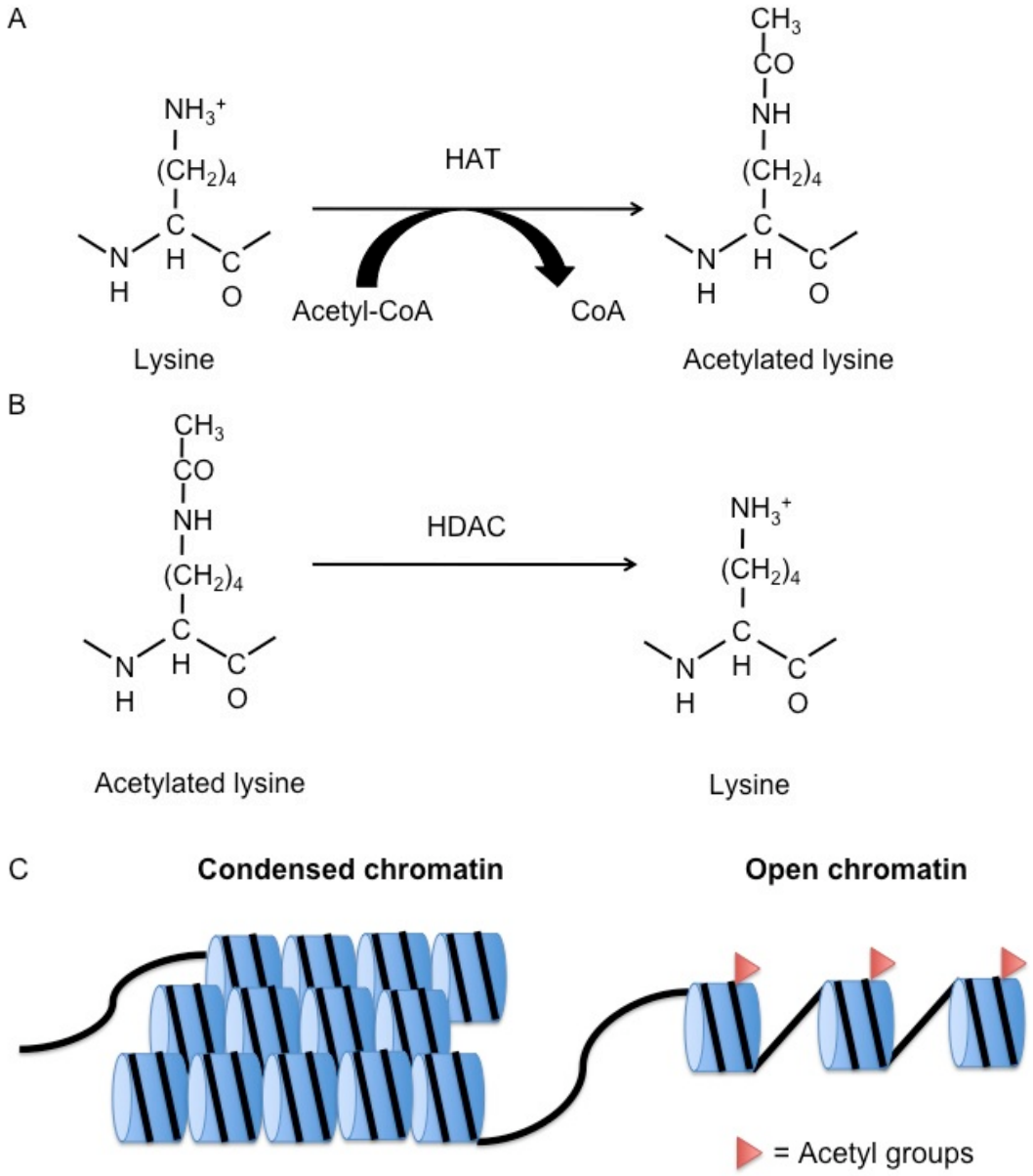

Figure 1-2. Histone lysine acetylation and deacetylation. (*A*) A lysine residue is acetylated by the activity of a HAT. Acetylated lysine loses the positive charge on the side-chain. Acetyl-CoA is used as a co-factor for the HAT activity. (*B*) Acetylated lysine residue is deacetylated by the activity of an HDAC. Unacetylated lysine is positively charged. (*C*) The open and condensed chromatin states. Cylinders represent core histones, black lines represent DNA and red arrows represent acetyl groups.

the shared catalytic component of three complexes in budding yeast: SAGA, SLIK and ADA complexes (Fig. 1-3A). Of note, the SAGA complex contains multiple functional modules, including a deubiquitinase module that uses Ubp8 to remove ubiquitin attached to histones (Fig. 1-3B; Weake and Workman 2012). The MYST family has four complexes in budding yeast, NuA4, piccolo NuA4, NuA3 and SAS complexes (Fig. 1-3C). As lysine acetylation usually weakens the interaction between DNA and histones, the HAT complexes are critically involved in transcriptional activation as well as DNA damage repair (reviewed in Lee and Workman 2007).

The enzymes removing the acetyl groups from histone lysine residues are known as histone deacetylases (HDACs). Enzymes with HDAC activities are divided into three classes, based on sequence homology (Table 1-1). Like HATs, HDACs also function in multi-subunit complexes. The most pertinent HDAC complex to the thesis is the silent information regulator (SIR complex), whose catalytic subunit Sir2 is a Class III HDAC (Table 1-1).

Another important type of histone modification is histone phosphorylation. Earlier studies mostly focused on the phosphorylation of serine and threonine residues of histones. For instance, histone H3 Ser10 phosphorylation plays an important role in regulating cell cycle progression while histone H2A Ser129 phosphorylation is key to DNA damage repair (reviewed by Rossetto *et al.* 2012). The yeast core histones contain 14 tyrosine residues in total, but prior to our work, only two residues had been found to be phosphorylated: H2B Tyr40, whose phosphorylation regulates histone gene expression during cell cycle (Mahajan *et al.* 2012), and H3 Tyr 100, whose phosphorylation regulates ubiquitination-dependent proteolysis of histone H3 (Singh *et al.* 2009). The

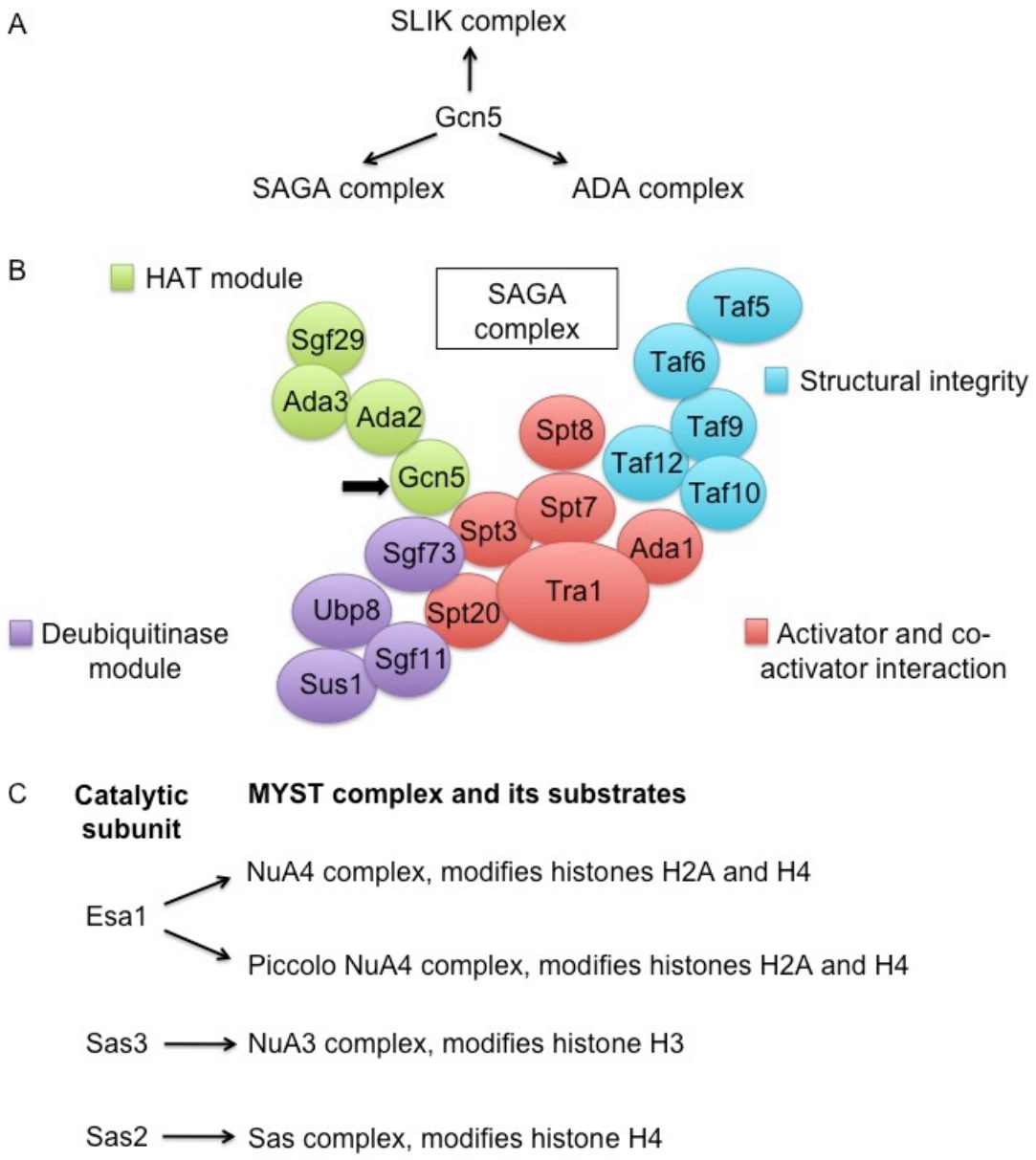

Figure 1-3. HAT complexes in budding yeast. (*A*) Gcn5 is the shared catalytic subunit of three GNAT HAT complexes. (*B*) The largest complex, SAGA, contains four different modules, the HAT module, the deubiquitinase module, the activator/co-activator-interaction module and the module maintaining the structural integrity of the complex. Gcn5 is highlighted with a black arrow. Of note, Ubp8 carries out the deubiquitinase function of the SAGA complex. (*C*) There are the four HAT complexes belonging to the MYST family in budding yeast. Shown are the catalytic subunits and the histone substrates for each family.

Table 1-1. The three classes of HDACs in budding yeast. The catalytic features and members of each class are highlighted in the table.

Class	I	II	III
Catalytic feature	Zn^{2+}-dependent	Zn^{2+}-dependent	NAD^{+}-dependent
Members and the associated complexes	Rpd3 (Rpd3S and Rpd3L complexes) Hos1 (associates with Tup1-Ssn6) Hos2 (Set3 complex)	Hda1 (associates with Hda2-Hda3) Hos3	Sir2 (SIR and RENT complex) Hst1* Hst2* Hst3* Hst4*

Note: * indicates proteins whose interacting complexes have been less rigorously defined than the other HDACs.

functional importance of the other tyrosine residues has not been characterized in detail, but it was reported that yeast strains with alanine substitutions of H2A Tyr58, H3 Tyr41 or H4 Tyr72 were inviable or had reduced fitness (Nakanishi *et al.* 2008). Therefore, it remains possible that additional histone tyrosine residues are phosphorylated, a topic presented in Chapter 5.

Histone lysine methylation is also a well-established form of modification with important physiological functions (Table 1-2). In budding yeast, histone H3 contains three methylation sites, Lys4, Lys36 and Lys79 that have been characterized to date. The respective methyltransferases and demethylases are summarized in Table 1-2 (reviewed by Martin and Zhang 2005; Kooistra and Helin 2012). Of note, the catalytic activities of both groups of modifying enzymes are dependent on small molecule metabolites. Histone methyltransferases are S-adenosylmethionine (SAM)-dependent and histone demethylases are α-ketoglutarate-dependent.

Interestingly, in addition to modifications on individual histone residues, histone tails were found to undergo proteolytic cleavage *in vivo* (Reviewed in Azad and Tomar 2014). As simplified in Fig. 1-1, structural studies revealed that the globular domains of histones are embedded at the center of the core nucleosome, whereas the histone tails lack an ordered structure and protrude towards the surface of the nucleosomes. Consequently, the histone tails play important roles in regulating the core histones' interaction with DNA and the chromatin-associated enzymes. Thus far the most-established histone tail cleavage is H3 N-terminal clipping. This modification was found to occur *in vivo* in both yeast (Santos-Rosa *et al.* 2009) and animal cells (Duncan *et al.* 2008). Several enzymes have been suggested to be the H3 clipping protease, including

Table 1-2. Histone H3 lysine methylation sites and their physiological functions in budding yeast. The methyltransferase, demethylase and physiological functions of each modification are summarized in the table.

Properties	H3 Lys4	H3 Lys36	H3 Lys79
Methyltransferase SAM-dependent	Set1 complex	Set2 complex	Dot1
Demethylase Fe(II) and α-ketoglutarate-dependent	Jhd2	Jhd1/Rph1/Gis1	Unknown
Physiological functions of methylation	Silencing Transcriptional activation	Transcriptional elongation	Silencing DNA damage response Meiosis

cathespin L in mouse embryonic stem cells (Duncan *et al.* 2008), glutamate dehydrogenase in animal tissue extracts (Mandal *et al.* 2013) and the vacuolar protease Prb1 in yeast (Xue *et al.* 2014).

Chromatin silencing and its regulatory mechanisms

As different chromatin modifying complexes are targeted to different parts of the genome, the accessibility of the DNA at different genomic loci varies greatly, resulting in a phenomenon known as position effect variegation (PEV). The concept of PEV was established by the observation that the context of the chromatin determines the expression of the inserted gene. And in budding yeast, three genomic regions are known to repress expression of inserted genes: the *HM* silent mating type loci, the telomeres and the rDNA repetitive arrays (Fig. 1-4; reviewed in Kueng *et al.* 2013). This phenomenon is known as chromatin silencing, and is thought to have important physiological implications for the respective regions: Telomeric silencing helps reduce homologous recombination between repetitive sequences of different telomeres, thus preventing chromosomal fusion. rDNA silencing helps reduce homologous recombination between different rDNA repeats, thus preventing the formation of extrachromosomal rDNA circles. Silencing at the *HM* loci keeps the cryptic copies of mating information silenced, thus enabling yeast cells to maintain a single mating status and stable cell type in the absence of mating-type switching signal (reviewed in Kueng *et al.* 2013).

Chromatin silencing is primarily established and maintained by the deacetylase activity of Sir2. As discussed earlier, Sir2 carries out histone lysine deacetylation, using

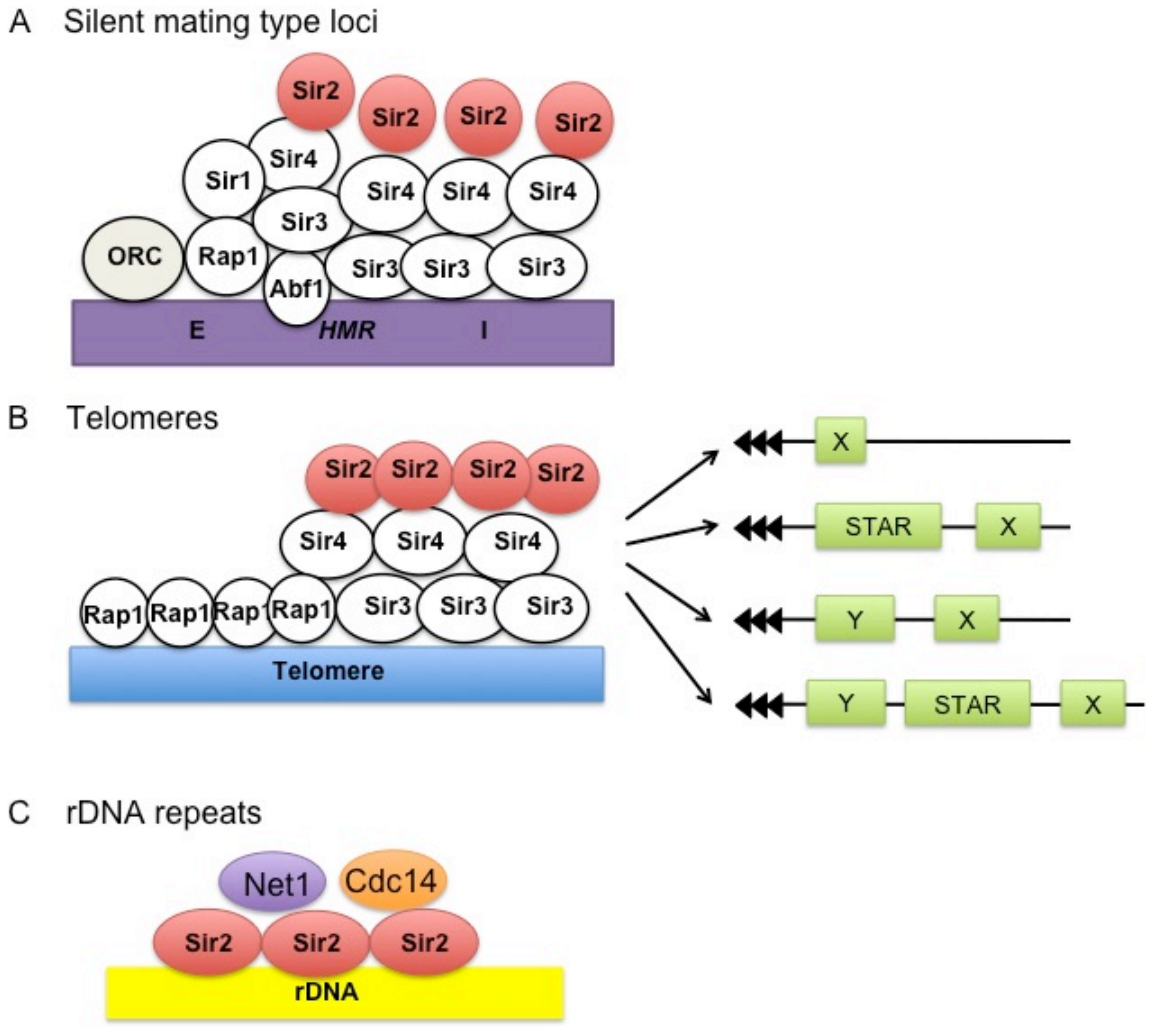

Figure 1-4. Three genomic regions in budding yeast undergo chromatin silencing. Sir2, highlighted in red, is the catalytic component of the Sir complex. (*A*) Transcription factors Rap1, Abf1 and Orc1 help with the recruitment of the SIR complex to the *HM* loci (shown is the *HMR* locus). (*B*) Transcription factor Rap1 facilitates the recruitment of the SIR complex to telomeres (left). Different telomeres contain different numbers and combinations of the X- and Y-repeats and STAR silencer elements (right). Triple black triangles represent the $TG_{1\text{-}3}$ repeats at the chromosomal ends. (*C*) Sir2 forms a homotrimer within the rDNA repeats, to form part of the RENT complex.

NAD^+ as a co-factor (Table 1-1). Except Sir2, the compositions of the silencing complexes and the mechanisms of silencing are different for the three silent loci, with the telomeres and the *HM* loci being more similar to each other, and the rDNA locus having distinct features (reviewed in Kueng *et al.* 2013; Fig. 1-4). The *HM* loci contain two *cis*-acting silencer sequences, E and I, which are recognized by transcriptional factors Abf1 and Rap1. Rap1 and Abf1 help recruit Sir3 and Sir4 through direct physical interactions. Orc1 of the origin replication complex is also associated with the *HM* loci, and is thought to recruit Sir1 (Fig. 1-4A). Telomeric silencing is initiated by the Rap1 transcription factor, which recognizes and binds the terminal $TG_{1\text{-}3}$ (Thymine-guanidine) repeats at the ends of chromosomes. Unlike the two *HM* loci, which have similar structures, different telomeres vary greatly in terms of their subtelomeric sequences and their silencer elements. Whereas all telomeres contain X-elements, some telomeres also contain Y-elements or STAR sequences (Fig. 1-4B). The diversity in subtelomeric sequences and structures determines that different telomeres have different strengths of silencing. It was shown that the strength of telomere position effect (TPE), i.e. the telomere-specific form of PEV, varies greatly from telomere to telomere. Despite these differences, both the *HM* loci and the telomeres showing strong TPE were thought to be silenced following a sequential model, where the initial histone deacetylation carried out by Sir2 creates binding sites for Sir3 and Sir4, which in turn facilitate the spreading of the SIR complex across the silent loci.

Unlike the *HM* loci and the telomeres, rDNA silencing does not require Sir3 or Sir4. Instead, Sir2 forms a homotrimer at the rDNA locus (Fig. 1-4C). Together with

Net1 and Cdc14, Sir2 forms part of the RENT complex, which carries out rDNA silencing.

In addition to histone deacetylation, other kinds of histone modifications have been shown to have auxiliary roles in chromatin silencing. For example, the Set1 complex, which carries out methylation on histone H3 Lys4, was found to be important for silencing at all three loci. Deletions of individual components of the complex result in defective silencing (Nislow *et al* 1997; Krogan *et al* 2002). The Set1 complex is thought to regulate silencing by facilitating the establishment of the boundary between heterochromatic and euchromatic regions (Santos-Rosa *et al.* 2004; Venkatasubrahmanyam *et al.* 2007).

Crosstalk between metabolism and chromatin function

Classic biochemical studies led to the idea that most metabolic enzymes are localized within mitochonria or to the cytosol, so their enzymatic activities were expected to have little impact on chromatin regulation. In recent years, growing evidence suggests that there are multiple ways in which metabolism and metabolic proteins intersect with chromatin function. The earliest known crosstalk mechanism is through the activity of a signal transduction pathway, in which an upstream sensor detects changes in the cellular metabolite levels and culminates in the nuclear translocation of a downstream effector. Upon nuclear translocation, the downstream effector regulates gene expression either directly acting as a transcription factor, or indirectly through recruiting chromatin regulatory complexes (Fig. 1-5A). The most-established example of this form of crosstalk is the AMP kinase pathway (reviewed in Gut and Verdin 2013).

Interestingly, recent studies have shown that some metabolic proteins are directly localized to the nucleus. These nuclear-localized metabolic proteins influence chromatin regulation by two distinct mechanisms. In one mechanism, the metabolic enzymes carry out their usual metabolic reaction inside the nucleus. It is known that many chromatin regulatory complexes require small molecule metabolites for their catalytic activities. As noted above, HATs require acetyl-CoA as a co-factor to add acetyl groups to histone lysine residues (Fig. 1-2A). Class III HDACs, on the other hand, use NAD^+ as a co-factor to remove acetyl groups (Table 1-1). Methyltransferases use S-adenosylmethionine (SAM) as a co-factor, whereas JMJC-domain containing histone lysine demethylases use α-ketoglutarate to remove methyl groups from lysines (Table 1-2). Therefore, if a nuclear metabolic protein catalyzes a reaction that involves the metabolites used by chromatin regulators, its metabolic activity may result in changes in the nuclear levels of these metabolites, thus controlling the activity of chromatin regulators (Fig. 1-5B). For example, the acetyl-CoA biosynthetic machinery has been found to have a separate nuclear pool in both yeast and mammalian cells. Since acetyl-CoA concentration is a rate-limiting factor for HAT activities, the nuclear acetyl-CoA biosynthetic machinery directly determines global histone acetylation levels (Takahashi *et al.* 2006; Wellen and Hatzivassiliou *et al.* 2009). Another example of regulation by metabolite levels comes from the NAD^+ metabolic pathways. It has been found that altering nuclear NAD^+ levels causes changes in chromatin silencing, because Sir2's catalytic activity is dependent on this metabolite (Sandmeier *et al.* 2002). Also, Tdh3, which encodes the yeast glyceraldehyde-3-phosphate dehydrogenase, was found to have a nuclear pool. Since Tdh3 uses NAD^+ as a co-factor, its enzymatic activity influences the nuclear levels of

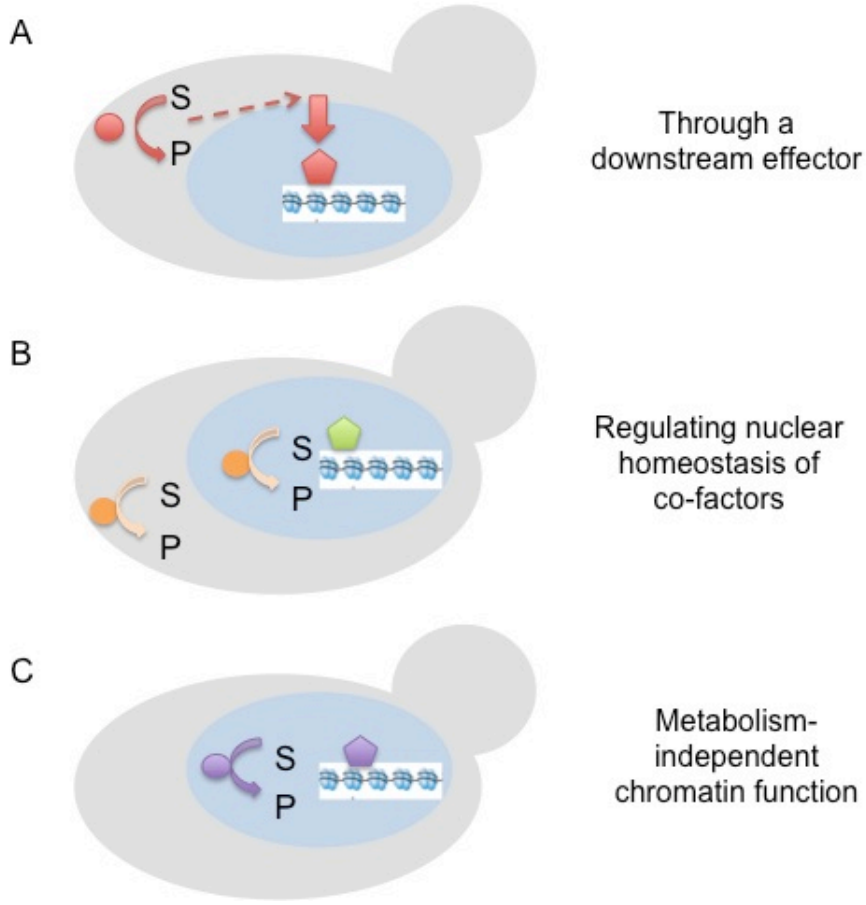

Figure 1-5. Three different mechanisms link can metabolism to chromatin regulation. Circles represent metabolic proteins and diamonds represent chromatin regulators. S = substrate and P = product. (*A*) A cytoplasmic sensor of a signal transduction pathway detects changes in levels of a metabolite synthesized in the cytoplasm. This culminates in the nuclear translocation of a downstream effector, which directly or indirectly influence chromatin regulation. (*B*) The metabolic protein has a nuclear pool, where it catalyzes its usual metabolic reactions. When the reaction involves a metabolite that is rate-limiting to a chromatin regulator, the metabolic activity directly determines the activity of the chromatin regulator. Shown is an example in which the product of the nuclear metabolic enzyme is used as a co-factor for the chromatin regulator. (*C*) The metabolic protein has a distinct function in the nucleus, which allows it to act as a chromatin regulator itself.

NAD^+ available to Sir2, thus impacting chromatin silencing (Ringel *et al.* 2013).

Not all nuclear metabolic proteins function in the nucleus by altering the levels of metabolites. Instead, some metabolic proteins have evolved a distinct function in the nucleus (Fig. 1-5C). For example, tumor-specific pyruvate kinase M2 (PKM2) translocates to the nucleus upon EGF receptor activation in cancer cells. Inside the nucleus, PKM2 phosphorylates histone H3 Thr11 instead of its usual metabolic substrate. Importantly, PKM2 uses the same kinase domain to carry out its nuclear function and its cytoplasmic function, as mutations in the kinase domain abolished both functions (Yang *et al.* 2012). Another example of a metabolic protein with a distinct nuclear function is the yeast lysine biosynthetic enzyme, Lys20. Lys20 catalyzes the first committed step of lysine biosynthesis in budding yeast. Intriguingly, earlier work showed that Lys20 is highly abundant in the nucleus (Chen *et al.* 1997), raising the question of whether this enzyme has a distinct nuclear activity. Recent work from the Pillus lab showed that when the *LYS20* gene is expressed on a high copy 2 micron plasmid, it suppresses the DNA damage sensitivity phenotype of hypomorphic alleles of the essential HAT *ESA1*. Lys20's function in DNA damage repair does not require its catalytic residues for lysine biosynthesis (Scott and Pillus 2009), but requires a separate domain that is localized to the C terminus of the protein (unpublished, Torres Machorro *et al.*). Lys20 is directly recruited to the break sites, where it facilitates the recruitment of the INO80 chromatin remodeling complex (unpublished, Torres Machorro *et al.*).

Amino acid metabolism and chromatin regulation

The work with Lys20 raised the question of whether other amino acid metabolic enzymes have chromatin regulatory functions. This is an attractive idea for two reasons. First, many amino acid anabolic and catabolic reactions involve metabolites used by chromatin regulators, including NAD^+, α-ketoglutarate, SAM and others. Second, amino acid metabolic proteins are ancient enzymes with a great diversity of catalytic features. It is known that many enzymes in the carbohydrate metabolic pathways have distinct nuclear functions. For example, hexokinase 2 acts as transcription factors in the nucleus (reviewed in Gancedo and Flores 2008). By contrast, relatively few instances of chromatin-directed functions have been characterized for amino acid metabolic proteins.

Overview of the thesis

In Chapter 2, an *in silico* screen was used to reveal undiscovered amino acid metabolic proteins with functions in chromatin regulation. The roles of the glutamate dehydrogenase homologs, Gdh1 and Gdh3, in telomeric silencing were studied in detail in Chapter 2 and Appendix A. Chapter 3 focuses on the discovery of threonine metabolic proteins as regulators of rDNA silencing, and Chapter 4 describes the finding that Arg82 is a regulator of telomeric silencing. Chapter 5 is a collaborative study that revealed a role of H2A Tyr57 in transcriptional elongation. Taken together, these chapters used the powerful tool of yeast genetics to uncover a series of new chromatin regulatory mechanisms.

References

Adams RL, Wente SR. 2013. Uncovering nuclear pore complexity with innovation. *Cell* **152**: 1218-1221.

Azad GK, Tomar RS. 2014. Proteolytic clipping of histone tails: the emerging role of histone proteases in regulation of various biological processes. *Mol Biol Rep* **41**: 2717-2730.

Bannister AJ, Kouzarides T. 2011. Regulation of chromatin by histone modifications. *Cell Res* **21**: 381-395.

Chen S, Brockenbrough JS, Dove JE, Aris JP. 1997. Homocitrate synthase is located in the nucleus in the yeast *Saccharomyces cerevisiae*. *J Biol Chem* **272**: 10839-10846.

Duncan EM, Muratore-Schroeder TL, Cook RG, Garcia BA, Shabanowitz J, Hunt DF, Allis CD. 2008. Cathepsin L proteolytically processes histone H3 during mouse embryonic stem cell differentiation. *Cell* **135**: 284-294.

Gancedo C, Flores CL. 2008. Moonlighting proteins in yeasts. *Microbiol Mol Biol Rev* **72**: 197-210.

Gut P, Verdin E. 2013. The nexus of chromatin regulation and intermediary metabolism. *Nature* **502**: 489-498.

Kooistra SM, Helin K. 2012. Molecular mechanisms and potential functions of histone demethylases. *Nat Rev Mol Cell Biol* **13**: 297-311.

Kouzarides T. 2007. Chromatin modifications and their function. *Cell* **128**: 693-705.

Krogan NJ, Dover J, Khorrami S, Greenblatt JF, Schneider J, Johnston M, Shilatifard A. 2002. COMPASS, a histone H3 (Lysine 4) methyltransferase required for telomeric silencing of gene expression. *J Biol Chem* **277**: 10753-10755.

Kueng S, Oppikofer M, Gasser SM. 2013. SIR proteins and the assembly of silent chromatin in budding yeast. *Annu Rev Genet*.

Lee KK, Workman JL. 2007. Histone acetyltransferase complexes: one size doesn't fit all. *Nat Rev Mol Cell Biol* **8**: 284-295.

Mahajan K, Fang B, Koomen JM, Mahajan NP. 2012. H2B Tyr37 phosphorylation suppresses expression of replication-dependent core histone genes. *Nat Struct Mol Biol* **19**: 930-937.

Mandal P, Verma N, Chauhan S, Tomar RS. 2013. Unexpected histone H3 tail-clipping activity of glutamate dehydrogenase. *J Biol Chem* **288**: 18743-18757.

Martin C, Zhang Y. 2005. The diverse functions of histone lysine methylation. *Nat Rev Mol Cell Biol* **6**: 838-849.

Nakanishi S, Sanderson BW, Delventhal KM, Bradford WD, Staehling-Hampton K, Shilatifard A. 2008. A comprehensive library of histone mutants identifies nucleosomal residues required for H3K4 methylation. *Nat Struct Mol Biol* **15**: 881-888.

Nislow C, Ray E, Pillus L. 1997. SET1, a yeast member of the trithorax family, functions in transcriptional silencing and diverse cellular processes. *Mol Biol Cell* **8**: 2421-2436.

Ringel AE, Ryznar R, Picariello H, Huang KL, Lazarus AG, Holmes SG. 2013. Yeast Tdh3 (glyceraldehyde 3-phosphate dehydrogenase) is a Sir2-interacting factor that regulates transcriptional silencing and rDNA recombination. *PLoS Genet* **9**: e1003871.

Rossetto D, Avvakumov N, Côte J. 2012. Histone phosphorylation: a chromatin modification involved in diverse nuclear events. *Epigenetics* **7**: 1098-1108.

Sandmeier JJ, Celic I, Boeke JD, Smith JS. 2002. Telomeric and rDNA silencing in *Saccharomyces cerevisiae* are dependent on a nuclear NAD^+ salvage pathway. *Genetics* **160**: 877-889.

Santos-Rosa H, Bannister AJ, Dehe PM, Geli V, Kouzarides T. 2004. Methylation of H3 lysine 4 at euchromatin promotes Sir3p association with heterochromatin. *J Biol Chem* **279**: 47506-47512.

Santos-Rosa H, Kirmizis A, Nelson C, Bartke T, Saksouk N, Côte J, Kouzarides T. 2009. Histone H3 tail clipping regulates gene expression. *Nat Struct Mol Biol* **16**: 17-22.

Scott EM, Pillus L. 2010. Homocitrate synthase connects amino acid metabolism to chromatin functions through Esa1 and DNA damage. *Genes Dev* **24**: 1903-1913.

Singh RK, Kabbaj MH, Paik J, Gunjan A. 2009. Histone levels are regulated by phosphorylation and ubiquitylation-dependent proteolysis. *Nat Cell Biol* **11**: 925-933.

Takahashi H, McCaffery JM, Irizarry RA, Boeke JD. 2006. Nucleocytosolic acetyl-coenzyme a synthetase is required for histone acetylation and global transcription. *Mol Cell* **23**: 207-217.

Venkatasubrahmanyam S, Hwang WW, Meneghini MD, Tong AH, Madhani HD. 2007. Genome-wide, as opposed to local, anti-silencing is mediated redundantly by the euchromatic factors Set1 and H2A.Z. *Proc Natl Acad Sci U S A* **104**: 16609-16614.

Weake VM, Workman JL. 2012. SAGA function in tissue-specific gene expression. *Trends Cell Biol* **22**: 177-184.

Wellen KE, Hatzivassiliou G, Sachdeva UM, Bui TV, Cross JR, Thompson CB. 2009. ATP-citrate lyase links cellular metabolism to histone acetylation. *Science* **324**: 1076-1080.

Xue Y, Vashisht AA, Tan Y, Su T, Wohlschlegel JA. 2014. Prb1 is required for clipping of the histone H3 N-terminal tail in *Saccharomyces cerevisiae. PLoS One* **9**: e90496.

Yang W, Xia Y, Hawke D, Li X, Liang J, Xing D, Aldape K, Hunter T, Alfred Yung WK, Lu Z. 2012. PKM2 phosphorylates histone H3 and promotes gene transcription and tumorigenesis. *Cell* **150**: 685-696.

Chapter 2. The Gdh1 glutamate dehydrogenase regulates telomeric silencing through modulating α-ketoglutarate, recruitment of the SIR complex and histone H3 clipping

Abstract

Growing evidence suggests that metabolism and chromatin dynamics are not separate processes but that they functionally intersect in many ways. Lys20, a lysine biosynthetic enzyme, was previously shown to have an unexpected function in DNA damage repair, raising the question of whether other amino acid metabolic proteins participate in chromatin regulation. Using an *in silico* screen combined with silencing reporter assays, we demonstrate that four additional amino acid metabolic proteins potentially regulate chromatin silencing in budding yeast. Analysis of the Gdh1 glutamate dehydrogenase reveals that this protein participates in telomeric silencing. The silencing function is dependent on Gdh1's metabolic activity and is linked to its consumption of α-ketoglutarate. Further manipulations of α-ketoglutarate levels reveal a key regulatory role for this metabolite in telomeric silencing. The *GDH1* deletion mutant shows diminished recruitment of the Silent Information Regulator (SIR) complex and elevated histone H3 clipping at the telomeres. Genetic analysis suggests that H3 clipping inhibits telomeric silencing *in vivo.* Therefore, the Gdh1 glutamate dehydrogenase appears to modulate telomeric silencing by controlling α-ketoglutarate, the recruitment of the SIR complex and histone H3 clipping.

Introduction

In eukaryotic nuclei, DNA is wrapped around histones to form nucleosomes, the basic subunits of chromatin (reviewed in Kornberg and Lorch 1999). The physical and chemical properties of chromatin are regulated by at least two types of enzymatic activities: chromatin remodeling and post-translational modifications of histones and chromatin-associated proteins (reviewed in Kouzarides 2007; Rando and Winston 2012). These enzymatic activities directly determine the accessibility of DNA for transcription, replication, and repair.

In *Saccharomyces cerevisiae*, condensed chromatin silences transcription in three regions: at telomeres, within the ribosomal DNA (rDNA) and at the *HM* silent mating-type loci (*HMR* and *HML*). In order to establish and maintain silencing during each cell cycle, transcription factors such as Rap1 bind to specific DNA sequences, thus facilitating the recruitment of the SIR complex (reviewed in Kueng *et al.* 2013). Sir2 is the catalytic component of the SIR complex, which uses NAD^+ as a co-factor to deacetylate histones H3 and H4 in newly deposited nucleosomes. Initial deacetylation by Sir2 creates binding sites for Sir3 and Sir4, which regulate the spreading of Sir2 at the telomeres and the silent mating-type loci (Rusche *et al.* 2002).

A growing field in the study of chromatin is the intersection of epigenetic and chromatin dynamics with cellular metabolic processes (reviewed in Wellen and Thompson 2012). Although most metabolic proteins localize to the cytoplasm and thus may influence chromatin indirectly through signaling cascades, a number of metabolic proteins are found in the nucleus. These nuclear-localized metabolic proteins can regulate

chromatin dynamics through at least two distinct mechanisms. In one, the proteins catalyze metabolic reactions in the nucleus and thus modulate the levels of substrates or co-factors available to chromatin modifying enzymes (reviewed in Gut and Verdin 2013). For instance, the acetyl-CoA synthesizing machinery has a separate nuclear pool in both yeast and mammalian cells, and its metabolic activity directly determines the amount of acetyl-CoA as a co-factor available for lysine acetyltransferases (Takahashi *et al.* 2006; Wellen and Hatzivassiliou *et al.* 2009). In an alternative mechanism, metabolic proteins have evolved distinct nuclear functions. For example, the mammalian pyruvate kinase PKM2 is translocated to the nucleus when the EGF receptor is activated, where it phosphorylates histone H3 instead of its usual metabolic substrate (Yang *et al.* 2012). A second example is *LYS20,* which encodes the yeast homocitrate synthase. This protein is constitutively localized to the nucleus (Chen *et al.* 1997). It acts as a dosage suppressor of the DNA damage sensitivity of *esa1-414,* an allele of the essential lysine acetyltransferase encoded by *ESA1.* Lys20 is thus defined as a moonlighting protein (Copley 2012; Jeffery 2009), because its function in DNA damage repair requires its nuclear localization signal but not its lysine biosynthetic activity (Scott and Pillus 2010). The previous findings with Lys20 prompted us to ask if other amino acid metabolic proteins function in chromatin regulation. This was an attractive possibility for two reasons: first, cells may adjust gene expression in response to fluctuating levels of amino acids, and second, amino acid metabolic proteins are ancient proteins with a rich repertoire of biochemical activities, making them ideal candidates to evolve multiple functions. Using a virtual screen combined with silencing reporter assays, we identified a number of candidate proteins with potential functions in chromatin regulation. Among

these, we focused on the role of glutamate dehydrogenase Gdh1 in the regulation of telomeric silencing. We report that α-ketoglutarate is an important regulatory metabolite for telomeric silencing and that Gdh1 regulates histone H3 clipping and binding of the SIR complex to the telomeres.

Results

A screen for amino acid metabolic enzymes with chromatin function

Based on our knowledge of Lys20, we designed an *in silico* screen as outlined in Fig. 2-1. The screen began with a search of the yeast proteome for proteins annotated to participate in amino acid metabolism. Next, in order to increase the likelihood of finding candidates that directly act on chromatin, we identified proteins with reported nuclear pools (Table 2-1). Known transcription factors were removed from the list because their nuclear functions have been established. Finally, we selected candidates based on two additional criteria: that they catalyze a reaction involving metabolite(s) required by known chromatin regulators, or that they share a similar biochemical feature as known chromatin regulators. The first criterion potentially reveals enzymes that regulate the homeostasis of metabolites involved in chromatin regulation. The second criterion is based on the idea that many multifunctional proteins take advantage of the same biochemical features for distinct activities. For instance, PKM2 uses the same kinase domain for phosphorylating both protein and metabolite substrates (Yang *et al.* 2012).

The screen identified nine candidates with potential functions in chromatin regulation: Arg82, Gdh1, Gdh3, Hom2, Hom6, Hpa3, Lys20, Lys21 and Utr4. Notably, the screen not only recovered Lys20 and its homolog Lys21, but also Arg82 (also known

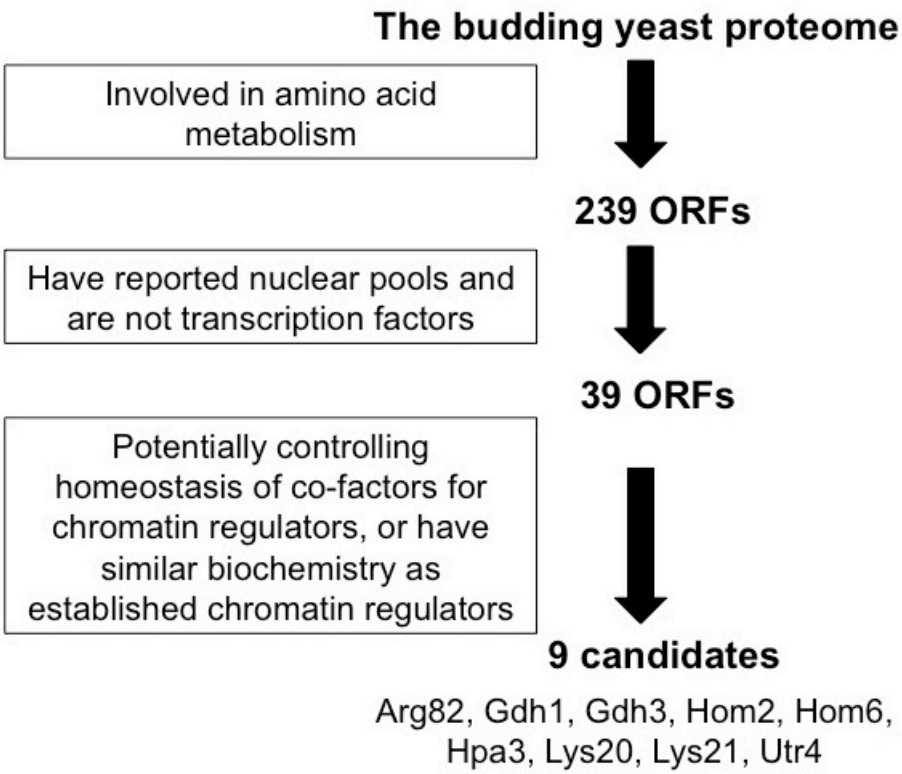

Figure 2-1. The *in silico* screen identified nine proteins that potentially function in chromatin regulation. The search was performed using the 'Advanced Search Engine' in the *Saccharomyces* Genome Database: yeastmine.yeastgenome.org/yeastmine/begin.do Search criteria for each step are boxed at left.

as Ipk2), another established moonlighting protein (Dubois *et al.* 2000; Odom *et al.* 2000). Therefore, the screen proved a promising method for discovering metabolic proteins with chromatin regulatory functions. The metabolic functions and known biochemical properties of the seven new candidate proteins are briefly summarized in Table S1A. Notably, all candidates had reported genetic or physical interactions with chromatin regulators defined by the *Saccharomyces* Genome Database (Table 2-1A) (Cherry *et al.* 2012; http://www.yeastgenome.org), although most of these interactions were identified by high-throughput screens that have not been independently validated.

A subset of candidate genes has potential roles in chromatin silencing

To assess the candidates' roles in chromatin function, we took advantage of a yeast strain in which reporter genes were integrated at the three silenced regions (Roy and Runge 2000). Of note, we grew the null strains in synthetic complete (SC) medium throughout this study, because the SC medium is made with a defined composition of nitrogen sources (Materials and Methods) and is likely to introduce fewer experimental variables for analyzing strains deleted for amino acid metabolic genes.

We first assessed rDNA silencing in the mutant strains. The rDNA locus has an *ADE2-CAN1* reporter cassette inserted at the 25S transcription unit. *CAN1* encodes a plasma membrane permease that imports arginine. Natural silencing within the rDNA locus represses *CAN1* expression, thus blocking the import of the toxic arginine analog canavanine (Fig. 2-2A). Mutants with rDNA silencing defects, for example *esa1-414* (Clarke *et al.* 2006), are sensitive to canavanine, because elevated import and incorporation of canavanine compromise protein functions. The *gdh1Δ, hom2Δ* and

hom6Δ strains were sensitive to canavanine, suggesting that these genes may normally promote rDNA silencing (Fig. 2-2A).

The reporter strain also has the *URA3* gene inserted on the right arm of telomere V (*TELV-R).* Cells expressing *URA3* are sensitive to 5-fluoroorotic acid (5-FOA). Natural silencing at *TELV-R* represses *URA3* transcription, allowing cells to grow on 5-FOA. Defective silencing, such as that caused by *SIR2* deletion, results in cell death on 5-FOA (Aparicio *et al.* 1991). Deletion of *HOM6, ARG82* and *GDH1* resulted in varying degrees of 5-FOA sensitivity (Fig. 2-2B), suggesting that their gene products normally promote telomeric silencing. Notably, unlike the *sir2Δ* mutant, the *gdh1Δ* strain exhibited a distinct phenotype: it showed small colony size and delayed growth on 5-FOA (Fig. 2-2B). This is consistent with two possibilities. One is that silencing is not abolished but is delayed in this mutant. A second is that *GDH1* deletion increases switching between the transcriptional 'off' and 'on' state per cell cycle, such as the deletion of *CAC1*, a component of the CAF1 chromatin assembly complex which has a similar phenotype on 5-FOA (Enomoto *et al.* 1997; Kaufman *et al.* 1997; Monson *et al.* 1997).

For monitoring silent mating type control, the reporter strain carries the *TRP1* gene at the *HMR* silent mating-type locus. Natural silencing at *HMR* represses *TRP1* transcription, causing poor growth on medium lacking tryptophan. Loss of silencing in the *sir2Δ* strain improved growth on SC-Trp (Aparicio *et al.* 1991). In contrast to *sir2*Δ, deletion of *HOM6* and *ARG82* worsened growth on SC-Trp (Fig. 2-2C), suggesting that *HMR* silencing is enhanced in these mutants. The phenotype for the *arg82Δ* mutant was unexpected because it was reported to have a mating defect (Dubois and Messenguy 1994) whereas enhanced *HM* silencing usually results in a higher mating efficiency. We

Figure 2-2. Gene products of *ARG82, GDH1*, *HOM2* and *HOM6* contribute to chromatin silencing. Wild type (WT) (LPY4654), *esa1-414* (LPY11113), *sir2Δ* (LPY4977), *gdh1Δ* (LPY15970), *gdh3Δ* (LPY15972), *hom2Δ* (LPY15962), *hom6Δ* (LPY17406), *hpa3Δ* (LPY15966)*, arg82Δ* (LPY15968) and *utr4Δ* (LPY15964) strains carry the rDNA*::ADE2-CAN1, TELVR::URA3* and *hmrΔE::TRP1* silencing reporters. The *esa1-414* and *sir2Δ* mutants served as controls with established silencing defects. (*A*) Deletion of *GDH1*, *HOM2* or *HOM6* caused defects in rDNA reporter silencing on SC-Ade-Arg+canavanine, where decreased growth indicates defective rDNA silencing. (*B*) Deletion of *ARG82, GDH1* or *HOM6* caused defective telomeric silencing as measured on 5-FOA, where decreased growth indicates defective telomeric silencing. (*C*) Deletion of *ARG82* and *HOM6* enhanced *HMR* silencing. Silencing was measured on SC-Trp, where decreased growth indicates enhanced *HMR* silencing.

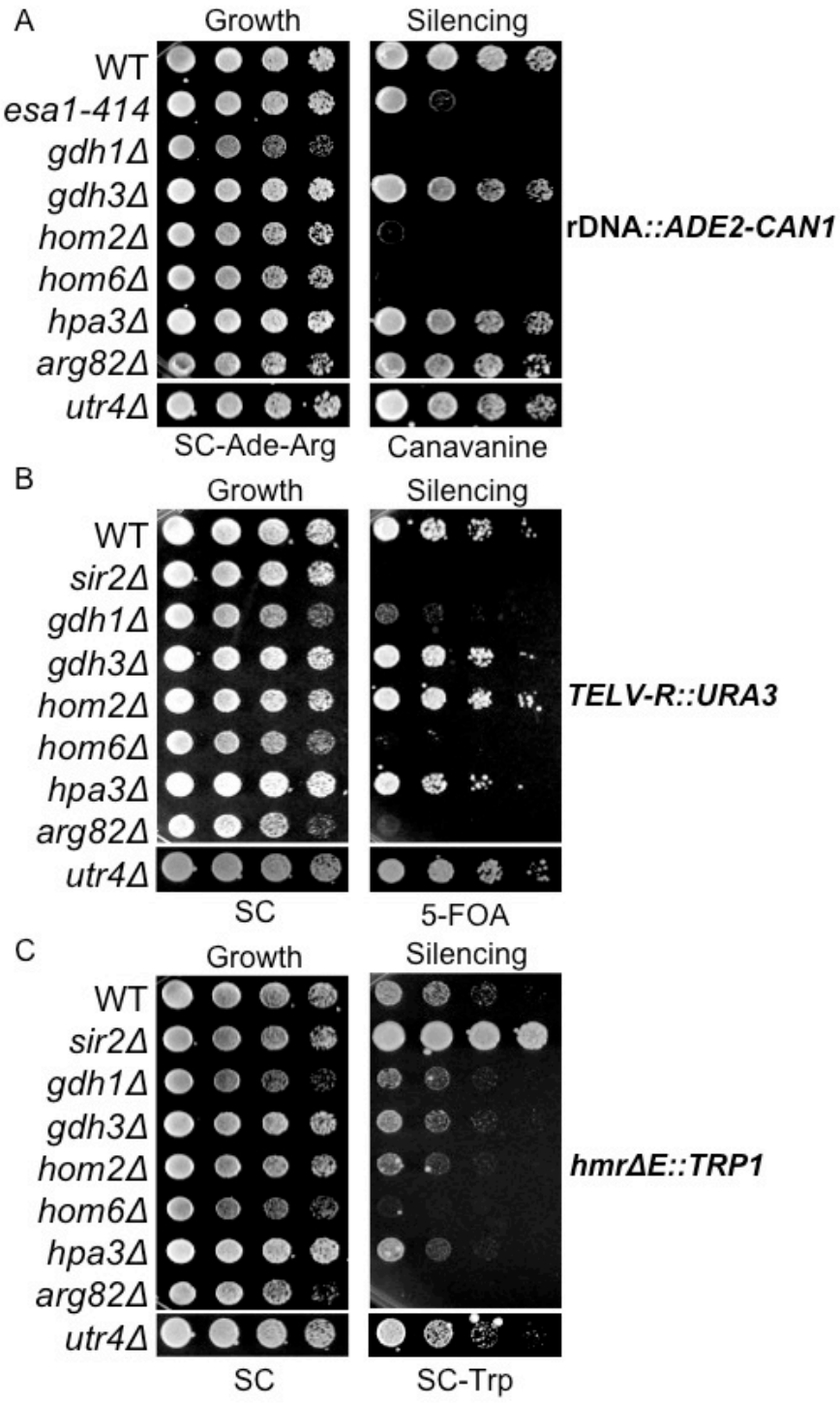
A
Growth
Silencing
WT
esa1-414
gdh1Δ
gdh3Δ
hom2Δ
hom6Δ
hpa3Δ
arg82Δ
utr4Δ
rDNA::ADE2-CAN1
SC-Ade-Arg
Canavanine
B
Growth
Silencing
WT
sir2Δ
gdh1Δ
gdh3Δ
hom2Δ
hom6Δ
hpa3Δ
arg82Δ
utr4Δ
TELV-R::URA3
SC
5-FOA
C
Growth
Silencing
WT
sir2Δ
gdh1Δ
gdh3Δ
hom2Δ
hom6Δ
hpa3Δ
arg82Δ
utr4Δ
hmrΔE::TRP1
SC
SC-Trp

confirmed that the *arg82Δ* mutant is not a tryptophan auxotroph (not shown), and therefore *ARG82* may influence mating through multiple mechanisms, perhaps in a manner shared by *PLC1*, which is upstream of *ARG82* and similarly enhances *HMR* silencing when deleted (Galdieri *et al* 2013),

Taken together, the deletion of *ARG82, HOM6, HOM2* and *GDH1* altered silencing of integrated reporter genes, whereas the deletion of *UTR4, HPA3* and *GDH3* had no apparent effect. We turned our focus to *GDH1* because it encodes the broadly conserved glutamate dehydrogenase enzyme that lies at the nexus between the citric acid cycle and nitrogen metabolism. Dysregulation of this enzyme has been directly associated with congenital hyperinsulinism (reviewed in James *et al.* 2009), and is indirectly implicated in cancer through the glutamine production pathway (reviewed in Burgess 2013). Therefore, it is of great importance to understand the role of GDH in chromatin regulation in addition to its role in metabolism.

Gdh1 is a positive regulator of telomeric silencing

Since the silencing reporters are metabolic in nature and Gdh1 is a metabolic protein, we examined the role of Gdh1 in silencing through independent assays. Recent studies showed that 5-FOA-based telomeric silencing assays may give false-positive results when mutants elevate ribonucleotide reductase (RNR) activities (Takahashi and Schulze *et al.* 2011; Rossmann *et al.* 2011). One way to eliminate the confounding effect is to supplement the 5-FOA assay with 10mM hydroxyurea (HU) (Rossmann *et al.* 2011), an RNR inhibitor. Adding HU did not rescue the 5-FOA sensitivity of *gdh1Δ TELV-R::URA3*, suggesting that the 5-FOA readout is likely the true reflection of *gdh1Δ*'s

silencing defect (Fig. 2-3A). Also, since the *TELV-R::URA3* reporter was constructed at an artificially truncated telomere, we assessed Gdh1's function at natural telomeres. A hallmark of silenced telomeres is the binding of the SIR complex. Chromatin immunoprecipitation (ChIP) revealed that the *gdh1Δ* mutant exhibited a significant reduction of Sir2 binding at all natural telomeric loci studied (Fig. 2-3C) that was not a result of global reduction of Sir2 levels (Fig. 2-3B). In contrast, Sir2 binding was unaffected at the *HMR* locus (Fig. 2-3C), consistent with the result of the *hmrΔE::TRP1* reporter assay. Sir3 binding was also reduced at the telomeres (Fig. 2-S1A). To directly assess the effect of the loss of the SIR complex in the *gdh1Δ* mutant, we evaluated the transcript levels of three genes close to their respective native telomeres (Fig. 2-3D). We found a moderate but significant increase in gene expression in the *gdh1Δ* mutant (Fig. 2-3D). Although more modest than the effect of deleting *SIR2* (Fig. 2-3D), these results parallel those of the silencing reporter assay in which the remaining silencing activity is likely to be mediated by the residual presence of Sir complex at the telomeres. These independent assays collectively support a role for Gdh1 in telomeric silencing through modulating the recruitment of the SIR complex.

In contrast to the silencing effects for telomeres, we found that the rDNA::*ADE2-CAN1* reporter assay was confounded by a silencing-independent effect of Gdh1 on *CAN1*. A *gdh1Δ* strain with *CAN1* at its endogenous locus was hypersensitive to canavanine (Fig. 2-S2A), suggesting that Gdh1 influences canavanine sensitivity outside the context of rDNA. In an independent assay, the *gdh1Δ* mutant did not show obvious changes in silencing a *URA3* reporter integrated at the *NTS1* spacer region (Smith and Boeke 1997) (Fig. 2-S2B). We did observe decreased Sir2 binding at the rDNA *NTS1*

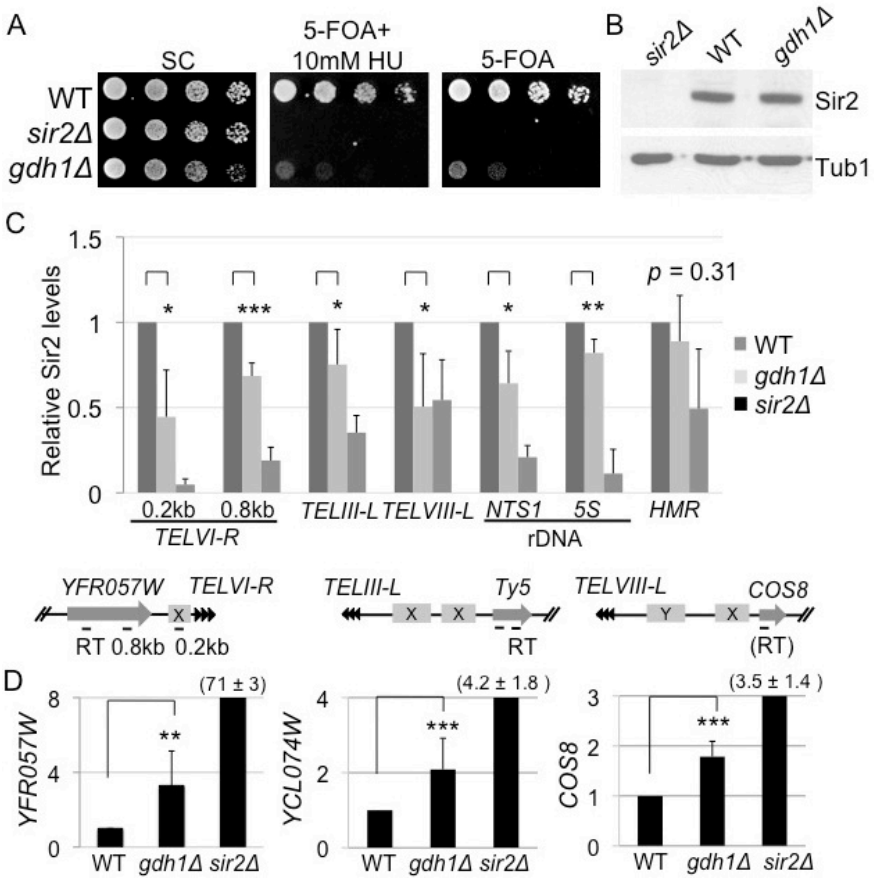

Figure 2-3. Independent assays support *GDH1*'s function in telomeric silencing. (*A*) The *gdh1Δ* silencing phenotype on 5-FOA was not a result of elevated RNR activity. WT (LPY4916), *sir2Δ* (LPY4979) and *gdh1Δ* (LPY16033) strains were assayed on 5-FOA with 10mM hydroxyurea (HU), a RNR inhibitor. (*B*) Sir2 protein levels were unaffected in the *gdh1Δ* mutant. Whole cell extracts of WT (LPY5), *gdh1Δ* (LPY16026) and *sir2Δ* (LPY11) were immunoblotted with antiserum for Tub1 (loading control) or Sir2. (*C*) Sir2 binding was significantly reduced in the *gdh1Δ* mutant. Sheared chromatin was prepared from strains in (*B*). Approximate positions of the primers used for ChIP analysis are indicated. Approximate positions of primers for expression analysis are indicated as RT. For *COS8*, the same primers were used for both ChIP and expression analysis (RT). Subtelomeric structures are indicated, including designations of the X and Y elements (boxed) and the $TG_{1\text{-}3n}$ repeats (arrowheads). Sir2 enrichment at each locus was normalized to an established ChrV control locus (Hess *et al.* 2004) with WT set to 1 for each experiment. Data represent averages from 2-4 independent experiments. For all experiments of this study, *p*-values were calculated using the one-tailed Student's t-test. * = $p < 0.05$, ** = $p < 0.01$, *** = $p < 0.005$. (*D*) Expression of telomere-proximal transcripts was increased in the *gdh1Δ* mutant. The mRNA from strains in (*B*) was analyzed by quantitative RT-PCR, normalized to *ACT1* with the WT value set to 1. Data represent averages from 3-5 experiments.

spacer (Fig. 2-3C) and a mild increase in the rDNA recombination rate (Gottlieb and Esposito 1989) (Fig. 2-S2C).

We also assessed the effect of *GDH1* deletion on the *HML* silent mating-type locus. The *gdh1Δ* strain silenced *HML* as strongly as the wild type strain (Fig. 2-S3A). Quantitative mating analysis showed that the deletion of *GDH1* moderately improved mating in the *MATα* strain (Fig. 2-S3B), suggesting that Gdh1 may have a minor role in the regulation of silent mating type.

Due to *gdh1Δ* mutant's modest effect on the *HM* locus and within the rDNA, we concluded that Gdh1's major chromatin silencing function is at telomeric heterochromatin. Further, since the 5-FOA-based telomeric silencing assay was a true reflection of the natural telomeric silencing status in the *gdh1Δ* mutant, we used it for further genetic analyses.

Both glutamate dehydrogenase paralogs contribute to telomeric silencing

In *S. cerevisiae*, Gdh1 has a paralog, Gdh3 (Avendano *et al.* 1997). Although the two proteins are 97% similar in amino acid sequence, the genes are differentially regulated by carbon sources: Gdh1 is expressed and active in both glucose- and ethanol-fueled media, whereas Gdh3 is only detectable and active in ethanol (DeLuna *et al.* 2001). Our screen identified Gdh3 as a potential chromatin regulator, but the deletion of *GDH3* did not affect telomeric silencing in glucose (Fig. 2-2B). We speculate this is because of *GDH3*'s low level of expression in glucose. Increased gene dosage of *GDH3* suppressed the telomeric silencing defect of the *gdh1Δ* mutant (Fig. 2-4A). Also, deletion of either single *GDH* gene only caused a mild loss of silencing in ethanol-fueled medium

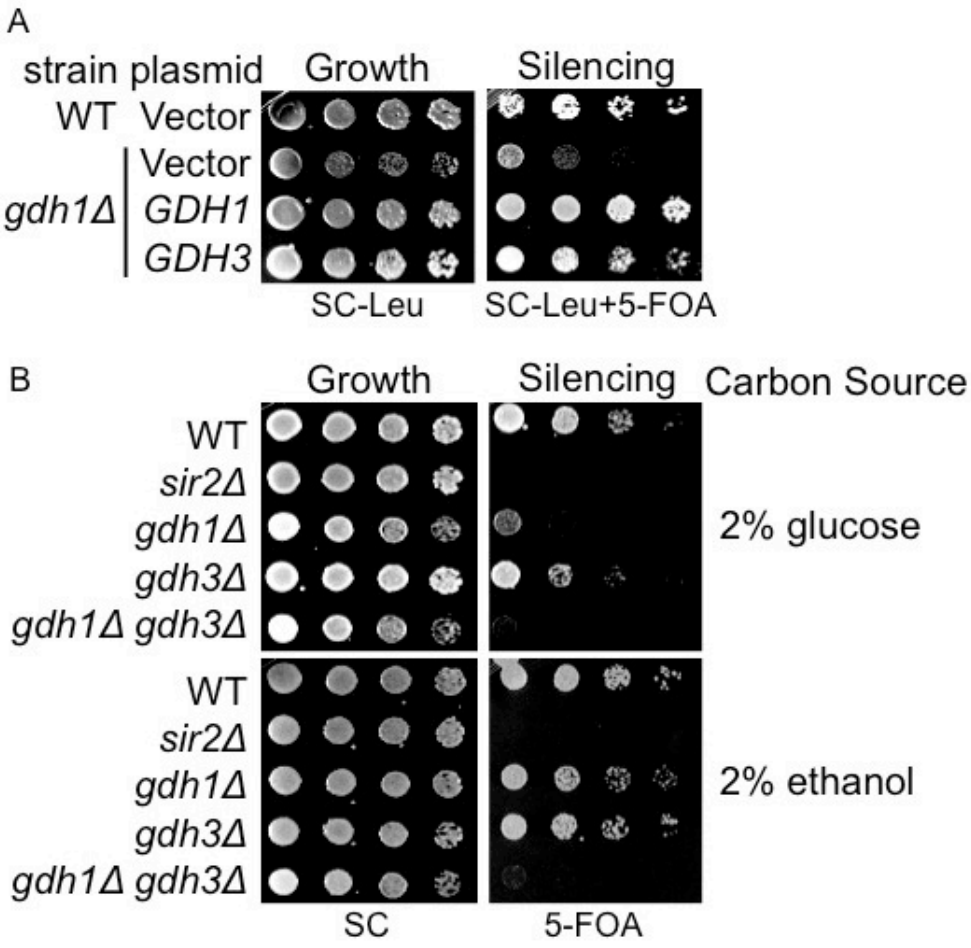

Figure 2-4. Gdh3 also contributes to telomeric silencing. (*A*) Increased dosage of *GDH3* suppressed *gdh1Δ*'s silencing defect. WT and *gdh1Δ* strains were transformed with 2μ plasmids: vector (pRS425), *GDH1* (pLP2764) or *GDH3* (pLP2662). Silencing was assessed on SC-Leu+5-FOA. (*B*) *GDH1* and *GDH3* single and double mutants showed different telomeric silencing phenotypes on glucose and ethanol-fueled media. WT (LPY4916), *sir2Δ* (LPY4979), *gdh1Δ* (LPY16033), *gdh3Δ* (LPY16785) and *gdh1Δ gdh3Δ* (LPY17916) strains were plated on 5-FOA with the indicated carbon sources.

(Fig. 2-4B), suggesting that the two paralogs may have overlapping functions in telomeric silencing when they are both expressed. Moreover, the *gdh1Δ gdh3Δ* double mutant showed defective telomeric silencing in both glucose- and ethanol-fueled media (Fig. 2-4B). Therefore, both proteins contribute to telomeric silencing, with Gdh1 as the primary player when glucose is the carbon source.

Gdh1's silencing function depends on its metabolic activity

We next asked if the metabolic function of Gdh1 accounts for its role in telomeric silencing. The established functions of Gdh1 and Gdh3 in *S. cerevisiae* are in nitrogen assimilation: the enzymes catalyze the synthesis of glutamate from α-ketoglutarate and ammonium (Fig. 2-5A). Of note, budding yeast has an alternative pathway to synthesize glutamate, using the glutamate synthase encoded by *GLT1* (Fig. 2-5A).

Studies on GDH from *Clostridium symbiosum* reported that the Asp165 residue is required for catalysis, because a D165S mutant lost its catalytic activity *in vitro* without affecting substrate binding (Dean *et al.* 1994) and sequence alignment revealed that this catalytic residue is conserved in *S. cerevisiae*. We constructed a plasmid-borne *gdh1-D150S* mutant Myc-tagged and expressed from its endogenous promoter. The mutant protein had stable expression compared to wild type (Fig. 2-5B), demonstrating that the mutation did not perturb protein stability. The catalytic activity of the *gdh1-D150S* mutant was assessed *in vivo* by a growth assay. The assay is based on the principle that the *gdh1Δ gdh3Δ glt1Δ* triple mutant strain cannot catalyze the anabolic reactions to synthesize glutamate from ammonium sulfate (Fig. 2-5A), and thus grows poorly in ammonium sulfate-based minimal medium. Transformation of wild type *GDH1* rescued

Figure 2-5. The metabolic activity of the Gdh homologs is important for telomeric silencing. (*A*) The catalytic Asp residue is conserved in *S. cerevisiae* Gdh1. Top: the enzymatic reaction catalyzed by the GDH enzymes. Bottom: Alignment of the *C. symbiosum* GDH with *S. cerevisiae* Gdh1. Boxed is the conserved catalytic Asp residue at position 165 in the *Clostridium* protein. (*B*) *gdh1-D150S*-13Myc was stably expressed. *gdh1Δ* (LPY16026) cells were transformed with vector (pRS316), *GDH1*-13Myc (pLP2833) or *gdh1-D150S*-13Myc (pLP2834). Whole cell extracts were immunoblotted for Myc or Tub1 (loading control). (*C*) The *gdh1-D150S* mutant had diminished catalytic activity required to assimilate ammonium. The *gdh1Δ gdh3Δ glt1Δ* strain (LPY17131) was transformed with vector (pRS315), *GDH1* (pLP2631) or *gdh1-D150S* (pLP2638) and assayed for growth. (*D*) The conserved Asp residue contributes to Gdh1's function in telomeric silencing. WT and *gdh1Δ gdh3Δ* cells were transformed with vector (pRS425), *GDH1* (pLP2764) or *gdh1-D150S* (pLP2698) and telomeric silencing was assessed. (*E*) Colony counting assay on SC-Ura confirmed the lack of silencing activity of the *gdh1-D150S* mutant. Assay was described in Materials and Methods.

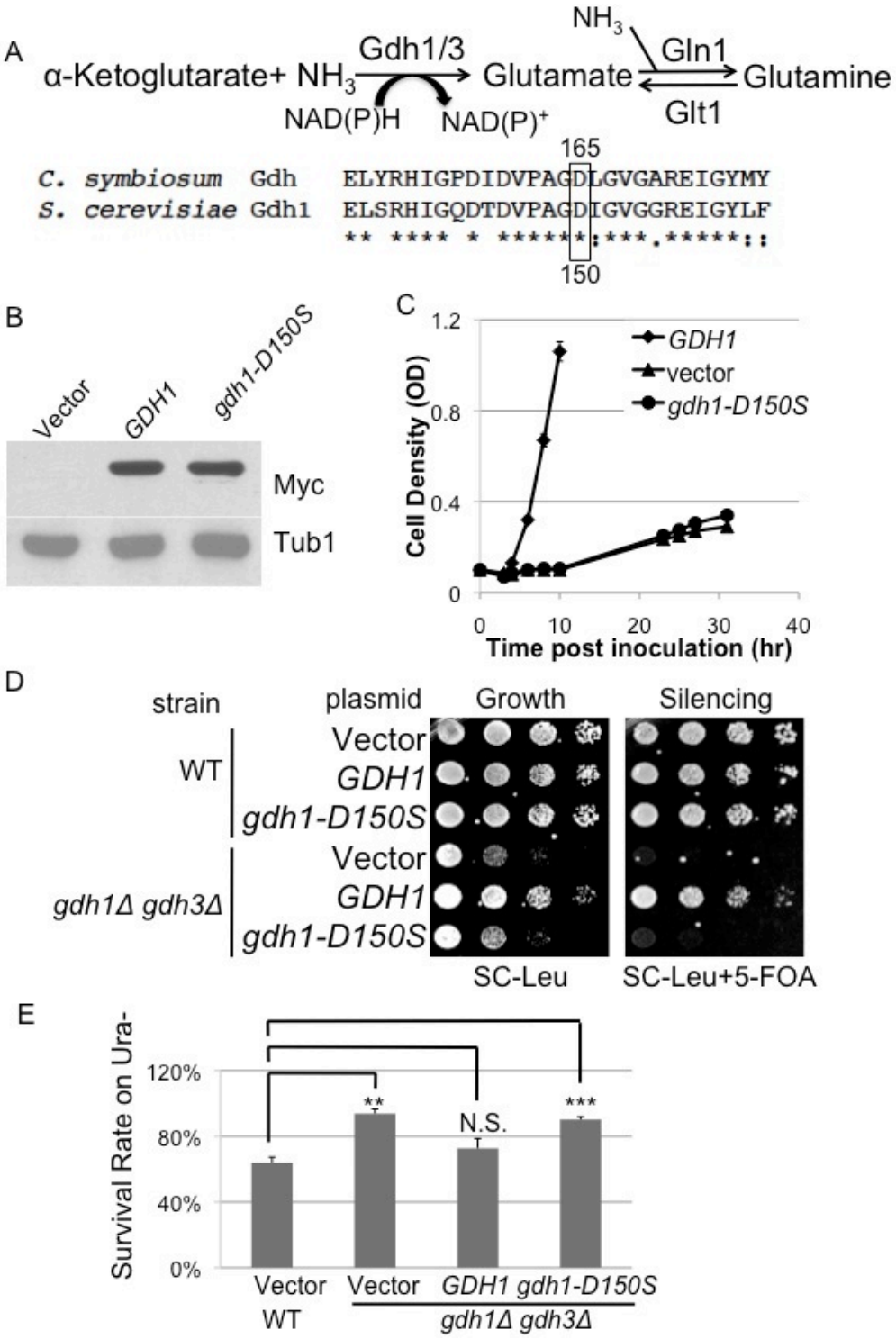
A
α-Ketoglutarate+ NH3
Gdh1/3
NAD(P)H
NAD(P)+
Glutamate
NH3
Gln1
Glt1
Glutamine
165
C. symbiosum Gdh ELYRHIGPDIDVPAGDLGVGAREIGYMY
S. cerevisiae Gdh1 ELSRHIGQDTDVPAGDIGVGGREIGYLF
150
B
Vector
GDH1
gdh1-D150S
Myc
Tub1
C
GDH1
vector
gdh1-D150S
Cell Density (OD)
Time post inoculation (hr)
D
strain
plasmid
Growth
Silencing
WT
Vector
GDH1
gdh1-D150S
gdh1Δ gdh3Δ
Vector
GDH1
gdh1-D150S
SC-Leu
SC-Leu+5-FOA
E
Survival Rate on Ura-
120%
80%
40%
0%
**
N.S.
***
Vector
WT
Vector
GDH1
gdh1-D150S
gdh1Δ gdh3Δ

the growth defect of the triple mutant, whereas the *D150S* mutant was unable to do so (Fig. 2-5C). Therefore, the *D150S* mutant had lost much of its catalytic activity *in vivo*. Since Gdh1 and Gdh3 were reported to form hetero-hexamers (DeLuna *et al.* 2001), we assessed the silencing function of the *gdh1-D150S* mutant in the *gdh1Δ gdh3Δ* background to avoid potential dominant negative effects. The *gdh1-D150S* mutant failed to suppress the telomeric silencing defect of the *gdh1Δ gdh3Δ* strain, as demonstrated by dilution assay (Fig. 2-5D) and independently counting colonies grown on medium lacking uracil (Fig. 2-5E). Some silencing activity was observed upon prolonged incubation, likely due to low or residual metabolic activity of the D150S mutant. Hence, we conclude that the metabolic activity of Gdh1 is required for its full silencing function.

Elevated α-ketoglutarate levels result in telomeric silencing defects

Since catalysis promoted by Gdh1 is linked to its silencing function, we asked whether it acts through modulating the levels of co-factors required for chromatin regulators. Sir2 uses NAD^+ as a co-factor to deacetylate its substrates (Imai *et al*. 2000). Since Gdh1 also uses $NAD(P)^+$ as a co-factor, it was possible that Gdh1's metabolic activity influences the nuclear pool of NAD^+. To test this hypothesis, we took advantage of a nuclear NAD^+ reporter assay that consists of a plasmid-borne NadR-AD transcriptional activator and a yeast strain with a NadR binding-site box integrated at the promoter of the *HIS3* gene (Fig. 2-6A). The levels of free NAD^+ in the nucleus influence the binding affinity of NadR-AD for the NAD box, thus modulating the ability of the strain to grow on medium lacking histidine (Anderson *et al.* 2003). In this assay the *gdh1Δ* mutant showed similar growth as the wild type strain (Fig. 2-6A), and so it is

unlikely that *GDH1* influences telomeric silencing through controlling nuclear NAD^+ levels.

We next considered the possibility that Gdh1 regulates telomeric silencing through modulating α-ketoglutarate levels. This metabolite is known to be a co-factor for chromatin regulators such as the JMJC-domain containing demethylases (reviewed in Schneider and Shilatifard 2006). The *gdh1Δ* mutant has reduced ability to use α-ketoglutarate as a substrate to assimilate ammonium (Fig. 2-5A), and showed an ~33% increase in α-ketoglutarate levels when grown in ammonium sulfate-based SC medium (DeLuna *et al.* 2001). To assess whether elevated α-ketoglutarate levels could contribute to the *gdh1Δ* silencing defect, we took two separate approaches. First, we transformed *gdh1*Δ with plasmid-borne *IDP1*, which encodes the mitochondrial NADP-specific isocitrate dehydrogenase that is known to contribute to the synthesis of α-ketoglutarate. Increased dosage of *IDP1* further worsened telomeric silencing in *gdh1Δ* cells by ~50% (Fig. 2-6B), consistent with the concept that these two genetic manipulations had additive effects on increasing α-ketoglutarate levels. In an independent approach, we deleted the gene *MKS1*, because a previous study showed that this mutant caused a 600% increase in α-ketoglutarate levels (Feller *et al.* 1997). The *mks1Δ* mutant showed an even stronger telomeric silencing defect than the *gdh1Δ* mutant (Fig. 2-6C). These findings suggest that α-ketoglutarate levels are important regulators of telomeric silencing.

It is worth noting that no experimental tool has yet been developed to evaluate nuclear levels of α-ketoglutarate. Nonetheless, we found that adding a strong nuclear export (NES) signal to Gdh1 caused a moderate loss of telomeric silencing (Fig. 2-S4B), suggesting that the nuclear pool of α-ketoglutarate may be altered when Gdh1 is depleted

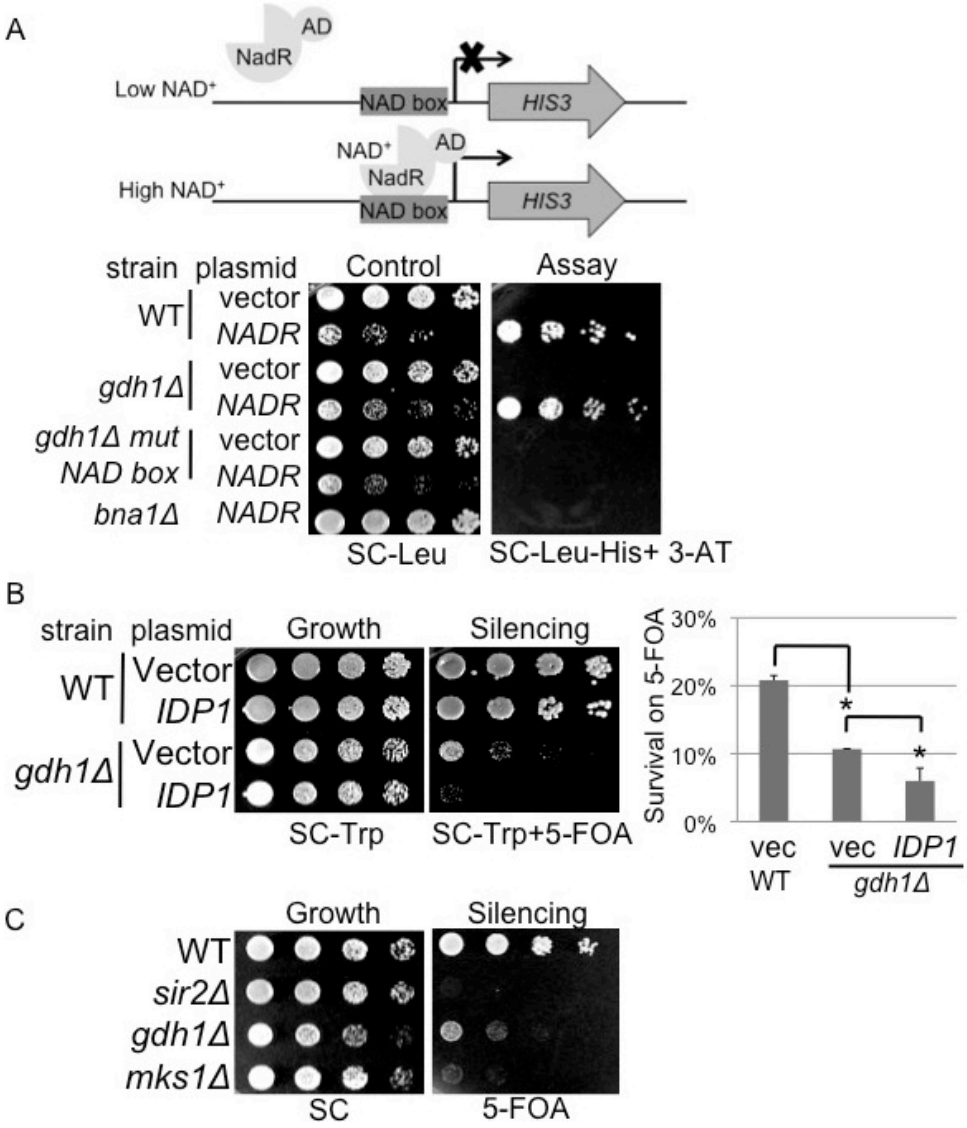

Figure 2-6. Gdh1 likely regulates telomeric silencing through modulating α-ketoglutarate levels. (*A*) The *gdh1Δ* cells have normal levels of nuclear NAD^+. WT (LPY20466) and *gdh1Δ* (LPY20477) reporter strains were transformed with vector (pLP3227) or NADR-AD (pLP3228). Nuclear NAD^+ levels were measured by growth on SC-His-Trp+ 10mM 3-amino-1,2,4-triazole (3-AT). 3-AT prevents leaky transcription of *HIS3*. The *bna1Δ* strain (LPY20468) was a positive control for reduced NAD^+ levels and the *gdh1Δ* strain with mutant NAD boxes (LPY20480) was a negative control to test for NadR-AD-specific effects. (*B*) Increased dosage of *IDP1* worsened telomeric silencing in *gdh1Δ*. WT and *gdh1Δ* cells transformed with vector (pRS314) or *IDP1* (pLP3238) were assayed on SC-Trp+5-FOA. Survival rate on 5-FOA was quantified as described in Materials and Methods. (*C*) Deletion of *MKS1* caused defective telomeric silencing. WT, *sir2Δ*, *gdh1Δ* and *mks1Δ* (LPY16796) strains were assayed on 5-FOA.

from the nucleus. Also, we observed moderate recruitment of Gdh1 to telomeric loci as well as the rDNA-*NTS1* (Fig. 2-S4C), and thus it is possible that Gdh1 influences α-ketoglutarate levels at these loci.

Gdh1 is a negative regulator of H3 N-terminal clipping *in vivo*

Histone H3 clipping refers to the proteolytic cleavage of the H3 N-terminal tail that is subject to post-translational modifications. Knowledge of its physiological function is limited to its role in transcriptional activation. As an example, enhanced H3 clipping was found to increase H3 turnover at the promoters of sporulation-induced genes (Santos-Rosa *et al.* 2009). Clipping was originally attributed to an unidentified serine protease, and the cleavage site was proposed to be H3-S22 (Santos-Rosa *et al.* 2009). Recent studies suggest a debatable role of glutamate dehydrogenase in H3 clipping. For example, GDH purified from microsomes of chicken liver clips histone H3 *in vitro* (Mandal *et al.* 2013). By contrast, another study showed that Gdh1 was present in a fraction with clipping activity, but whole cell extracts from *gdh1Δ* cells growing in rich medium did not affect clipping *in vitro* (Xue *et al.* 2014). This same study reported that a vacuolar protease encoded by *PRB1* has H3 clipping activity. Since the H3 N-terminal tail is established to be important for telomeric silencing (Thompson *et al.* 1994; Martin *et al.* 2004), we asked whether Gdh1 has a role in H3 clipping *in vivo* and if so, whether this contributes to its function in telomeric silencing.

Nuclear extracts were prepared from log-phase cells growing in ammonium sulfate-based SC medium followed by immunoblotting to evaluate both intact and clipped H3. The *gdh1Δ* mutant showed increased global H3 clipping (Fig. 2-7A), with the

increase dependent on the Gdh1 Asp150 catalytic site residue. Therefore, it appears that Gdh1 has an inhibitory role on H3 clipping *in vivo.*

We next asked by ChIP if the deletion of *GDH1* affects H3 clipping at telomeres. We used a yeast histone shuffle strain in which the chromosomal loci encoding H3-H4 were deleted and in which viability was maintained by a plasmid carrying N-terminally Flag-tagged H3 and untagged H4 (Nathan and Ingvarsdottir *et al.* 2006). In these experiments, Flag ChIP detects unclipped H3 and H3-CT ChIP detects both clipped and unclipped H3. The ratio of Flag/H3-CT thus represents the percentage of unclipped H3 relative to total H3. The deletion of *GDH1* significantly reduced the Flag: H3-CT ratio at the telomeres, consistent with an increase in H3 clipping. By contrast, the mutant showed minimal effect on H3 clipping at the *HMR-E* silencer (Fig. 2-7B). Moreover, the elevation of H3 clipping diminished further away from *TELVI-R* (2kb), suggesting that Gdh1 affects H3 clipping locally at this telomere (Fig. 2-7B).

It was reported that histone H3K4 methylation inhibits H3 clipping (Santos-Rosa *et al.* 2009), and that *JHD2* encodes a demethylase that uses α-ketoglutarate as a co-factor to demethylate trimethylated H3K4 (Liang and Klose *et al.* 2007). Therefore, it is possible that increased α-ketoglutarate levels in the *gdh1Δ* mutant hyperactivate Jhd2, leading to spurious erasure of the H3K4 trimethylation mark and thus promoting clipping. To test this idea, we first asked whether increased dosage of *JHD2* would increase clipping just like the *gdh1Δ* mutant. This was indeed the case (Fig. 2-S5A). Next, we asked if H3K4 tri-methylation levels are reduced in the *gdh1Δ* mutant. Global H3K4 di- and trimethylation levels did not change in the *gdh1Δ* mutant (Fig. 2-S5B). Furthermore, we found that there was in fact an increase in H3K4Me3 trimethylation at

Figure 2-7. Gdh1 is a negative regulator of histone H3 N-terminal clipping. (*A*) H3 N-terminal clipping was increased in the *gdh1Δ* mutant. Nuclear extracts were prepared from WT (LPY4916) and *gdh1Δ* (LPY16033) strains transformed with vector (pRS314), *GDH1* (pLP3082) or *gdh1-D150S* (pLP3083), and immunoblotted for H3-CT and Tub1 (loading control). N-terminally clipped H3 was highlighted by the asterisk. Blots from two sets of independent extracts were quantified. (*B*) H3 N-terminal clipping was increased at telomeres in the *gdh1Δ* mutant. WT (LPY19789) and *gdh1Δ* (LPY19794) histone shuffle strains carried H3 with an N-terminal Flag tag (pLP2129). Anti-Flag antibody precipitated unclipped H3 whereas anti-H3-CT antibody precipitated both clipped and unclipped H3. Flag and H3-CT signals at each locus were normalized to the respective signals for the control locus *ACT1*. The Flag/H3-CT ratio for the WT strain was set to 1 for each experiment. Data represent the averages from 2-3 ChIP experiments. (*C*) The H3S22A mutation interferes with H3 clipping. Nuclear extracts of strains were prepared from WT and *gdh1Δ* strains carrying plasmid-borne WT H3-H4 (pLP1775) or H3S22A-H4 (pLP2438), and blotted anti-H3-CT or anti-Tub1 (loading control). (*D*) The H3S22A mutation improved silencing in both the WT and the *gdh1Δ* background. The strains used in (*C*) were assayed on 5-FOA. (*E*) Gdh1's metabolic activity regulates telomeric silencing through both clipping-dependent and -independent mechanisms. In this cell model, the nucleus is highlighted in blue with the cytoplasm shown in grey.

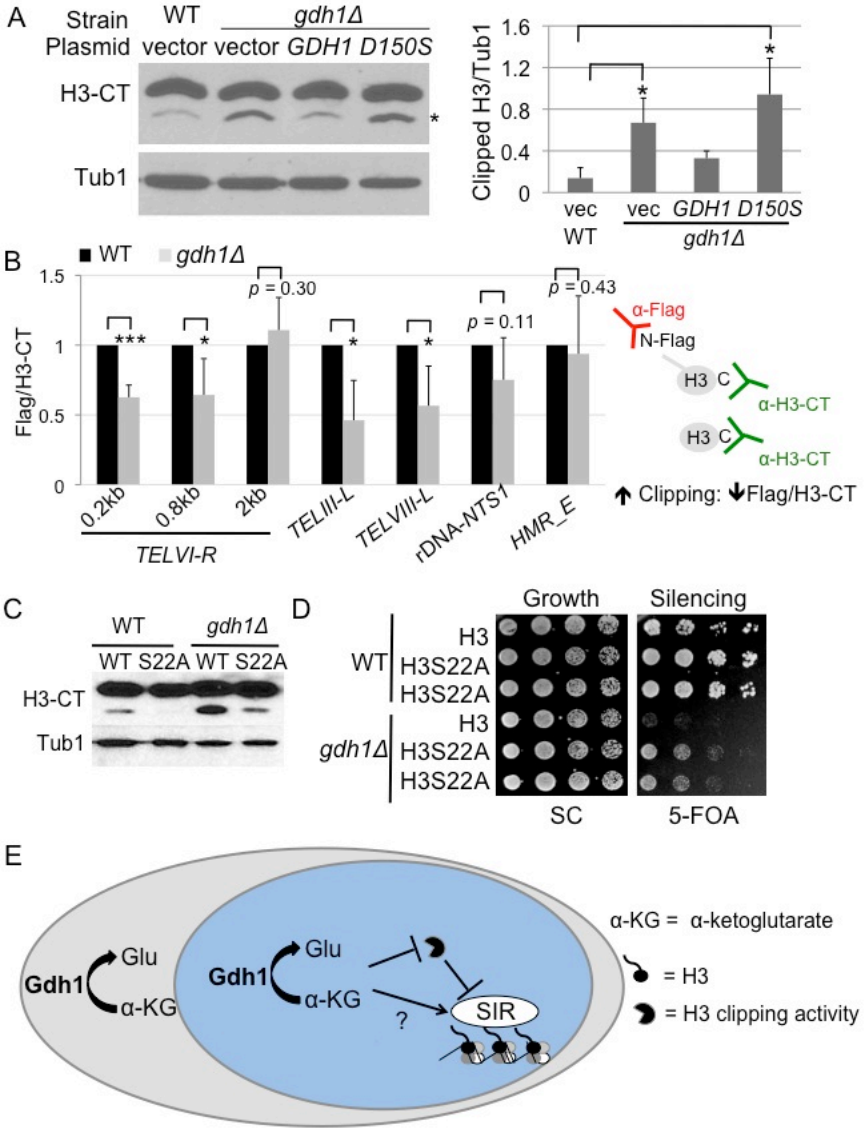
A
Strain
Plasmid
WT
vector
gdh1Δ
vector
GDH1 D150S
H3-CT
Tub1
Clipped H3/Tub1
vec WT
vec
GDH1 D150S
gdh1Δ
B
WT
gdh1Δ
Flag/H3-CT
p = 0.30
p = 0.11
p = 0.43
0.2kb
0.8kb
2kb
TELVI-R
TELIII-L
TELVIII-L
rDNA-NTS1
HMR_E
α-Flag
N-Flag
H3 C
α-H3-CT
Clipping: Flag/H3-CT
C
WT
gdh1Δ
WT S22A WT S22A
H3-CT
Tub1
D
Growth
Silencing
WT
gdh1Δ
H3
H3S22A
H3S22A
SC
5-FOA
E
Gdh1
Glu
α-KG
SIR
?
α-KG = α-ketoglutarate
= H3
= H3 clipping activity

TELVI-R and *TELIII-L* in the *gdh1Δ* mutant (Fig. 2-S5C), suggesting that Gdh1 does not regulate H3 clipping through a Jhd2-dependent pathway.

Gdh1 regulates telomeric silencing through both clipping- dependent and independent mechanisms

Previous studies demonstrated that N-terminal truncation of H3 diminished telomeric silencing (Thompson *et al* 1994). Since we found that deletion of *GDH1* simultaneously increased H3 clipping and decreased telomeric silencing, we asked if elevated clipping contributed to the silencing defect in the *gdh1Δ* mutant. To address this question, we first used the established *H3Δ3-29* mutant as a genetically clipped form of H3 (Zhang *et al.* 1998). This mutant was very defective for the silencing of *TELV-R::URA3,* and the *gdh1*Δ *H3Δ3-29* double mutant was just as defective (Fig. 2-S6A). Furthermore, although Ser22 was proposed to be the H3 clipping site (Santos-Rosa *et al.* 2009, Xue *et al.* 2014), little work has been done to evaluate its function *in vivo*. We found that the H3S22A mutation reduced, although did not abolish H3 clipping in both WT and *gdh1Δ* yeast (Fig. 2-7C; Fig. 2-S6B), consistent with the idea that cleavage can occur at this site *in vivo.* The H3S22A mutation improved silencing of the telomeric reporter gene in both wild type and the *gdh1Δ* mutant (Fig. 2-7D). The H3S22A mutation also improved Sir2 and Sir3 binding at *TELVI-R* and *TELIII-L* in the wild type background (Fig. 2-S6C-D), suggesting that H3 clipping generally has a negative impact on telomeric silencing *in vivo*. The H3S22A mutation improved Sir3 binding in the *gdh1Δ* mutant at *TELIII-L* but not *TELVI-R* (Fig. 2-S6C-D). Given that the H3S22A mutation also improved silencing of the reporter gene inserted at *TELV-R,* it appears that

both clipping-dependent and -independent mechanisms contribute to Gdh1's function in silencing. We did not observe the loss of Sir2 binding in the *gdh1Δ* mutant in the histone shuffle strains (Fig. 2-S6C-D), nor did we observe improved Sir2 binding by the H3S22A mutation. This may relate to earlier studies demonstrating that lowered histone dosage in shuffle strains altered chromatin functions such as DNA damage repair (Liang *et al.* 2012). It is possible that the lowered histone dosage in the shuffle strain suppressed Gdh1's effect on Sir2 binding and that Sir3 and Sir2 binding may be differentially affected in response to such dosage changes.

Discussion

In this study, our *in silico* screen revealed that four proteins with established roles in amino acid metabolism also have potential functions in chromatin silencing. We observed that the Gdh1 and Gdh3 glutamate dehydrogenases both regulate telomeric silencing, with Gdh1 acting as the primary regulator when glucose is the carbon source, whereby it regulates the recruitment of the SIR complex to the telomeres. We showed through genetic experiments that increased α-ketoglutarate levels generally diminish telomeric silencing, and that the loss of Gdh1 contributes to the promotion of H3 clipping both globally and at the telomeres *in vivo.*

Deletion of four candidate metabolic proteins altered chromatin silencing

Increasing evidence suggests that multiple pathways connect metabolism to chromatin regulation and epigenetic processes (reviewed in Gut and Verdin 2013; Kaelin and McKnight 2013). In particular, chromatin silencing is influenced by the activity of

the NAD^+ metabolic pathways (Sandmeier *et al.* 2002). We found that deletion of *ARG82, GDH1, HOM2,* and *HOM6* exhibited silencing defects. The gene products of these candidates represent three distinct metabolic pathways: synthesis of inositol polyphosphate, assimilation of ammonium and synthesis of methionine and threonine. We showed that Gdh1's role in telomeric silencing is dependent on its metabolic activity, and that high α-ketoglutarate levels are generally detrimental to telomeric silencing. Future studies will establish if Hom2, Hom6 and Arg82 contribute to chromatin-mediated silencing through metabolism-dependent or -independent mechanisms.

It is noteworthy that our *in silico* search revealed that 39 amino acid metabolic proteins have reported nuclear pools, many of which were eliminated by our stringent search criteria (Table 2-S1B). We are aware of the fact that these proteins may regulate chromatin functions in unexpected ways. For example, these proteins may use the same catalytic site for entirely different biochemical reactions (Khersonsky and Tawfik 2010). Further, the candidate genes whose deletion did not show any silencing phenotypes may regulate other aspects of chromatin function, such as DNA damage repair or other elements of transcriptional regulation.

α-ketoglutarate is an important metabolic regulator of telomeric silencing

Recent studies revealed that oncogenic mutations in human isocitrate dehydrogenase result in the synthesis of 2-hydroyglutarate (2-HG) instead of α-ketoglutarate. 2-HG competitively inhibits JMJC domain histone demethylases, resulting in increased H3K9 methylation (Turcan, Rohle and Goenka *et al.* 2012; Lu *et al.* 2012). Our work demonstrates that elevated α-ketoglutarate levels caused telomeric silencing

defects (Fig. 2-6B-C). These findings collectively suggest that it is crucial to maintain the homeostasis of α-ketoglutarate, as both low and high levels have detrimental effects on chromatin functions. This point will be particularly important when developing therapies against IDH mutant-bearing tumors, because strategies to compensate for the low production of α-ketoglutarate may cause unwanted secondary effects.

Gdh1 is a negative regulator of H3 N-terminal clipping

Glutamate dehydrogenase extracted from chicken liver microsomes was shown to clip free and chromatin-bound H3 *in vitro* (Mandal *et al.* 2013). We asked if Gdh1 clips H3 in budding yeast *in vivo*. Contrary to that possibility, the deletion of *GDH1* increased H3 clipping globally, and the increase was dependent on the conserved catalytic residue controlling its metabolic activity (Fig. 2-7A). This suggests that Gdh1 normally inhibits rather than catalyzes H3 N-terminal clipping in budding yeast *in vivo.*

Earlier work showed that H3K4 trimethylation inhibits clipping both *in vitro* and *in vivo* (Santos-Rosa *et al.* 2009). We asked whether Jhd2, which specifically demethylates the H3K4 trimethylation mark, mediates the effect of α-ketoglutarate on H3 clipping. We found that increased dosage of Jhd2 increased H3 clipping (Fig. 2-S5A). However, we did not observe any loss of the H3K4 trimethylation mark in the *gdh1Δ* mutant (Fig. 2-S5B-C). These findings suggest that although Jhd2 could be a regulator of H3 clipping *in vivo,* elevated Jhd2 activity was unlikely to be the cause of increased clipping in the *gdh1Δ* mutant.

Previous studies showed that H3 clipping is diminished with the addition of serine protease inhibitors, hence supporting the proposal that Ser22 is the cleavage site *in vivo*

(Santos-Rosa *et al.* 2009, Xue *et al.* 2014). In this work, we found that the H3S22A mutation greatly reduced H3 clipping in the nuclear extracts (Fig. 2-7C). Nonetheless, residual H3 clipping was observed (Fig. 2-S6B), suggesting that alternative or additional cleavage site(s) exist *in vivo.* Interestingly, earlier studies reported cleavage at Lys23/27 *in vitro* (Mandal *et al* 2013; Xue *et al* 2014), so these residues may be sites of clipping *in vivo.*

We found that reduced H3 clipping by the S22A mutation correlates with increased telomeric silencing (Fig. 2-7D) and improved telomeric SIR binding (Fig. 2-S6C-D). In the *gdh1Δ* mutant, the S22A mutation improved silencing of the reporter gene inserted at *TELV-R* and restored Sir3 binding at *TELIII-L* (Fig. 2-7D; Fig. 2-S6D), with no obvious effect on Sir3 binding at *TELVI-R.* These results suggest that Gdh1 regulates telomeric silencing through both clipping-dependent and -independent mechanisms. Analysis of Sir2 binding in the *gdh1Δ* histone shuffle mutant was confounded by altered histone dosage (Fig. 2-S6C-D), and future work with an integrated H3S22A allele will be worthy to address this question.

In sum, we identified glutamate dehydrogenase homologs Gdh1 and Gdh3 as positive regulators of telomeric silencing. Gdh1's silencing function requires its catalytic activity, and high α-ketoglutarate levels are generally detrimental to silencing. Gdh1 represses H3 N-terminal clipping and regulates the recruitment of the SIR complex to the telomeres. This study lends new evidence for the emerging concept that epigenetic processes are tightly regulated by cellular metabolic status, and that mutations in metabolic genes may cause diseases through changes both in the cytoplasm and in the nucleus.

Materials and Methods

Yeast strains and plasmids

Strains are listed in Table S2. All mutants are null alleles except *esa1-414* (Clarke *et al.* 2006). Gene deletions were constructed by amplifying *kanMX* from the *Saccharomyces* Genome Deletion Project strains (oligonucleotides listed in Table S4) and transforming into the silencing reporter strain (Roy and Runge 2000). Strains for the *GDH1* study were backcrossed before use. Double mutants were constructed through standard crosses. Histone shuffle strains were chromosomally deleted for both *HHT-HHF* loci and were originally covered with a plasmid carrying the wild type copy of *HHT2-HHF2* (Ahn *et al.* 2005). Histone mutant strains were made by transforming the shuffle strains with plasmids carrying histone mutants and counter-selecting the wild type plasmid.

Plasmids are listed in Table S3. Each gene was subcloned from the Yeast Genomic Tiling Library (Open Biosystems, Jones *et al.* 2008), including endogenous 5' and 3' sequences. Detailed cloning information is available upon request. The D150S mutation was introduced by site-directed mutagenesis using primers listed in Table S4. Plasmid-borne Myc-tagged Gdh1 was constructed by replacing the natural stop codon of *GDH1* with an XmaI site using primers oLP1598 and oLP1599 and ligating the digested plasmid with an XmaI-digested DNA fragment containing 13Myc and a terminator sequence made by amplification of pLP1651 with primers oLP1629 and oLP1753.

Growth assays and silencing reporter assays

SC medium was made with 0.67% ammonium sulfate-based yeast nitrogen base without amino acids (Difco) supplemented with amino acids (standard lab recipe). For all experiments of this study, freshly thawed/transformed cells were inoculated in 3mL SC medium for 2 days before plating/diluting for log-phase growth. For dilution assays, A_{600}=1OD of culture (~ 6×10^6 cells) was pelleted, resuspended in 1mL H_2O, plated in five-fold serial dilutions, and incubated at 30°C. For rDNA silencing assays, strains were plated on SC-Ade-Arg (growth control) and SC-Ade-Arg+8μg/mL L-canavanine (Sigma). For *HM* silencing assays, strains were plated on SC (growth control) and SC-Trp (silencing). For telomeric silencing assays, strains were plated on SC (growth control) and SC+1g/L 5-FOA (US Biological). For the nuclear NAD^+ assays, strains were plated on SC-Leu (growth control) and SC-Leu-His+10mM 3-AT (Sigma). Images were captured after 1.5- 3 days. To assess the catalytic activity of *gdh1-D150S,* starter cultures of transformants were diluted to A_{600} of 0.1 in minimal medium (0.67% ammonium sulfate-based yeast nitrogen base supplemented with required amino acids and 2% glucose). A_{600} was measured at indicated times. Quantification of growth on media lacking uracil was done by plating 200-500 log-phase cells on SC-Trp (control) or SC-Trp-Ura (silencing) media. Quantification of survival rate on 5-FOA was done by plating 500-1000 log-phase cells on SC-Trp (control) and SC-Trp+ 5-FOA (silencing). For both quantitative assays, cells were counted 48 hours after plating.

mRNA quantification

Starter cultures were diluted in 50mL SC medium and harvested at A_{600} of 0.8-1.0

(~5×10^6 - 6.5×10^6 cells per mL). RNA was extracted using the hot acid phenol method (Collart and Oliviero 2001), except that harvested cells were resuspended in sodium acetate buffer (50mM sodium acetate pH5.3, 10mM EDTA). RNA was reverse transcribed with random hexamers using TaqMan Reverse Transcription Reagents (Life Technologies). cDNA was diluted 5- or 10-fold and analyzed by real-time PCR on DNA Engine Opticon 2 (MJ Research) with primers for *YFR057W* and *ACT1* (Table S4).

Chromatin immunoprecipitation

Strains were grown as for mRNA quantification. Chromatin immunoprecipitation (ChIP) was performed as described (Darst *et al.* 2008). Briefly, sheared chromatin was incubated overnight at 4°C with anti-Sir2 (1:1000, Garcia *et al.* 2002), anti-Flag (1:1000, Sigma) or anti-H3-CT (1:500, Millipore). Input DNA and IP samples were diluted 10-fold and analyzed by real-time PCR (primers listed in Table S4). Anti-Flag specificity was verified with an untagged strain (not shown).

Preparation of yeast nuclei and whole cell extract

Strains were grown as for mRNA quantification. Nuclei were prepared as described (Kizer *et al.* 2006). Whole cell extract was prepared by resuspending each A_{600}= 1.0 of cells in 25µl phosphate buffered saline with protease inhibitors and vortexing with glass beads. Protein samples were denatured by boiling in sample loading buffer.

Protein immunoblotting

Proteins were separated on SDS-polyacrylamide gels (18% acrylamide for the separation of histones and 8% for the other proteins) and transferred to 0.2μm nitrocellulose. Primary antisera used were anti-H3-CT (1:10,000, Millipore) anti-Myc (1:10,000, Evan *et al.* 1985), anti-Sir2 (1:10,000, Garcia *et al.* 2002) and anti-β-tubulin (1:10,000, Bond *et al.* 1986). Secondary antisera used were goat anti-mouse for anti-Myc or goat anti-rabbit (conjugated to horseradish peroxidase, 1:10,000, Promega). Signals were detected with Pierce ECL substrate (Thermo Scientific) on Hyblot CL films (Denville Scientific). Quantification was done using ImageJ.

Supplementary Materials and Methods

Yeast strains

The chromosomal *GDH1* locus was tagged by amplifying the 13Myc-kanMX cassette from pLP1651 (Longtine *et al.* 1998) with oligonucleotides OLP1629 and OLP1630 and transforming into the WT W303 strain. The NES used was a variant of the strong NES from PKI with the sequence ELALKLAGLDINLI (Gadal *et al.* 2001). A 13Myc-Gly-Gly-NES-kanMX fragment was integrated to tag the C-terminus of Gdh1 by amplifying this cassette from pLP2829 with OLP1629 and OLP1630 and transforming into the WT W303 strain.

Silencing and rDNA recombination assays

For the rDNA*::mURA3* silencing assay, strains were plated on SC (growth control) and SC-Ura (silencing). For the canavanine sensitivity test, strains were plated on SC-Arg (growth control) and SC-Arg+0.75μg/mL L-canavanine (Sigma).

To measure the rDNA recombination rate, strains were grown in SC-Ade-Arg to an A_{600} of 0.8-1.0. 400-500 cells were plated on yeast peptone dextrose with adenine (YPAD), incubated at 30°C for 2 days, then moved to 4°C to promote color development. 1500-2500 colonies were assessed for each strain. Half-sectored colonies originated from cells that had lost the *ADE2* reporter at the first mitotic division. The recombination rate was calculated as the number of half-sectored colonies divided by the total number of colonies.

Quantitative mating assay

Query strains were grown in SC and mating testers were grown in YPAD. Approximately 500 log-phase cells were either plated in triplicate on YPAD or mixed with an equal number of mating tester cells (LPY78 or LPY142). After 3hrs of incubation at 30°C, the mating mixtures were plated on minimal medium in triplicate. Raw mating efficiency was calculated as the number of diploids (i.e. colonies growing on the minimal plate) divided by the number of haploids (i.e. colonies growing on the YPAD plate). Mating efficiency for the WT strain was set to 1.

Immunoblotting and chromatin IP

Experimental procedures were described in Materials. Anti-Sir3 (Palladino *et al.* 1993) was diluted 1:2000 for ChIP and 1:5000 for immunoblotting. Anti-Myc was diluted 1:250 for ChIP and precipitated with protein G sepharose beads (GE Healthcare).

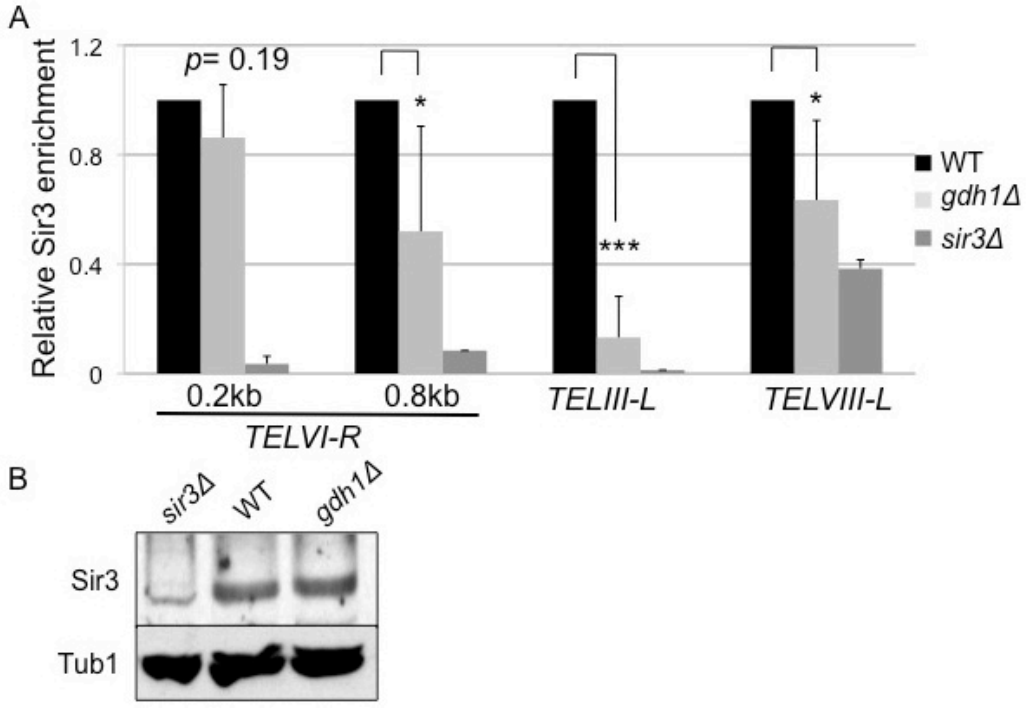

Figure 2-S1. Sir3 binding is reduced at three telomeric loci in the *gdh1Δ* mutant. (*A*) Telomeric Sir3 binding was significantly reduced in the *gdh1Δ* mutant. WT (LPY5), *gdh1Δ* (LPY16026) and *sir3Δ* (LPY10) strains were analyzed by ChIP for the indicated loci and the ChrV intergenic control locus. The WT values were set to 1. Data represent the averages from 3 independent experiments. (*B*) Sir3 protein levels were unchanged in the *gdh1Δ* mutant. Whole cell extracts from the strains used in (*A*) were immunoblotted for Sir3 or Tub1 (loading control).

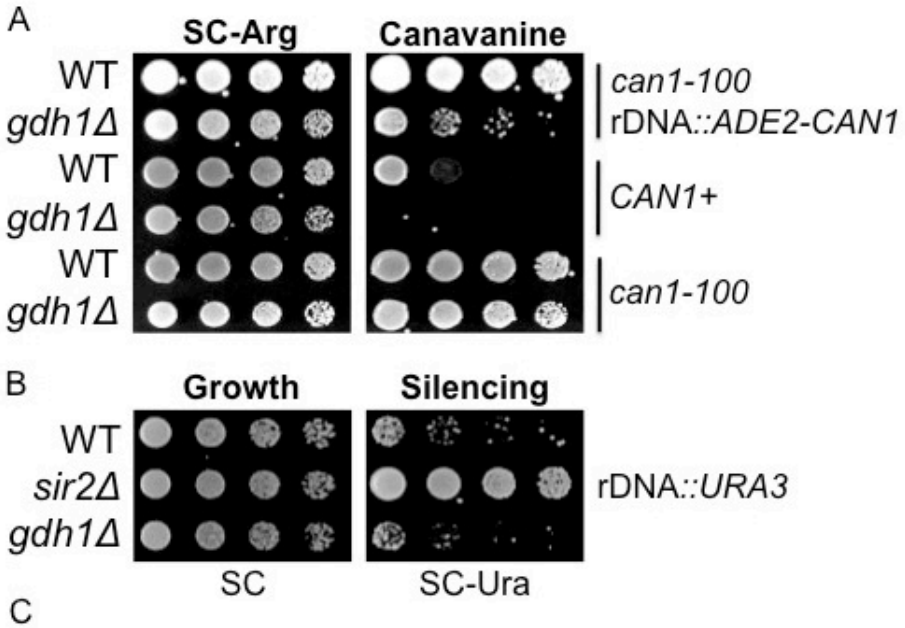

C

Strain	Recombination Rate	*p*-value
WT	0.002 ± 0.001	
gdh1Δ	0.004 ± 0.002	0.091
sir2Δ	0.018 ± 0.005	0.0009

Figure 2-S2. *GDH1* has a minimal role in rDNA silencing. (*A*) The *gdh1Δ* strain showed canavanine sensitivity in a silencing-independent manner. The following strains were plated on SC-Arg (control) and SC-Arg+canavanine (0.75 μg/mL): WT rDNA::*ADE2-CAN1* (LPY4909), *gdh1Δ* rDNA::*ADE2-CAN1* (LPY16019), WT *CAN1* (LPY17954), *gdh1Δ CAN1* (LPY17951), WT *can1-100* (LPY5) and *gdh1Δ can1-100* (LPY16026). Note that this was a lower concentration of canavanine than used in the silencing assay. Decreased growth indicates increased sensitivity to canavanine. (*B*) rDNA silencing at *NTS1* was unaffected in the *gdh1Δ* mutant. WT (LPY2446), *sir2Δ* (LPY2445) and *gdh1Δ* (LPY16009) strains carried the rDNA Ty *mURA3* insertion and silencing was assessed on SC-Ura. Increased growth indicates defective silencing. (*C*) Mitotic recombination within the rDNA array was mildly elevated in the *gdh1Δ* mutant. WT (LPY4909), *gdh1Δ* (LPY16019) and *sir2Δ* (LPY5013) strains were assessed as described in Supplementary Materials and Methods. Data represent the averages from 3-4 independent experiments.

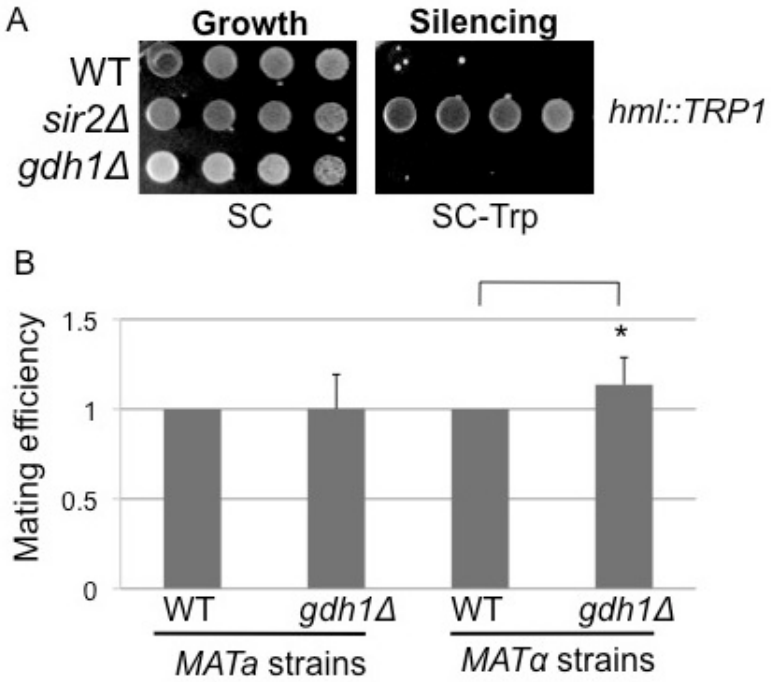

Figure 2-S3. Gdh1 has a modest role in *HM* silencing. (*A*) Silencing at the *HML* locus was unaffected in the *gdh1Δ* mutant. WT (LPY309), *sir2Δ* (LPY1401) and *gdh1Δ* (LPY18979) strains were plated on SC-Trp, where increased growth indicates defective silencing. (*B*) *MAT*α mating efficiency was moderately increased in the *gdh1Δ* mutant. *MAT*a WT (LPY5), *MAT*α WT (LPY79), *MAT*a *gdh1Δ* (LPY16026) and *MAT*α *gdh1Δ* (LPY16560) strains were assessed as described in Supplementary Materials and Methods. Data represent the averages from 5 independent experiments.

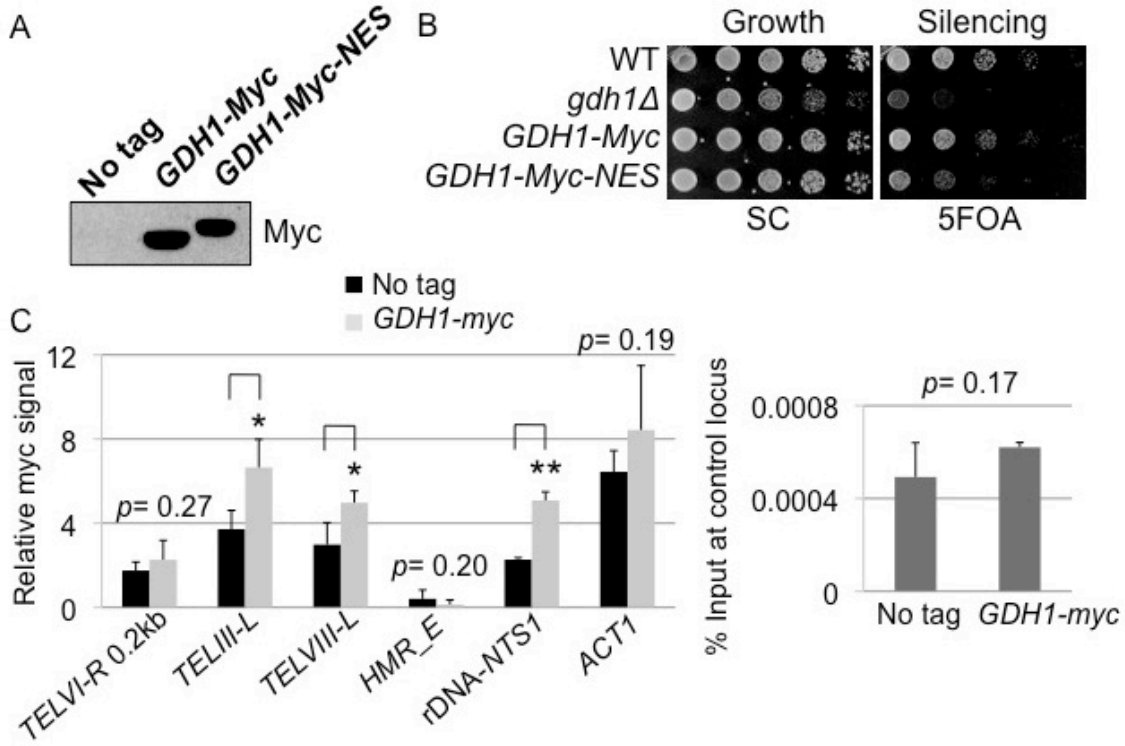

Figure 2-S4. Reducing the nuclear pool of Gdh1 results in a moderate telomeric silencing defect. (*A*) Gdh1-13Myc and Gdh1-13Myc-NES were stably expressed. Whole cell extracts from non-tagged WT (LPY5), *GDH1-13Myc* (LPY16784) and *GDH1-13Myc-NES* (LPY17738) strains were immunoblotted for Myc. (*B*) Ectopic integration of a NES at the C terminus of Gdh1 caused a moderate telomeric silencing defect. WT, *gdh1Δ, GDH1-13Myc* (LPY16782)*, GDH1-13Myc-NES* (LPY17736) strains were assayed on 5-FOA for telomeric silencing. (*C*) Gdh1 was moderately recruited to some telomeres and the rDNA-NTS1 locus. No tag (LPY5) and *GDH1-myc* (LPY16784) strains were analyzed by ChIP. Signal at each locus was normalized to that at the ChrV control locus, in which no myc enrichment was found.

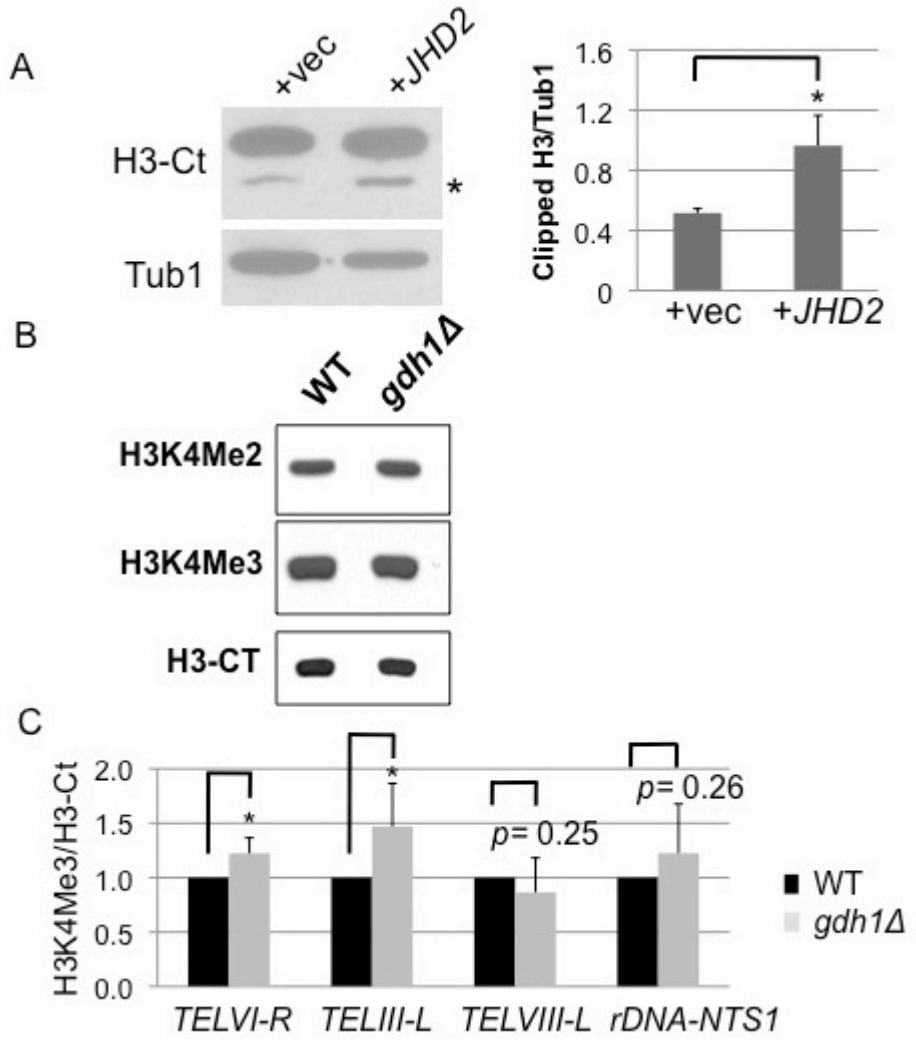

Figure 2-S5. Gdh1 does not regulate H3 clipping through a Jhd2-dependent pathway. (*A*) Increased dosage of *JHD2* elevated H3 clipping. Nuclear extracts were prepared from WT cells transformed with vector (pRS315) or *JHD2* (pLP3181) and immunoblotted for H3-CT or Tub1 (loading control). Quantification represent the averages from two independent transformants. (*B*) H3K4 di- and tri-methylation levels remained unchanged in the *gdh1Δ* mutant. Whole cell extract of WT (LPY5) and *gdh1Δ* (LPY16026) were blotted with the indicated antibody. (*C*) H3K4 trimethylation mark was increased rather than decreased at some telomeres in the *gdh1Δ* mutant. ChIP experiments were done with non-histone shuffle WT (LPY5) and *gdh1Δ* (LPY16026) strains. H3K4Me3 and H3-Ct signals at each locus were normalized to those at the control *ACT1* locus. The WT ratio of H3K4Me3 to H3-CT was set to 1 for each experiment. Data represent the averages from 2-3 experiments.

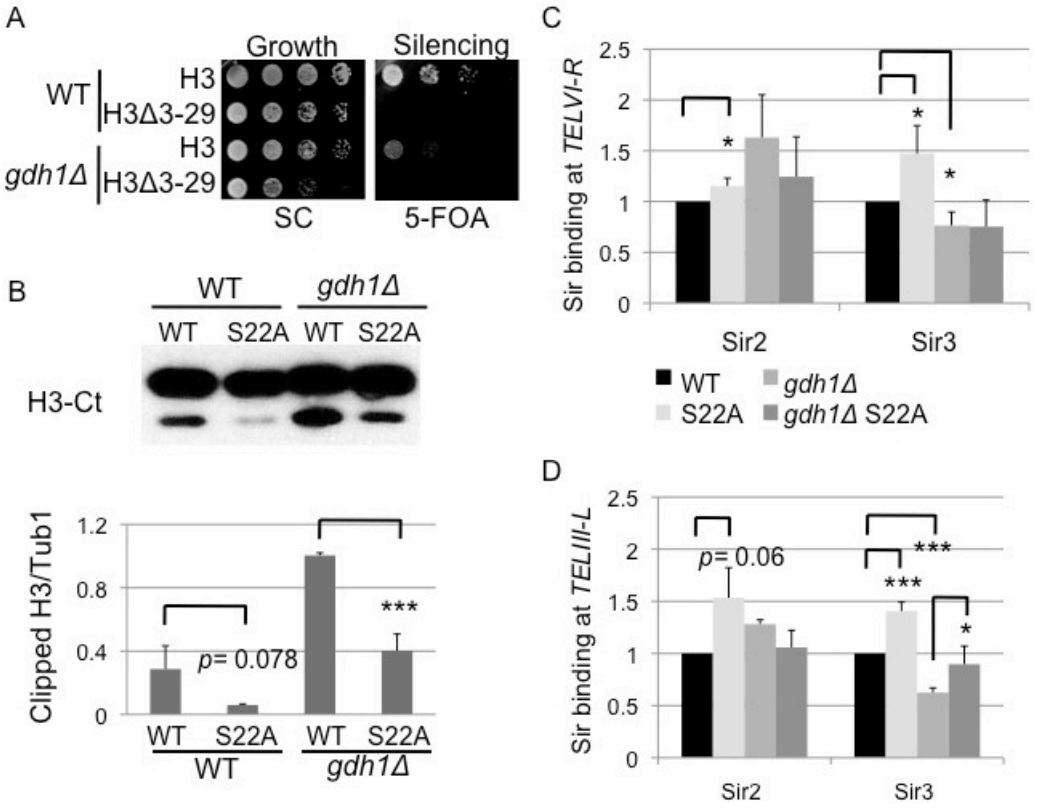

Figure 2-S6. The S22A mutation reduces H3 clipping *in vivo.* (*A*) The H3Δ3-29 mutation was epistatic to the *gdh1Δ* mutant with respect to telomeric silencing. WT and *gdh1Δ* strains with H3-H4 (pLP1490) or H3Δ3-29-H4 (pLP1491) were assayed on 5-FOA. (*B*) Longer exposure of the immunoblot in Figure 7C shows that H3 clipping is not completely abolished by the S22A mutation *in vivo.* Quantification of the immunoblot was based on results from two independent sets of nuclear extracts. (*C*)-(*D*) The H3S22A mutation had different effects on Sir2 and Sir3 binding in the histone shuffle strains than the non-shuffle strains. Strains from Figure S5B were analyzed by ChIP for the indicated loci and the ChrV intergenic control locus. WT value is set to 1 for each experiment.

Table 2-S1. Information on amino acid metabolic proteins with reported nuclear pools. (*A*) Summary of metabolic function, co-factor binding and nuclear interactors of candidate proteins (http:://www. yeastgenome.org, Cherry *et al.* 2012).

Candidate	Metabolic Function	Co-factor	Examples of Nuclear Interactors
Arg82	Regulates arginine-, phosphate-, and nitrogen-responsive genes	ATP	Transcription factors Nuclear kinases
Gdh1	Glutamate dehydrogenase	NADP+	Gdh3
Gdh3	Glutamate dehydrogenase	NADP+	Gdh1 Component of the RSC complex (Htl1) HAT (Hpa2) *YEL057C,* encodes an unknown protein in telomere maintenance
Hom2	Aspartic beta semi-aldehyde dehydrogenase (Methionine-Threonine synthesis)	NADP+	Nup84 nuclear pore complex Cell cycle control proteins
Hom6	Homoserine dehydrogenase (Methionine-Threonine synthesis)	NADP+	HAT and HDAC complexes dsDNA break repair machinery INO80 chromatin remodeling complex Nup84 nuclear pore complex
Hpa3	D-amino acid N-acetyltransferase	Acetyl-CoA	RNA binding proteins
Utr4	Enolase phosphatase	-	RNA binding proteins SWR1 chromatin remodeling complex

Table 2-S1. Information on amino acid metabolic proteins with reported nuclear pools, continued. (*B*) Brief information of non-candidate amino acid metabolic proteins with reported nuclear pools.

ORF	Gene	Enzymatic activity of the encoding protein
YBR145W	*ADH5*	Alcohol dehydrogenase isoenzyme V
YMR009W	*ADI1*	Acireductone dioxygenease involved in the methionine salvage pathway
YDR035W	*ARO3*	3-deoxy-D-arabino-heptulosonate-7-phosphate (DAHP) synthase
YBR249C	*ARO4*	3-deoxy-D-arabino-heptulosonate-7-phosphate (DAHP) synthase
YPR060C	*ARO7*	Chorismate mutase
YHR137W	*ARO9*	Aromatic aminotransferase II
YLR155C	*ASP3-1*	Cell-wall L-asparaginase II involved in asparagine catabolism
YJR148W	*BAT2*	Cytosolic branched-chain amino acid aminotransferase
YPL111W	*CAR1*	Arginase
YLR438W	*CAR2*	L-ornithine transaminase (OTAse)
YLL018C	*DPS1*	Aspartyl-tRNA synthetase
YBR281C	*DUG2*	Probable di- and tri-peptidase
YNL135C	*FPR1*	Peptidyl-prolyl cis-trans isomerase (PPIase)
YML004C	*GLO1*	Monomeric glyoxalase I
YJR070C	*LIA1*	Deoxyhypusine hydroxylase
YPR118W	*MRI1*	5'-methylthioribose-1-phosphate isomerase
YIL145C	*PAN6*	Pantothenate synthase
YLR044C	*PDC1*	Major of three pyruvate decarboxylase isozymes
YLR134W	*PDC5*	Minor isoform of pyruvate decarboxylase
YOR323C	*PRO2*	Gamma-glutamyl phosphate reductase
YPL273W	*SAM4*	S-adenosylmethionine-homocysteine methyltransferase
YGR208W	*SER2*	Phosphoserine phosphatase of the phosphoglycerate pathway
YOL052C	*SPE2*	S-adenosylmethionine decarboxylase
YPR069C	*SPE3*	Spermidine synthase
YJR130C	*STR2*	Cystathionine gamma-synthase
YDL080C	*THI3*	Probable alpha-ketoisocaproate decarboxylase
YCR053W	*THR4*	Threonine synthase
YDR354W	*TRP4*	Anthranilate phosphoribosyl transferase of the tryptophan biosynthetic pathway
YGL026C	*TRP5*	Tryptophan synthase
YGR185C	*TYS1*	Cytoplasmic tyrosyl-tRNA synthetase

Table 2-S2. Strains used in this study

Strain (alias)	Genotype	References /Sources
LPY5	*MATa ade2-1 can1-100 his3-11 leu2-3,112 trp1-1 ura3-1* (W303-1a)	R. Rothstein
LPY10	*MATa sir3Δ::TRP1*	
LPY11	*MATa sir2Δ::HIS3*	
LPY78*	*MATα his4*	P. Schatz
LPY79	*MATα* W303	
LPY142*	*MATa his4*	P. Schatz
LPY309	*MATa hml::TRP1*	
LPY1401	*MATa sir2Δ::HIS3 hml::TRP1*	
LPY2445*	*MATα his3Δ200 leu2Δ1 ura3-52 sir2Δ::HIS3 with* rDNA *Ty mURA3 insertion*	Smith and Boeke. 1997
LPY2446*	*MATα his3Δ200 leu2Δ1 ura3-52 with* rDNA *Ty mURA3 insertion*	Smith and Boeke. 1997
LPY4654	*MATα hmrΔE::TRP1 rDNA::ADE2-CAN1 TELV-R::URA3*	Roy and Runge. 2000
LPY4909	*MATα* rDNA*::ADE2-CAN1*	Clarke *et al.* 2006
LPY4916	*MATa TELV-R::URA3*	Clarke *et al*. 2006
LPY4977	*MATα sir2Δ::HIS3 hmrΔE::TRP1* rDNA*::ADE2-CAN1 TELV-R::URA3*	Clarke *et al*. 2006
LPY4979	*MATα sir2Δ::HIS3 TELV-R::URA3*	Clarke *et al.* 2006
LPY5013	*MATα sir2Δ::TRP1* rDNA*::ADE2-CAN1*	
LPY11113	*MATa esa1-414 hmrΔE::TRP1* rDNA*::ADE2-CAN1 TELV-R::URA3*	
LPY15962	*MATα hom2Δ::kanMX hmrΔE::TRP1* rDNA*::ADE2-CAN1 TELV-R::URA3*	
LPY15964	*MATα utr4Δ::kanMX hmrΔE::TRP1* rDNA*::ADE2-CAN1 TELV-R::URA3*	
LPY15966	*MATα hpa3Δ::kanMX hmrΔE::TRP1* rDNA*::ADE2-CAN1 TELV-R::URA3*	
LPY15968	*MATα arg82Δ::kanMX hmrΔE::TRP1* rDNA*::ADE2-CAN1 TELV-R::URA3*	
LPY15970	*MATα gdh1Δ::kanMX hmrΔE::TRP1* rDNA*::ADE2-CAN1 TELV-R::URA3*	
LPY15972	*MATα gdh3Δ::kanMX hmrΔE::TRP1* rDNA*::ADE2-CAN1 TELV-R::URA3*	
LPY16009*	*MATα his3Δ200 leu2Δ1 ura3-52 gdh1Δ::kanMX with* rDNA *Ty mURA3 insertion*	

Table 2-S2. Strains used in this study, continued

Strain (alias)	Genotype	Reference /Source
LPY16019	*MATα gdh1Δ::kanMX* rDNA*::ADE2-CAN1*	
LPY16026	*MATa gdh1Δ::kanMX*	
LPY16033	*MATα gdh1Δ::kanMX TELV-R::URA3*	
LPY16155	*MATα hht1-hhf1Δ::kanMX hht2-hhf2Δ::kanMX hta2-htb2Δ::HPH TELV-R::URA3*+pLP2438	
LPY16161	*MATα hht1-hhf1Δ::kanMX hht2-hhf2Δ::kanMX hta2-htb2Δ::HPH TELV-R::URA3*+pLP2438	
LPY16162	*MATα gdh1Δ::kanMX hht1-hhf1Δ::kanMX hht2-hhf2Δ::kanMX hta2-htb2Δ::HPH TELV-R::URA3*+pLP2438	
LPY16560	*MATα gdh1Δ::kanMX*	
LPY16782	*MATa GDH1-13Myc::kanMX TELV-R::URA3*	
LPY16784	*MATa GDH1-13Myc::kanMX*	
LPY16785	*MATa gdh3Δ::kanMX TELV-R::URA3*	
LPY16796	*MATα mks1Δ::kanMX TELV-R::URA3*	
LPY17131*	*MATα his3Δ1 leu2Δ0 met15Δ0 ura3Δ0 gdh1Δ::kanMX gdh3Δ::kanMX glt1Δ::kanMX*	
LPY17406	*MATα hom6Δ::kanMX hmrΔE::TRP1* rDNA*::ADE2-CAN1 TELV-R::URA3*	
LPY17736	*MATa GDH1-13Myc-NES::kanMX TELV-R::URA3*	
LPY17738	*MATα GDH1-13Myc-NES::kanMX*	
LPY17916	*MATα gdh1Δ::kanMX gdh3Δ::kanMX TELV-R::URA3*	
LPY17951	*MATa ade2-1 CAN1 his3-11,15 leu2-3,112 trp1-1 ura3-1 gdh1Δ::kanMX*	
LPY17954	*MATa ade2-1 CAN1 his3-11,15 leu2-3,112 trp1-1 ura3-1*	
LPY18415	*MATα jhd2Δ::kanMX gdh1Δ::kanMX TELV-R::URA3*	
LPY18669	*MATα jhd2Δ::kanMX TELV-R::URA3*	
LPY18979	*MATa gdh1Δ::kanMX hml::TRP1*	
LPY19789	*MATα hht1-hhf1Δ::kanMX hht2-hhf2Δ::kanMX hta2-htb2Δ::HPH* +pLP2129	
LPY19794	*MATα gdh1Δ::kanMX hht1-hhf1Δ::kanMX hht2-hhf2Δ::kanMX hta2-htb2Δ::HPH* +pLP2129	
LPY20021	*MATa gdh1Δ::kanMX hht1-hhf1Δ::kanMX hht2-hhf2Δ::kanMX hta2-htb2Δ::HPH TELV-R::URA3* +pLP1490	

Table 2-S2. Strains used in this study, continued

Strain (alias)	Genotype	References /Sources
LPY20023	*MATa gdh1Δ::kanMX hht1-hhf1Δ::kanMX hht2-hhf2Δ::kanMX hta2-htb2Δ::HPH TELV-R::URA3*+pLP1491	
LPY20665	*MATα hht1-hhf1Δ::kanMX hht2-hhf2Δ::kanMX hta2-htb2Δ::HPH TELV-R::URA3* +pLP1490	
LPY20695	*MATα hht1-hhf1Δ::kanMX hht2-hhf2Δ::kanMX hta2-htb2Δ::HPH TELV-R::URA3* +pLP1491	
LPY20466*	*leu2 his3* (4×NAD boxes)-*HIS3* (YSH896)	Ringel *et al.* 2013/ S. Holmes
LPY20468*	*bna1Δ leu2 his3* (4×NAD boxes)-*HIS3*+ BSH484 (YSH898)	Ringel *et al.* 2013/ S. Holmes
LPY20470	*MATα hht1-hhf1Δ::kanMX hht2-hhf2Δ::kanMX hta2-htb2Δ::HPH TELV-R::URA3*+pLP1775	
LPY20623	*MATα gdh1Δ::kanMX hht1-hhf1Δ::kanMX hht2-hhf2Δ::kanMX hta2-htb2Δ::HPH TELV-R::URA3*+pLP1775	
LPY20477*	*gdh1Δ::kanMX leu2 his3* (4×NAD boxes)-*HIS3*	
LPY20480*	*gdh1Δ::kanMX leu2 his3* (4×mutated NAD boxes)-*HIS3*	

Note: Unless otherwise noted, strains were constructed during this study or are part of the standard lab collection. All strains are in the W303 background, except where indicated (*).

Table 2-S3. Plasmids used in this study

Plasmid (alias)	Description	Reference/Source
pRS314	vector *TRP1* CEN	Sikorski and Hieter 1989
pRS315	vector *LEU2* CEN	Sikorski and Hieter 1989
pRS316	vector *URA3* CEN	Sikorski and Hieter 1989
pRS424	vector *TRP1* 2μ	Christianson *et al.* 1992
pRS425	vector *LEU2* 2μ	Christianson *et al.* 1992
pLP1490	pRS414-*HHT2 HHF2*	Zhang *et al.* 1998
pLP1491	pRS414-*hht2Δ3-29 HHF2*	Zhang *et al.* 1998
pLP1651	pFA6a-13Myc-kanMX	Longtine *et al.* 1998
pLP1775	pRS314-*HHT2 HHF2*	
pLP2129	pRS314-*FLAG-HHT2 HHF2*	Nathan and Ingvarsdottir *et al.* 2006
pLP2438	pRS314-*hht2S22A HHF2*	Nakanishi *et al.* 2008
pLP2637	pRS315-*GDH1*	
pLP2638	pRS315-*gdh1-D150S*	
pLP2662	pRS425-*GDH3*	
pLP2698	pRS425-*gdh1-D150S*	
pLP2764	pRS425-*GDH1*	
pLP2829	pFA6a-13Myc-Gly-Gly-NES-kanMX	
pLP2833	pRS316-*GDH1-13Myc*	
pLP2834	pRS316-*gdh1-D150S-13Myc*	
pLP3082	pRS314-*GDH1*	
pLP3083	pRS314-*gdh1-D150S*	
pLP3181	pRS315-*JHD2*	
pLP3227	pACT2 (V172)	Ringel *et al.* 2013/S. Holmes
pLP3228	pACT2-NadR-AD (BSH 484)	Ringel *et al.* 2013/S. Holmes
pLP3238	pRS314-*IDP1*	

Note: Unless otherwise noted, plasmids were constructed during this study or are part of the standard lab collection.

Table 2-S4. Oligos used in this study

Oligo #	Oligo Name	Sequence(5'-3')	Source/Reference
764	*TELVI-R* 0.75KB F	ATATATGCACTAGTTGCACTAGGCG	Jacobson S
765	*TELVI-R* 0.75KB R	CTTCCAGTAAATTTCTCTTTGAGTGG	Jacobson S
776	rDNA.5S.f	CATGGAGCAGTTTTTTCCGC	Emre *et al.* 2005
777	rDNA.5S.r	TACAAGCACTCATGTTTGCCG	Emre *et al.* 2005
778	*TELVI-R*.200.f	AAATGGCAAGGGTAAAAACCAG	Emre *et al.* 2005
779	*TELVI-R*.200.r	TCGGATCACTACACACGGAAAT	Emre *et al.* 2005
798	*ACT1*_F1	GGTGGTTCTATCTTGGCTTC	Darst *et al.* 2008
799	*ACT1*_R1	ATGGACCACTTTCGTCGTAT	Darst *et al.* 2008
852	rDNA NTS1-1f	AGGGCTTTCACAAAGCTTCC	Huang and Moazed 2003
853	rDNA NTS1-1r	TCCCCACTGTTCACTGTTCA	Huang and Moazed 2003
871	ChrV_sense	GTGTTTGACCCGAGGGTATG	Hess *et al.* 2004
872	ChrV_antisense	TAAGGTCCACACCGTCATCA	Hess *et al.* 2004
1516	*HOM2*_5_KO	CGACGGAGAAGAAGGAGAC	
1517	*HOM2*_3_KO	CTTGGGTCAGCGAGAGAATTAC	
1520	*GDH1*_5_KO	CACGTCCAATCAGCAGAGAG	
1521	*GDH1*_3_KO	CAATAAGCCTGGTGTCCAATC	
1522	*GDH3*_5_KO	CCGTTCAGTTTGCTTGATTG	
1523	*GDH3*_3_KO	CACTATCCCCCTTCAAATTG	
1524	*UTR4*_5_KO	CCTTGCGGCCACTTATAG	
1525	*UTR4*_3_KO	CTATTTCGCGCCTCTGTG	
1528	*ARG82*_5_KO	GACAGGCTTGTTGTGTGTG	
1529	*ARG82*_3_KO	CATAGCAGCCGGTTTTTC	
1530	*HPA3*_5_KO	CCCGACATTCAGACGTACAC	
1531	*HPA3*_3_KO	GACGGTGTCCATTGCTTATATAG	
1556	*gdh1-D150S* F	GACGTGCCAGCTGGTTCTATCGGTGTTGGTGGTC	
1557	*gdh1-D150S* R	GACCACCAACACCGATAGAACCAGCTGGCACGTC	

Table 2-S4. Oligos used in this study, continued

Oligo #	Oligo Name	Sequence(5'-3')	Source /Reference
1598	*GDH1* XmaI F	CCAAGGTGATGTATTTCCCGGGGTCT AAAAGAAAGAAAAGAGG	
1599	*GDH1* XmaI R	CCTCTTTTCTTTCTTTTAGACCCCGGG AAATACATCACCTTGG	
1629	*GDH1*_CMyc F	CAAGTTTCATCAAGGTCTCTGATGCT ATGTTTGACCAAGGTGATGTATTTCG GATCCCCGGGTTAATTAA	
1630	*GDH1*_CMyc R	AAAAGAAAGAACTTTTTATGAACTTT CCTCTTTTCTTTCTTTTAGACTATGAA TTCGAGCTCGTTTAAAC	
1753	XmaI_pFA6a_R	TCCCCCCGGGGGACGAGGCAAGCTA AACAG	
1769	*HOM6*_new5KO	CAATAACGCACATGGTGG	
1770	*HOM6*_new3KO	GCCCCATGACATGGATGAG	

Note: Unless otherwise noted, oligos were designed during this study.

Acknowledgements

We thank A.L. Torres-Machorro for critical discussion throughout the course of the work. We also thank M. Oki, S. Holmes, K. Runge and D. Notani for oligo sequences and reagents, and lab members for comments on the manuscript. This work was initiated with funding from the NIH and continued with support from the UC Cancer Research Coordinating Committee and the UCSD Academic Senate Committee on Research.

Chapter 2, in full, is currently under review for publication in *Genes and Development*, and may appear as Su XB and Pillus L 2014. The Gdh1 Glutamate Dehydrogenase Regulates Telomeric Silencing Through Modulating α-ketoglutarate, Recruitment of the SIR Complex and Histone H3 clipping. The dissertation author was the primary investigator and author of this paper.

References

Ahn SH, Cheung WL, Hsu JY, Diaz RL, Smith MM, Allis CD. 2005. Sterile 20 kinase phosphorylates histone H2B at serine 10 during hydrogen peroxide-induced apoptosis in *S. cerevisiae. Cell* **120**: 25-36.

Anderson RM, Latorre-Esteves M, Neves AR, Lavu S, Medvedik O, Taylor C, Howitz KT, Santos H, Sinclair DA. 2003. Yeast life-span extension by calorie restriction is independent of NAD fluctuation. *Science* **302**: 2124-2126.

Aparicio OM, Billington BL, Gottschling DE. 1991. Modifiers of position effect are shared between telomeric and silent mating-type loci in *S. cerevisiae. Cell* **66**: 1279-1287.

Avendano A, Deluna A, Olivera H, Valenzuela L, Gonzalez A. 1997. *GDH3* encodes a glutamate dehydrogenase isozyme, a previously unrecognized route for glutamate biosynthesis in *Saccharomyces cerevisiae. J Bacteriol* **179**: 5594-5597.

Bond JF, Fridovich-Keil JL, Pillus L, Mulligan RC, Solomon F. 1986. A chicken-yeast chimeric beta-tubulin protein is incorporated into mouse microtubules *in vivo. Cell* **44**: 461-468.

Burgess DJ. 2013. Metabolism: Glutamine connections. *Nat Rev Cancer* **13**: 293.

Chen S, Brockenbrough JS, Dove JE, Aris JP. 1997. Homocitrate synthase is located in the nucleus in the yeast *Saccharomyces cerevisiae. J Biol Chem* **272**: 10839-10846.

Cherry JM, Hong EL, Amundsen C, Balakrishnan R, Binkley G, Chan ET, Christie KR, Costanzo MC, Dwight SS, Engel SR *et al.* 2012. *Saccharomyces* Genome Database: the genomics resource of budding yeast. *Nucleic Acids Res* **40**: D700-705.

Christianson TW, Sikorski RS, Dante M, Shero JH, Hieter P. 1992. Multifunctional yeast high-copy-number shuttle vectors. *Gene* **110**: 119-122.

Clarke AS, Samal E, Pillus L. 2006. Distinct roles for the essential MYST family HAT Esa1p in transcriptional silencing. *Mol Biol Cell* **17**: 1744-1757.

Collart MA, Oliviero S. 2001. Preparation of yeast RNA. *Curr Protoc Mol Biol* Chapter **13**: Unit13.12.

Copley SD. 2012. Moonlighting is mainstream: paradigm adjustment required. *Bioessays* **34**: 578-588.

Darst RP, Garcia SN, Koch MR, Pillus L. 2008. Slx5 promotes transcriptional silencing and is required for robust growth in the absence of Sir2. *Mol Cell Biol* **28**: 1361-1372.

Dean JL, Wang XG, Teller JK, Waugh ML, Britton KL, Baker PJ, Stillman TJ, Martin SR, Rice DW, Engel PC. 1994. The catalytic role of aspartate in the active site of glutamate dehydrogenase. *Biochem J* **301**: 13-16.

DeLuna A, Avendano A, Riego L, Gonzalez A. 2001. NADP-glutamate dehydrogenase isoenzymes of *Saccharomyces cerevisiae*. Purification, kinetic properties, and physiological roles. *J Biol Chem* **276**: 43775-43783.

Dubois E, Messenguy F. 1994. Pleiotropic function of ArgRIIIp (Arg82p), one of the regulators of arginine metabolism in *Saccharomyces cerevisiae*. Role in expression of cell-type-specific genes. *Mol Gen Genet* **243**: 315-324.

Dubois E, Dewaste V, Erneux C, Messenguy F. 2000. Inositol polyphosphate kinase activity of Arg82/ArgRIII is not required for the regulation of the arginine metabolism in yeast. *FEBS Lett* **486**: 300-304.

Ehrentraut S, Weber JM, Dybowski JN, Hoffmann D, Ehrenhofer-Murray AE. 2010. Rpd3-dependent boundary formation at telomeres by removal of Sir2 substrate. *Proc Natl Acad Sci U S A* **107**: 5522-5527.

Emre NC, Ingvarsdottir K, Wyce A, Wood A, Krogan NJ, Henry KW, Li K, Marmorstein R, Greenblatt JF, Shilatifard A et al. 2005. Maintenance of low histone ubiquitylation by Ubp10 correlates with telomere-proximal Sir2 association and gene silencing. *Mol Cell* **17**: 585-594.

Enomoto S, McCune-Zierath PD, Gerami-Nejad M, Sanders MA, Berman J. 1997. RLF2, a subunit of yeast chromatin assembly factor-I, is required for telomeric chromatin function in vivo. *Genes Dev* **11**: 358-370.

Evan GI, Lewis GK, Ramsay G, Bishop JM. 1985. Isolation of monoclonal antibodies specific for human c-myc proto-oncogene product. *Mol Cell Biol* **5**: 3610-3616.

Feller A, Ramos F, Pierard A, Dubois E. 1997. Lys80p of *Saccharomyces cerevisiae*, previously proposed as a specific repressor of *LYS* genes, is a pleiotropic regulatory factor identical to Mks1p. *Yeast* **13**: 1337-1346.

Gadal O, Strauss D, Kessl J, Trumpower B, Tollervey D, Hurt E. 2001. Nuclear export of 60s ribosomal subunits depends on Xpo1p and requires a nuclear export sequence-containing factor, Nmd3p, that associates with the large subunit protein Rpl10p. *Mol Cell Biol* **21**: 3405-3415.

Galdieri L, Chang J, Mehrotra S, Vancura A. 2013. Yeast phospholipase C is required for normal acetyl-CoA homeostasis and global histone acetylation. *J Biol Chem* **288**: 27986-27998.

Garcia SN, Pillus L. 2002. A unique class of conditional sir2 mutants displays distinct silencing defects in *Saccharomyces cerevisiae. Genetics* **162**: 721-736.

Gottlieb S, Esposito RE. 1989. A new role for a yeast transcriptional silencer gene, *SIR2*, in regulation of recombination in ribosomal DNA. *Cell* **56**: 771-776.

Gut P, Verdin E. 2013. The nexus of chromatin regulation and intermediary metabolism. *Nature* **502**: 489-498.

Hess D, Liu B, Roan NR, Sternglanz R, Winston F. 2004. Spt10-dependent transcriptional activation in *Saccharomyces cerevisiae* requires both the Spt10 acetyltransferase domain and Spt21. *Mol Cell Biol* **24**: 135-143.

Huang J, Moazed D. 2003. Association of the RENT complex with nontranscribed and coding regions of rDNA and a regional requirement for the replication fork block protein Fob1 in rDNA silencing. *Genes Dev* **17**: 2162-2176.

James C, Kapoor RR, Ismail D, Hussain K. 2009. The genetic basis of congenital hyperinsulinism. *J Med Genet* **46**: 289-299.

Jeffery CJ. 2009. Moonlighting proteins--an update. *Mol Biosyst* **5**: 345-350.

Jones GM, Stalker J, Humphray S, West A, Cox T, Rogers J, Dunham I, Prelich G. 2008. A systematic library for comprehensive overexpression screens in *Saccharomyces cerevisiae*. *Nat Methods* **5**: 239-241.

Kaelin WG,Jr, McKnight SL. 2013. Influence of metabolism on epigenetics and disease. *Cell* **153**: 56-69.

Kaufman PD, Kobayashi R, Stillman B. 1997. Ultraviolet radiation sensitivity and reduction of telomeric silencing in *Saccharomyces cerevisiae* cells lacking chromatin assembly factor-I. *Genes Dev* **11**: 345-357.

Khersonsky O, Tawfik DS. 2010. Enzyme promiscuity: a mechanistic and evolutionary perspective. *Annu Rev Biochem* **79**: 471-505.

Kizer KO, Xiao T, Strahl BD. 2006. Accelerated nuclei preparation and methods for analysis of histone modifications in yeast. *Methods* **40**: 296-302.

Kornberg RD, Lorch Y. 1999. Twenty-five years of the nucleosome, fundamental particle of the eukaryote chromosome. *Cell* **98**: 285-294.

Kouzarides T. 2007. Chromatin modifications and their function. *Cell* **128**: 693-705.

Kueng S, Oppikofer M, Gasser SM. 2013. SIR Proteins and the Assembly of Silent Chromatin in Budding Yeast. *Annu Rev Genet*. **47**:275-306.

Liang D, Burkhart SL, Singh RK, Kabbaj MH, Gunjan A. 2012. Histone dosage regulates DNA damage sensitivity in a checkpoint-independent manner by the homologous recombination pathway. *Nucleic Acids Res* **40**: 9604-9620.

Liang G, Klose RJ, Gardner KE, Zhang Y. 2007. Yeast Jhd2p is a histone H3 Lys4 trimethyl demethylase. *Nat Struct Mol Biol* **14**: 243-245.

Longtine MS, McKenzie A, 3rd, Demarini DJ, Shah NG, Wach A, Brachat A, Philippsen P, Pringle JR. 1998. Additional modules for versatile and economical PCR-based gene deletion and modification in *Saccharomyces cerevisiae. Yeast* **14**: 953-961.

Lu C, Ward PS, Kapoor GS, Rohle D, Turcan S, Abdel-Wahab O, Edwards CR, Khanin R, Figueroa ME, Melnick A *et al.* 2012. IDH mutation impairs histone demethylation and results in a block to cell differentiation. *Nature* **483**: 474-478.

Imai S, Armstrong CM, Kaeberlein M, Guarente L. 2000. Transcriptional silencing and longevity protein Sir2 is an NAD-dependent histone deacetylase. *Nature* **403**: 795-800.

Mandal P, Verma N, Chauhan S, Tomar RS. 2013. Unexpected Histone H3 Tail-clipping Activity of Glutamate Dehydrogenase. *J Biol Chem* **288**: 18743-18757.

Martin AM, Pouchnik DJ, Walker JL, Wyrick JJ. 2004. Redundant roles for histone H3 N-terminal lysine residues in subtelomeric gene repression in *Saccharomyces cerevisiae. Genetics* **167**: 1123-1132.

Monson EK, de Bruin D, Zakian VA. 1997. The yeast Cac1 protein is required for the stable inheritance of transcriptionally repressed chromatin at telomeres. *Proc Natl Acad Sci U S A* **94**: 13081-13086.

Nakanishi S, Sanderson BW, Delventhal KM, Bradford WD, Staehling-Hampton K, Shilatifard A. 2008. A comprehensive library of histone mutants identifies nucleosomal residues required for H3K4 methylation. *Nat Struct Mol Biol* **15**: 881-888.

Nathan D, Ingvarsdottir K, Sterner DE, Bylebyl GR, Dokmanovic M, Dorsey JA, Whelan KA, Krsmanovic M, Lane WS, Meluh PB *et al.* 2006. Histone sumoylation is a negative regulator in *Saccharomyces cerevisiae* and shows dynamic interplay with positive-acting histone modifications. *Genes Dev* **20**: 966-976.

Odom AR, Stahlberg A, Wente SR, York JD. 2000. A role for nuclear inositol 1,4,5-trisphosphate kinase in transcriptional control. *Science* **287**: 2026-2029.

Palladino F, Laroche T, Gilson E, Axelrod A, Pillus L, Gasser SM. 1993. SIR3 and SIR4 proteins are required for the positioning and integrity of yeast telomeres. *Cell* **75**: 543-555.

Rossmann MP, Luo W, Tsaponina O, Chabes A, Stillman B. 2011. A common telomeric gene silencing assay is affected by nucleotide metabolism. *Mol Cell* **42**: 127-136.

Rando OJ, Winston F. 2012. Chromatin and transcription in yeast. *Genetics* **190**: 351-387.

Ringel AE, Ryznar R, Picariello H, Huang KL, Lazarus AG, Holmes SG. 2013. Yeast Tdh3 (glyceraldehyde 3-phosphate dehydrogenase) is a Sir2-interacting factor that regulates transcriptional silencing and rDNA recombination. *PLoS Genet* **9**: e1003871.

Roy N, Runge KW. 2000. Two paralogs involved in transcriptional silencing that antagonistically control yeast life span. *Curr Biol* **10**: 111-114.

Rusche LN, Kirchmaier AL, Rine J. 2002. Ordered nucleation and spreading of silenced chromatin in *Saccharomyces cerevisiae*. *Mol Biol Cell* **13**: 2207-2222.

Sandmeier JJ, Celic I, Boeke JD, Smith JS. 2002. Telomeric and rDNA silencing in Saccharomyces cerevisiae are dependent on a nuclear NAD(+) salvage pathway. *Genetics* **160**: 877-889.

Santos-Rosa H, Kirmizis A, Nelson C, Bartke T, Saksouk N, Cote J, Kouzarides T. 2009. Histone H3 tail clipping regulates gene expression. *Nat Struct Mol Biol* **16**: 17-22.

Schneider J, Shilatifard A. 2006. Histone demethylation by hydroxylation: chemistry in action. *ACS Chem Biol* **1**: 75-81.

Scott EM, Pillus L. 2010. Homocitrate synthase connects amino acid metabolism to chromatin functions through Esa1 and DNA damage. *Genes Dev* **24**: 1903-1913.

Sikorski RS, Hieter P. 1989. A system of shuttle vectors and yeast host strains designed for efficient manipulation of DNA in *Saccharomyces cerevisiae*. *Genetics* **122**: 19-27.

Smith JS, Boeke JD. 1997. An unusual form of transcriptional silencing in yeast ribosomal DNA. *Genes Dev* **11**: 241-254.

Takahashi H, McCaffery JM, Irizarry RA, Boeke JD. 2006. Nucleocytosolic acetyl-coenzyme a synthetase is required for histone acetylation and global transcription. *Mol Cell* **23**: 207-217.

Takahashi YH, Schulze JM, Jackson J, Hentrich T, Seidel C, Jaspersen SL, Kobor MS, Shilatifard A. 2011. Dot1 and histone H3K79 methylation in natural telomeric and *HM* silencing. *Mol Cell* **42**: 118-126.

Thompson JS, Ling X, Grunstein M. 1994. Histone H3 amino terminus is required for telomeric and silent mating locus repression in yeast. *Nature* **369**: 245-247.

Turcan S, Rohle D, Goenka A, Walsh LA, Fang F, Yilmaz E, Campos C, Fabius AW, Lu C, Ward PS *et al.* 2012. IDH1 mutation is sufficient to establish the glioma hypermethylator phenotype. *Nature* **483**: 479-483.

Wellen KE, Hatzivassiliou G, Sachdeva UM, Bui TV, Cross JR, Thompson CB. 2009. ATP-citrate lyase links cellular metabolism to histone acetylation. *Science* **324**: 1076-1080.

Wellen KE, Thompson CB. 2012. A two-way street: reciprocal regulation of metabolism and signalling. *Nat Rev Mol Cell Biol* **13**: 270-276.

Wyrick JJ, Holstege FC, Jennings EG, Causton HC, Shore D, Grunstein M, Lander ES, Young RA. 1999. Chromosomal landscape of nucleosome-dependent gene expression and silencing in yeast. *Nature* **402**: 418-421.

Xue Y, Vashisht AA, Tan Y, Su T, Wohlschlegel JA. 2014. *PRB1* Is required for clipping of the histone H3 N-terminal tail in *Saccharomyces cerevisiae. PLoS One* **9**: e90496.

Yang W, Xia Y, Hawke D, Li X, Liang J, Xing D, Aldape K, Hunter T, Alfred Yung WK, Lu Z. 2012. PKM2 phosphorylates histone H3 and promotes gene transcription and tumorigenesis. *Cell* **150**: 685-696.

Yang B, Britton J, Kirchmaier AL. 2008. Insights into the impact of histone acetylation and methylation on Sir protein recruitment, spreading, and silencing in *Saccharomyces cerevisiae. J Mol Biol* **381**: 826-844.

Zhang W, Bone JR, Edmondson DG, Turner BM, Roth SY. 1998. Essential and redundant functions of histone acetylation revealed by mutation of target lysines and loss of the Gcn5p acetyltransferase. *EMBO J* **17**: 3155-3167

Chapter 3. Threonine metabolic enzymes Hom2 and Hom6 positively regulate rDNA silencing

Introduction

In budding yeast, threonine and methionine are synthesized through a branching pathway initiated with L-aspartate as the primary substrate. L-aspartate is converted into the intermediate metabolite homoserine through a three-step pathway involving aspartate kinase Hom3, aspartic β-semialdehyde dehydrogenase Hom2, and homoserine dehydrogenase Hom6. Homoserine is further processed by branching pathways to synthesize threonine or methionine (Fig. 3-1).

Hom2 and Hom6 were identified as candidates with potential chromatin functions by the *in silico* screen (Fig. 2-1). This was based on the idea that they both use NADPH as co-factors, and thus potentially regulate the nuclear pool of NAD^+ available to Sir2 (Fig. 3-1). Furthermore, methionine is a precursor to S-adenosylmethioine (SAM). Therefore, the activities of Hom2 and Hom6 potentially influence the nuclear pool of SAM available to histone methyltransferases (Fig. 3-1).

The silencing reporter assays revealed that both the *hom2Δ* and the *hom6Δ* mutants exhibited defective rDNA silencing (Fig. 2-2A). Furthermore, the *hom6Δ* mutant also exhibited defective telomeric silencing and elevated *HMR* silencing (Fig. 2-2B; Fig. 2-2C). Additionally, high throughput screens revealed that deletion of *HOM3*, *HOM2* or *HOM6* caused DNA damage sensitivities (Table 3-1; Cherry *et al.* 2012; http:://www.yeastgenome.org). Also, deletion of *THR1*, which encodes the first enzyme

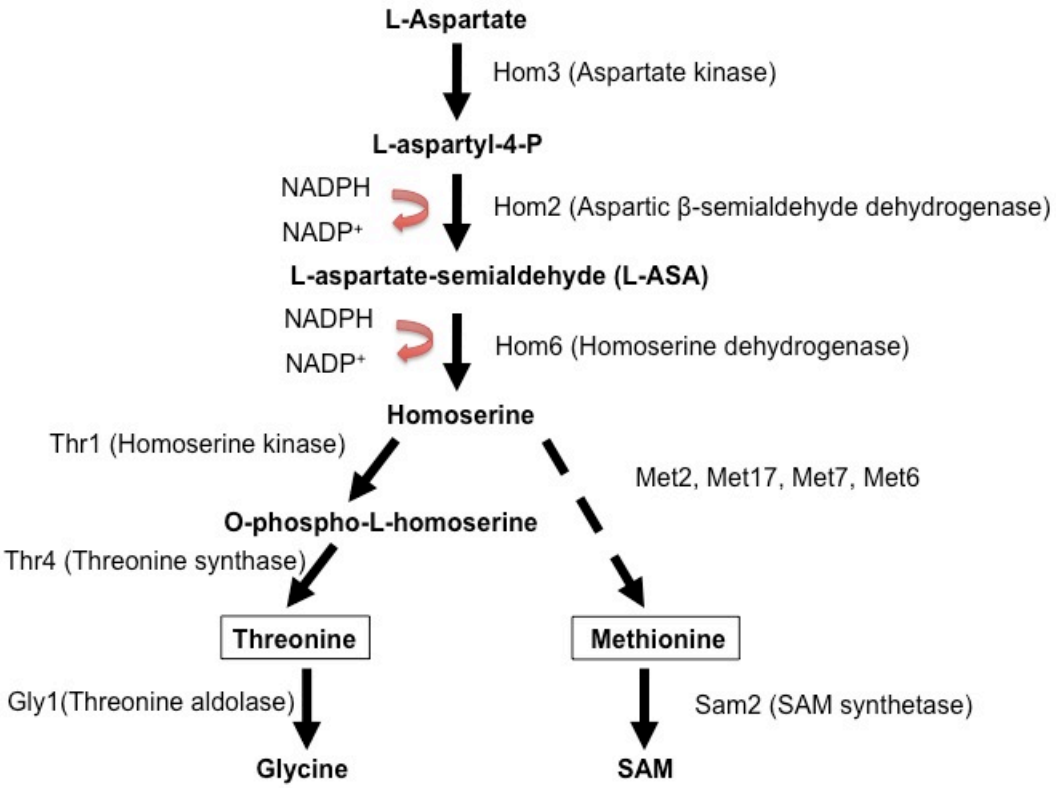

Figure 3-1. The metabolic activities of Hom2 and Hom6. Diagram showing the threonine-methionine biosynthetic superpathway in budding yeast. The multi-step methionine synthesis pathway was not shown in detail for simplicity.

Table 3-1. Summary of DNA damage phenotypes of strains deleted for genes encoding enzymes in the methionine-threonine biosynthetic pathway. Threonine biosynthetic mutants were shown to be sensitive to a wide range of drugs that induce DNA damage (http:://www.yeastgenome.org, Cherry *et al.* 2012). A few examples were shown in this table. Red color represents sensitivity and white color indicates no reported sensitivity. CPT= camptothecin, HU = hydroxyurea and MMS = methyl methanesulfonate.

Strain	CPT	Cisplatin	Doxorubicin	HU	MMS
hom3Δ					
hom2Δ					
hom6Δ					
thr1Δ					
met2Δ					

in the threonine biosynthetic pathway, similarly caused DNA damage sensitivity. In contrast, deletion of *MET2*, which encodes the first enzyme in the methionine biosynthetic pathway, does not have any reported DNA damage sensitivities (Table 3-1). Since DNA damage sensitivity is often caused by defects in chromatin regulation (reviewed in Hampsey 1997), it is possible that Hom2 and Hom6 regulate both chromatin silencing and DNA damage repair.

Interestingly, threonine and methionine metabolism have been associated with chromatin regulation in mouse embryonic stem cells. Of note, since both threonine and methionine are essential amino acids for animals, their influence on chromatin regulation is determined by the respective catabolic reactions. In mouse embryonic stem cells, threonine dehydrogenase breaks down threonine to form glycine and acetyl-CoA, and therefore its catalytic activity directly influences the amount of acetyl-CoA available to histone acetyltransferase (Alexander *et al.* 2011). However, threonine dehydrogenase is absent from the budding yeast proteome, and L-threonine is instead converted into glycine and acetaldehyde in a reaction catalyzed by threonine aldolase (Fig. 3-1). Therefore, threonine aldolase does not regulate acetyl-CoA levels directly in budding yeast. Threonine metabolism is also coupled to SAM metabolism in mouse embryonic stem cells. Upon threonine depletion, SAM levels were reduced and histone methylation was diminished (Shyh-Chang *et al.* 2013). Although the SAM metabolic pathways are different in budding yeast, methionine is converted into SAM by the SAM synthetase, Sam2 (Fig. 3-1). Therefore Hom2 and Hom6 might influence chromatin regulation through modulating the levels of methionine and SAM.

Earlier results showed that Hom2 and Hom6 had rDNA silencing defects (Fig. 2-2A). Hence, this chapter focuses primarily on the role of threonine biosynthesis in rDNA silencing. I found that deletion of all genes in the threonine but not the methionine biosynthetic pathway resulted in rDNA silencing defects. The rDNA silencing defect of the null mutants was partially suppressed by the addition of threonine, but not methionine. In addition, the Hom6 catalytic mutant retained partial rDNA silencing function, indicating that Hom6 might also regulate silencing through a threonine metabolism-independent mechanism. Depletion of Hom6 from the nucleus modestly reduced the strength of rDNA silencing, suggesting that the nuclear pool of this enzyme contributes to rDNA silencing.

Results

Independent assays support *HOM6*'s role in regulating rDNA silencing

The *hom6Δ* mutant showed reduced silencing of the *CAN1* reporter inserted at the 5S locus of the rDNA array (Fig. 2-2A). To assess whether this phenotype truly reflects Hom6's function in rDNA silencing and is not caused by an intrinsic sensitivity to canavanine, a *hom6Δ CAN1* control strain was constructed. This strain was only weakly sensitive to canavanine, indicating that Hom6 represses *CAN1* expression in the context of rDNA silencing (Fig. 3-2A). Therefore, the rDNA::*ADE2-CAN1* reporter assay was a valid method for assessing the silencing phenotype of the *hom6Δ* strain and was used for further genetic analyses.

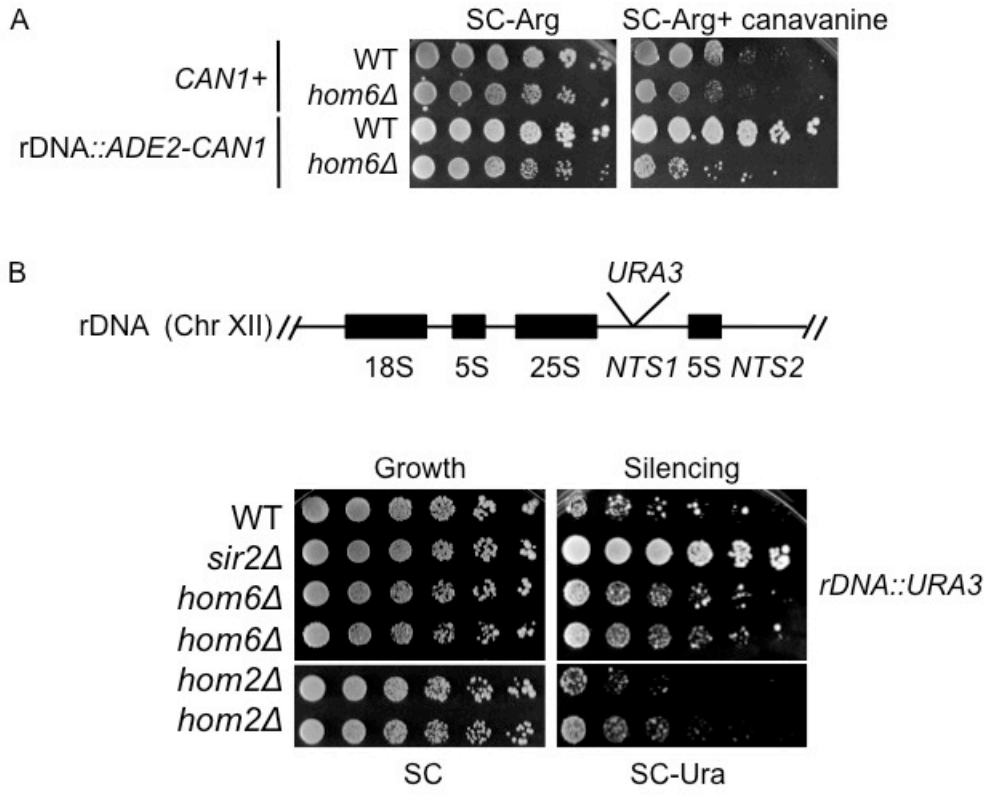

Figure 3-2. Independent assays support Hom6's positive regulatory role in rDNA silencing. (*A*) Hom6 represses *CAN1* transcription when it is inserted at the rDNA locus, not the endogenous *CAN1* locus. WT *CAN1+* (LPY17812), *hom6Δ CAN1+* (LPY18196), WT rDNA::*ADE2-CAN1* (LPY4909) and *hom6Δ* rDNA::*ADE2-CAN1* (LPY17411) strains were plated on SC-Arg (growth control) and SC-Arg + canavanine (0.75 μg/mL). (*B*) Hom6 also regulates silencing of a *URA3* reporter inserted at the rDNA *NTS1* spacer region, shown by modestly increased growth in the absence of uracil. Top: Diagram showing the insertion site of the silencing reporter. Bottom: WT (LPY2446), *sir2Δ* (LPY2447), two independent *hom6Δ* strains (LPY16037 and LPY16038) and two independent *hom2Δ* strains (LPY16011 and LPY16012) were plated on SC (growth control) and SC-Ura (silencing) media. Increased growth indicates defective rDNA silencing. The *sir2Δ* strain served as a positive control for silencing defect.

As an independent way of assessing *HOM6*'s function in rDNA silencing, *HOM6* was deleted from another rDNA reporter strain. In this strain, a *URA3* reporter gene was inserted at the *NTS1* spacer region of the rDNA array (Fig. 3-2A). The expression of *URA3* is normally repressed by rDNA silencing, and therefore the WT strain grew poorly on medium lacking uracil. When silencing is defective, for example, when *SIR2* was deleted, *URA3* expression was elevated and cells grew better on SC-Ura. Deletion of *HOM6* moderately improved growth on SC-Ura (Fig. 3-2B), suggesting that Hom6 also regulates silencing at the *NTS1* spacer region of the rDNA repeats. In contrast, deletion of *HOM2* did not change the expression of *URA3* (Fig. 3-2B), indicating that the role of Hom6 in silencing at the *NTS1* spacer may be independent of Hom2. Such differential regulation within the rDNA has been previously observed for enzymes participating in the same metabolic pathway (Koch and Pillus 2009).

Threonine but not methionine biosynthesis regulates rDNA silencing

Since Hom2 and Hom6 participate in the common pathway for the synthesizing threonine and methionine (Fig. 3-1) and deletion of both genes resulted in an rDNA silencing defect (Figure 2-2A), the question was raised of whether rDNA silencing is regulated by the levels of methionine, threonine, or both.

To address this question, two independent approaches were taken. First, the effects of deleting *MET2* or *THR1* were examined, because they encode the first enzymes catalyzing the two branching pathways. The *thr1Δ* mutant was defective for rDNA silencing, whereas the *met2Δ* mutant showed normal silencing (Fig. 3-3A).

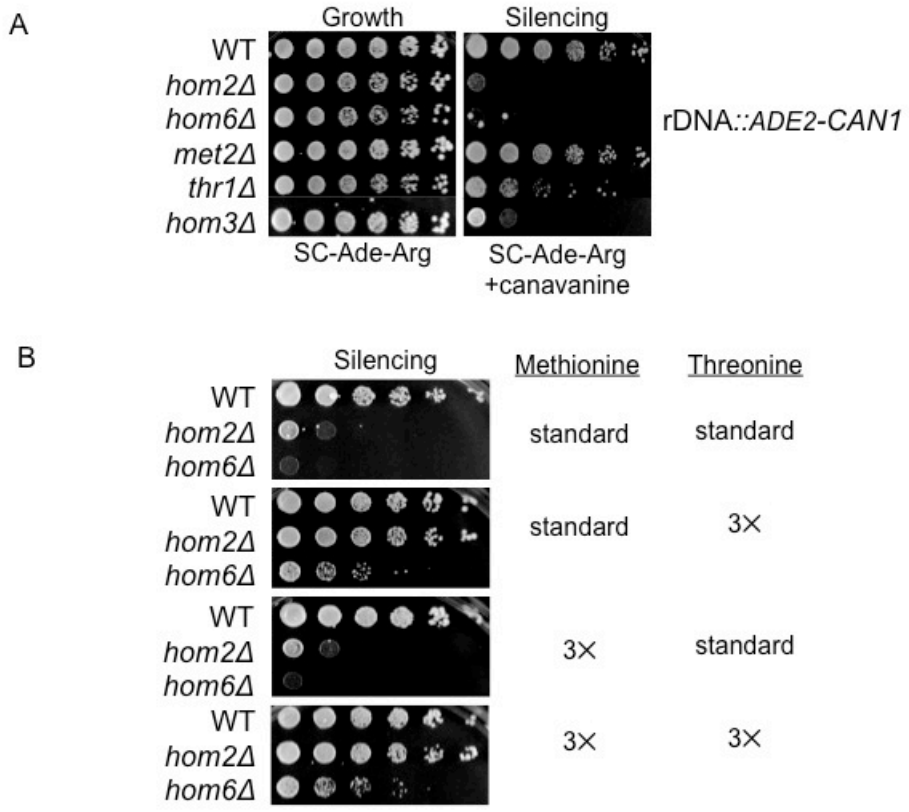

Figure 3-3. rDNA silencing is regulated by the threonine, but not methionine biosynthetic pathway. (*A*) Deletion of *THR1* but not *MET2* resulted in rDNA silencing defect. WT (LPY4909), *hom2Δ* (LPY16020), *hom6Δ* (LPY17411), *hom3Δ* (LPY16907), *thr1Δ* (LPY16837) and *met2Δ* (LPY16821) strains were plated on SC-Ade-Arg (growth control) and SC-Ade-Arg + 8 μg/mL canavanine (silencing). (*B*) Elevated concentration in the plates of threonine but not methionine improved the rDNA silencing defect of the *hom2Δ* and *hom6Δ* mutants. WT (LPY4909), *hom2Δ* (LPY16020), *hom6Δ* (LPY17411) strains were plated on SC-Ade-Arg + 8 μg/mL canavanine to assess rDNA silencing. 'Standard' indicates medium made with the standard amount of threonine (10 g/L) and methionine (1 g/L), whereas 3× indicates media containing 3× the standard amount of the indicated amino acid.

Deletion of *HOM3* also caused an rDNA silencing defect (Fig. 3-3A). These results suggest that the levels of threonine rather than methionine regulate rDNA silencing. Of note, although the *thr1Δ* mutant exhibited an rDNA silencing defect, its phenotype was weaker than the phenotype of *hom3Δ*, *hom2Δ* or *hom6Δ* mutants. This suggests that these mutants influence rDNA silencing through both threonine- dependent and independent pathways.

The second approach was to add back increased amounts of methionine or threonine to the medium in the rDNA silencing assay. Elevated concentration of threonine partially rescued the rDNA silencing defect of the *hom2Δ* and *hom6Δ* mutants, whereas that of methionine did not (Fig. 3-3B). Increased concentrations of both threonine and methionine did not further improve silencing compared to increased threonine (Fig. 3-3B). This result supports the idea that the concentration of threonine (or its metabolites), rather than that of methionine, regulates rDNA silencing. Additionally, adding back threonine only partially rescued the rDNA silencing defect of the *hom6Δ* mutant, suggesting that Hom6 might also regulate rDNA silencing through a threonine metabolism-independent pathway.

The catalytic mutant of Hom6 retains partial rDNA silencing function

The crystal structure and the mechanism of catalysis have been established for the budding yeast Hom6 (DeLaBarre *et al.* 2000). It was shown that the Hom6-D219L mutant abolished catalytic activity without compromising structural integrity (DeLaBarre *et al.* 2000). The D219L mutant was constructed and expressed under the endogenous promoter on a 2-micron plasmid. The *hom6-D219L* mutant was unable to suppress the

methionine-threonine auxotrophy phenotype of the *hom6Δ* mutant, but partially suppressed the silencing defect of the mutant (Fig. 3-4). This result is consistent with the idea that Hom6 regulates rDNA silencing through both threonine metabolism- dependent and independent pathways.

Hom6 has a nuclear pool and nuclear-localized Hom6 contributes to its rDNA silencing function

A high throughput screen using GFP-tagged strains demonstrated that Hom6 has a nuclear pool (http://yeastgfp.yeastgenome.org). To validate this result, sequence encoding a thirteen-Myc epitope was integrated at the 3' end of the chromosomal *HOM6*. Protein immunoblotting validated the stable expression of the Myc-tagged Hom6 (Fig. 3-5A). Immunofluorescence analysis showed that Hom6-Myc is broadly distributed in the cytoplasm, the mitochondria and the nucleus (Fig. 3-5B). To study whether the nuclear pool of Hom6 is important for rDNA silencing, a strong nuclear export sequence (NES, Gadal *et al.* 2001) was integrated after the Myc tag. The Hom6-Myc-NES mutant was expressed at a similar level as the Hom6-Myc strain (Fig. 3-5A), and was able to synthesize threonine and methionine normally (not shown), demonstrating that the tagged construct was biochemically active and stable. It moderately reduced Hom6's function in rDNA silencing (Fig. 3-5C), suggesting that the nuclear pool of Hom6 contributes to its rDNA silencing function.

Hom6 has a complex role in telomeric silencing

The initial screen showed that the *hom6Δ* mutant had defect in silencing the *URA3* gene integrated at *TELV-R* (Fig. 2-2B). To validate this result, RT-qPCR was performed

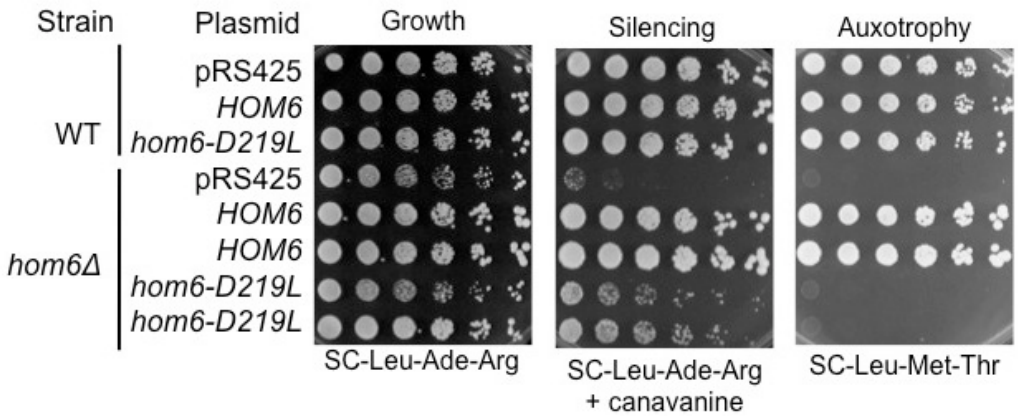

Figure 3-4. The hom6-D219L mutant retains partial silencing activity. WT (LPY4909) and *hom6Δ* (LPY17411) strains were transformed with empty vector (pRS425), *HOM6* (pLP2629) and *hom6-D219L* (pLP2754). The transformants were plated on SC-Ade-Arg-Leu (growth control), SC-Ade-Arg-Leu + 8 μg/mL canavanine (silencing) and SC-Leu-Thr-Met (auxotrophy). Two independent transformants of the *hom6Δ* mutant were assessed.

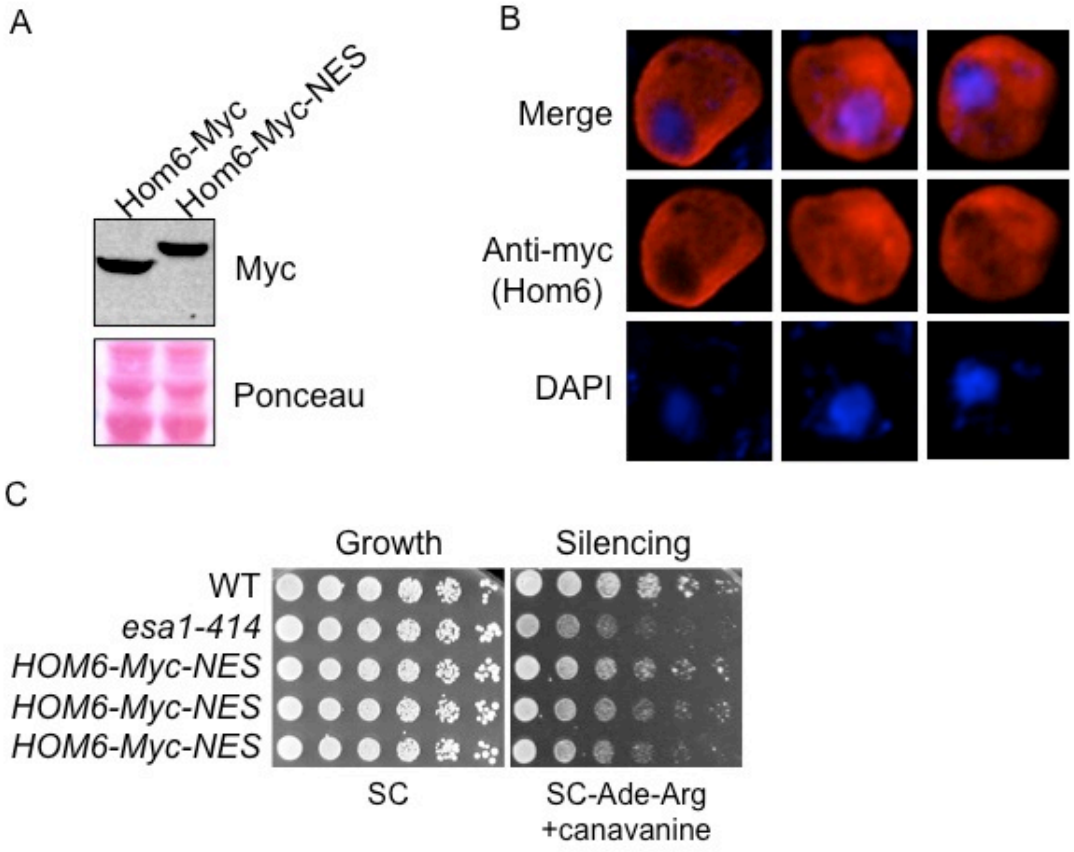

Figure 3-5. Hom6 is partially localized to the nucleus. (*A*) Myc-tagged Hom6 is stably expressed with or without the NES signal. Whole cell extracts of Hom6-Myc (LPY16779) and Hom6-Myc-NES (LPY17330) were blotted with anti-Myc antibody. Ponceau staining indicated equal loading. (*B*) Hom6 is partially localized to the nucleus. The Hom6-Myc strain was visualized by immunofluorescence, where the red signal represents Myc-tagged Hom6 and the blue signal indicates DAPI staining for DNA. (*C*) The Hom6-Myc-NES mutant grew normally on medium lacking methionine and threonine. WT (LPY4909), *esa1-414* (LPY11113) and three independent *HOM6-Myc-NES* (LPY17330, LPY17331 and LPY17332) strains were plated on SC-Ade-Arg (growth control), SC-Thr-Met (Auxotrophy) and SC-Ade-Arg + canavanine (silencing). The *esa1-414* strain was used as a positive control for reduced rDNA silencing.

on RNA prepared from the mutant. WT and mutant cDNA was analyzed with primers detecting transcription of *YFR057W*, an ORF that is normally repressed by the SIR complex recruited to *TELVI-R*. The expression of *YFR057W* was modestly, though significantly, upregulated in the *hom6Δ* mutant (Fig. 3-6A). *HOM6* was also deleted from an independent reporter strain carrying a *URA3-TRP1* reporter cassette at *TELVII-L*. For this reporter strain, decreased silencing results in elevated expression of *URA3* and *TRP1* and better growth on the respective dropout media. Interestingly, the *hom6Δ* strain showed reduced growth on both SC-Ura and SC-Trp, indicating that this mutation improved telomeric silencing (Fig. 3-6B). Therefore, the role of Hom6 on telomeric silencing varies depending on the subtelomeric sequence and/or structure. Earlier work demonstrated a similar finding with other mutants (Pryde and Louis 1999), and therefore Hom6 may be another example of a silencing regulator with telomere-specific effects.

Variability issues in this study

During this study, it was noted that the *hom6Δ* strain was highly variable in terms of colony morphology and growth rate. The colony sizes were not uniform after streaking and individual *hom6Δ* spores dissected from the same diploid had different growth rates and damage (Fig. 3-7A)/silencing phenotypes (Fig. 3-7B). Also, when a *hom6Δ* strain transformed with a plasmid-borne *HOM6-myc* was examined by immunofluorescence, the Myc-signal was unevenly distributed from cell to cell, with some cells having intense signals and other cells having no signals. Additionally, it was noted that for all the threonine metabolic heterozygotes, full tetrads were only obtained if dissection was done immediately after spore formation, indicating some lethality in meiosis or germination.

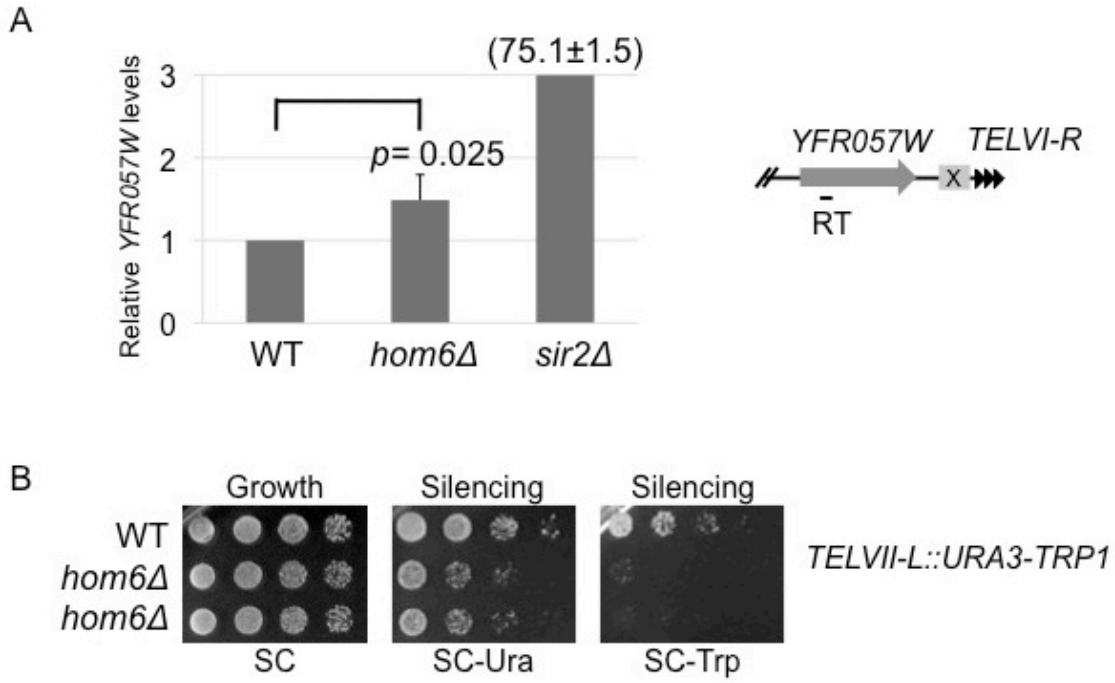

Figure 3-6. Hom6 regulates different telomeres differently. (*A*) Deletion of *HOM6* resulted in a modest increase in *YFR057W* levels. RNA was extracted from WT (LPY5), *hom6Δ* (LPY16562) and *sir2Δ* (LPY11) and cDNA was made as described in Materials and Methods. The transcript level of *YFR057W* was normalized to *ACT1* and the WT value was set to 1 for each experiment. Average represents 2-3 independent experiments and *p*-value was calculated using one-tailed Student t-test. (*B*) Deletion of *HOM6* improved silencing at *TELVII-L.* WT (LPY2202) and two independent *HOM6* knockouts (LPY16193 and LPY16194) were plated on SC (growth control), SC-Ura (silencing) and SC-Trp (silencing). Reduced growth on dropout media indicates improved silencing.

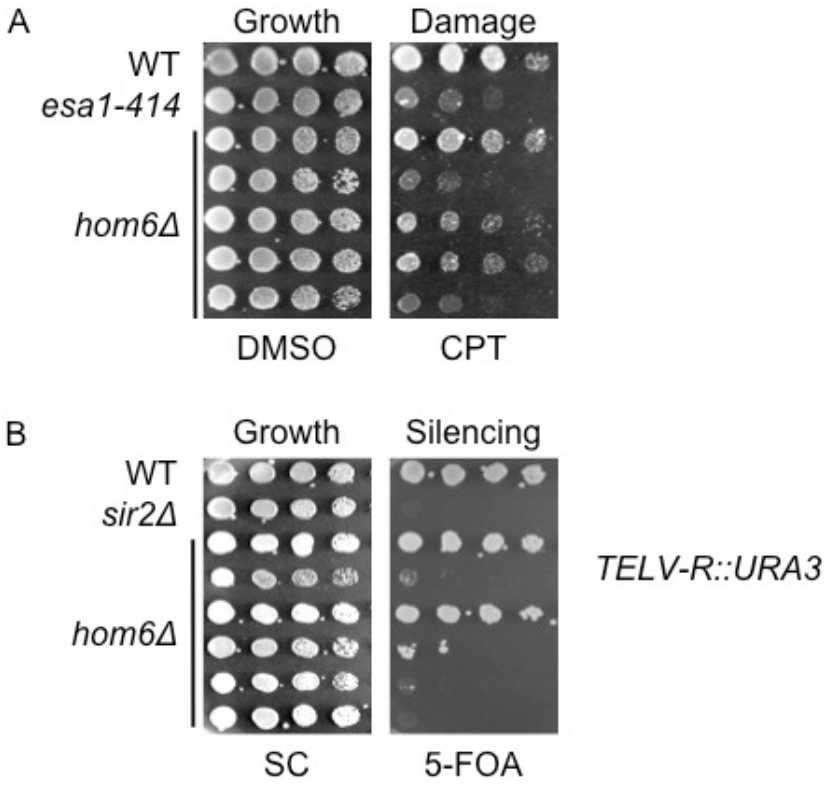

Figure 3-7. Independent *hom6Δ* strains showed variations in DNA damage and telomeric silencing phenotypes. (*A*) Independent *hom6Δ* strains had different sensitivities to DNA damage agent camptothecin (CPT). WT (LPY5), *esa1-414* (LPY4774) and independent *hom6Δ* haploid strains were plated on DMSO (solvent control) or 40 µg/mL CPT (damage). The *esa1-414* strain served as a positive control for sensitivity to CPT. (*B*) Independent *hom6Δ* strains had different telomeric silencing phenotypes. WT (LPY4916), *sir2Δ* (LPY4979) and independent *hom6Δ* haploid strains were plated on SC (growth control) or 5-FOA (silencing). The *sir2Δ* strain served as a positive control for telomeric silencing defect.

There are a few possible explanations for the variable results. The first possibility is that Hom6 regulates partitioning of materials during cell division, perhaps resulting in uneven distribution of mitochondria and plasmids to daughter cells. The second possibility is that Hom6 regulates the formation of extrachromosomal circles. Accumulation of extrachromosomal circles has been found to result in variable phenoypes (Dobson *et al.* 2005). Additional studies will be required to determine if either of these explanations is true in the case of *hom6*Δ, or if there is some other underlying source of phenotypic variability.

Discussion

In Chapter 4, the chromatin functions of threonine metabolic genes were examined with a series of genetic experiments. These experiments suggest that the threonine rather than the methioine biosynthetic pathway regulates rDNA silencing in budding yeast. In addition, Hom6 potentially regulates rDNA silencing through both threonine metabolism- dependent and independent pathways, as supported by three findings: 1) the *thr1Δ* mutant had a weaker silencing defect than the *hom6Δ* mutant; 2) adding back threonine only partially rescued *hom6Δ*'s silencing defect; 3) the Hom6-D219L catalytic mutant retained partial silencing activities. Further, Hom6 might also be involved in the regulation of telomeric silencing, but its impact on silencing is telomere-specific.

The variability issue of the *hom6Δ* strain needs to be resolved

One issue that hindered the progress of this study was that the *hom6Δ* strain showed variable phenotypes, as described in Results. To address this issue, a few technical modifications could be applied to future studies. A covering plasmid containing the WT copy of *HOM6* should be used during genetic crosses, to alleviate the potential uneven distribution problem during meiosis. Additionally, extrachromosomal circles could be removed by a plasmid-borne FLP recombinase (Tsalik and Gartenberg 1998). Experiments involving the knockout mutant in this chapter should be validated when the new strains are constructed. Further, the potential mechanisms suggested above could be evaluated experimentally.

Genetic interactions between different threonine metabolic genes

Although all threonine biosynthetic mutants exhibited rDNA silencing defects, the extent of the defect was different. Therefore, in order to assess the relative importance of each intermediate metabolite in silencing, double mutants deleted for *HOM6* and another threonine biosynthetic gene should be made.

Hom6's interaction with known chromatin regulators

In this chapter, Hom6 was shown to have multiple rDNA and telomeric silencing phenotypes using reporter assays. To further establish Hom6's effect on silencing, global SIR protein levels and SIR binding at the three silent loci should be analyzed. Also, since the threonine metabolic pathway has been linked to histone methylation levels in mouse

embryonic stem cells (Shyh-Chang *et al.* 2013), histone methylation status should be analyzed for the *hom6Δ* mutant with immunoblot and chromatin IP experiments.

Analysis of additional Hom6 catalytic mutants

The *hom6-D219L* mutant was found to retain partial rDNA silencing functions. One caveat with the experiment was that the leucine codon used in the mutagenesis primer was the non-preferred codon in budding yeast. Although apparently normal levels of expression were observed, an additional D219L mutant should be made with the preferred leucine codon. To support the finding with the D219L mutant, the silencing function of other known catalytic mutants of Hom6 should also be tested (DeLaBarre *et al.* 2000). Additionally, the catalytic mutants should be tested for telomeric and *HMR* silencing, as well as for the reported DNA damage phenotypes of the *hom6Δ* mutant.

Materials and Methods

Yeast strains and plasmids

The deletion strains were made by amplifying the *KanMX* knockout cassette using oligonucleotides listed in Table 3-4 and transforming the PCR products into the WT strain. Correct gene knockout was validated by molecular genotyping.

The *HOM6-Myc* strain was constructed by amplifying the *Myc-KanMX* cassette from plasmid pLP1651, using oligos oLP1627 and oLP1628. The *HOM6-Myc-NES* strain was constructed by amplifying the *Myc-NES-KanMX* cassette from plasmid pLP2829, using oligos oLP1627 and 1628.

A 3.4kb HindIII-PstI fragment containing *HOM6* was digested from the yeast tiling library plasmid YGpM25e07 (pLP2592) and subcloned into HindIII-PstI digested pbluescript vector or pRS425 to make pbluescript-*HOM6* (pLP2630) or pRS425-*HOM6* (pLP2629). Of note, the PstI site was not carried by the genomic sequence but was present on the tiling library plasmid, adjacent to the cloning site.

The D219L mutation was introduced into pbluescript-*HOM6* (pLP2630) by site-directed mutagenesis, using oligos oLP1558 and oLP1559. This resulted in pbluescript-*hom6-D219L* (pLP2640). A HindIII-XmaI fragment containing *hom6-D219L* was ligated into pRS425 to make pRS425-*hom6-D219L* (pLP2754).

Dilution assays for growth and silencing

Cells were grown in 3mL YPAD or dropout medium for 2 days at 30°. A_{600} of 1.0 was pelleted and washed once with H_2O before plating at 5-fold serial dilutions. Of note, the washing step was important because residual methionine and threonine were found to enable *hom6Δ* growth on medium lacking threonine and methionine. Silencing was assessed on media indicated in the figures and figure legends.

RNA extraction and cDNA preparation

Starter cultures were diluted in 50mL SC medium and harvested at A_{600} of 0.8-1.0. RNA was extracted as described (Collart and Oliviero 2001), except that harvested cells were resuspended in sodium acetate buffer (50mM sodium acetate pH5.3, 10mM EDTA). RNA was reverse transcribed with random hexamers using TaqMan Reverse Transcription Reagents. cDNA was diluted 5- fold and analyzed by real-time PCR on

DNA Engine Opticon 2 with oligos for *YFR057W* and *ACT1*.

Table 3-2. Yeast strains used in Chapter 3

Strain (alias)	Genotype	Source/reference
LPY5	W303 *MATa* (W303-1a)	R. Rothstein
LPY11	W303 *MATa sir2Δ::HIS3*	
LPY2202	*MATα ade2 his4 leu2-3,112 lys2 trp1 ura3-52 TELVII-L::URA3-TRP1*	Gottschling *et al.* 1990
LPY2446	*MATα his3Δ200 leu2Δ1 ura3-52* with rDNA *Ty mURA3* insertion	Smith and Boeke 1997
LPY2447	*MATα his3Δ200 leu2Δ1 ura3-52 sir2Δ::HIS3* with rDNA *Ty mURA3* insertion	Smith and Boeke 1997
LPY4774	W303 *MATa esa1-414*	
LPY4909	W303 *MATα* rDNA*::ADE2-CAN1*	Clarke *et al.* 2006
LPY4916	W303 *MATa TELV-R::URA3*	
LPY4979	W303 *MATα sir2Δ::HIS3 TELV-R::URA3*	
LPY11113	W303 *MATα esa1-414 hmrΔE::TRP1* rDNA*::ADE2-CAN1 TELV-R::URA3*	
LPY16011	*MATα his3Δ200 leu2Δ1 ura3-52 hom2Δ::kanMX* with rDNA *Ty mURA3* insertion	
LPY16012	*MATα his3Δ200 leu2Δ1 ura3-52 hom2Δ::kanMX* with rDNA *Ty mURA3* insertion	
LPY16020	W303 *MATα hom2Δ::kanMX* rDNA*::ADE2-CAN1*	
LPY16037	*MATα his3Δ200 leu2Δ1 ura3-52 hom6Δ::kanMX* with rDNA *Ty mURA3* insertion	
LPY16038	*MATα his3Δ200 leu2Δ1 ura3-52 hom6Δ::kanMX* with rDNA *Ty mURA3* insertion	
LPY16193	*MATα ade2 his4 leu2-3,112 lys2 trp1 ura3-52 hom6Δ::kanMX TELVII-L::URA3-TRP1*	
LPY16194	*MATα ade2 his4 leu2-3,112 lys2 trp1 ura3-52 hom6Δ::kanMX TELVII-L::URA3-TRP1*	
LPY16779	*MATα* rDNA*::ADE2-CAN1 HOM6-13Myc::kanMX*	
LPY16821	*MATα met2Δ::kanMX* rDNA*::ADE2-CAN1*	
LPY16837	*MATα thr1Δ::kanMX* rDNA*::ADE2-CAN1*	
LPY16907	*MATα hom3Δ::kanMX* rDNA*::ADE2-CAN1*	
LPY17330	W303 *MATα hmrΔE::TRP1* rDNA*::ADE2-CAN1 TELV-R::URA3 hom6-13Myc-NES::kanMX*	
LPY17331	W303 *MATα hmrΔE::TRP1* rDNA*::ADE2-CAN1 TELV-R::URA3 hom6-13Myc-NES::kanMX*	
LPY17332	W303 *MATα hmrΔE::TRP1* rDNA*::ADE2-CAN1 TELV-R::URA3 hom6-13Myc-NES::kanMX*	
LPY17411	*MATα hom6Δ::kanMX* rDNA*::ADE2-CAN1*	
LPY17812	W303 *MATa CAN1*	
LPY18196	W303 *MATa CAN1 hom6Δ::kanMX*	

Table 3-3. Plasmids used in Chapter 3

Plasmid	Description	Source/Reference
pRS425	Vector *LEU2* 2-micron	Christianson *et al.* 1992
pLP1651	pFA6a-13Myc-kanMX	Longtine *et al.* 1998
pLP2629	pRS425-*HOM6*	
pLP2592	YGpM25e07	Jones *et al.* 2008
pLP2630	pbluescript-*HOM6*	
pLP2640	pbluescript-*hom6-D219L*	
pLP2754	pRS425-*hom6-D219L*	
pLP2829	pFA6a-13Myc-Gly-Gly-NES-KanMX	

Note: Unless otherwise stated, all plasmids listed were part of the standard lab collection or constructed during this study.

Table 3-4. Oligonucleotides used in Chapter 3

Oligo #	Name	Sequence
798	*ACT1*_For	GGTGGTTCTATCTTGGCTTC
799	*ACT1*_Rev	ATGGACCACTTTCGTCGTAT
1516	*HOM2*_KO_For	CGACGGAGAAGAAGGAGAC
1517	*HOM2*_KO_Rev	CTTGGGTCAGCGAGAGAATTAC
1558	*hom6-D219L*_For	GATTTGAATGGGTTGCTTGTTGCTAGA AAGG
1559	*hom6-D219L*_Rev	CCTTTCTAGCAACAAGCAACCCATTC AAATC
1604	*MET2*_KO_For	CAGCTGCGTCCAATAGATGAG
1605	*MET2*_KO_Rev	CGGTAACTCGTGTGCTCTCATTC
1608	*THR1*_KO_For	CCTTCAAACCGTGATCCTG
1609	*THR1*_KO_Rev	GAAGGAAAACTTCCCCAAG
1606	*HOM3*_newKO_For	CTTTCCGTACGCAGTCTTCTC
1607	*HOM3*_newKO_Rev	GTCAGTGATGGGGATTTGC
1627	*HOM6*_C-Myc_For	GTTACTGCCGCTGGTGTTTTGGGTGAT GTTATCAAGATTGCTCAAAGACTTCG GATCCCCGGGTTAATTAA
1628	*HOM6*_C-Myc_Rev	ATCTATTTATATATAAATATACCTATG TTTTTATATGTCTGTTTACTGATGAAT TCGAGCTCGTTTAAAC
1769	*HOM6*_newKO_For	CAATAACGCACATGGTGG
1770	*HOM6*_newKO_Rev	GCCCCATGACATGGATGAG
1815	*YFR057W*_For	CTAGTGTCTATAGTAAGTGCTCGG
1816	*YFR057W*_Rev	CTCTAACATAACTTTGATCCTTACTCG

References

Alexander PB, Wang J, McKnight SL. 2011. Targeted killing of a mammalian cell based upon its specialized metabolic state. *Proc Natl Acad Sci U S A* **108**: 15828-15833.

Cherry JM, Hong EL, Amundsen C, Balakrishnan R, Binkley G, Chan ET, Christie KR, Costanzo MC, Dwight SS, Engel SR, Fisk DG, Hirschman JE, Hitz BC, Karra K, Krieger CJ, Miyasato SR, Nash RS, Park J, Skrzypek MS, Simison M, Weng S, Wong ED. 2012. *Saccharomyces* Genome Database: the genomics resource of budding yeast. *Nucleic Acids Res* **40**: D700-5.

Christianson TW, Sikorski RS, Dante M, Shero JH, Hieter P. 1992. Multifunctional yeast high-copy-number shuttle vectors. *Gene* **110**: 119-122.

Clarke AS, Samal E, Pillus L. 2006. Distinct roles for the essential MYST family HAT Esa1p in transcriptional silencing. *Mol Biol Cell* **17**: 1744-1757.

Collart MA, Oliviero S. 2001. Preparation of yeast RNA. *Curr Protoc Mol Biol* Chapter **13**: Unit13.12.

DeLaBarre B, Thompson PR, Wright GD, Berghuis AM. 2000. Crystal structures of homoserine dehydrogenase suggest a novel catalytic mechanism for oxidoreductases. *Nat Struct Biol* **7**: 238-244.

Dobson MJ, Pickett AJ, Velmurugan S, Pinder JB, Barrett LA, Jayaram M, Chew JS. 2005. The 2 micron plasmid causes cell death in *Saccharomyces cerevisiae* with a mutation in Ulp1 protease. *Mol Cell Biol* **25**: 4299-4310.

Gadal O, Strauss D, Kessl J, Trumpower B, Tollervey D, Hurt E. 2001. Nuclear export of 60s ribosomal subunits depends on Xpo1p and requires a nuclear export sequence-containing factor, Nmd3p, that associates with the large subunit protein Rpl10p. *Mol Cell Biol* **21**: 3405-3415.

Gottschling DE, Aparicio OM, Billington BL, Zakian VA. 1990. Position effect at S. cerevisiae telomeres: reversible repression of Pol II transcription. *Cell* **63**: 751-762.

Hampsey M. 1997. A review of phenotypes in *Saccharomyces cerevisiae. Yeast* **13**: 1099-1133.

Jones GM, Stalker J, Humphray S, West A, Cox T, Rogers J, Dunham I, Prelich G. 2008. A systematic library for comprehensive overexpression screens in Saccharomyces cerevisiae. *Nat Methods* **5**: 239-241.

Koch MR, Pillus L. 2009. The glucanosyltransferase Gas1 functions in transcriptional silencing. *Proc Natl Acad Sci U S A* **106**: 11224-11229

Longtine MS, McKenzie A,3rd, Demarini DJ, Shah NG, Wach A, Brachat A, Philippsen P, Pringle JR. 1998. Additional modules for versatile and economical PCR-based gene deletion and modification in *Saccharomyces cerevisiae. Yeast* **14**: 953-961.

Pryde FE, Louis EJ. 1999. Limitations of silencing at native yeast telomeres. *EMBO J* **18**: 2538-2550.

Shyh-Chang N, Locasale JW, Lyssiotis CA, Zheng Y, Teo RY, Ratanasirintrawoot S, Zhang J, Onder T, Unternaehrer JJ, Zhu H, Asara JM, Daley GQ, Cantley LC. 2013. Influence of threonine metabolism on S-adenosylmethionine and histone methylation. *Science* **339**: 222-226.

Smith JS, Boeke JD. 1997. An unusual form of transcriptional silencing in yeast ribosomal DNA. *Genes Dev* **11**: 241-254.

Tsalik EL, Gartenberg MR. 1998. Curing *Saccharomyces cerevisiae* of the 2 micron plasmid by targeted DNA damage. *Yeast* **14**: 847-852.

Chapter 4. *ARG82* regulates rDNA, telomeric and *HM* silencing

Introduction

In eukaryotic cells, inositol-phospholipid (IP) metabolism plays important roles in diverse signaling pathways. The metabolic pathway is initiated by the activity of phospholipase C (Plc1), which hydrolyzes the plasma membrane-associated phosphatidylinositol 4,5-bisphosphate (PIP_2) to form diacylglycerol (DAG) and inositol 1,4,5-trisphosphate (IP_3). Both DAG and IP_3 serve as second messengers of multiple signal transduction pathways (Nelson and Cox 2013). In addition, IP_3 can be further phosphorylated to yield various forms of inositol polyphosphates (IPs) (Fig. 4-1, adapted from York *et al.* 2005). In budding yeast, the kinase Arg82 (also known as Ipk2) catalyzes the sequential phosphorylation of IP_3 to form IP_4 and IP_5. IP_5 can be further modified by two alternative pathways. In one pathway, IP_5 is converted into an inositol pyrophosphate (PP-IP) PP-IP_4 by Kcs1, whereas in the other, IP_5 is phosphorylated by Ipk1 to make IP_6, which is turn modified by Kcs1 or Vip1 to make different forms of PP-IP_5.

Because of the structural and chemical diversities of the IPs and PP-IPs, each molecule has potentially a unique signaling capability. IPs and PP-IPs have been implicated in a number of nuclear processes. For example, IP_4 was reported to promote the physical interaction between HDAC3 and the DAD domain of NCOR2 in human cell lines (Watson *et al.* 2012). Also, the mammalian IP_6 was found to stimulate the non-homologous end joining pathway of DNA repair *in vitro* (Hanakahi *et al.* 2000). Further, increased production of PP-IP_4 caused telomere shortening through the activity of Tel1,

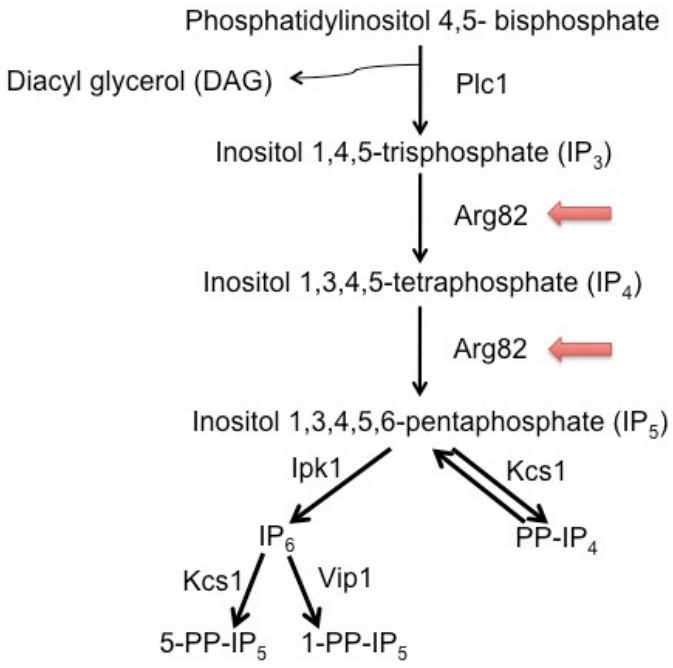

Figure 4-1. Diagram showing the inositol polyphosphate metabolic pathway in budding yeast. PIP_2 is hydrolyzed by Plc1 into DAG and IP_3, the latter of which serves as the precursor to other IPs and PP-IPs. Arg82 (highlighted by the red arrows) phosphorylates IP_3 to synthesize IP_4 and subsequently IP_4 into IP_5. IP_5 has two fates. First, it can be phosphorylated by Kcs1 to make pyrophosphate PP-IP_4. Alternatively, it can be first modified by Ipk1 to make IP_6, which is then phosphorylated by Kcs1 or Vip1 to make different forms of PP-IP_5.

which is the yeast homologue of the ATM kinase (York *et al.* 2005).

Arg82 was recovered in our initial screen for amino acid metabolic genes with silencing phenotypes (Fig. 2-1), based on the speculation that its kinase activity potentially regulates chromatin silencing through phosphorylation of nuclear substrates. Interestingly, Arg82 has already been established to be a moonlighting protein with chromatin functions. This protein was originally identified as a transcriptional activator that regulates the expression of arginine metabolic genes (Béchet *et al.* 1970). Later, two independent studies suggested that Arg82 carries out the sequential phosphorylation of IP_3 and IP_4 (Saiardi *et al.* 1999; Odom *et al.* 2000). Further, mutational studies demonstrated that the catalytic residues important for the IP kinase activity of Arg82 are dispensable for its function as a transcriptional activator, whereas the residues important for transcriptional activation are dispensable for its function as an IP kinase (Dubois *et al.* 2000, Dubois *et al.* 2002). Hence, Arg82 is a classic example of a moonlighting protein because it uses separate domains to carry out two distinct activities (Gancedo and Flores 2008).

In our screen, the *arg82Δ* mutant reduced telomeric silencing and improved *HMR* silencing (Fig. 2-2B and Fig. 2-2C), while it had no apparent effect on rDNA silencing (Fig. 2-2A). In addition, earlier studies showed that the *arg82Δ* mutant had other chromatin phenotypes, such as sensitivity to DNA damage and telomere lengthening (York *et al.* 2000). These two phenotypes were attributed to the lowered production of IPs and PP-IPs in the *arg82Δ* mutant, although the catalytic mutants of Arg82 were not tested during this study. Curiously, telomere elongation is usually associated with increased silencing (Kyrion 1992). The *arg82Δ* mutant had longer telomeres (York *et al.*

2000) but reduced telomeric silencing (Fig. 2-2B). Therefore, Arg82 might influence telomeric length and telomeric silencing through distinct pathways.

In this chapter, Arg82's functions in telomeric, *HM* silent mating type loci and rDNA silencing were validated with independent methods. In addition, structural-functional analyses were used to determine the domain required for its role in silencing. Moreover, mutants encoding other enzymes in the inositol polyphosphate biosynthetic pathway were assessed for functions in telomeric silencing.

Results

Validation of Arg82's function in *HM* silencing

The initial screen revealed that deletion of *ARG82* enhanced silencing of the *TRP1* reporter integrated at the *HMR* locus because the *arg82Δ hmrΔE::TRP1* did not grow on SC-Trp media (Fig. 2-2C). This was an unexpected result, because this mutant was found to have mating defect (Dubois and Messenguy 1994). To ascertain that the loss of growth on SC-Trp was not due to tryptophan auxotrophy, an *arg82Δ TRP1* strain was constructed. This strain did not exhibit any growth defect on SC-Trp, indicating that the readout of the *hmrΔE::TRP1* reporter assay reflected silencing defect rather than tryptophan auxotrophy (Fig. 3-2A). Therefore, Arg82 is likely to regulate mating and *HM* silencing through distinct mechanisms.

Arg82's effect on the other silent mating-type locus, *HML*, was assessed in an *arg82Δ hml::TRP1* reporter strain. In this strain, the expression of the *TRP1* reporter is normally repressed by silencing at the *HML* locus, causing the WT strain to grow poorly

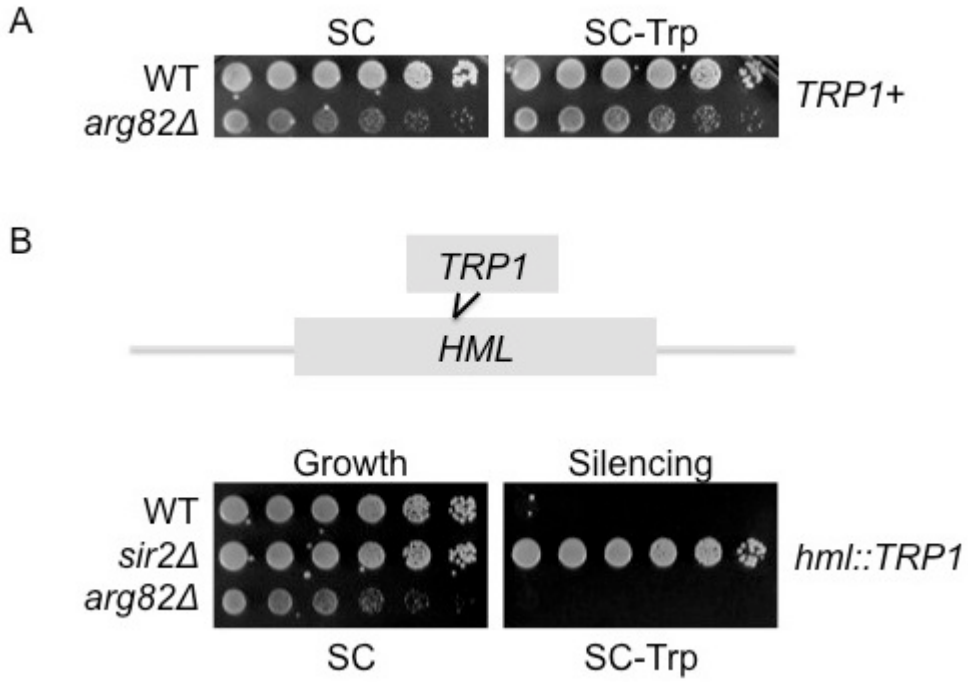

Figure 4-2. Deletion of *ARG82* did not affect growth on SC-Trp or silencing of the *HML* locus. (*A*) Arg82 does not regulate *TRP1* expression outside the context of *HM* silencing. WT *TRP1* (LPY19291) and *arg82Δ TRP1* (LPY19288) strains were plated on SC (control) and SC-Trp (auxotrophy). (*B*) Deletion of *ARG82* did not change *HML* silencing. The WT (LPY254), *sir2Δ* (LPY1401) and *arg82Δ* (LPY20374) strains all carried the *hml::TRP1* reporter. The strains were assayed on SC-Trp (silencing), where increased growth suggests *HML* silencing defect. A starting A_{600} of 5.0 was plated at 5-fold serial dilutions.

on medium lacking tryptophan. Defective silencing, such as that caused by *SIR2* deletion, leads to increased growth on medium without tryptophan. The *arg82Δ* mutant showed similar growth as the WT strain (Fig. 4-2B). It was difficult to dissect if the mutant further enhanced silencing at the *HML* locus because transcription of the *hml::TRP1* reporter was strongly repressed even in the WT background.

Further dissection of Arg82's function in rDNA silencing

The *arg82Δ* strain did not show any rDNA silencing phenotype in the initial screen (Fig. 2-2A). Nevertheless, a low canavanine concentration (8μg/mL) was used for the screen to achieve a stringent cut-off. Ana Lilia Torres Machorro studied the rDNA silencing phenotype of the *arg82Δ* strain on media containing 32μg/mL canavanine, and found that the mutant exhibited silencing defect (Fig. 4-3A). Hence, *ARG82* may also have a role in controlling rDNA silencing at the 5S locus. Notably, the *arg82Δ CAN1* strain is known to have increased resistance to canavanine (Bechet *et al* 1970), thus the readout of the reporter assay might have underestimated Arg82's function in rDNA silencing. Silencing at the rDNA locus is also known to repress the recombination between the repetitive rDNA sequences (Gottlieb and Esposito 1989). The *arg82Δ* strain did not show any change in the rDNA recombination rate (Fig. 4-3B), indicating that Arg82 is not involved in the repression of rDNA recombination.

Arg82 is also required for the repression of an endogenous telomeric transcript

The *TELV-R::URA3* reporter assay showed that Arg82 positively regulates telomeric silencing (Fig. 2-2B). To validate this result, Arg82's effect on an endogenous

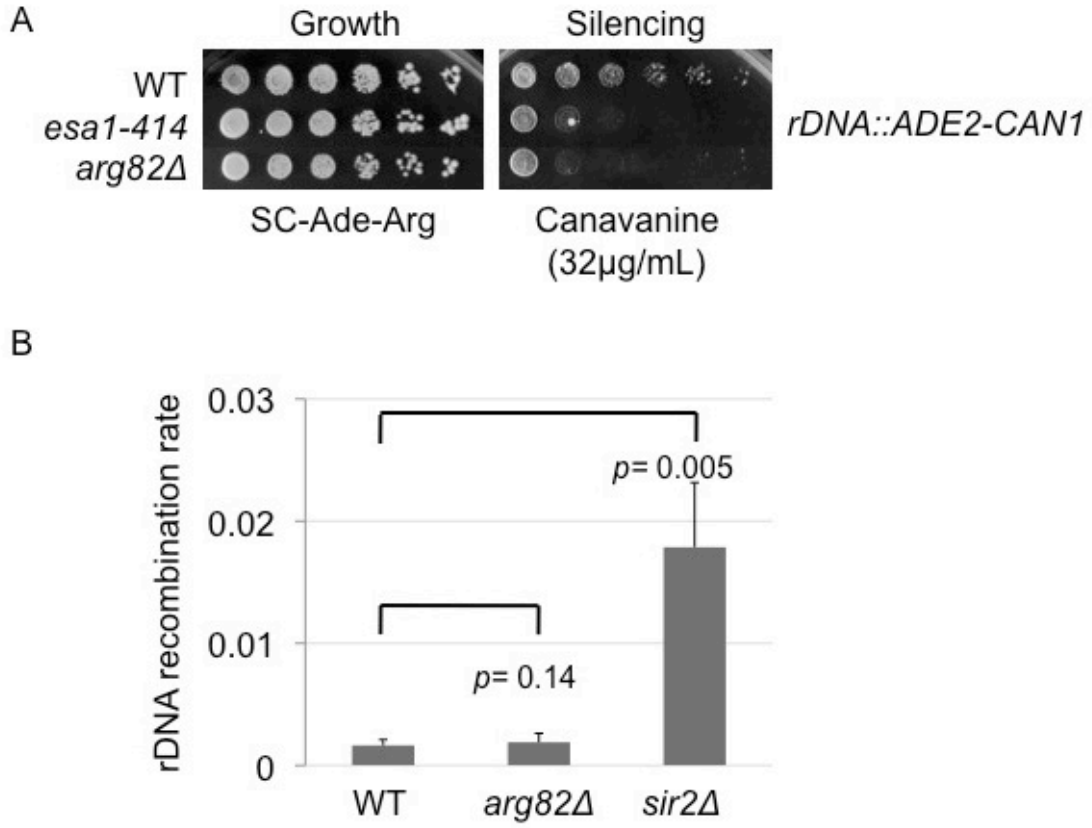

Figure 4-3. Arg82's function in rDNA silencing is revealed by elevated concentration of canavanine. (*A*) The *arg82Δ rDNA::ADE-CAN1* strain was sensitive to 32 µg/mL of canavanine. WT (LPY4909), *esa1-414* (LPY4911) and *arg82Δ* (LPY16022) strains were plated on SC-Ade-Arg + 32 µg/mL canavanine to assess rDNA silencing. The *esa1-414* strain served as a control for defective rDNA silencing. Data was generated by Ana Lilia Torres Machorro. (*B*) Arg82 does not regulate rDNA recombination. rDNA recombination rates of WT(LPY4909), *arg82Δ* (LPY16022) and *sir2Δ* (LPY5013) strains were measured as described in Materials and Methods. The *sir2Δ* strain served as a control for increased rDNA recombination. Data represent averages of three independent experiments.

telomeric gene was studied. The *YFR057W* open reading frame is located close to *TELVI-R* and its transcription is repressed by SIR complex-dependent silencing (Wyrick *et al.* 1999). Deletion of *ARG82* significantly increased the transcript levels of *YFR057W* in the BY4741 background, suggesting that Arg82 also regulates silencing at natural telomeres (Fig. 4-4A). Additionally, when previously published microarray data was compared for the *arg82Δ, sir2Δ, sir3Δ* and *sir4Δ* mutants (Wyrick *et al.* 1999; Worley *et al.* 2013), at least one third of the subtelomeric genes upregulated by each *SIR* deletion was also upregulated in the *arg82Δ* mutant (Fig. 4-4B). This suggests that Arg82 has a significant role in repressing expression of subtelomeric genes. A list of genes co-regulated by the SIR complex and *ARG82* was included in Table 4-1.

Structural- functional analyses of Arg82

Previously, Arg82 was shown to use two separate domains for its transcriptional activator function and for its IP kinase activity (Fig. 4-5A). Amino acids 282-303 were shown to be important for the transcriptional activator function, because the Arg82-Δ282-303 mutant lost its transcriptional activator activity while maintaining the IP kinase activity (Dubois *et al.* 2002). On the other hand, the Asp131 residue of Arg82 is part of the P*XXX*D*X*K*X*G signature motif that forms hydrogen bond with the ADP-ribose group (Holmes and Jogl 2006). The *arg82-D131A* mutation abolished the IP kinase activity of Arg82 both *in vitro* and *in vivo*, while having no effect on the transcriptional activator activity (Dubois *et al.* 2000; Dubois *et al.* 2002). Although these domains were well-defined, few studies have assessed their relative functions in suppressing the myriad of phenotypes of the *arg82Δ* mutant. Therefore, the two mutants were constructed and

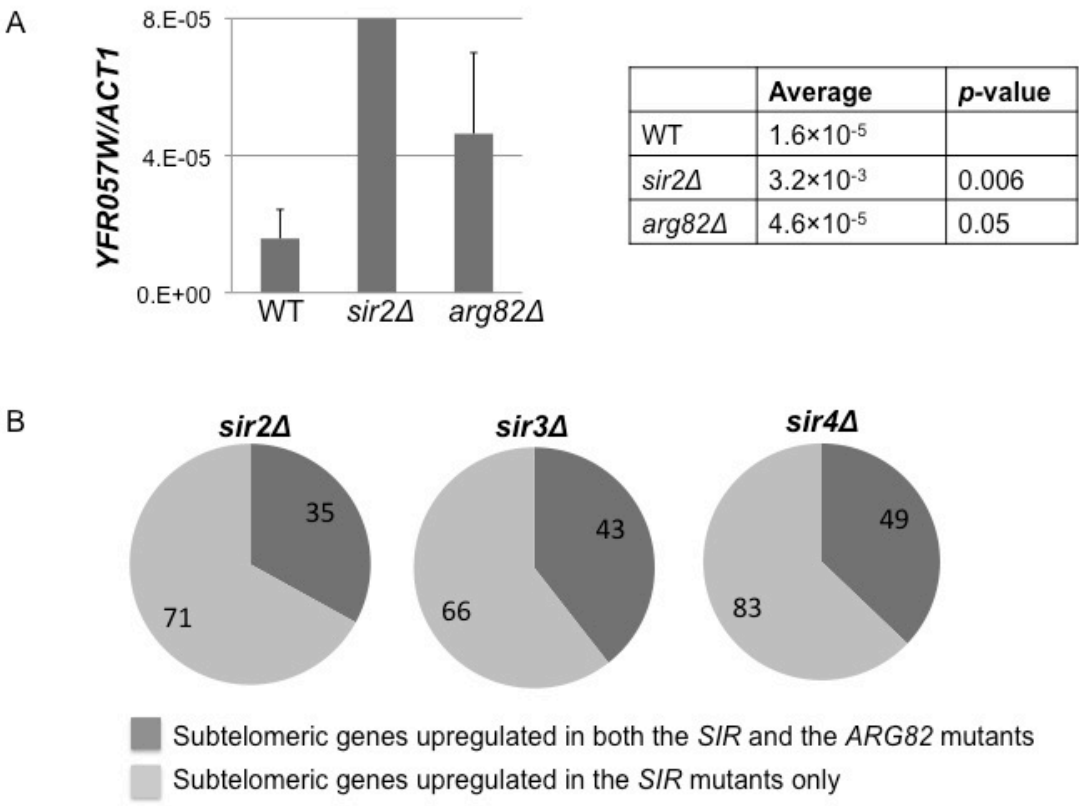

	Average	*p*-value
WT	1.6×10^{-5}	
sir2Δ	3.2×10^{-3}	0.006
arg82Δ	4.6×10^{-5}	0.05

Figure 4-4. Arg82 regulates silencing of endogenous telomeric genes. (*A*) cDNA was prepared from WT BY4741 (LPY6496), *arg82Δ* (LPY15944) and *sir2Δ* (LPY6634) strains as described in Materials and Methods. cDNA was analyzed with primers for the indicated transcripts. Data represent averages of three independent experiments. (*B*) Arg82 and SIR co-regulate silencing of subtelomeric genes. Data was summarized from published microarray data (Wyrick *et al.* 1999; Worley *et al.* 2013). Co-regulated genes were listed in Table 4-1.

Table 4-1. List of subtelomeric genes co-regulated by the *SIR* genes and *ARG82*

SIR	**Subtelomeric genes that are upregulated in both the *SIR* and the *ARG82* mutants**
sir2Δ	*AAD10, ARR1, COS1, COS3, COS4, COS5, COS6, COS8, FET4, GIT1, LYS1, PHO11, THI5, YAR064W, YAR068W, YAR070C, YCR101C, YDR543C, YEL074W, YEL075C, YER189W, YFL061W, YFL063W, YFL065C, YFL067W, YGR294W, YHL049C, YHR218W, YIR042C, YJR162C, YLR465C, YNL337W, YNR077C, YOR392W, YPR202W*
sir3Δ	*ARR1, CHA1, COS1, COS3, COS4, COS5, COS8, FET4, GIT1, HXK1, LYS1, PHO11, THI5, YAR064W, YAR068W, YAR069C, YAR070C, YBL107C, YDR542W, YDR543C, YDR544C, YEL070W, YEL074W, YEL076C, YER189W, YFL063W, YFL064C, YFL068W, YGR294W, YHL044W, YHL049C, YHR218W, YIR042C, YJR162C, YKL222C, YLR465C, YNL335W, YNL337W, YNR077C, YOR392W, YPR196W, YPR202W, YPR203W*
sir4Δ	*AAD10, ARR1, CHA1, COS1, COS3, COS4, COS5, COS6, COS8, COS9, FET4, GIT1, LYS1, MAL31, MAL33, PAU3, PHO11, PHO12, PHO89, RPN12, THI5, YAL069W, YAR062W, YAR064W, YAR066W, YAR069C, YAR070C, YBL107C, YCR101C, YDL247W, YDR543C, YEL070W, YER185W, YER186C, YER189W, YGR293C, YHL044W, YHL049C, YHR217C, YHR218W, YIR042C, YJR160C, YJR162C, YKL223W, YLR463C, YNL335W, YNL337W, YNR077C, YPR202W*

and expressed on a plasmid in the *arg82Δ* strains. The *arg82-Δ282-303* mutant fully rescued the slow growth, the DNA damage sensitivity and the temperature sensitivity of the *arg82Δ* mutant (Fig. 4-5B), indicating that Arg82's role as a transcriptional activator is not needed for the respective cellular functions. The *arg82-Δ282-303* mutant also rescued the *HM* and telomeric silencing defects of the *arg82Δ* mutant (Fig. 4-5C), suggesting that the transcriptional activator function of Arg82 does not contribute to its role in silencing.

The *arg82-D131A* mutant fully suppressed the slow growth phenotype of the *arg82Δ* mutant. In addition, it partially suppressed the mutant's sensitivities to high temperature, and DNA damage, as measured by growth on HU and MMS. This finding suggests that the IP kinase activity of Arg82 is necessary but not sufficient for its role in damage and heat responses. Further, the *arg82-D131A* mutant did not rescue the *HM* silencing defect of the *arg82Δ* mutant (Fig. 4-5), suggesting that the IP kinase activity of Arg82 is required for its role in *HM* silencing. Surprisingly, the *arg82-D131A* mutant rescued the telomeric silencing phenotype of the *arg82Δ* mutant (Fig. 4-5). This result suggests that Arg82 may have a thus-far undefined domain for the regulation of telomeric silencing.

Analyzing the effects of genes encoding other IP metabolic enzymes

As an independent approach to examine Arg82's function in silencing, null mutants were generated for other IP kinase metabolic genes. The *plc1Δ* and the *kcs1Δ* mutants exhibited sensitivity to high temperature HU and MMS, whereas the *vip1Δ* and *ipk1Δ* mutants did not (Fig. 4-6A). This result suggests that the production of PP-IP_4 is

Figure 4-5. Arg82 uses different domains for different functions. (*A*) Diagram showing the two domains required for the two distinct activities of Arg82. (*B*) The two domains of Arg82 are required for different functions of Arg82. The WT (LPY4916) and *arg82Δ* (LPY16036) strains carried the *TELV-R::URA3* reporter. They were transformed with empty vector (pRS315), pRS315-*ARG82* (pLP3313), pRS315-*arg82-D131A* (pLP3315), and pRS315-*arg82-Δ282-303* (pLP3314). The transformants were plated on the indicated media to measure temperature sensitivity, damage sensitivity and telomeric silencing. All plates used in this figure were SC-Leu. (*C*) The IP kinase domain of Arg82 regulates *HMR* silencing. The WT(LPY4913) and *arg82Δ* (LPY17130) strains carried the *hmrΔE::TRP1* reporter. The strains were transformed with the same plasmids as (*B*) and were plated on SC-Leu-Trp to assess silencing.

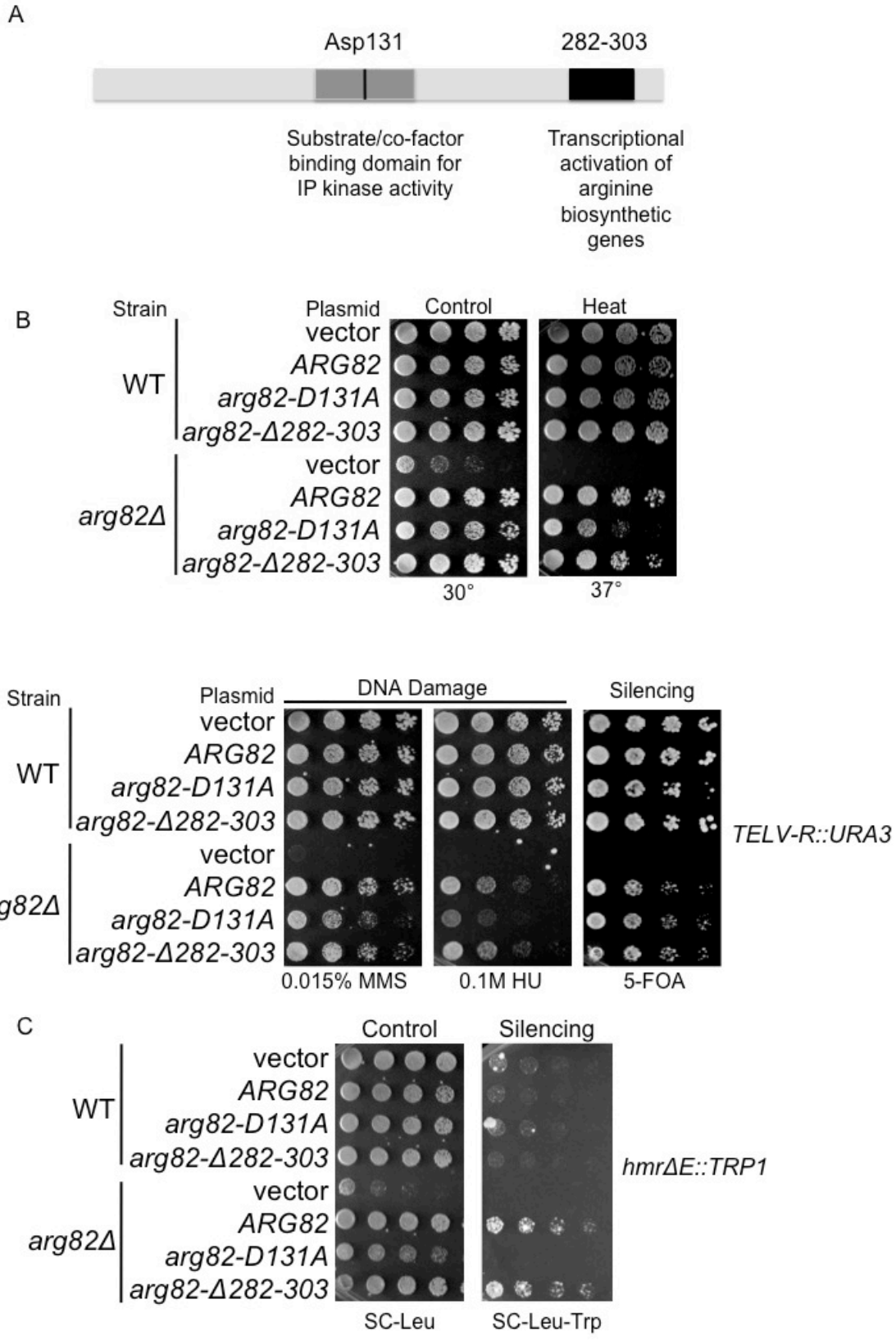
A
Asp131
282-303
Substrate/co-factor binding domain for IP kinase activity
Transcriptional activation of arginine biosynthetic genes
B
Strain
Plasmid
Control
Heat
WT
arg82Δ
vector
ARG82
arg82-D131A
arg82-Δ282-303
30°
37°
Strain
Plasmid
DNA Damage
Silencing
0.015% MMS
0.1M HU
5-FOA
TELV-R::URA3
C
Control
Silencing
SC-Leu
SC-Leu-Trp
hmrΔE::TRP1

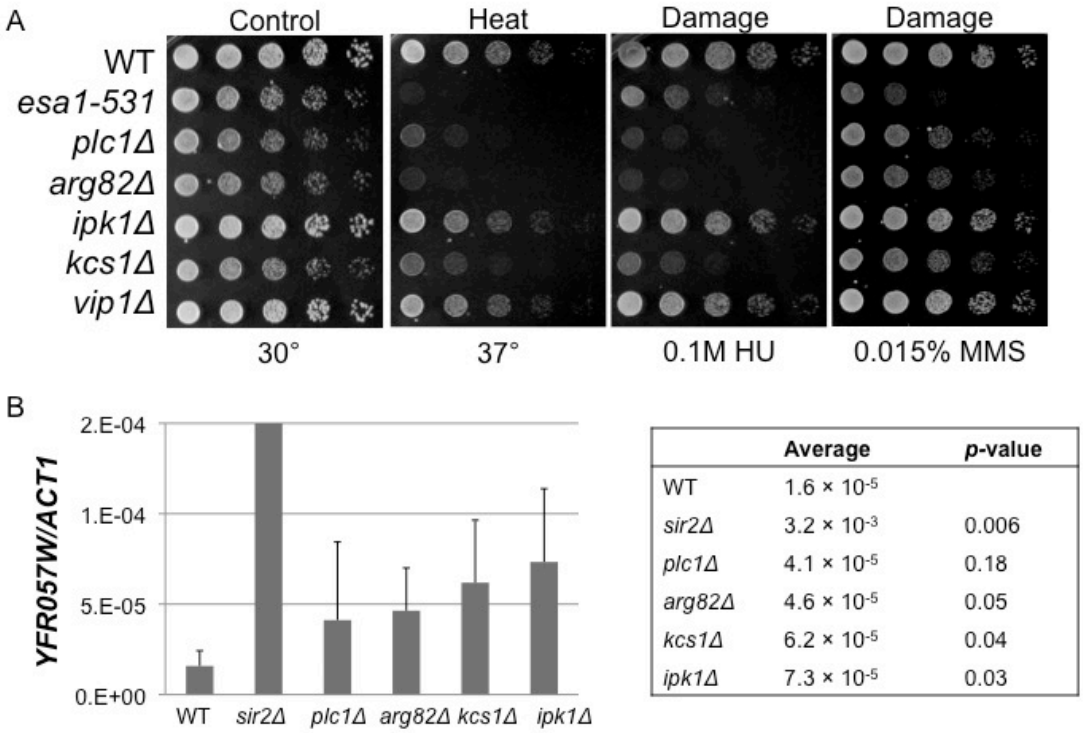

	Average	*p*-value
WT	1.6×10^{-5}	
sir2Δ	3.2×10^{-3}	0.006
plc1Δ	4.1×10^{-5}	0.18
arg82Δ	4.6×10^{-5}	0.05
kcs1Δ	6.2×10^{-5}	0.04
ipk1Δ	7.3×10^{-5}	0.03

Figure 4-6. Different IP kinase mutants exhibited different subsets of phenotypes. (*A*) Like Arg82, Plc1 and Kcs1 are involved in responding to heat and DNA damage stress. The WT (LPY6496), *esa1-531* (LPY14758), *plc1Δ* (LPY14140), *arg82Δ* (LPY15944), *ipk1Δ* (LPY16573), *kcs1Δ* (LPY17057), *vip1Δ* (LPY17128) strains were plated on SC-based media to assess sensitivity to heat and damage. The *esa1-531* strain served as a control for increased sensitivity to heat and damage. (*B*) cDNA was prepared from strain in (*A*) and *sir2Δ* (LPY6634) as described in Materials and Methods. cDNA was analyzed with primers for the indicated transcripts. Data represent averages of 2-3 independent experiments.

likely to be important for coping with heat stress and DNA damage.

In addition, all of the IP kinase mutants were defective for silencing the subtelomeric *YFR057W* gene (Fig. 4-6B). This is in contrast to the finding that the IP kinase domain of Arg82 was dispensable for its role in telomeric silencing (Fig. 4-5B). Therefore, future work is needed to fully understand the role of IP kinase metabolism in chromatin regulation.

Discussion

In Chapter 5, further evidence was presented to support Arg82's role in *HM,* telomeric and rDNA silencing. Suppression analysis using the two Arg82 mutants revealed that the different domains of Arg82 are required to respond to various stresses, and for silencing functions. Analysis of additional mutants in the IP kinase metabolic pathway showed that the PP-IP_4 not the PP-IP_5 pathway is required for responding to DNA damage, whereas both pathways are needed for regulating telomeric silencing.

Arg82's function in *HM* silencing

Arg82's function in *HMR* silencing was shown to be dependent on the catalytic residue of its IP kinase activity (Fig. 4-5C). Interestingly, an earlier study suggested that *HMR* silencing was elevated in the *plc1Δ* mutant. This phenotype was attributed to an effect of Plc1 on the expression of *HXT* genes involved in glucose metabolism and acetyl-CoA synthesis (Galdieri *et al.* 2013). It is likely that Arg82 controls *HMR* silencing through a similar pathway. To test this idea, genetic manipulations that restore *HMR* silencing in the *plc1Δ* mutant could be applied to the *arg82Δ* mutant. For example,

deletion of an HDAC encoded by *HDA1*, or deletion of a *HXT* transcriptional repressor encoded by *MTH1* was shown to suppress the *HM* silencing phenotype of the *plc1Δ* mutant. Construction of the *arg82Δ hda1Δ* and *arg82Δ mth1Δ* double mutants would help to assess whether Arg82 and Plc1 regulate *HMR* silencing through the same molecular pathway.

Arg82's function in telomeric silencing

Asp131, the catalytic residue for the IP kinase activity of Arg82 was shown to be dispensable for the silencing of the telomeric reporter gene (Fig. 4-5B). Intriguingly, deletion of other genes in the IP metabolic pathway also de-repressed the transcription of the subtelomeric *YFR057W* gene (Fig. 4-6A). These two results seemingly contradict each other, as the former suggests that the IP metabolic pathway is not required for telomeric silencing, whereas the latter suggests that it is.

One possible explanation for these results is that a feedback mechanism exists for the IP metabolic pathway, such that cells respond to the deletion of downstream genes by down-regulating the activity or expression of Arg82. This idea could be assessed by measuring *ARG82* mRNA levels or IP_4 and IP_5 levels in the other IP kinase mutants. Another possible explanation is that the D131A mutation did not fully abolish Arg82's IP kinase function in the W303 background. This idea could be tested by examining known gene targets of the IP kinase pathway in the presence of the D131A mutant. Also, other kinase mutants of Arg82 could be used to validate the result of the D131A mutant.

Another general direction that could be pursued is the search for the chromatin modifying complex(es) that coordinate Arg82's effect on telomeric silencing. For

example, Sir protein levels and binding at the telomeres should be assessed in the *arg82Δ* mutant. Additionally, IP kinases have been associated with various HDACs in the literature. For example, IP_4 was shown to act as a molecular 'glue' promoting the interaction between HDAC3 and SMRT in mammalian cells (Watson *et al.* 2012). Also, PP-IPs were found to activate the activity of the Rpd3L complex in response to environmental stress in budding yeast (Worley *et al.* 2013). Further, Plc1 was found to regulate *HM* silencing in a HAT-dependent manner, as mentioned earlier (Galdieri *et al.* 2013). Since multiple HDACs are known to regulate telomeric silencing, genetic interactions between *ARG82* and different *HDAC*s should be assessed.

Arg82's function in general stress response

The mutational analysis suggested that the catalytic residue for IP kinase activity was only partially required for Arg82's function in heat and DNA damage stress response. Although the D131A mutant was established to abolish the IP kinase activity of Arg82 (Dubois *et al.* 2002), it is possible that compensating enzymes or pathways exist in the strain backgrounds we used. Therefore, it is important to validate the results with independent kinase mutants of Arg82.

Arg82's function in rDNA silencing

In the experiment performed by Ana Lilia Torres Macchorro, the *arg82Δ* mutant was shown to exhibit an rDNA silencing defect when the reporter strain was challenged with a higher concentration of canavanine (Fig. 4-3A). Interestingly, the *arg82Δ* mutant was shown to have increased resistance to canavanine when *CAN1* is at its endogenous locus (Bechet *et al.* 1970). Therefore, the *arg82Δ* mutant may have a stronger rDNA

silencing phenotype than that portrayed by the *CAN1*-based reporter assay. To fully assess Arg82's role in rDNA silencing, other silencing assays should be used, such as using a non-*CAN1*-based reporter system, or measuring the binding of SIR proteins at the rDNA locus.

Materials and Methods

Yeast strains and plasmids

Strains, plasmids and oligos used in this study are listed in Tables 5-2, 5-3 and 5-4, respectively. The BY4741 haploid strains used for *YFR057W* expression analysis were obtained by dissecting heterozygous diploid strains from the Resgen collection (Winzeler *et al*. 1999). The *ARG82* open reading frame, together with its native promoter and 3' untranslated regions was amplified from the yeast tiling library plasmid with 5'-phosphorylated oLP1541 and oLP1552. The PCR product was cloned into pRS315 to generate pLP3133. The *arg82*-D131A and the *arg82-Δ282-303* mutants were generated by overlapping PCR, using oligos listed in Table 4-3, and cloned into pRS315 to generate pLP3135 and pLP3134, respectively.

Dilution assays for growth and silencing

Strains were grown in 3mL SC for 2 days before plating. The exception is the rDNA silencing assays, for which the starter cultures were grown in 3mL of SC-Ade-Arg. Unless otherwise stated, dilution assays represent 5-fold serial dilutions, starting from an A_{600} of 1.0. Plates were incubated at 30° and images were captured after 3-5 days of growth.

Measurement of the rDNA recombination rate

Strains were grown in SC-Ade-Arg and harvested at A_{600} of 0.8-1. 400-500 cells were plated on YPAD, incubated at 30° for 2 days, and subsequently moved to 4° to promote color development. 1500-2500 colonies were assessed for each strain. Half-sectored colonies originated from cells that had lost the *ADE2* reporter after the first mitotic division. Recombination rate was calculated as the number of half-sectored colonies divided by the total number of colonies.

RNA extraction

2-day old starter cultures were diluted in 50mL SC medium and grown overnight until reaching A_{600} of 0.8-1.0. RNA was extracted as described (Collart and Oliviero 2001), with the adaptation that the harvested cells were resuspended in sodium acetate buffer (50mM sodium acetate pH5.3, 10mM EDTA). RNA was reverse transcribed with random hexamers using TaqMan Reverse Transcription Reagents. cDNA was diluted 5-fold and analyzed by real-time PCR on DNA Engine Opticon 2 with oligos for *YFR057W* and *ACT1*.

Acknowledgements

Ana Lilia Torres Machorro generated the data for Fig. 4-3A.

Table 4-2. Yeast strains used in Chapter 4

Strain	Genotype	Source /Reference
LPY5 (W303-1a)	*MATa ade2-1 can1-100 his3-11,15 leu2-3,112 trp1-1 ura3-1*	R. Rothstein
LPY254	W303 *MATα hml::TRP1*	R. Sternglanz
LPY1401	W303 *MATa hml::TRP1 sir2Δ::HIS3*	
LPY4909	W303 *MATα rDNA::ADE2-CAN1*	Clarke *et al.* 2006
LPY4911	W303 *MATα esa1-414 rDNA::ADE2-CAN1*	Clarke *et al.* 2006
LPY4913	W303 *MATα hmrΔE::TRP1*	Clarke *et al.* 2006
LPY4916	W303 *MATa TELV-R::URA3*	Clarke *et al.* 2006
LPY5013	W303 *MATα sir2Δ::HIS3 rDNA::ADE2-CAN1*	
LPY6496	*MATa his3Δ1 leu2Δ0 LYS2 MET15 ura3Δ0*	
LPY6634	*MATa his3Δ1 leu2Δ0 LYS2 MET15 ura3Δ0 sir2Δ::kanMX*	
LPY14140	*MATa his3Δ1 leu2Δ0 LYS2 MET15 ura3Δ0 plc1Δ::kanMX*	
LPY14758	*MATα his3Δ1 leu2Δ0 LYS2 MET15 ura3Δ0 esa1Δ::kanMX* + CEN *URA3 esa1-531*	
LPY15944	*MATa his3Δ1 leu2Δ0 LYS2 MET15 ura3Δ0 arg82Δ::kanMX*	
LPY16022	W303 *MATα arg82Δ::kanMX rDNA::ADE2-CAN1*	
LPY16036	W303 *MATα arg82Δ::kanMX TELV-R::URA3*	
LPY16573	*MATα his3Δ1 leu2Δ0 LYS2 MET15 ura3Δ0 ipk1Δ::kanMX*	
LPY17057	*MATa his3Δ1 leu2Δ0 LYS2 MET15 ura3Δ0 kcs1Δ::kanMX*	
LPY17128	*MATa his3Δ1 leu2Δ0 LYS2 MET15 ura3Δ0 vip1Δ::kanMX*	
LPY17130	W303 *MATα hmrΔE::TRP1 arg82Δ::kanMX*	
LPY19288	W303 *MATα arg82Δ::kanMX TRP1*	
LPY19291	W303 *MATα TRP1*	
LPY20374	W303 *MATa arg82Δ::kanMX hml::TRP1*	

Note: Unless otherwise stated, all strain used in Chapter 4 were made during this study or part of the standard lab collection.

Table 4-3. Plasmids used in Chapter 4

Plasmid #	Description
pRS315	Vector, CEN, *LEU2*
pLP3313	pRS315- *ARG82*
pLP3314	pRS315- *arg82-Δ282-303*
pLP3315	pRS315- *arg82-D131A*

Table 4-4. Oligonucleotides used in Chapter 4

Oligo #	Name	Sequence
798	*ACT1*_For	GGTGGTTCTATCTTGGCTTC
799	*ACT1*_Rev	ATGGACCACTTTCGTCGTAT
1541	*ARG82*-3'UTR	GAAGCTCCAGTTTGTGTGG
1552	*ARG82*-5'-1.1kb	CCGGATCCTCCAAGGAAAGCTGGTGGTAG
1815	*YFR057W*_For	CTAGTGTCTATAGTAAGTGCTCGG
1816	*YFR057W*_Rev	CTCTAACATAACTTTGATCCTTACTCG
2104	*arg82-D131A*_For	CCTAATATACTTGCAATAAAATTAGGC
2105	*arg82-D131A*_Rev	GCCTAATTTTATTGCAAGTATATTAGG
2106	*arg82-Δ282-303*_For	GACAAACTTATGCGAGGAAGCAGCGAAGG
2107	*arg82-Δ282-303*_Rev	CCTTCGCTGCTTCCTCGCATAAGTTTGTC

References

Bechet J, Greenson M, Wiame JM. 1970. Mutations affecting the repressibility of arginine biosynthetic enzymes in Saccharomyces cerevisiae. *Eur J Biochem* **12**: 31-39.

Clarke AS, Samal E, Pillus L. 2006. Distinct roles for the essential MYST family HAT Esa1p in transcriptional silencing. *Mol Biol Cell* **17**: 1744-1757.

Desai P, Guha N, Galdieri L, Hadi S, Vancura A. 2009. Plc1p is required for proper chromatin structure and activity of the kinetochore in Saccharomyces cerevisiae by facilitating recruitment of the RSC complex. *Mol Genet Genomics* **281**: 511-523.

Dubois E, Dewaste V, Erneux C, Messenguy F. 2000. Inositol polyphosphate kinase activity of Arg82/ArgRIII is not required for the regulation of the arginine metabolism in yeast. *FEBS Lett* **486**: 300-304.

Dubois E, Messenguy F. 1994. Pleiotropic function of ArgRIIIp (Arg82p), one of the regulators of arginine metabolism in Saccharomyces cerevisiae. Role in expression of cell-type-specific genes. *Mol Gen Genet* **243**: 315-324.

Dubois E, Scherens B, Vierendeels F, Ho MM, Messenguy F, Shears SB. 2002. In Saccharomyces cerevisiae, the inositol polyphosphate kinase activity of Kcs1p is required for resistance to salt stress, cell wall integrity, and vacuolar morphogenesis. *J Biol Chem* **277**: 23755-23763.

Galdieri L, Chang J, Mehrotra S, Vancura A. 2013. Yeast phospholipase C is required for normal acetyl-CoA homeostasis and global histone acetylation. *J Biol Chem* **288**: 27986-27998.

Galdieri L, Chang J, Mehrotra S, Vancura A. 2013. Yeast phospholipase C is required for normal acetyl-CoA homeostasis and global histone acetylation. *J Biol Chem* **288**: 27986-27998.

Gancedo C, Flores CL. 2008. Moonlighting proteins in yeasts. *Microbiol Mol Biol Rev* **72**: 197-210.

Hanakahi LA, Bartlet-Jones M, Chappell C, Pappin D, West SC. 2000. Binding of inositol phosphate to DNA-PK and stimulation of double-strand break repair. *Cell* **102**: 721-729.

Holmes W, Jogl G. 2006. Crystal structure of inositol phosphate multikinase 2 and implications for substrate specificity. *J Biol Chem* **281**: 38109-38116.

Kyrion G, Boakye KA, Lustig AJ. 1992. C-terminal truncation of RAP1 results in the deregulation of telomere size, stability, and function in Saccharomyces cerevisiae. *Mol Cell Biol* **12**: 5159-5173.

Odom AR, Stahlberg A, Wente SR, York JD. 2000. A role for nuclear inositol 1,4,5-trisphosphate kinase in transcriptional control. *Science* **287**: 2026-2029.

Saiardi A, Erdjument-Bromage H, Snowman AM, Tempst P, Snyder SH. 1999. Synthesis of diphosphoinositol pentakisphosphate by a newly identified family of higher inositol polyphosphate kinases. *Curr Biol* **9**: 1323-1326.

Watson PJ, Fairall L, Santos GM, Schwabe JW. 2012. Structure of HDAC3 bound to co-repressor and inositol tetraphosphate. *Nature* **481**: 335-340.

Winzeler EA, Shoemaker DD, Astromoff A, Liang H, Anderson K, Andre B, Bangham R, Benito R, Boeke JD, Bussey H et al. 1999. Functional characterization of the S. cerevisiae genome by gene deletion and parallel analysis. *Science* **285**: 901-906.

Worley J, Luo X, Capaldi AP. 2013. Inositol pyrophosphates regulate cell growth and the environmental stress response by activating the HDAC Rpd3L. *Cell Rep* **3**: 1476-1482.

Wyrick JJ, Holstege FC, Jennings EG, Causton HC, Shore D, Grunstein M, Lander ES, Young RA. 1999. Chromosomal landscape of nucleosome-dependent gene expression and silencing in yeast. *Nature* **402**: 418-421.

York SJ, Armbruster BN, Greenwell P, Petes TD, York JD. 2005. Inositol diphosphate signaling regulates telomere length. *J Biol Chem* **280**: 4264-4269.

Tyrosine phosphorylation of histone H2A by CK2 regulates transcriptional elongation

Harihar Basnet[1,2], Xue B. Su[3], Yuliang Tan[1], Jill Meisenhelder[5], Daria Merkurjev[1,4], Kenneth A. Ohgi[1], Tony Hunter[5], Lorraine Pillus[3] & Michael G. Rosenfeld[1]

Post-translational histone modifications have a critical role in regulating transcription, the cell cycle, DNA replication and DNA damage repair[1]. The identification of new histone modifications critical for transcriptional regulation at initiation, elongation or termination is of particular interest. Here we report a new layer of regulation in transcriptional elongation that is conserved from yeast to mammals. This regulation is based on the phosphorylation of a highly conserved tyrosine residue, Tyr 57, in histone H2A and is mediated by the unsuspected tyrosine kinase activity of casein kinase 2 (CK2). Mutation of Tyr 57 in H2A in yeast or inhibition of CK2 activity impairs transcriptional elongation in yeast as well as in mammalian cells. Genome-wide binding analysis reveals that CK2α, the catalytic subunit of CK2, binds across RNA-polymerase-II-transcribed coding genes and active enhancers. Mutation of Tyr 57 causes a loss of H2B mono-ubiquitination as well as H3K4me3 and H3K79me3, histone marks associated with active transcription. Mechanistically, both CK2 inhibition and the H2A(Y57F) mutation enhance H2B deubiquitination activity of the Spt-Ada-Gcn5 acetyltransferase (SAGA) complex, suggesting a critical role of this phosphorylation in coordinating the activity of the SAGA complex during transcription. Together, these results identify a new component of regulation in transcriptional elongation based on CK2-dependent tyrosine phosphorylation of the globular domain of H2A.

To assess potential tyrosine phosphorylation events in H2A, we individually mutated every tyrosine residue in H2A to phenylalanine and expressed the mutants in 293T cells. Mutation of Tyr 39 and Tyr 57 resulted in a decrease in tyrosine phosphorylation compared to the wild-type protein, indicating that these residues might be phosphorylated (Fig. 1a). Mass spectrometry confirmed phosphorylation of these residues in histone extracts from 293T cells (Supplementary Table 1). The Tyr 57 residue, along with neighbouring residues, is conserved from yeast to mammals (Fig. 1b), and is present in all variants of H2A (Extended Data Fig. 1a). In budding yeast, where genetic manipulation of histones is possible, mutation of the corresponding residue to alanine is lethal, suggesting a critical structural and/or functional contribution of this tyrosine residue[2,3]. Analysis of histones in wild-type mononucleosomes and those containing the H2A(Y57F) mutant showed similar stoichiometry, suggesting that the Y57F mutation is unlikely to affect the structural integrity of nucleosomes (Extended Data Fig. 1b). Hence, we tested whether the structurally conservative substitution of tyrosine with phenylalanine would

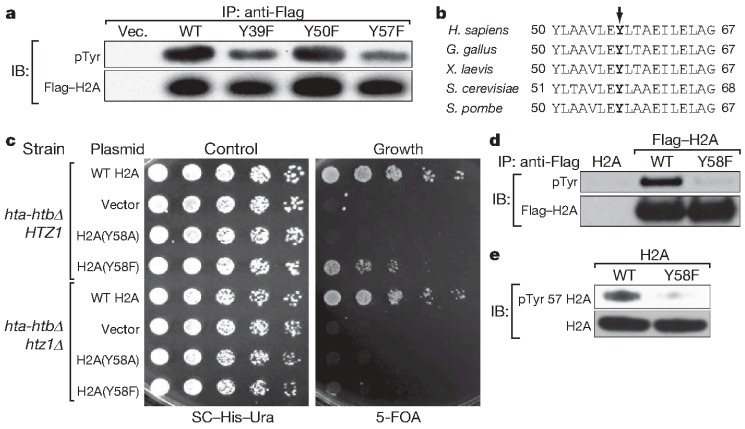

Figure 1 | The conserved Tyr 57 residue in H2A is phosphorylated. **a**, Tyr 57 in H2A is phosphorylated in 293T cells. Flag-tagged H2A mutants were expressed in 293T cells, immunoprecipitated (IP) under denaturing conditions, and immunoblotted (IB) as indicated. Vec., vector; WT, wild type. **b**, Tyr 57 in H2A is highly conserved. Comparison of H2A sequence surrounding the Tyr 57 residue (arrow) in different organisms. *H.*, *Homo*; *G.*, *Gallus*; *X.*, *Xenopus*; *S.*, *Saccharomyces* (for *cerevisiae*); *S.*, *Schizosaccharomyces* (for *pombe*). **c**, Tyr 58 in H2A is functionally important in yeast. Fivefold serial dilutions of the yeast strains lacking H2A (*hta*) and H2B (*htb*) but containing pJH33 (*HTA1-HTB1 HHF2-HHT2 URA3* CEN) were transformed as indicated, and the transformants were plated on SC (synthetic complete supplement)–His–Ura for growth control and 5-fluoroorotic acid (5-FOA) for the removal of pJH33. **d**, **e**, Tyr 58 in H2A is phosphorylated in *S. cerevisiae*. **d**, Flag-tagged wild-type H2A and H2A(Y58F) were immunoprecipitated under denaturing conditions and immunoblotted as indicated. **e**, Whole-cell extracts from yeast strains were prepared under denaturing conditions and immunoblotted as indicated. Data represent three independent experiments.

[1]Howard Hughes Medical Institute, Department of Medicine, University of California San Diego, La Jolla, California 92093, USA. [2]Biomedical Sciences Graduate Program, School of Medicine, University of California San Diego, La Jolla, California 92093, USA. [3]Division of Biological Sciences, Section of Molecular Biology, UCSD Moores Cancer Center, University of California San Diego, La Jolla, California 92093-0347, USA. [4]Bioinformatics and Systems Biology Program, Department of Bioengineering, University of California San Diego, La Jolla, California 92093, USA. [5]Molecular and Cell Biology Laboratory, Salk Institute for Biological Studies, La Jolla, California 92037, USA.

produce a different phenotype in yeast. Tyr 58 in yeast H2A corresponds to Tyr 57 in mammalian H2A. The H2A(Y58F) mutant was viable and exhibited a slow growth phenotype (Fig. 1c). Notably, the same mutation proved to be lethal in the *HTZ1* (the gene encoding H2AZ (also known as H2AFZ)) null background, and double mutation of the tyrosine residue in both H2A and H2AZ resulted in an extremely slow growth phenotype (Fig. 1c and Extended Data Fig. 1c). Next, we tested if this site is phosphorylated in yeast. Immunoprecipitated Flag-tagged H2A(Y58F) showed reduced tyrosine phosphorylation compared to the wild-type protein (Fig. 1d), suggesting that this residue is phosphorylated.

To confirm Tyr 57 phosphorylation and investigate its function, an antibody specific for phosphorylated Tyr (pTyr) 57 H2A was developed. This antibody detected proteins corresponding to the size of H2A and ubiquitinated H2A in 293T cells (Extended Data Fig. 1d). Peptide blocking assays and dot blot assays verified the specificity of the antibody and treatment with calf intestinal phosphatase further validated its phospho-specificity (Extended Data Fig. 1d–f). Use of this antibody confirmed Tyr 58 phosphorylation in yeast H2A (Fig. 1e). Collectively, these results demonstrate that Tyr 57 in H2A is phosphorylated and that this phosphorylation is conserved from yeast to mammals.

To identify the kinase(s) that mediate(s) phosphorylation of Tyr 57 in H2A in mammals, we performed mass spectrometry analysis of proteins interacting with H2A in 293T cells. To be consistent with yeast, we used H2AX (also known as H2AFX), a common H2A variant that has closer sequence homology to yeast H2A, for co-immunoprecipitation and *in vitro* kinase assays. Mass spectrometry data revealed that the CK2α catalytic subunit of CK2 interacts preferentially with H2A(Y57F) compared to wild-type H2A (Supplementary Table 2). This interaction was further verified by immunoblotting, which revealed a higher level of CK2α associated with H2A(Y57F) (Fig. 2a). One implication of this interaction is that CK2 may phosphorylate Tyr 57 in H2A, and the Y57F mutation stabilizes the enzyme–substrate interaction, analogous to substrate trapping approaches that have been successfully used to identify substrates of tyrosine phosphatases[4]. Although CK2 is considered primarily to be a Ser/Thr kinase, two studies have reported its tyrosine phosphorylation activity, thus implicating it as a dual-specificity kinase[5,6]. To investigate the potential roles of CK2 in H2A Tyr 57 phosphorylation, we tested whether CK2α phosphorylates the tyrosine residue (Tyr 57) in H2A in an *in vitro* assay using full-length H2A or nucleosomes. The kinase assay revealed that CK2α phosphorylates Tyr 57 in H2A, acting preferentially in the context of nucleosomes (Fig. 2b). This phosphorylation was inhibited by tetrabromobenzimidazole (TBBz), a chemical inhibitor of CK2[7]. To further establish the tyrosine kinase activity of CK2α, we performed phosphoamino acid analysis (PAA) of phosphorylated H2A from nucleosomes using [γ-^{32}P]ATP. We found that CK2α phosphorylates tyrosine as well as serine residues in H2A, but does not phosphorylate threonine residues, and that Tyr 57 is a phosphorylation site, as demonstrated by the reduced tyrosine phosphorylation in H2A(Y57F) compared to wild-type H2A (Extended Data Fig. 2a).

Next we investigated whether CK2 is necessary for H2A Tyr 57 phosphorylation *in vivo*. CK2α knockdown in 293T cells reduced the level of Tyr 57 phosphorylation in H2A (Fig. 2c), supporting an *in vivo* role of CK2α in regulating this phosphorylation. Moreover, a dose-dependent decrease in H2A Tyr 57 phosphorylation was observed upon treatment with TBBz (Fig. 2d), further supporting the role of CK2 in Tyr 57 phosphorylation in H2A. Together, these results provide strong evidence for a function of CK2 in H2A Tyr 57 phosphorylation.

To investigate the physiological significance of Tyr 57 phosphorylation in H2A, we examined in yeast the impact of the H2A(Y58F) mutation on other important histone marks. We found that the H2A(Y58F) mutation resulted in a loss of H2B mono-ubiquitination, as well as trimethylation of H3K4 and H3K79 (Fig. 3a). H3K27 acetylation showed a modest increase, and all other histone modifications tested were unaffected (Extended Data Fig. 3a). Notably, the Y57F mutation also lowered the level of H2A mono-ubiquitination in 293T cells (Extended Data Fig. 3b, c). The role of H2A Tyr 58 phosphorylation as a potential regulator of H2B mono-ubiquitination is of particular significance because this modification has an established role in transcriptional elongation[8,9], thus potentially linking H2A Tyr 58 phosphorylation to transcriptional elongation. Further, yeast with the H2A(Y58F) mutation exhibited increased sensitivity to 6-azauracil (Extended Data Fig. 3d), indicating a defect in transcriptional elongation[10].

To assess the role of Tyr 58 phosphorylation in transcriptional elongation, binding of RNA polymerase II (Pol II) in actively transcribed genes was evaluated by chromatin immunoprecipitation (ChIP) followed by quantitative real-time polymerase chain reaction (qPCR). Pol II binding was reduced in the gene body of a housekeeping gene, *PYK1*, as well as a number of heat-shock-induced genes[11] upon heat shock in the H2A(Y58F) mutant (Fig. 3b). Pol II binding was further reduced in H2A(Y58F) and H2AZ(Y65F) mutants (Fig. 3b). The decrease in Pol II binding in the H2A(Y58F) mutant was not due to reduced Pol II expression (Extended Data Fig. 3e). Consistent with the defect in transcriptional elongation, a decreased level of messenger RNA of the corresponding genes was observed in H2A(Y58F) mutants (Extended Data Fig. 3f), whereas H2AZ(Y65F) mutation alone caused only a mild defect in transcription of heat-shock-induced genes (Extended Data Fig. 3g). Furthermore, in 293T cells, H2A Tyr 57 phosphorylation, like H2B mono-ubiquitination, was correlated with transcriptional elongation events, as demonstrated when transcriptional elongation was blocked with flavopiridol treatment[12], and induced by washing out the drug (Extended Data Fig. 3h). H3K4me2, a control histone mark, did not change in this assay (Extended Data Fig. 3h). Collectively, these results indicate a conserved role of Tyr 57/58 phosphorylation in H2A in regulating transcriptional elongation.

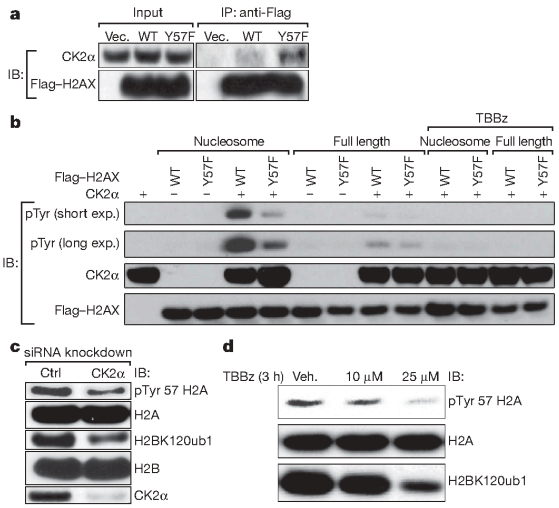

Figure 2 | CK2 phosphorylates Tyr 57 in H2A. **a**, CK2α interacts preferentially with the H2A(Y57F) mutant. Flag-tagged wild-type (WT) H2AX and H2AX(Y57F) were expressed in 293T cells, immunoprecipitated (IP) and immunoblotted (IB). **b**, CK2 phosphorylates Tyr 57 in H2A in nucleosomes *in vitro*. *In vitro* kinase assays were performed using recombinant glutathione *S*-transferase (GST)-CK2α, and full-length or nucleosomal Flag-tagged H2AX purified from 293T cells, and were immunoblotted to examine tyrosine phosphorylation. **c**, **d**, CK2 phosphorylates Tyr 57 in H2A *in vivo*. **c**, CK2α was knocked down in 293T cells, and nuclear extracts were immunoblotted. Ctrl indicates scrambled short interfering RNA (siRNA). **d**, Nuclear extract from 293T cells treated with vehicle (Veh.) or TBBz for 3 h were immunoblotted. Data represent three independent experiments.

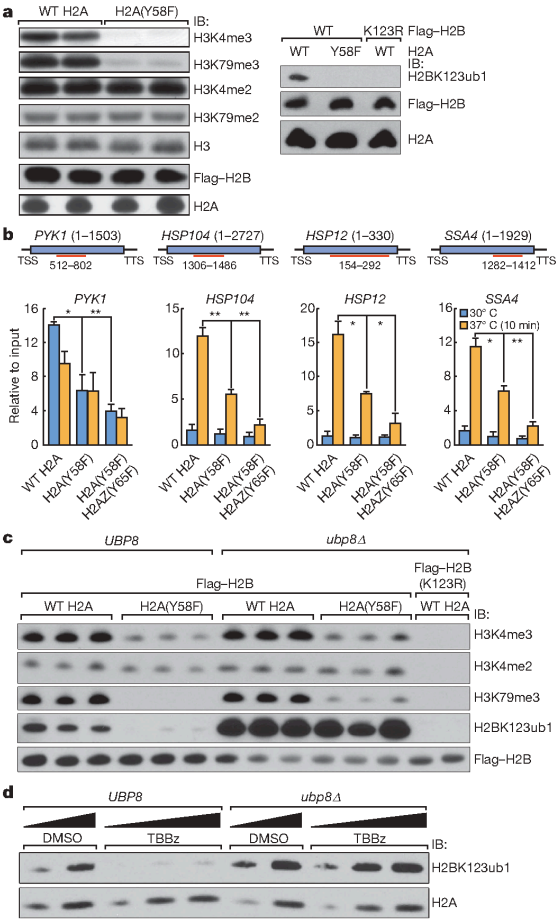

Figure 3 | The H2A(Y58F) mutation enhances H2B deubiquitination, and impairs transcriptional elongation in yeast. **a**, The H2A(Y58F) mutation affects several histone modifications. Whole-cell extracts from indicated strains were immunoblotted (IB). **b**, H2A(Y58F) mutation impairs transcriptional elongation. Pol II binding in the indicated genes was measured by ChIP-qPCR in yeast strains grown at 30 °C or at 37 °C for 10 min ($(n = 3$, mean ± s.e.m.), $*P < 0.05$, $**P < 0.01$). The ORF of the genes and the regions amplified by the primer pairs are shown. *P* values were calculated by two-tailed Student's *t*-tests. TSS, transcription start site; TTS, transcription termination site. **c**, *UBP8* deletion rescues the defect in H2B mono-ubiquitination in the H2A(Y58F) mutant yeast. Whole-cell extracts from indicated yeast strains were immunoblotted. **d**, CK2 prevents the deubiquitination of H2B. Wild-type (*UBP8*) or *ubp8Δ* cells were treated with vehicle (dimethylsulphoxide, DMSO) or TBBz (25 μM) for 3 h and whole-cell extracts were immunoblotted. Data represent three independent experiments.

To address the mechanism through which H2A Tyr 57/58 phosphorylation regulates H2B mono-ubiquitination, we examined the recruitment of proteins known to be involved in establishing H2B mono-ubiquitination, such as Paf1, Rtf1 and Rad6 (refs 13–15), by ChIP-qPCR. The binding of Paf1 and Rtf1 was comparable in wild-type and H2A(Y58F) yeast strains, whereas Rad6 binding was slightly reduced in the genes tested in the H2A(Y58F) mutant strain (Extended Data Fig. 4a–c). The effect of the H2A(Y58F) mutation was further evaluated in yeast lacking *UBP8*, which encodes a major H2B deubiquitinase that is a component of the SAGA complex. Deletion of *UBP8* restored H2B mono-ubiquitination in the H2A(Y58F) mutant to the wild-type level (Fig. 3c), suggesting that the defect in H2B mono-ubiquitination in the H2A(Y58F) mutant occurs through Ubp8 deubiquitinase activity, and not through defective ubiquitination machinery. Likewise, CK2 inhibition reduced H2B mono-ubiquitination in wild-type yeast while having no effect in *UBP8* mutants (Fig. 3d), further supporting the role of CK2-mediated H2A Tyr 58 phosphorylation in preventing H2B deubiquitination. Notably, despite the complete rescue of H2B mono-ubiquitination, *UBP8* deletion only partially rescued H3K79me3, and the level of H3K4me3 remained low in the H2A(Y58F) mutant (Fig. 3c). Furthermore, deletion of *UBP8* did not rescue defects in Pol II binding, the transcript levels, or the slow growth phenotype of the H2A(Y58F) mutant (Extended Data Fig. 4d–f). These results suggest that the physiological effects of Tyr 58 mutation in H2A are linked to, but extend beyond, the loss of H2B mono-ubiquitination.

Next, we investigated whether knockdown or inhibition of CK2 phenocopies the effects of H2A(Y58F) mutation in the regulation of transcriptional elongation. Consistent with the result in yeast, H2B mono-ubiquitination was reduced upon CK2α knockdown or inhibition of CK2 kinase activity in 293T cells (Fig. 2c, d). Likewise, Pol II binding in active genes in LNCaP human prostate carcinoma cells was impaired in gene bodies but not in the promoter regions upon CK2 inhibition, as determined by ChIP followed by sequencing (ChIP-seq) (Fig. 4a). A travelling ratio plot of Pol II[16,17] showed a significant shift in CK2-inhibited cells (Fig. 4a), suggesting that CK2 kinase activity is required for transcriptional elongation in gene bodies. In agreement with this, dihydrotestosterone (DHT)-induced transcriptional activation of androgen-receptor-regulated genes was impaired in LNCaP cells treated with TBBz (Extended Data Fig. 5a).

To understand the molecular aspects of the role of CK2 in transcriptional elongation, genome-wide localization of CK2α in LNCaP cells was determined by ChIP-seq. Like Pol II, CK2α showed binding to actively transcribed genes across gene bodies, although its binding profile was distinct from that of Pol II (Fig. 4b). Meta-analysis of the top 10% of active genes, based on global run-on sequencing results in LNCaP cells[18], revealed that CK2α globally co-localizes with Pol II (Fig. 4c). Consistent with the genome-wide binding pattern, CK2α immunoprecipitated with the phosphorylated carboxy-terminal domain (CTD) of Pol II, which is localized in the promoters (pSer 5) and gene bodies (pSer 2) of active genes (Extended Data Fig. 5b). We also found CK2α binding in intergenic regions that co-localized with H3K4me1 and H3K27ac marks, histone modifications that co-localize with active enhancers[19], and LNCaP cell-type-specific androgen receptor enhancers (Fig. 4d and Extended Data Fig. 5c), suggesting that the intergenic CK2α peaks are in enhancer regions. Inhibition of CK2 also caused stalling of Pol II in the androgen-receptor-bound enhancers (Fig. 4e, Extended Data Fig. 5d), underpinning the function of CK2 in transcriptional elongation in both gene bodies and enhancers.

We asked if CK2 also regulates transcriptional elongation in yeast, and if so, whether H2A Tyr 58 phosphorylation is a key player, among the many other substrates of CK2[20]. Inhibition of CK2 kinase activity resulted in a decrease in the recruitment of Pol II in both the promoter region as well as gene bodies of the tested genes in wild-type yeast, but did not have additive effects in the H2A(Y58F) yeast (Fig. 4f). It is noteworthy that both CK2 inhibition and H2A(Y58F) mutation did not result in promoter-proximal pausing in the genes tested, consistent with the observation that regulation by promoter-proximal pausing is rare in yeast[21]. Collectively, these results demonstrate that CK2 has a deeply conserved role in transcriptional elongation both in gene bodies and enhancers, and that H2A Tyr 58 phosphorylation is critical in this regulation.

This study identifies a new H2A modification, phosphorylation of Tyr 57/58, which provides new insight into how two important protein complexes, SAGA and Paf1, with opposite enzymatic effects on H2B mono-ubiquitination, might be coordinated during transcriptional elongation. The data further emphasize the key significance of this delicate coordination as demonstrated by defects in transcriptional elongation upon mutation of the conserved phosphorylation site. A moderate increase

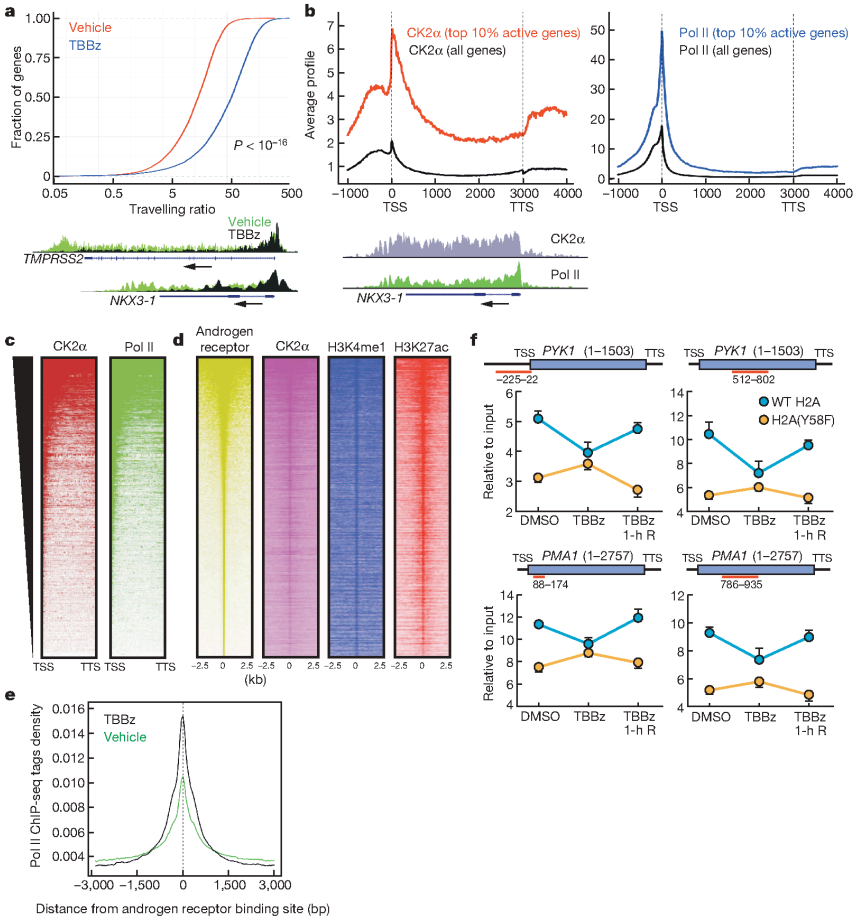

Figure 4 | CK2 regulates transcriptional elongation. **a**, CK2 kinase activity is required for promoter-proximal pause release in mammalian cells. The Pol II travelling ratio was plotted for LNCaP cells treated with vehicle or TBBz for 2.5 h ($P < 10^{-16}$). *P* value was calculated using a Kolmogorov–Smirnov test. Overlay of Pol II occupancy in representative genes (*TMPRSS2* and *NKX3-1*) are shown. **b**, **c**, CK2α binds across the actively transcribed genes globally. **b**, CK2α and Pol II occupancy were determined in the top 10% active genes ($n = 3{,}162$) and all genes by CEAS[24]. The length of all gene bodies is normalized to 3 kilobases (kb). Enrichment of CK2α and Pol II at a representative active gene (*NKX3-1*) is shown. **c**, Heat map of Pol II and CK2α binding profile in top 10% active genes from transcription start site to transcription termination site is shown. **d**, CK2α binds to active enhancers. Heat maps of androgen receptor CK2α, H3K4me1 (ref. 18), and H3K27ac (ref. 18) signals over androgen-receptor-enriched regions[18] in LNCaP cells were determined. **e**, CK2 regulates transcriptional elongation in enhancers. Shown are Pol II ChIP tag density plots centred at androgen-receptor-enriched enhancers. bp, base pairs. **f**, H2A Tyr 58 phosphorylation is critical for CK2-mediated regulation of transcriptional elongation in yeast. Cells expressing either wild-type H2A or H2A(Y58F) mutant were treated with vehicle (DMSO, dimethylsulphoxide) or TBBz (25 μM) for 3 h, or treated with TBBz for 3 h followed by 1-h inhibition release (TBBz 1-h R), and Pol II binding in the indicated genes was measured by ChIP-qPCR ($n = 3$, mean ± s.e.m.). The ORF of the genes and the regions amplified by the primer pairs are shown. Data represent two independent experiments for ChIP-seq (**a**–**e**) and three for ChIP-qPCR (**f**).

in Gcn5–SAGA-mediated H3K27 acetylation[22] in the H2A(Y58F) mutant yeast suggests that phosphorylation may antagonize multiple activities of SAGA. Such antagonism could explain the partial rescue of the defects in the H2A(Y58F) mutant upon deletion of *UBP8*, as the other modules of SAGA remain functional in the absence of Ubp8[23]. Although unlikely, the potential role in transcriptional elongation of the hydroxyl group of Tyr 58, rather than phosphorylation itself, cannot yet be dismissed. Assays using synthetic nucleosomes with constitutively phosphorylated H2A Tyr 57/58 may ultimately be used to further define the role of this site in transcriptional elongation. This study also emphasizes the functional significance of the tyrosine kinase activity of CK2, and encourages the search for other tyrosine substrates of CK2. Importantly, the identification of a highly conserved role of CK2 in regulating transcriptional elongation in both gene bodies and enhancer regions adds yet another layer to understanding transcription.

Online Content Methods, along with any additional Extended Data display items and Source Data, are available in the online version of the paper; references unique to these sections appear only in the online paper.

Received 5 December 2013; accepted 5 August 2014.
Published online 24 September 2014.

1. Kouzarides, T. Chromatin modifications and their function. *Cell* **128,** 693–705 (2007).
2. Nakanishi, S. *et al.* A comprehensive library of histone mutants identifies nucleosomal residues required for H3K4 methylation. *Nature Struct. Mol. Biol.* **15,** 881–888 (2008).
3. Matsubara, K., Sano, N., Umehara, T. & Horikoshi, M. Global analysis of functional surfaces of core histones with comprehensive point mutants. *Genes Cells* **12,** 13–33 (2007).

4. Flint, A. J., Tiganis, T., Barford, D. & Tonks, N. K. Development of 'substrate-trapping' mutants to identify physiological substrates of protein tyrosine phosphatases. *Proc. Natl Acad. Sci. USA* **94,** 1680–1685 (1997).
5. Wilson, L. K., Dhillon, N., Thorner, J. & Martin, G. S. Casein kinase II catalyzes tyrosine phosphorylation of the yeast nucleolar immunophilin Fpr3. *J. Biol. Chem.* **272,** 12961–12967 (1997).
6. Vilk, G. *et al.* Protein kinase CK2 catalyzes tyrosine phosphorylation in mammalian cells. *Cell. Signal.* **20,** 1942–1951 (2008).
7. Pagano, M. A. *et al.* 2-Dimethylamino-4,5,6,7-tetrabromo-1*H*-benzimidazole: a novel powerful and selective inhibitor of protein kinase CK2. *Biochem. Biophys. Res. Commun.* **321,** 1040–1044 (2004).
8. Xiao, T. *et al.* Histone H2B ubiquitylation is associated with elongating RNA polymerase II. *Mol. Cell. Biol.* **25,** 637–651 (2005).
9. Tanny, J. C., Erdjument-Bromage, H., Tempst, P. & Allis, C. D. Ubiquitylation of histone H2B controls RNA polymerase II transcription elongation independently of histone H3 methylation. *Genes Dev.* **21,** 835–847 (2007).
10. Uptain, S. M., Kane, C. M. & Chamberlin, M. J. Basic mechanisms of transcript elongation and its regulation. *Annu. Rev. Biochem.* **66,** 117–172 (1997).
11. Ferguson, S. B. *et al.* Protein kinase A regulates constitutive expression of small heat-shock genes in an Msn2/4p-independent and Hsf1p-dependent manner in *Saccharomyces cerevisiae*. *Genetics* **169,** 1203–1214 (2005).
12. Chao, S.-H. & Price, D. H. Flavopiridol inactivates P-TEFb and blocks most RNA Polymerase II transcription *in vivo*. *J. Biol. Chem.* **276,** 31793–31799 (2001).
13. Robzyk, K., Recht, J. & Osley, M. A. Rad6-dependent ubiquitination of histone H2B in yeast. *Science* **287,** 501–504 (2000).
14. Wood, A., Schneider, J., Dover, J., Johnston, M. & Shilatifard, A. The Paf1 complex is essential for histone monoubiquitination by the Rad6–Bre1 complex, which signals for histone methylation by COMPASS and Dot1p. *J. Biol. Chem.* **278,** 34739–34742 (2003).
15. Ng, H. H., Dole, S. & Struhl, K. The Rtf1 component of the Paf1 transcriptional elongation complex is required for ubiquitination of histone H2B. *J. Biol. Chem.* **278,** 33625–33628 (2003).
16. Rahl, P. B. *et al.* c-Myc regulates transcriptional pause release. *Cell* **141,** 432–445 (2010).
17. Reppas, N. B., Wade, J. T., Church, G. M. & Struhl, K. The transition between transcriptional initiation and elongation in *E. coli* is highly variable and often rate limiting. *Mol. Cell* **24,** 747–757 (2006).
18. Wang, D. *et al.* Reprogramming transcription by distinct classes of enhancers functionally defined by eRNA. *Nature* **474,** 390–394 (2011).
19. Heintzman, N. D. *et al.* Histone modifications at human enhancers reflect global cell type-specific gene expression. *Nature* **459,** 108–112 (2009).
20. Meggio, F. & Pinna, L. A. One-thousand-and-one substrates of protein kinase CK2? *FASEB J.* **17,** 349–368 (2003).
21. Wade, J. T. & Struhl, K. The transition from transcriptional initiation to elongation. *Curr. Opin. Genet. Dev.* **18,** 130–136 (2008).
22. Suka, N., Suka, Y., Carmen, A. A., Wu, J. & Grunstein, M. Highly specific antibodies determine histone acetylation site usage in yeast heterochromatin and euchromatin. *Mol. Cell* **8,** 473–479 (2001).
23. Henry, K. W. *et al.* Transcriptional activation via sequential histone H2B ubiquitylation and deubiquitylation, mediated by SAGA-associated Ubp8. *Genes Dev.* **17,** 2648–2663 (2003).
24. Shin, H., Liu, T., Manrai, A. K. & Liu, X. S. CEAS: cis-regulatory element annotation system. *Bioinformatics* **25,** 2605–2606 (2009).

Supplementary Information is available in the online version of the paper.

Acknowledgements We acknowledge M. Ghassemian for assistance in mass spectrometry analysis. We also acknowledge K. Arndt for providing the *UBP8* null yeast strain. CK2 constructs were provided by D. Litchfield. We acknowledge J. Hightower for assistance in figure preparation. We acknowledge K. Tumaneng and I. Bassets for critical reading of the manuscript and D. J. Forbes for discussion. This work was supported by grants NS034934, DK039949, DK018477, HL065445 and CA173903 from NIH to M.G.R., UC-CRCC to L.P., NIH-GM033279 support for X.B.S. and NCI CA82683 grant to T.H. M.G.R. is an Investigator with the HHMI. T.H. is a Frank and Else Schilling American Cancer Society Professor and holds the Renato Dulbecco Chair in Cancer Research.

Author Contributions M.G.R. and H.B. conceived the idea and wrote the manuscript with contributions from L.P., X.B.S. and T.H. M.G.R. and H.B. designed the experiments with mammalian cells, and H.B. performed the experiments. L.P., X.B.S. and H.B. designed the yeast experiments, and X.B.S. and H.B. performed the experiments. Y.T. did the bioinformatics analysis. D.M. aligned the ChIP-seq data. K.A.O. prepared the ChIP-seq library, and conducted the high-throughput sequencing. T.H. designed the PAA experiments, and J.M. performed the experiments. All authors read the manuscript, and approve the content.

Author Information ChIP-seq data has been deposited in the Gene Expression Omnibus database under accession number GSE58607. Reprints and permissions information is available at www.nature.com/reprints. The authors declare no competing financial interests. Readers are welcome to comment on the online version of the paper. Correspondence and requests for materials should be addressed to M.G.R. (mrosenfeld@ucsd.edu) or L.P. (lpillus@ucsd.edu).

METHODS

Cell culture, short interfering RNA, primers, plasmids, transfection, antibodies and kinase inhibitors. LNCaP and 293T cells were cultured in F12 medium supplemented with 10% fetal bovine serum (FBS) and glutamine. For the DHT-treatment experiments, LNCaP cells were cultured in deficient DME high glucose medium with 5% FBS (charcoal dextran filtered) for 3–4 days. Short interfering RNA (siRNA) against CK2α was from Santa Cruz (sc-29918). Cells were transfected using lipofectamine 2000 (Invitrogen) using the manufacturer's protocol. Mutagenesis was done using Quikchange Lightening Mutagenesis Kit following the manufacturer's recommended protocol. The following antibodies were used in this study: pTyr 57 H2A antibody was generated by Biomatik Company using pTyr 57 H2A peptide as an antigen (LE(pY)LTAEILELAGNC), purified, and positively selected using a pTyr 57 H2A peptide column, and negatively selected using a Tyr 57 H2A peptide column; anti-H2A (Abcam no. ab18255), anti-CK2α (Abcam no. ab 70774), anti-H2BK120ub1 (Cell Signaling no. 5546S), anti-Flag (Sigma M2), anti-RNA polymerase II (Santa Cruz N-20 (for mammalian cells), Abcam no. ab817 (for yeast cells)), anti-pSer 2 Pol II (Abcam no. ab5095), anti-pSer 5 Pol II (Abcam no. ab5131), anti-pTyr (Millipore no. 05-321 (4G10)), anti-H2A (yeast) (Active Motif no. 39236), anti-H4K4me3 (Active Motif no. 39159), anti-H3K4me2 (Millipore no. 07-030), anti-H3K4me1 (Millipore no. 07-436), anti-pSer 10-H3 (Millipore no. 06-570), anti-H3K27ac (Abcam no. ab4729), anti-H3K79me2 (Active Motif no. 39924), anti-H3K36me2 (Active Motif no. 39255) and anti-H2AK119ub (Cell Signaling no. 8240S). TBBz and flavopiridol were from Sigma. Primers used in this study are listed in Supplementary Table 3.

Chromatin immunoprecipitation. Cells were grown to 90–95% confluence, fixed with 1% formaldehyde for 15 min for Pol II ChIP, and with di-succinimidyl glutarate (DSG) for 45 min followed by 10 min fixation with 1% formaldehyde for CK2α ChIP. Fixations were performed at room temperature. To terminate crosslinking, fixed cells were incubated with glycine (1.25 mM) for 10 min. Nuclei were prepared as described[25], which were then sonicated in lysis buffer (150 mM NaCl, 1% Triton X-100, 20 mM Tris pH 8.0, 0.1% SDS) using a Bioruptor to fragment chromatin to less than 500 base pairs (bp). Chromatin was pre-cleared with Protein-G magnetic beads, and then immunoprecipitated using 5 μg of antibody per 10-cm plate for each sample. The chromatin antibody mix was incubated with 35 μl protein G-conjugated Dyna beads for 4 h at 4 °C, washed three times with wash buffer (1% Triton X-100, 50 mM Tris pH 8.0, 10% glycerol) with increasing concentrations of NaCl (150 mM, 300 mM and 400 mM), and two times with Tris-EDTA buffer. DNA was eluted in 1% SDS in Tris-EDTA buffer for 45 min at 37 °C, crosslinking was reversed overnight at 65 °C, and DNA was purified using Qiagen columns. Yeast ChIP was performed using 300–400 μg DNA and 2 μg antibody using the protocol as described[26] with some modifications. In brief, cells were fixed for 15 min, and then incubated with glycine at a final concentration of 2.5 mM for 5 min, and cells were lysed using glass beads (5 × 5 min beating with 2 min on ice intervals). Cells were then sonicated to obtain chromatin fragments of less than 1 kb, and the rest of the protocol was similar to the mammalian cells. All the buffers used included fresh complete protease inhibitors (Roche), 1 mM PMSF, 2 mM Na_3VO_4, 10 mM β-glycerol phosphate and 10 mM NaF.

Statistical analysis. *P* values for ChIP-qPCR and reverse transcription (RT)–PCR were calculated by two-tailed Student's *t*-tests, type two using Microsoft Excel. The statistical significance of the change of travelling ratio between control and CK2-inhibitor-treated samples was determined using two-tailed Kolmogorov–Smirnov test. In yeast experiments, independent transformants that were processed separately were considered biological replicates, and in mammalian experiments, cells cultured in different plates, and processed separately were considered biological replicates. In the analyses, *n* represents the number of biological replicates. All independent experiments are biological replicates.

Identification of ChIP-seq peaks. ChIP-seq peaks were identified using HOMER (http://sdcsb.ucsd.edu/resources/homer/). A 200-bp sliding window was used for transcription factors and a 500-bp sliding window was used for histone modifications with the requirement that two peaks are at least 500 bp apart for transcription factors, and 1,250 bp for histone modifications to avoid redundant peak identification. Tag density was calculated by using HOMER and average signal profiles surrounding androgen-receptor-enriched regions were generated with CEAS[24] (cis-regulatory element annotation system) which were visualized with Java TreeView (http://jtreeview.sourceforge.net).

ChIP-seq alignment. DNA was ligated to specific adaptors followed by high-throughput sequencing on Illumina's HiSeq 2000 system according to the manufacturer's instructions. The first 48 bp for each sequence tag returned was aligned to the hg18 (human) assembly using Bowtie2. The data were visualized by preparing custom tracks on the UCSC genome browser by using HOMER. The total number of mappable reads was normalized to 10^7 for each experiment presented.

ChIP-seq data deposition. ChIP-seq data has been deposited in the Gene Expression Omnibus database under accession number GSE58607. Other published sequencing data used in the study are described in ref. 18.

Travelling ratio calculation. The Pol II travelling ratio was defined as the relative ratio of Pol II density in the promoter-proximal region and the gene body. The promoter proximal region refers to the window from −50 bp to +300 bp surrounding the TSS, and the gene body refers to regions from 300 bp downstream of the TSS to 13 kb from the TSS for genes longer than 13 kb, or to the transcription termination site for genes shorter than 13 kb. The significance of the change of the travelling ratio between control and CK2-inhibitor-treated samples was determined by two-tailed Kolmogorov–Smirnov test.

***In vitro* kinase assay and phosphoamino acid analysis (PAA).** *In vitro* kinase reactions were performed with 100 ng of recombinant GST-tagged CK2α (expressed in *E. coli* with 0.2 mM isopropyl-β-D-thiogalactoside induction for 3 h at 30 °C) in 1× kinase buffer (20 mM Tris-HCl, 50 mM KCl, 10 mM $MgCl_2$ pH 7.5) with the addition of 0.2 mM ATP for cold reactions (and 10 μM ATP mixed with 10 μCi of [γ-^{32}P]ATP for the radioactive reactions). The substrates (Flag-tagged wild-type H2AX and H2AX(Y57F)) were purified from 293T cells expressing Flag-tagged H2AX constructs. For the full-length proteins, histone extracts were immunoprecipitated using Flag antibody, then washed several times with wash buffer (1% Triton X-100, 900 mM NaCl, 20 mM Tris 8.0), treated with calf intestinal phosphatase for 30 min at 37 °C, washed a few more times with wash buffer, and eluted with 3× Flag peptides. Mononucleosomes were prepared as described[25] with minor changes in micrococcal nuclease digestion. In brief, nuclei were isolated from 15-cm fully confluent plates, and DNA was digested in 1.2 ml total volume with 2.5 μl micrococcal nuclease (NEB no. M0247S) for 10 min at 37 °C, and the reaction was stopped by adding 5 mM EGTA, and mononucleosomes were collected by centrifugation. Mononucleosomes were immunoprecipitated with Flag antibody, washed four times with buffer A (340 mM sucrose, 10 mM HEPES pH 7.5, 10% glycerol, 1.5 mM MgCl2, 10 mM KCl) followed by three washes with kinase reaction buffer, then treatment with 500 μM FSBA (Sigma no. F9128-25MG) for 25 min at 37 °C to irreversibly inhibit any potential kinases interacting with the nucleosome. Samples were washed three times with kinase buffer, treated with calf intestinal phosphatase for 30 min at 37 °C, and washed a further three times with buffer A. The bound nucleosomes were eluted with 3× Flag peptides in buffer A. The kinase reactions were carried out for 1 h at 30 °C. For PAA, the samples were separated by SDS–PAGE, transferred to polyvinylidene difluoride membrane, and the membrane corresponding to the mobility of phosphorylated H2AX was excised, and PAA using two-dimensional electrophoresis on thin layer cellulose plates was performed as described[27].

Whole-cell extracts, immunoprecipitation and cell fractionation. Yeast whole-cell extracts were prepared either by breaking the cells with glass beads in PBS or boiling the cells in denaturing buffer (2% SDS with 30 mM dithiothreitol) for 10 min. To immunoprecipitate the Flag-tagged proteins under denaturing conditions, whole-cell extracts were prepared as noted above in denaturing buffer, and the SDS concentration was adjusted to 0.1% by adding dilution buffer (150 mM NaCl, 1% Triton X-100, 20 mM Tris pH 8.0.), then immunoprecipitated overnight using anti-Flag (M2-Sigma) conjugated to agarose beads, and washed five times with dilution buffer. Bound proteins were eluted with 100 μg ml^{-1} 3× Flag peptides in Tris-buffered saline for 30 min at 8 °C twice and the eluted proteins were precipitated using tricholoroacetic acid. In 293T cells, whole-cell extracts for denaturing immunoprecipitation were prepared by boiling the cells in lysis buffer (1% SDS, 20 mM Tris pH 8.0, 10 mM dithiothreitol), and the SDS concentration was adjusted to 0.1% by adding dilution buffer before adding the Flag antibody for immunoprecipitation. Nuclear extracts were prepared using lysis buffer (10 mM HEPES pH 8.0, 1.5 mM $MgCl_2$, 10 mM KCl, 1% NP40) to lyse cell membranes; the supernatant is the cytosolic fraction and the pellet is the nuclear fraction. For co-immunoprecipitation, the nuclear pellet was re-suspended in lysis buffer (0.1% NP40, 150 mM NaCl, 20 mM Tris pH 8.0 and 10% glycerol) and sonicated to disrupt the nuclei and chromatin. The antibody and nuclear extract were incubated overnight with 5 μg of CK2α antibody or 20 μl of M2 Flag antibody conjugated to magnetic beads. The beads were washed three times with the same lysis buffer, and the proteins bound to the beads were analysed by mass spectrometry or by immunoblotting.

Mass spectrometry. Protein samples were prepared as described[28]. In brief, the protein samples were diluted in TNE buffer (50 mM Tris pH 8.0, 100 mM NaCl, 1 mM EDTA). RapiGest SF reagent (Waters Corp.) was added to the mix to a final concentration of 0.1% and samples were boiled for 5 min. TCEP (Tris (2-carboxyethyl) phosphine) was added to a final concentration of 1 mM and the samples were incubated at 37 °C for 30 min. Subsequently, the samples were carboxymethylated with 0.5 mg ml^{-1} of iodoacetamide for 30 min at 37 °C followed by neutralization with 2 mM TCEP (final concentration). Proteins samples prepared as above were digested with trypsin (trypsin:protein ratio 1:50) overnight at 37 °C. RapiGest was degraded and removed by treating the samples with 250 mM HCl at 37 °C for 1 h followed by centrifugation at 23,000*g* for 30 min at 4 °C. The soluble fraction

was then added to a new tube and the peptides were extracted and desalted using C18 desalting columns (Thermo Scientific).

Trypsin-digested peptides were analysed by ultra-high-pressure liquid chromatography (UPLC) coupled with tandem mass spectroscopy (MS/MS) using nano-spray ionization as described[29]. The nano-spray ionization experiments were performed using a TripleTof 5600 hybrid mass spectrometer (ABSCIEX) interfaced with nano-scale reversed-phase UPLC (Waters corporation nano ACQUITY) using a 20-cm, 75-micrometer inside diameter glass capillary tube packed with 2.5-μm C18 (130) CSH beads (Waters corporation). Peptides were eluted from the C18 column into the mass spectrometer using a linear gradient (5–80%) of ACN (acetonitrile) at a flow rate of 250 μl per min for 1 h. The buffers used to create the ACN gradient were: buffer A (98% H_2O, 2% ACN, 0.1% formic acid, and 0.005% TFA (trifluoroacetic acid)) and buffer B (100% ACN, 0.1% formic acid, and 0.005% TFA). MS/MS data were acquired in a data-dependent manner in which the MS1 (initial mass-to-charge-ratio (m/z) spectrum) data were acquired for 250 ms at an m/z of 400 to 1,250 Da and the MS2 (MS/MS or tandem MS) data were acquired from an m/z of 50 to 2,000 Da. The independent data acquisition parameters were as follows: MS1-TOF (time-of-flight) acquisition time of 250 ms, followed by 50 MS2 events of 48 ms acquisition time for each event. The threshold to trigger an MS2 event was set to 150 counts when the ion had the charge state +2, +3 or +4. The ion exclusion time was set to 4 s. Finally, the collected data were analysed using Protein Pilot 4.5 (ABSCIEX) for peptide identifications.

Yeast strains and yeast plasmids used in the study. Yeast strains and yeast plasmids used in the study are described in Supplementary Table 4.

25. O'Neill, L. P. & Turner, B. M. Immunoprecipitation of native chromatin: NChIP. *Methods* **31,** 76–82 (2003).
26. Strahl-Bolsinger, S., Hecht, A., Luo, K. & Grunstein, M. SIR2 and SIR4 interactions differ in core and extended telomeric heterochromatin in yeast. *Genes Dev.* **11,** 83–93 (1997).
27. Kamps, M. P. & Sefton, B. M. Acid and base hydrolysis of phosphoproteins bound to immobilon facilitates analysis of phosphoamino acids in gel-fractionated proteins. *Anal. Biochem.* **176,** 22–27 (1989).
28. Guttman, M. *et al.* Interactions of the NPXY microdomains of the low density lipoprotein receptor-related protein 1. *Proteomics* **9,** 5016–5028 (2009).
29. McCormack, A. L. *et al.* Direct analysis and identification of proteins in mixtures by LC/MS/MS and database searching at the low-femtomole level. *Anal. Chem.* **69,** 767–776 (1997).

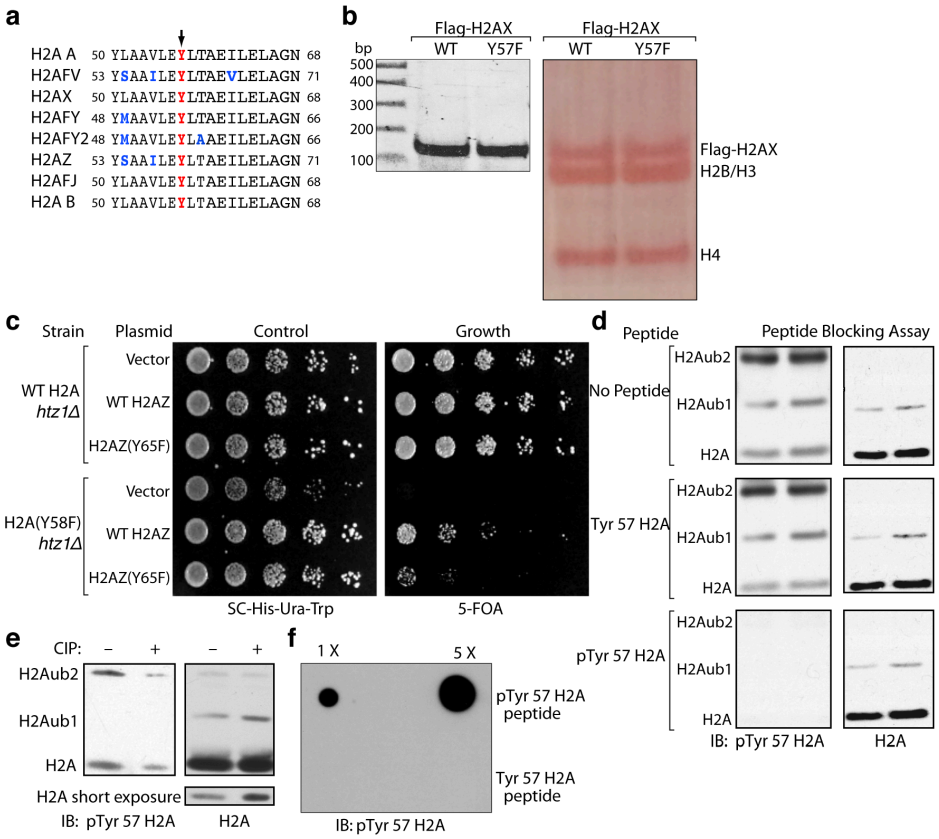

Extended Data Figure 1 | The conserved Tyr 57 residue in H2A is phosphorylated. **a**, The Tyr 57 residue is conserved in all variants of H2A. Sequences of H2A variants surrounding the Tyr 57 residue (arrow) in mammals is shown, particular variant residues are highlighted in blue. **b**, The Y57F mutation in H2A does not affect the structural integrity of nucleosomes. Mononucleosomes containing Flag-tagged wild-type H2AX or H2AX(Y57F) were immunoprecipitated, and histones and DNA were visualized by Ponceau staining (right) and by ultraviolet light (left), respectively. **c**, The H2A Tyr 58 residue has overlapping functions with the H2AZ Tyr 65 residue in yeast. Fivefold serial dilutions of the indicated transformants were plated on SC–His–Ura–Trp for growth and 5-FOA for the loss of pJH33. **d**, **e**, H2A Tyr 57 is phosphorylated in 293T cells. **d**, Nuclear extracts from 293T cells were immunoblotted (IB) with anti-pTyr 57 H2A pre-incubated with indicated peptides, and re-probed with anti-H2A. **e**, Histone extracts from 293T cells were treated with calf intestinal phosphatase (CIP) for 1 h at 37 °C, and immunoblotted. **f**, The anti-pTyr 57 H2A antibody specifically recognizes the H2A peptide phosphorylated at Tyr 57 but not the non-phosphorylated peptide. Indicated peptides were spotted on nitrocellulose, and probed with anti-pTyr 57 H2A. Data represent three independent experiments.

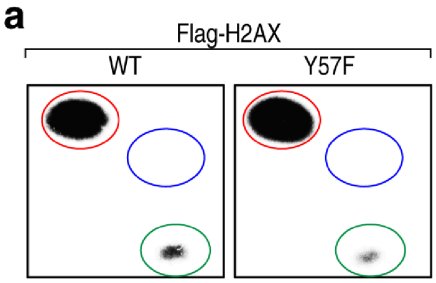

Extended Data Figure 2 | CK2α phosphorylates Tyr 57 in H2A. An *in vitro* kinase reaction was performed using recombinant GST-CK2α, 10 μCi of [γ-^{32}P]ATP supplemented with 10 μM cold ATP, and nucleosomes containing Flag-tagged wild-type H2AX or H2AX(Y57F) from 293T cells, and phosphoamino acid analysis of the phosphorylated Flag-tagged H2AX was performed. The red circle indicates pSer, the blue circle indicates pThr and the green circle indicates pTyr. Data represent two independent experiments.

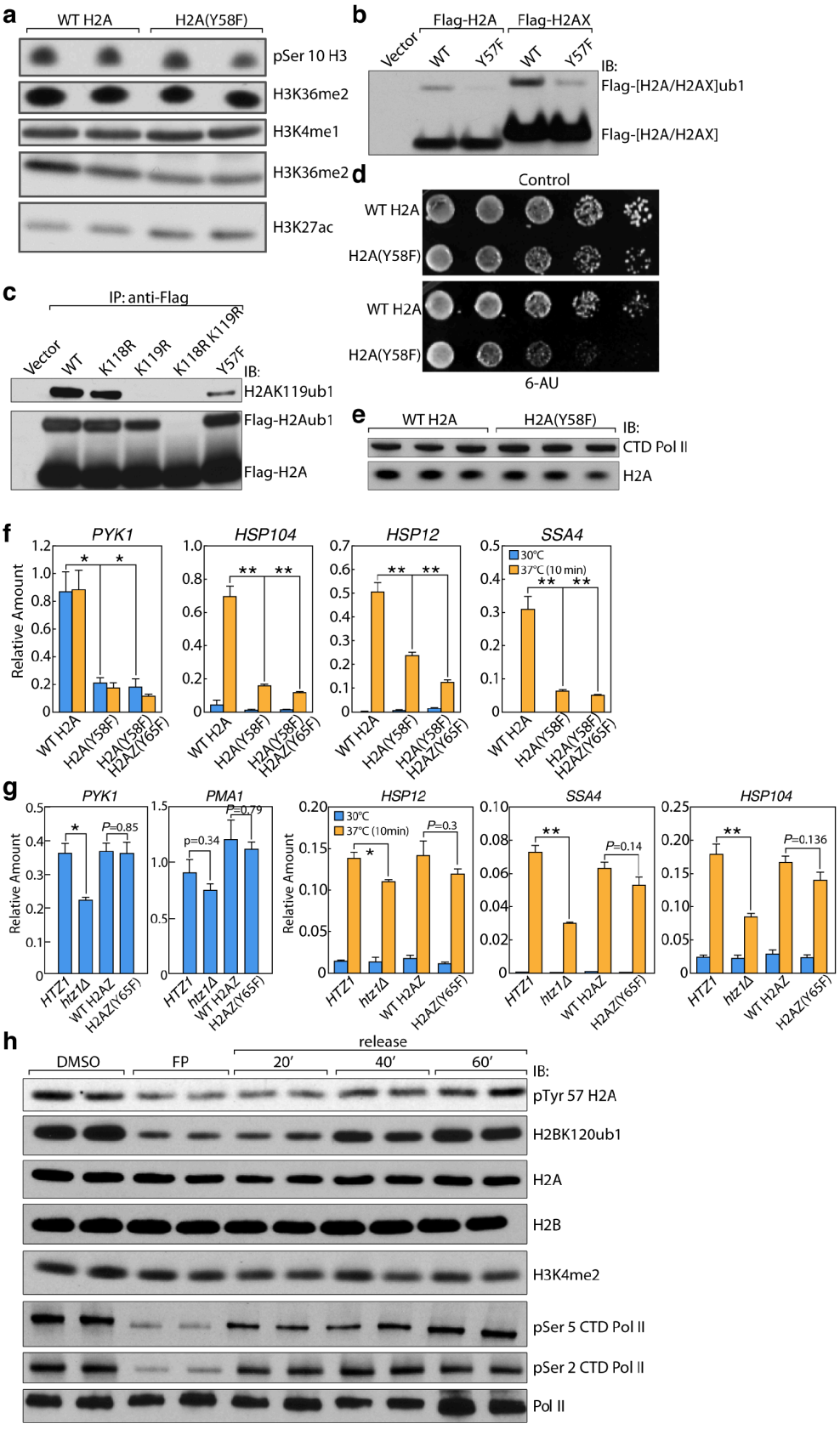
a
WT H2A
H2A(Y58F)
pSer 10 H3
H3K36me2
H3K4me1
H3K36me2
H3K27ac
b
Flag-H2A
Flag-H2AX
Vector
WT
Y57F
WT
Y57F
IB:
Flag-[H2A/H2AX]ub1
Flag-[H2A/H2AX]
c
IP: anti-Flag
Vector
WT
K118R
K119R
K118R K119R
Y57F
IB:
H2AK119ub1
Flag-H2Aub1
Flag-H2A
d
Control
WT H2A
H2A(Y58F)
WT H2A
H2A(Y58F)
6-AU
e
WT H2A
H2A(Y58F)
IB:
CTD Pol II
H2A
f
PYK1
HSP104
HSP12
SSA4
Relative Amount
30°C
37°C (10 min)
WT H2A
H2A(Y58F)
H2A(Y58F) H2AZ(Y65F)
g
PYK1
PMA1
HSP12
SSA4
HSP104
Relative Amount
30°C
37°C (10min)
P=0.85
p=0.34
P=0.79
P=0.3
P=0.14
P=0.136
HTZ1
htz1Δ
WT H2AZ
H2AZ(Y65F)
h
release
DMSO
FP
20′
40′
60′
IB:
pTyr 57 H2A
H2BK120ub1
H2A
H2B
H3K4me2
pSer 5 CTD Pol II
pSer 2 CTD Pol II
Pol II

Extended Data Figure 3 | H2A Tyr 57 phosphorylation regulates transcriptional elongation. **a**, H2A(Y58F) mutation does not affect several other histone marks. Whole-cell extracts from wild-type (WT) or H2A(Y58F) yeast cells were immunoblotted (IB). **b**, **c**, H2A(Y57F) mutation affects H2A ubiquitination in 293T cells. **b**, Flag-tagged wild-type H2A/H2AX and Y57F mutants were expressed in 293T cells, and mono-ubiquitination was assessed by immunoblotting with Flag antibody. **c**, The Flag-tagged H2A mutants were expressed in 293T cells, immunoprecipitated (IP) under denaturing conditions, and immunoblotted. **d**, H2A(Y58F) mutant cells are defective in transcriptional elongation. Fivefold serial dilutions of wild-type and H2A(Y58F) cells were plated on SC supplemented with NH_4OH (solvent) or 100 μg ml^{-1} 6-azauracil (6-AU). **e**, Pol II protein level is comparable in wild-type and H2A(Y58F) yeast. Whole-cell extracts from wild-type or H2A(Y58F) yeast were immunoblotted. **f**, H2A(Y58F) mutation affects transcription. Wild-type H2A, H2A(Y58F), and H2A(Y58F) H2AZ(Y65F) yeast were grown at 30 °C or shifted to 37 °C for 10 min. RNA was extracted and transcript levels of the indicated genes were measured by reverse-transcription–qPCR, and normalized to *SCR1*, a Pol III transcript ($n = 3$, mean ± s.e.m., $^*P < 0.05$, $^{**}P < 0.01$). *P* values were calculated with two-tailed Student's *t*-tests. **g**, H2AZ(Y65F) mutation alone in yeast does not affect transcription significantly. Wild type (*HTZ1*) transformed with vector, and *htz1Δ* strains transformed with vector (*htz1Δ*), *HTZ1* (WT H2AZ) or *HTZ1(Y65F)* (H2AZ(Y65F)) were grown at 30 °C (blue bars) or shifted to 37 °C for 10 min. (orange bars), and transcript levels of the indicated genes were measured as in **f** ($n = 3$, mean ± s.e.m., $^*P < 0.05$, $^{**}P < 0.01$). *P* values were calculated with two-tailed Student's *t*-tests. **h**, Tyr 57 in H2A is phosphorylated during transcriptional elongation. 293T cells were treated with vehicle (DMSO) or flavopiridol (FP) (1 μM) for 4.5 h, then flavopiridol was washed out (release). Cells were harvested at the indicated minute (') after release, and the nuclear extracts were immunoblotted. Data represent two (**a**, **d**, **h**) or three (**b**, **c**, **e**–**g**) independent experiments.

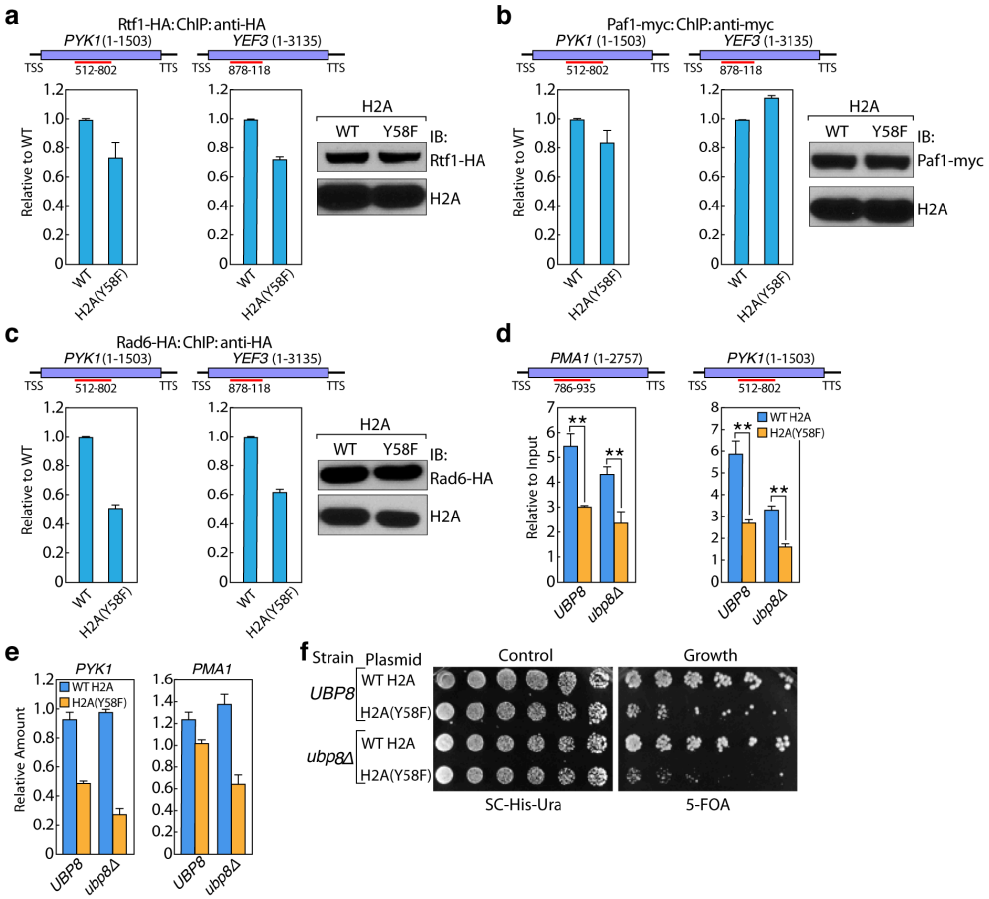

Extended Data Figure 4 | H2A(Y58F) mutation enhances H2B deubiquitination. a–c, The H2A Tyr 58 mutation has moderate to no effect on the recruitment of the H2B ubiquitination machinery. Binding of (**a**) Rtf1-HA, (**b**) Paf1-myc, and (**c**) Rad6-HA was measured by ChIP-qPCR in the indicated genes in wild-type and H2A(Y58F) yeast. Whole-cell extracts from the yeast strains were immunoblotted (IB) to compare the protein levels. ORF of the genes, and the region amplified by the primer pairs are shown ($n = 2$, mean ± s.e.m.). **d**, *UBP8* deletion does not rescue Pol II binding in the H2A(Y58F) mutant. Pol II binding in the indicated strains was measured by ChIP-qPCR. ($n = 3$, mean ± s.e.m., $*P < 0.05$, $**P < 0.01$). *P* values were calculated with two-tailed Student's *t*-tests. The ORF of the genes and the regions amplified by the primer pairs are shown. **e**, *UBP8* deletion does not rescue the defect in transcriptional output in the H2A(Y58F) yeast. The mRNA levels of the indicated genes were determined by RT–qPCR and normalized to the *SCR1* transcript. ($n = 2$, mean ± s.e.m.). **f**, *UBP8* deletion does not rescue the growth defect in the H2A(Y58F) yeast. *UBP8* and *ubp8Δ* strains expressing either wild-type (WT) H2A or H2A(Y58F) were plated at 2.5-fold serial dilutions on SC–His–Ura for growth and 5-FOA for the removal of pJH33. Data represent two (**a–c**, **e**, **f**) or three (**d**) independent experiments.

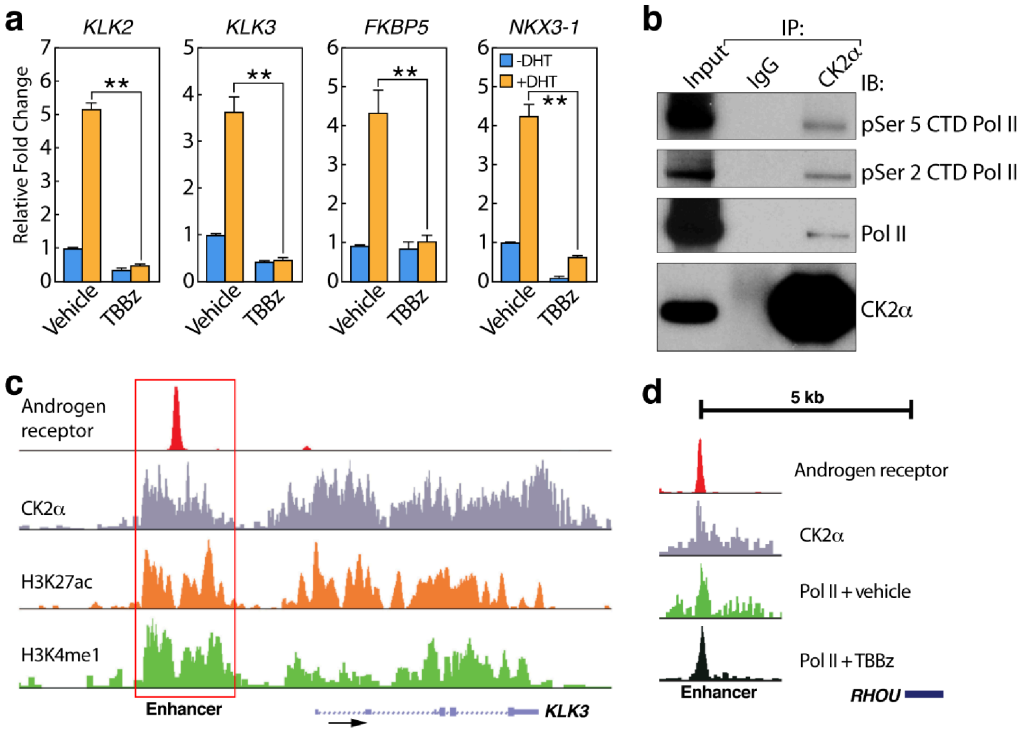

Extended Data Figure 5 | CK2 regulates transcriptional elongation. **a**, CK2 kinase activity is necessary for normal gene expression. LNCaP cells were treated with vehicle (DMSO) or TBBz (25 μM) for 60 min, and then treated with vehicle (ethanol) or 100 nM DHT for 90 min, and induction of the indicated androgen receptor (AR) target genes was measured by RT-qPCR ($n = 3$, mean ± s.e.m., $*P < 0.05$, $**P < 0.01$). *P* values were calculated with two-tailed Student's *t*-tests. **b**, Nuclear extracts from 293T cells were immunoprecipitated (IP) using CK2α antibody and immunoblotted (IB). **c**, Enrichment of CK2α, H3K4me1 (ref. 18), H3K27ac (ref. 18) and androgen receptor genes[18] at a representative androgen receptor enhancer (*KLK3*) is shown. **d**, Pol II tag density in cells treated with vehicle or TBBz at a representative *RHOU* enhancer is shown. Data represent two (**b**–**d**) or three (**a**) independent experiments; kb, kilobase.

Supporting information

Table 5-S1. Primers used in Chapter 5.

Mutagenesis primers

yHTZ1(Y65F)F	GACTGCTGTGTTGGAATTTTTGACTGCTGAAGTGC
yHTZ1(Y65F)R	GCACTTCAGCAGTCAAAAATTCCAACACAGCAGTC
yH2A(Y58A)F	CTTGACTGCTGTCTTGGAAGCTTTGGCCGCTGAAATTTTAG
yH2A(Y58A)R	CTAAAATTTCAGCGGCCAAAGCTTCCAAGACAGCAGTCAAG
yH2A-Y58FF	CTTGACTGCTGTCTTGGAATTTTTGGCCGCTGAAATTTTAG
yH2A-Y58FR	CTAAAATTTCAGCGGCCAAAAATTCCAAGACAGCAGTCAAG
hH2A-Y57FF	GCGGTGCTGGAATTTCTGACGGCCGAG
hH2A-Y57FR	CTCGGCCGTCAGAAATTCCAGCACCGC
hH2A(Y50F)F	GGCGCTCCAGTGTTCCTGGCAGCGGTG
hH2A(Y50F)R	CACCGCTGCCAGGAACACTGGAGCGCC
hH2A(Y39F)F	CTCCGCAAAGGCAACTTCTCCGAACGAGTCGGG
hH2A(Y39F)R	CCCGACTCGTTCGGAGAAGTTGCCTTTGCGGAG

Note: y = yeast; h = human

qPCR primers

SSA4 F	TTGTGGTACGCCTCTTGGAG
SSA4 R	CCTACGCTGACAACCAACCT
HSP12 F	TCTTCCAAGGTGTCCACGAC
HSP12 R	CCGGAAACATATTCGACGGC
PYK1 F2	GGTAAGATCTGTTCCCACAAGGGTG
PYK1 R2	CAAGTCACCTCTGGCAACCATAACAC
HSP104 F	ATGCCGACTCCACCACTAAA
HSP104 R	CTACGTTCAGCATCAAGGGC
KLK3 F	CAGAACTTTCTCCCCATTGC
KLK3 R	TGAGCCCCACAAAGAGAAAC
KLK2 F	TCAGCTGTGAGCATTCAACC
KLK2 R	TCTGGTGGAATCTGGGTTTC
FKBP5 F	ACAGTGTGTTCAGCGTTTGG
FKBP5 R	GGCAAAGAAAGCTCCCATTC
NKX3.1 F	AACGCCTCGTTTAGCGAAGA
NKX3.1 R	TGCCGTGGAACAAGATACCC
PMA1 F1	ACGATGACGCTGCATCTGAA
PMA1 R1	CGTCGTCGACACCGTGATTA

Table 5-S1. Primers used in Chapter 5, continued

qPCR primers

PMA1 F2	ACCGGTGACAACACTTTCGT
PMA1 R2	ACAAGCAGTCCAGACCAACA
PYK1 F1	CATATGATGCTAGGTACCTTTAGTGTCTTC
PYK1 R1	CAATCTTTCTAATCTAGACATTGTGATGATG
YEF3 F	TCTTGGGTAAATTGTTGCCAGG
YEF3 R	GTGCAAGAAGATAGTCATGTATGGGGTG
SCR1 F	CGCGGCTAGACACGGATT
SCR1 R	GCACGGTGCGGAATAGAGAA

Cloning primers

GST CKA1 F	ACTGACTGGATCCATGTCGGGACCCGTGCCAAGC
GST CKA1 R	ACTGACTGCGGCCGCTTACTGCTGAGCGCCAGCGGC

Table 5-S2. Yeast strains and plasmids used in Chapter 5.

Yeast strains

Strains (alias)	Genotype	Sources /References
LPY5	W303 *MATa*	
LPY8241	*MATα ubp8Δ::kanMX*	
LPY11654	*MATa htz1Δ::kanMX*	
LPY14461	*MATα hht1-hhf1Δ::kanMX hta1-htb1Δ::NatMX hta2-htb2Δ::HPH*+ pJH33	
LPY14828	LPY14461+ pLP2133 (no pJH33)	
LPY15980	*MATα hht1-hhf1Δ::kanMX hta1-htb1Δ::NatMX hta2-htb2Δ::HPH RTF1-HA::kanMX*+pLP2492	
LPY15981	*MATα hht1-hhf1Δ::kanMX hta1-htb1Δ::NatMX hta2-htb2Δ::HPH RTF1-HA::kanMX*+pLP3202	
LPY16021	*MATa hht1-hhf1Δ::kanMX hta1-htb1Δ::NatMX hta2-htb2Δ::HPH RAD6-HA::kanMX*+pLP2492	
LPY16024	*MATa hht1-hhf1Δ::kanMX hta1-htb1Δ::NatMX hta2-htb2Δ::HPH RAD6-HA::kanMX*+pLP3202	
LPY16265* (KY2248)	*MATα his3Δ200 lys2-128δ leu2Δ1 trp1Δ63 ura3-52 hta1-htb1Δ::LEU2 hta2-htb2Δ::kanMX ubp8Δ::NatMX*+pDC92	Arndt lab
LPY16266* (KY1600)	*MATα his3Δ200 lys2-128δ leu2Δ1 trp1Δ63 ura3-52 hta1-htb1Δ::LEU2 hta2-htb2Δ::kanMX*+pSAB6	Arndt lab
LPY16267*	LPY16266+pLP2492 (no pSAB6)	
LPY16269*	LPY16266+pLP3202 (no pSAB6)	
LPY16563*	LPY16265+pLP2492 (no pDC92)	
LPY16565*	LPY16265+pLP3202 (no pDC92)	
LPY17876	LPY14461+ pLP2492 (no pJH33)	
LPY17878	LPY14461+ pLP3202 (no pJH33)	
LPY18606	LPY14461+ pLP2908 (no pJH33)	
LPY18192	*MATα hht1-hhf1Δ::URA3 hta1-htb1Δ::NatMX hta2-htb2Δ::HPH*+ pLP2492	
LPY18194	*MATα hht1-hhf1Δ::URA3 hta1-htb1Δ::NatMX hta2-htb2Δ::HPH*+ pLP3202	
LPY19236	*MATa hht1-hhf1Δ::kanMX hta1-htb1Δ::NatMX hta2-htb2Δ::HPH htz1Δ::kanMX* +pJH33	

Table 5-S2. Yeast strains and plasmids used in Chapter 5, continued

Yeast strains

Strains	Genotype	Sources/ References
LPY19259	LPY19236+pLP2492	
LPY19261	LPY19236+pLP3202	
LPY19265	*MATα hht1-hhf1Δ::kanMX hta1-htb1Δ::NatMX hta2-htb2Δ::HPH PAF1-MYC::kanMX*+pLP2492	
LPY19266	*MATα hht1-hhf1Δ::kanMX hta1-htb1Δ::NatMX hta2-htb2Δ::HPH PAF1-MYC::kanMX*+pLP3202	
LPY19464	LPY14461+pLP3213 (no pJH33)	
LPY19806	LPY19236+pLP2252+pLP3202 (no pJH33)	
LPY19894	LPY19236+pLP3200+pLP3202 (no pJH33)	

Note: Except where indicated by *, all strains are in the W303 background. Unless otherwise stated, the strains were constructed during this study or are part of the Pillus lab collection.

Yeast plasmids

Plasmid (alias)	Description
pJH33	*HTA1-HTB1 HHF2-HHT2 URA3* CEN
pRS313	vector *HIS3* CEN
pRS314	vector *TRP1* CEN
pLP2133	pRS313-Flag-*HTA1-HTB1*
pLP2492	pRS313-*HTA1* Flag-*HTB1*
pLP2252	pRS314-*HTZ1*
pLP2908	pRS313-*HTA1*-Flag-*htb1-K123R*
pLP3200	pRS314-*htz1-Y65F*
pLP3202	pRS313-*hta1-Y58F*-Flag-*HTB1*
pLP3211	pRS313-Flag-*hta1-Y58A-HTB1*
pLP3213	pRS313-Flag-*hta1-Y58F-HTB1*

Acknowledgements

Chapter 5, in full, contains material published in *Nature* 2014. Basnet H, Su XB, Tan Y, Meisenhelder J, Merkurjev D, Ohgi KA, Hunter T, Pillus L and Rosenfeld MG. Tyrosine phosphorylation of histone H2A by CK2 regulates transcriptional elongation. The dissertation author was a contributing author to this material.

Chapter 6. Overview and Future Prospects

The unifying theme of this thesis was the identification of additional molecular pathways that regulate chromatin function. Using yeast genetics combined with molecular biology and biochemical techniques, a number of new chromatin modifiers were identified in the different chapters of the thesis.

Screening for amino acid metabolic proteins with chromatin functions

Chapters 2 was initiated with an *in silico* screen that identified a number of nuclear amino acid metabolic proteins with potential functions in chromatin regulation. The screen revealed that Gdh1, Hom2, Hom6 and Arg82 have functions in chromatin silencing, a result that was validated by independent assays in Chapter 3 and Chapter 4. Therefore, the screen proved to be a promising method to predict which metabolic proteins may have chromatin functions.

Interestingly, the screen recovered 39 amino acid metabolic proteins with reported nuclear pools, among which 7 candidates were assayed for silencing functions. It is possible that the other 32 proteins regulate chromatin function through unexpected ways. For example, although they may not directly have a role with the metabolites that were set as criteria for the screen, they might regulate levels of precursors to key metabolites or they may influence reactions controlling key metabolites through feedback mechanisms. Alternatively, they might exhibit catalytic promiscuity, such as using the same catalytic sites for entirely different reactions. Therefore, it is worthy of future work to construct

knockout mutants of these 32 genes, in particular the ones that showed DNA damage sensitivity in high throughput studies.

Glutamate dehydrogenase activity and telomeric silencing

Much of Chapter 2 and Appendix A focused on the chromatin functions of the glutamate dehydrogenase homologs, Gdh1 and Gdh3. Gdh1, in particular, regulates telomeric silencing by modulating the binding of the SIR complex and histone H3 clipping at the telomeres. The catalytic activity of Gdh1 was shown to be important for its effect on telomeric silencing and global H3 clipping.

One important aspect of this study is that the levels of α-ketoglutarate influence telomeric silencing. Future work needs to address the underlying molecular pathway for this influence. For instance, H3 clipping, binding of the SIR complex and histone methylation should be assessed in strains with constitutively elevated α-ketoglutarate levels.

Another conclusion of the study is that histone H3 clipping regulates telomeric silencing *in vivo*. Earlier work proposed a number of proteases with H3 clipping activities, including cathespin L, glutamate dehydrogenase and a vacuolar protease Prb1 (Duncan *et al.* 2008*;* Mandal *et al.* 2013; Xue *et al*. 2014). Our work showed that glutamate dehydrogenase inhibits rather than promotes H3 clipping *in vivo* (Fig. 2-7) and BLAST searches showed that cathespin L has no apparent homolog in budding yeast. Therefore, Prb1 is the most likely candidate, although it remains unclear whether this vacuolar protease enters the nucleus to act on nucleosomal H3. Future work needs to be done to study Prb1's subcellular localization under different growth conditions.

Chapter 2 demonstrated that Gdh1 regulates telomeric silencing through both H3 clipping- dependent and independent activities. The molecular pathway for the clipping-independent activity needs to be addressed in future studies. Notably, *GDH1* was shown to have genetic interactions with histone chaperones as well as a component of the RSC chromatin-remodeling complex (Fig. A-14; Fig. A-15). Therefore, future work needs to be done to understand the molecular basis of these interactions.

Threonine metabolism and rDNA silencing

Chapter 3 reported studies on the roles of the aspartic β-semialdehyde dehydrogenase (Hom2) and homoserine dehydrognase (Hom6) in rDNA silencing. Genetic analysis showed that Hom2 and Hom6 regulate rDNA silencing partly by modulating the levels of threonine. Additionally, Hom6 may also regulate rDNA silencing through a metabolism-independent activity.

The metabolite mediating the effects of Hom2 and Hom6 on silencing remains to be identified. Although SAM is the most likely candidate, synthesis of its direct precursor, methionine, was shown to be dispensable for rDNA silencing (Fig. 3-3). Acetyl-CoA and NAD^+ are other potential candidates. Acetyl-CoA is used by multiple threonine catabolic pathways (http://pathway.yeastgenome.org/YEAST/new-image?type=PATHWAY&object=THREOCAT2-PWY&detail-level=2). Therefore, histone acetylation levels should be measured in the threonine metabolic mutants. NADPH and NADH are used by threonine anabolic and catabolic pathways, thus nuclear NAD^+ levels may also be affected in the threonine mutants, potentially mediating silencing effects through Sir2 or the Sirtuins. The effect of Hom2 and Hom6 could be

dissected using a nuclear NAD^+ reporter assay such as that employed in Chapter 2 (Fig. 2-6A).

Since the Hom6 catalytic mutant D219L exhibited partial rDNA silencing function, it is possible that Hom6 is another example of a moonlighting protein. This result needs to be validated using independent metabolic mutants of Hom6. Also, truncation analysis or other domain-directed mutagenesis could be used to map the moonlighting domain of Hom6.

Inositol polyphosphate synthesis and silencing

In Chapter 4, Arg82 was shown to regulate silencing at all three loci. Since Arg82 is an established moonlighting protein, mutants inactivating one function but not the other were studied in the context of silencing. Interestingly, the Asp113 residue at the IP kinase domain was dispensable for telomeric silencing but was required for *HM* silencing, suggesting the possibility that Arg82 might use a thus-far unidentified functional domain to regulate telomeric silencing.

Future work is needed to validate the result with the D131A IP kinase mutant, including analyzing the effect of this mutant on the native telomeric transcripts and constructing other mutations inactivating the kinase domain. If this conclusion stands, truncation analysis will help to map the domain in Arg82 required for telomeric silencing.

Additional work is also needed to understand the molecular pathway connecting Arg82 to silencing. In particular, *ARG82*'s interactions with HDACs should be analyzed by genetic and molecular analysis, based on the reports that IPs and PP-IPs play

important roles in regulating the activities of the HDACs (Watson *et al.* 2012; Worley *et al.* 2013).

H2A Tyr57 phosphorylation and transcriptional elongation

Chapter 5 reported phosphorylation on the histone H2A Tyr57(58) residue in both yeast and mammalian cells. The H2A-Y58A mutant was shown to be inviable (Nakanishi *et al.* 2008), whereas the H2A-Y58F mutant exhibited slow growth phenotype (Fig. 5-1C). Detailed study revealed that the H2A-Y58F mutation reduced RNA polymerase II binding and levels of specific histone marks at actively transcribed regions. Casein kinase CK2 was shown to be the kinase phosphorylating mammalian H2A Tyr57 and inhibition of this kinase phenocopied the effect of the H2A-Y58F mutation in yeast.

Based on the findings in Chapter 5, a number of topics are worthy of future explorations. At the more general level, it will be interesting to assess the functions of the other tyrosine residues in the yeast histones. As discussed in Chapter 1 and Chapter 5, only 3 out of the 14 tyrosine residues have been shown to be phosphorylated in yeast. The functions/modifications of the other tyrosine residues remain largely unknown. Therefore, a genetic screen of Tyr mutants should be performed, to assess phenotypes such as damage sensitivity and cell cycle progression. In particular, the H3-Y41A and H4-Y72A mutations were shown to be lethal by the histone mutant screen (Nakanishi *et al.* 2008). It will be important to construct the Tyr to Phe mutants, to see if a hypomorph could be obtained for phenotypic analysis, and if they share any of the characteristics of the H2A-Y58F or Htz1-Y65F mutants.

There are also many specific questions to be addressed for the function of H2A Tyr58 phosphorylation. Chapter 5 focused on its function in transcriptional elongation. It is possible that this modification also participates in other aspects of chromatin regulation. Unpublished work demonstrated that the H2A-Y58F mutant was also sensitive to agents inducing DNA damage. Therefore, future work is needed to fully characterize the phenotypes of this mutant, such as cell morphology, cell cycle progression, chromatin silencing and so forth.

In Chapter 5, H2A Tyr58 phosphorylation was proposed to antagonize the activity of the SAGA complex. This was based on the finding that deletion of *UBP8*, which encodes the deubiquitinase component of the SAGA complex (Fig. 1-3B), restored H2B ubiquitination levels in the H2A-Y58F mutant (Fig. 5-3C). Nonetheless, *UBP8* deletion did not suppress the other phenotypes of the H2A-Y58F mutant (Fig. 5-3C; Fig. 5-S4E-F), suggesting that additional chromatin modifiers exist to mediate the effect of H2A Tyr58 phosphorylation. Since a moderate increase in H3 Lys27 acetylation was also observed (Fig. 5-S3A), it is possible that H2A Tyr phosphorylation also regulates other functional modules of the SAGA complex (Fig. 1-3B). Therefore, future work is needed to determine if the phenotypes of the tyrosine mutant could be suppressed by mutations inactivating the other functional modules of the SAGA complex.

Lastly, the PAF1 complex is known to be important for transcriptional elongation and for mediating H3 Lys4 methylation, H3 Lys79 methylation and H2B ubiquitination (reviewed in Tomson and Ardnt 2013). Therefore, it is highly likely that this complex may have some cross-talk with H2A Tyr58 phosphorylation. At the simplest level, the H2A-Y58F mutation did not significantly reduce the binding of the Rad6, Paf1 and Rtf1

components of the PAF1 complex to the actively transcribed regions (Fig. 5-S4A-D), indicating that H2A Tyr58 phosphorylation does not regulate the association of the PAF1 complex with chromatin. However, earlier work showed that an internal deletion mutant of Rtf1 exhibited similar phenotypes as the H2A-Y58F mutant (Warner *et al.* 2007). Therefore, it is possible that Tyr58 phosphorylation works by altering the physical interactions between Rtf1 and other components. This hypothesis could be tested genetically by combining the Y58F mutation with different truncation mutants of Rtf1, to ask if loss of any Rtf1 sequence suppresses the phenotypes of the Y58F mutation.

Summary

Taken together, the results reported here, motivated by the earlier discovery of a moonlighting role for the catabolic enzyme homocitrate synthase in DNA damage repair (Scott and Pillus 2009), have set the stage for a new approach to discover additional crosstalk mechanisms between metabolic proteins and chromatin regulation. Much remains to be learned, but as highlighted in this thesis, a number of amino acid metabolic proteins were shown to have diverse functions in chromatin regulation. Further work is needed to define the molecular pathways connecting the candidate proteins to chromatin function. Given that recent studies showed many diseases are associated with metabolic changes, continuing effort should be made to appreciate the impact of such changes to chromatin regulation.

References

Duncan EM, Muratore-Schroeder TL, Cook RG, Garcia BA, Shabanowitz J, Hunt DF, Allis CD. 2008. Cathepsin L proteolytically processes histone H3 during mouse embryonic stem cell differentiation. *Cell* **135**: 284-294.

Mandal P, Verma N, Chauhan S, Tomar RS. 2013. Unexpected Histone H3 Tail-clipping Activity of Glutamate Dehydrogenase. *J Biol Chem* **288**: 18743-18757.

Nakanishi S, Sanderson BW, Delventhal KM, Bradford WD, Staehling-Hampton K, Shilatifard A. 2008. A comprehensive library of histone mutants identifies nucleosomal residues required for H3K4 methylation. *Nat Struct Mol Biol* **15**: 881-888.

Tomson BN, Arndt KM. 2013. The many roles of the conserved eukaryotic Paf1 complex in regulating transcription, histone modifications, and disease states. *Biochim Biophys Acta* **1829**: 116-126.

Warner MH, Roinick KL, Arndt KM. 2007. Rtf1 is a multifunctional component of the Paf1 complex that regulates gene expression by directing cotranscriptional histone modification. *Mol Cell Biol* **27**: 6103-6115.

Watson PJ, Fairall L, Santos GM, Schwabe JW. 2012. Structure of HDAC3 bound to co-repressor and inositol tetraphosphate. *Nature* **481**: 335-340.

Worley J, Luo X, Capaldi AP. 2013. Inositol pyrophosphates regulate cell growth and the environmental stress response by activating the HDAC Rpd3L. *Cell Rep* **3**: 1476-1482.

Xue Y, Vashisht AA, Tan Y, Su T, Wohlschlegel JA. 2014. Prb1 is required for clipping of the histone H3 N-terminal tail in *Saccharomyces cerevisiae*. *PLoS One* **9**: e90496.

Appendix A. Further analysis of the Gdh1 and Gdh3 homologs

Introduction

The functions of Gdh1 and Gdh3 in telomeric silencing were established in Chapter 2. A number of additional analyses of the Gdh homologs were undertaken during this study, but were excluded from the manuscript presented in Chapter 2 due to length constraints. The results of these supporting experiments are reported here.

Results

Metabolic mutants of Gdh1 and Gdh3 do not have telomeric silencing activity

In Chapter 2, the D150S mutant of Gdh1 was shown to have lost both metabolic and telomeric silencing functions. The function of the conserved Asp residue in Gdh3 was also assessed. The *gdh3-D151S* mutant was unable to suppress the silencing defect of the *gdh1Δ gdh3Δ* mutant (Fig. A-1), suggesting that Gdh3 also needs this catalytic residue for its silencing activity.

Two other metabolic mutants of Gdh1 were generated. Crystallographic and photoaffinity labeling studies found that Glu275 and Ser276 of bovine Gdh bind to the NAD^+ co-factor (Smith *et al.* 2001; Cho *et al.* 1998). In budding yeast, the bovine Glu275 is substituted at position 248 with an Asp residue, which has similar chemical properties (Fig. A-2A). Therefore, a Gdh1 D248L S249A mutant was constructed in yeast. We also mutated a conserved Asp74 residue shown to bind α-ketoglutarate in the bovine Gdh (Smith *et al.* 2001). Expression of Myc-tagged Gdh1 mutant proteins was assessed in a *gdh1Δ* mutant strain. The mutant proteins were expressed with modest

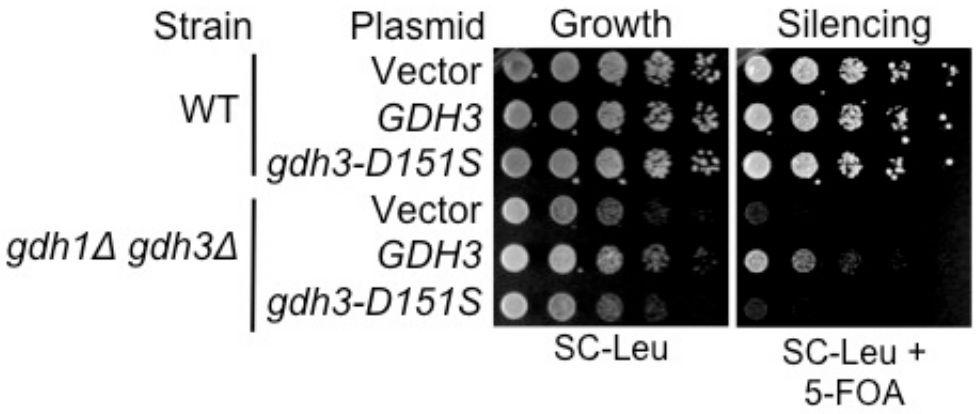

Figure A-1. The conserved Asp151 residue is also required for Gdh3's silencing activity. WT (LPY4916) and *gdh1Δ gdh3Δ* (LPY17916) strains were transformed with empty 2 micron vector (pRS425), *GDH3* (pLP2662) or *gdh3-D151S* (pLP2661). The transformants were plated on SC-Leu+5-FOA to assess telomeric silencing.

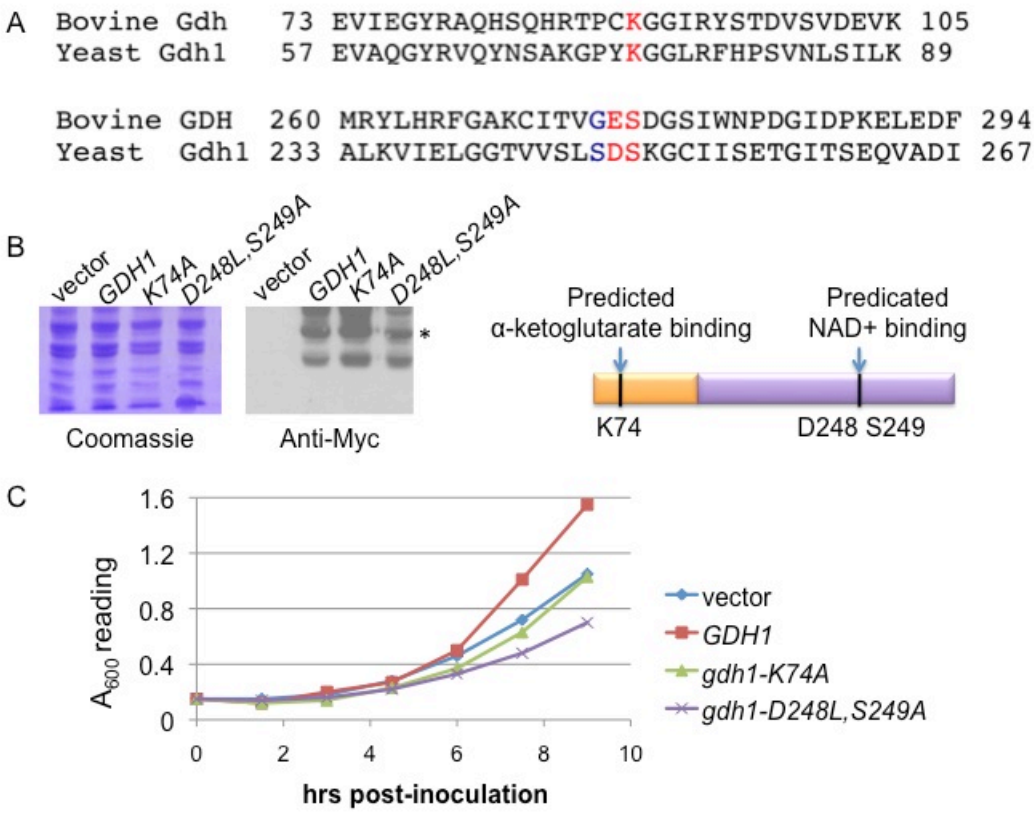

Figure A-2. Construction of additional metabolic mutants of Gdh1. (*A*) Alignment of bovine and yeast Gdh showed conservation of the predicted α-ketoglutarate and NAD^+ binding sites. The conserved residues are highlighted in red. (*B*) The Gdh1-K74A and Gdh1-D248L, S249A mutants were expressed, although expression levels changed modestly compared to the WT protein. A *gdh1Δ* strain (LPY16026) was transformed with vector (pLP316), *gdh1-K74A-Myc* (pLP2987) or *gdh1-D248L, S249A-Myc* (pLP2989). Whole cell extracts of the transformants were blotted with anti-Myc antibody. The predicted position of the Gdh1-myc protein is indicated with *. Both higher and lower molecular weight bands were observed, indicating possible proteolytic problems with the extract preparation. The Coomassie-stained acrylamide gel was shown on the left. (*C*) The *gdh1-K74A* and *gdh1-D248L, S249A* mutants were unable to suppress the metabolic defect of the *gdh1Δ* mutant. *gdh1Δ* (LPY16026) cells were transformed with empty vector (pRS315), *GDH1* (pLP2637), *gdh1-K74A* (pLP2970) or *gdh1-D248L,S249A* (pLP2939). Transformants were grown in SC-Leu media and A_{600} was monitored over time.

effects on the protein levels (Fig. A-2B). Both metabolic mutants tested were unable to suppress the slow growth phenotype of the *gdh1Δ* single mutant in ammonium-sulfate based medium (Fig. A-2C), indicating that they have lost most of the metabolic activity. The *gdh1-D248L, S249A* metabolic mutant could not suppress the silencing defect of the *gdh1Δ gdh3Δ* mutant, whereas the *gdh1-K74A* mutant poorly suppressed silencing in the *gdh1Δ gdh3Δ* strain (Fig. A-3). Because the growth assay measuring the metabolic activity followed only a short time period, it remains possible that the *gdh1-K74A* mutant had some residual metabolic activity (Fig. A-2C). In order to fully characterize these additional metabolic mutants, the metabolic growth assay should be repeated in the *gdh1Δ gdh3Δ glt1Δ* triple mutant background for an extended time period. Overall, it appears that like the D150S mutant, the other metabolic mutants of Gdh1 showed reduced silencing activities, supporting the idea that the silencing activity of Gdh1 is dependent on its metabolic function.

The alternative glutamate synthesis pathway plays a minor role in telomeric silencing

In budding yeast, glutamate biosynthesis is carried out by two independent pathways: one is catalyzed by the gene products of the *GDH* homologs, and the other is catalyzed by glutamine synthetase (encoded by *GLN1*) and NAD^+-dependent glutamate synthase (encoded by *GLT1*) (Fig. A-4A). Since the *GDH* homologs were shown to have functions in telomeric silencing in Chapter 2, it is possible that the alternative glutamate biosynthetic pathway also participates in telomeric silencing. However, when tested, I observed that the *glt1Δ* mutant exhibited only a minor silencing defect both on its own

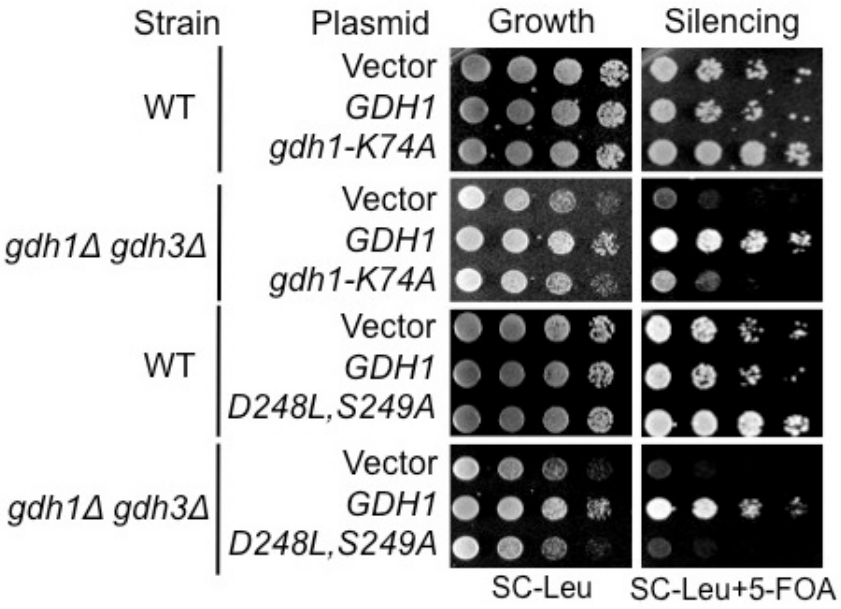

Figure A-3. Additional metabolic mutants of Gdh1 lost telomeric silencing activity. WT (LPY4916) and *gdh1Δ* (LPY16033) cells were transformed with empty vector (pRS315), *GDH1* (pLP2637), *gdh1-K74A* (pLP2970) or *gdh1-D248L, S249A* (pLP2939). Transformants were plated on SC-Leu + 5-FOA to assess telomeric silencing.

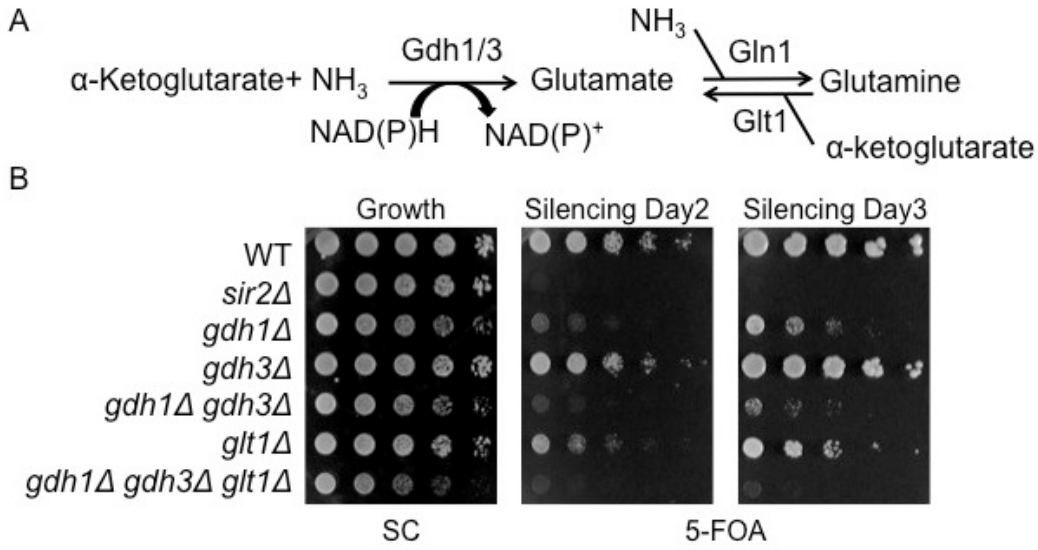

Figure A-4. Glt1 has a minor role in regulating telomeric silencing. (*A*) The anabolic pathways synthesizing glutamate in budding yeast. (*B*) The deletion of *GLT1* caused a mild defect in telomeric silencing. WT (LPY4916), *sir2Δ* (LPY4979), *gdh1Δ* (LPY16033), *gdh3Δ* (LPY16785), *gdh1Δ gdh3Δ* (LPY17916), *glt1Δ* (LPY18316), *gdh1Δ gdh3Δ glt1Δ* (LPY18576) were plated on 5-FOA to assess telomeric silencing. The *sir2Δ* strain served as a positive control for defective telomeric silencing.

and in combination with the *gdh1Δ gdh3Δ* mutant (Fig. A-4B), suggesting that the alternative glutamate synthesis pathway has only a minor role in the regulation of telomeric silencing.

Adding back glutamate partially rescues the silencing defects of the *GDH* mutants

In the absence of *GDH1,* yeast cells have reduced ability to assimilate ammonium to synthesize glutamate. Therefore, it is possible that the reduction in glutamate levels causes the telomeric silencing defect in the *GDH* deletion mutants. To test this possibility, the control and silencing plates were supplemented with 0.04% (w/v) glutamate (Fig. A-5). The addition of glutamate completely rescued the slow growth phenotype of the *GDH* mutants on the control plate, suggesting that the yeast strains were able to actively take up this metabolite from the medium (Fig. A-5). On the other hand, the added glutamate only partially rescued the silencing phenotypes of the *GDH* mutants (Fig. A-5) and higher glutamate concentrations did not further improve silencing (not shown). This suggests that the reduction in glutamate levels is not causing the silencing defects of *GDH* mutants. The partial rescue could be explained by the idea that the added glutamate stimulates metabolic pathways that actively consume α-ketoglutarate, and thus alleviate the negative impact of high α-ketoglutarate levels on telomeric silencing.

Gdh1 does not regulate telomeric silencing through controlling nitrogen catabolite repression

In budding yeast, genes encoding proteins involved in the use of non-preferred nitrogen sources are normally repressed when the preferred nitrogen source is present, a

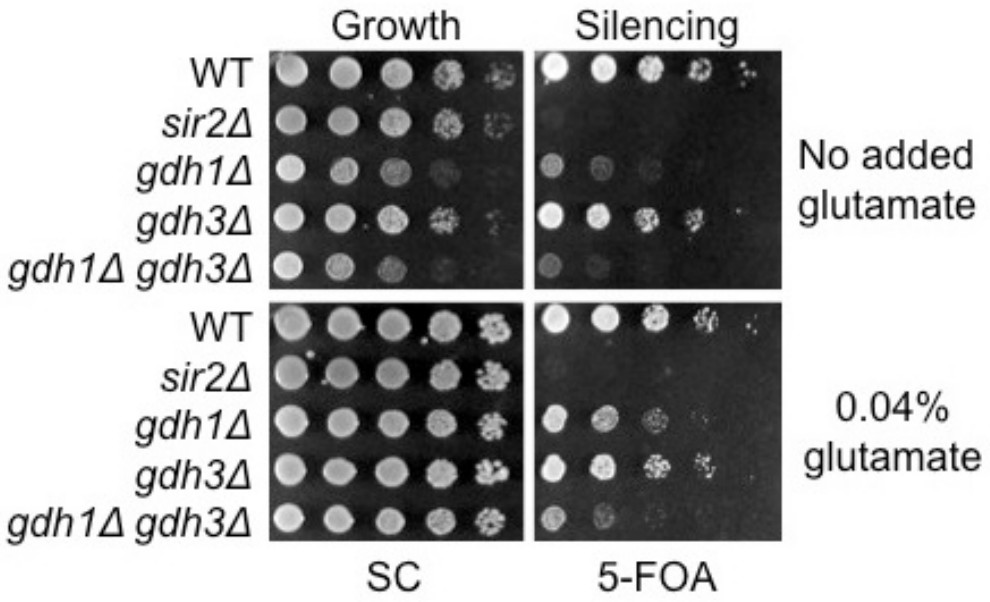

Figure A-5. Addition of glutamate completely rescued the growth defects but only weakly rescued the silencing defects of the *GDH* mutants. WT (LPY4916), *sir2Δ* (LPY4979), *gdh1Δ* (LPY16033), *gdh3Δ* (LPY16785) and *gdh1Δ gdh3Δ* (LPY17916) were plated on 5-FOA to assess telomeric silencing. Top plates: no additional glutamate was added to the 5-FOA media. Bottom plates: 0.04% (w/v) glutamate was supplemented to the 5-FOA media.

phenomenon termed nitrogen catabolite repression (reviewed by Ljungdahl and Daignan-Fornier 2012). When *GDH1* is deleted, yeast cells have a drastically reduced ability to assimilate ammonium and therefore respond to this change by lifting nitrogen catabolite repression. Therefore, it is possible that in the *GDH1* deletion mutant, a global gene expression change related to catabolite repression contributes to the mutant's telomeric silencing defect. To test this hypothesis, a *ure2Δ* strain was made as an independent way of relieving catabolite repression. The gene product of *URE2* normally sequesters the Gln3 transcriptional activator in the cytoplasm in the presence of preferred nitrogen source. Deletion of *URE2* results in constitutive activation of genes regulated by catabolite repression (reviewed by Ljungdahl and Daignan-Fornier 2012, Fig. A-6A). I observed that the *ure2Δ* mutant did not cause major changes to telomeric silencing (Fig. A-6B), suggesting that the removal of catabolite repression is unlikely to explain the *gdh1Δ* mutant's silencing phenotype.

Alternative nitrogen source and telomeric silencing

Pursuing the idea that the *gdh1Δ* mutant might be silencing-defective because of the use of alternative nitrogen sources, the WT and the *gdh1Δ* strains were assessed on growth media with 0.1% (w/v) proline, or with 0.15% (w/v) urea instead of ammonium sulfate (Fig. A-7). The WT strain did not show any change in telomeric silencing when grown in these alternative nitrogen sources, suggesting that telomeric silencing is not regulated by the use of proline or urea (Fig. A-7). The *gdh1Δ* mutant, in contrast, showed improved silencing in the presence of alternative nitrogen sources (Fig. A-7). This

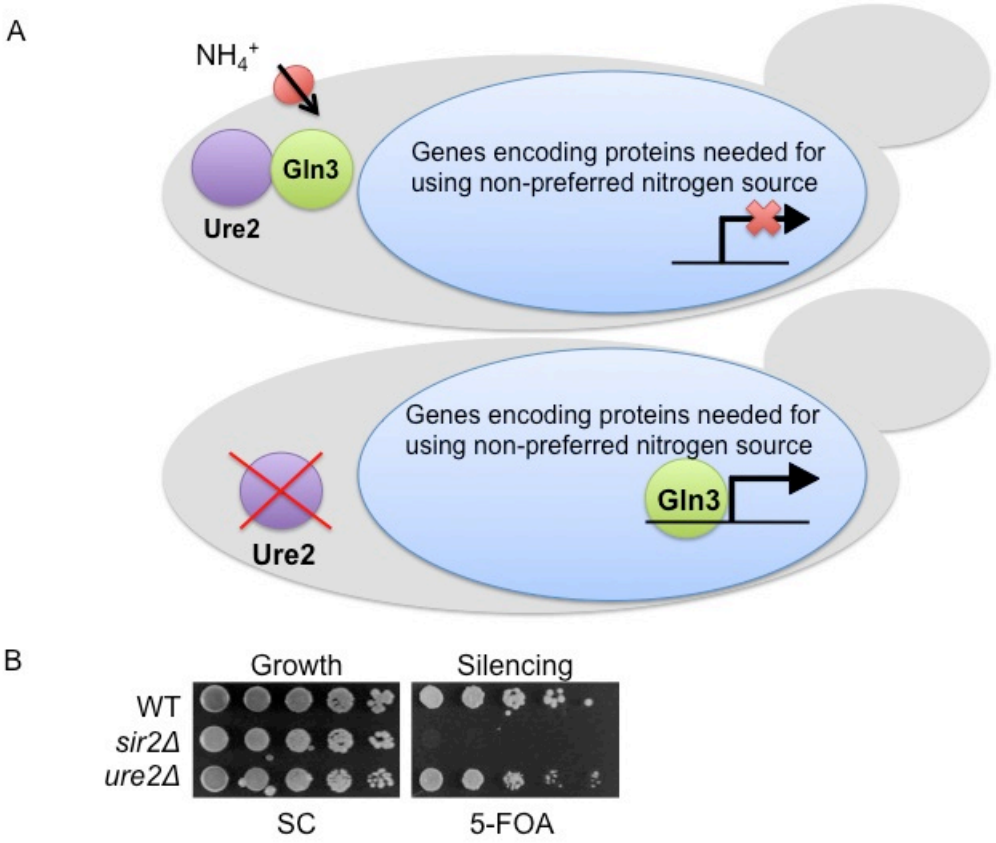

Figure A-6. Nitrogen catabolite repression is not a regulator of telomeric silencing. (*A*) Diagram demonstrating the mechanism of catabolite repression. In the presence of a preferred nitrogen source, e.g. NH_4^+, Ure2 sequesters Gln3 in the cytoplasm. When Ure2 is inactivated, the Gln3 transcriptional activator upregulates the expression of genes needed for the use of non-preferred nitrogen sources. (*B*) Deletion of *URE2* had little impact on telomeric silencing. WT (LPY4916), *sir2Δ* (LPY4979) and *ure2Δ* (LPY19570) strains were plated on 5-FOA to assess silencing.

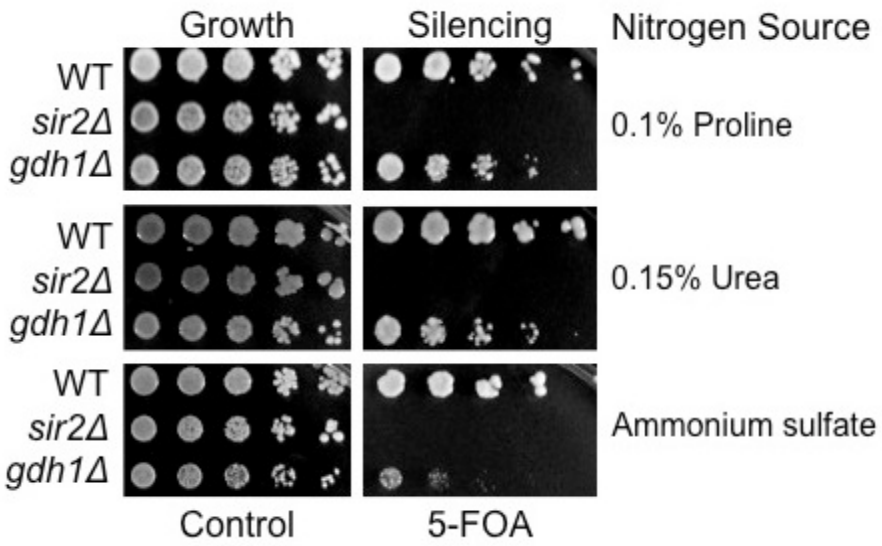

Figure A-7. Growth on alternative nitrogen sources rescued *gdh1Δ*'s telomeric silencing phenotype. WT (LPY4916), *sir2Δ* (LPY4979) and *gdh1Δ* (LPY16033) strains were plated on 0.1% (w/v) proline, 0.15% (w/v) urea or ammonium sulfate-based SC medium, with or without 5-FOA.

observation could be explained by the fact that the yeast metabolome undergoes major changes in the presence of alternative nitrogen sources, and α-ketoglutarate levels might be restored under these growth conditions. Overall, this finding suggests that the use of alternative nitrogen sources alone does not elicit changes in telomeric silencing.

Histone H3 clipping is further elevated by deletion of the *GDH* mutants under nitrogen starvation conditions

A high-throughput protein localization study suggested that Gdh1 has an increased nuclear pool under nitrogen starvation conditions (Breker *et al.* 2014; http://wws.weizmann.ac.il/molgen/loqate/). Chapter 2 established that Gdh1 has an inhibitory effect on histone H3 clipping when grown in synthetic complete medium. Here the effect of *GDH* deletions on H3 clipping was evaluated under nitrogen starvation conditions (Materials and Methods). Two independent experiments showed that H3 clipping was elevated in both the *gdh1Δ* and the *gdh1Δ gdh3Δ* mutants (Fig. A-8). Of note, total H3 levels were also increased in the *gdh1Δ gdh3Δ* mutant (Fig. A-8). Further experiments will be needed to allow quantification of these results. Overall, it appears that the Gdh homologs regulate both H3 levels and H3 clipping under nitrogen starvation conditions.

Increased dosage of *SIR2* or *SIR3* does not suppress the silencing phenotype of the *GDH* mutants

In Chapter 2, it was shown that global Sir2 or Sir3 protein levels did not change in the *gdh1Δ* mutant (Fig. 2-3B). To support this idea, the *GDH* mutants were transformed with *CEN* plasmids carrying *SIR2* or *SIR3*. Increased dosage of the *SIR* genes did not

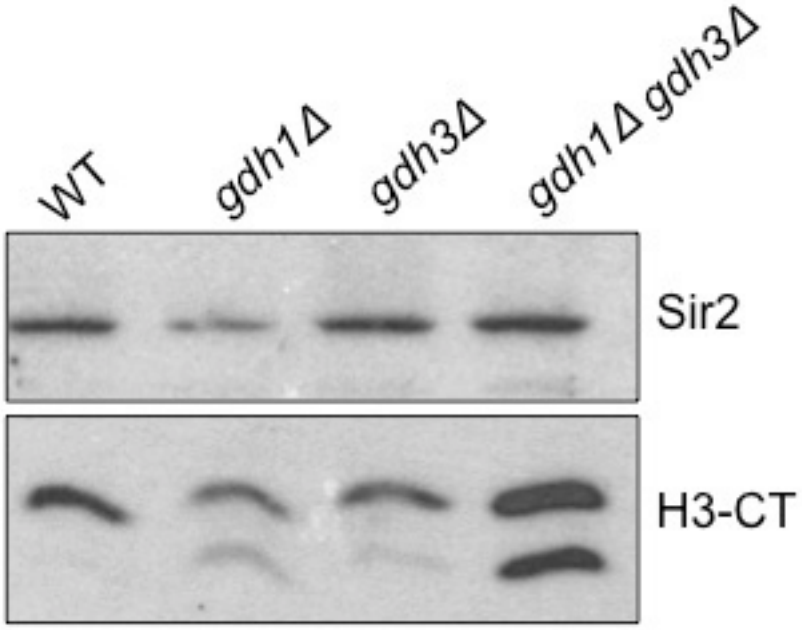

Figure A-8. H3 clipping was further increased when the *GDH* mutants were grown under nitrogen starvation conditions. Nuclear extracts were prepared from WT (LPY4916), *gdh1Δ* (LPY16033), *gdh3Δ* (LPY16785) and *gdh1Δ gdh3Δ* (LPY17916) mutants grown under nitrogen starvation conditions (Materials and Methods) and immunoblotted for Sir2 (loading control) and H3-CT.

Improve silencing in either the single or the double mutants (Fig. A-9). These findings suggest that Gdh1 does not regulate telomeric silencing by modulating levels of Sir proteins.

Increased gene dosage of histone demethylases worsened telomeric silencing in the *gdh1Δ* mutant

There are five JMJC-domain containing histone demethylases (Tu *et al.* 2007) encoded in the genome of budding yeast, among which Jhd1, Jhd2, Rph1 and Gis1 have established demethylase activities (Fig. A-10A). Since it is known that the JMJC-domain containing demethylases use α-ketoglutarate as a co-factor (reviewed by Shneider and Shilatifard 2006), it is possible that the elevated α-ketoglutarate levels in the *gdh1Δ* mutant resulted in their hyperactivity, which in turn reduced telomeric silencing. To test this idea, WT and *gdh1Δ* mutant strains were transformed with plasmids carrying each of the genes encoding the JMJC-domain containing demethylases (Fig. A-10B). Although increased dosage of these genes had little effect on the WT strain, they worsened the silencing defect of the *gdh1Δ* mutant (Fig. A-10B). This result suggests that the deletion of *GDH1* creates a condition in which increased dosage of demethylases diminish telomeric silencing.

Gdh1's effect on telomeric silencing is independent of the JMJC-domain containing histone demethylases

To test if the hyperactivation of histone demethylases caused the silencing defect in the *gdh1Δ* mutant, *JHD1*, *JHD2* and *RPH1* were deleted either singly or in combination with the *GDH1* deletion. The deletion of *JHD1* and *RPH1* did not alter

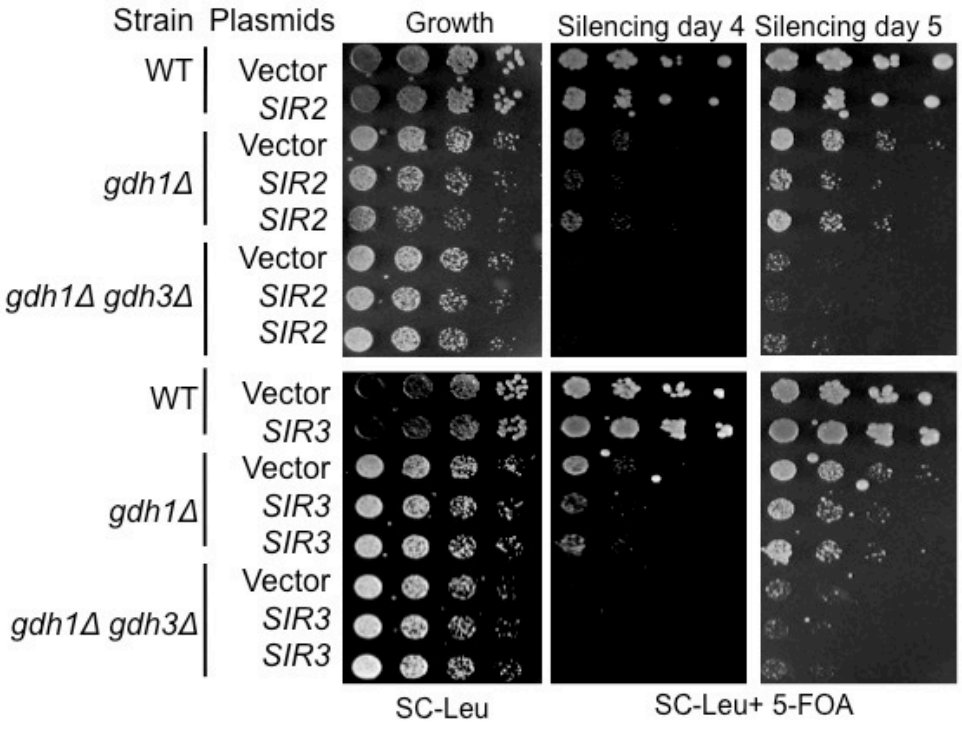

Figure A-9. Increased dosage of *SIR2* or *SIR3* did not rescue the silencing defect of the *GDH* single or double mutants. WT (LPY4916), *gdh1Δ* (LPY16033) or *gdh1Δ gdh3Δ* (LPY17916) strains were transformed with empty vector (pRS315), *SIR2* (pLP1237) or *SIR3* (pLP190) plasmids. Transformants were plated at 5-fold dilution, starting with A_{600} of 0.5. Two independent *SIR* transformants were plated for the *GDH* mutants.

A

Demethylase	Substrate	Reference
Jhd2	Tri-methylated H3K4	Liang *et al.* 2007
Jhd1	Tri-methylated H3K36	Fang *et al.* 2007; Kim and Buratowski 2007
Gis1	Methylated H3K36 (detail unclear)	Tu *et al.* 2007
Rph1	Tri- and di-methylated H3K36	Kim and Buratowski 2007

B

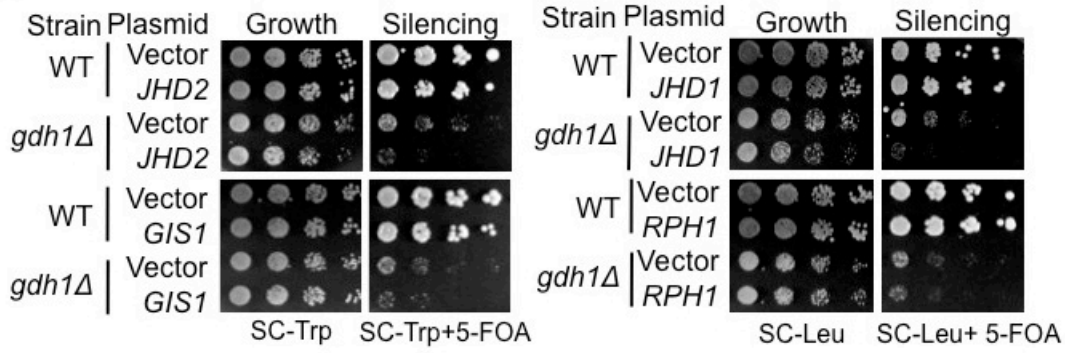

Figure A-10. Increased dosage of genes encoding JMJC-domain containing demethylases worsened the telomeric silencing defect of the *gdh1Δ* mutant to varying degrees. (*A*) Summary of the enzymatic activities of the yeast JMJC-domain containing demethylases. (*B*) WT (LPY4916) or *gdh1Δ* (LPY16033) strains were transformed with *JHD2* (pLP2928), *JHD1* (pLP2942), *RPH1* (pLP2930), *GIS1* (pLP2929) and the respective vector controls. The transformants were plated on the corresponding SC drop-out medium + 5-FOA to assess telomeric silencing.

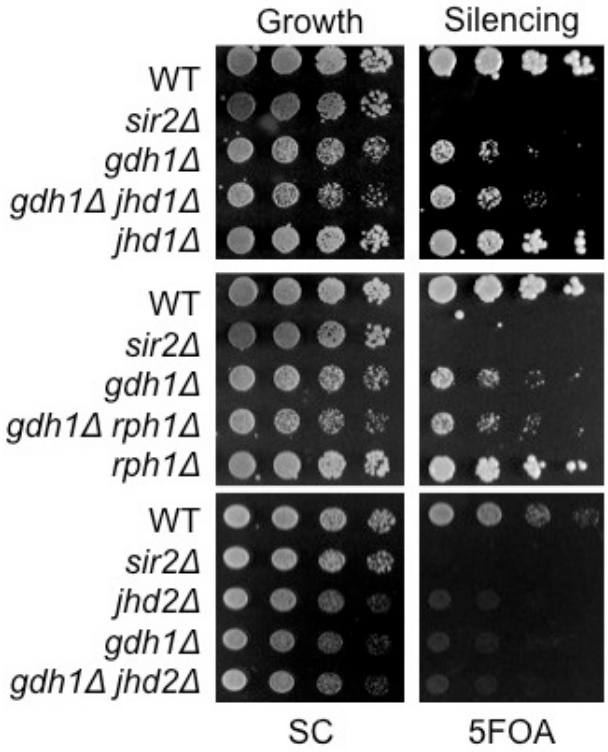

Figure A-11. Deletion of JMJC-domain containing demethylases did not suppress the silencing defect of the *gdh1Δ* mutant. WT (LPY4916), *sir2Δ* (LPY4979), *gdh1Δ* (LPY16033), *jhd1Δ* (LPY18873), *jhd2Δ* (LPY18880), *rph1Δ* (LPY18501), *gdh1Δ jhd1Δ* (LPY18673), *gdh1Δ jhd2Δ* (LPY18414), *gdh1Δ rph1Δ* (LPY18600) strains were plated on 5-FOA to assess silencing.

telomeric silencing, nor did they suppress the silencing defect of the *gdh1Δ* mutant (Fig. A-11). This finding suggests that Jhd1 and Rph1 are not major players in telomeric silencing. However, the deletion of *JHD2* reduced silencing of the reporter gene inserted at *TELV-R.* This is in contrast to the previous report that the *jhd2Δ* mutant modestly improved silencing at *TELVII-L* (Liang *et al.* 2007). This discrepancy was not unprecedented, as prior studies indicated that some mutants have opposing effects on the silencing of different telomeres (Fourel *et al.* 1999; Pryde and Louis 1999). The *gdh1Δ jhd2Δ* double mutant showed similar telomeric silencing defect as each single mutant, suggesting that they might function in a common pathway (Fig. A-11). However, earlier work suggested that H3K4 tri-methylation levels increased rather than decreased at the telomeres in the *gdh1Δ* mutant (Figure 2-S5C). Therefore, the genetic interaction between Jhd2 and Gdh1 appears to be complex and requires further examination.

Gdh1's effect on telomeric silencing is independent of the Set1 complex

It is known that histone H3 Lys4 methylation carried out by the Set1 complex is an important regulator of telomeric silencing (Fig. A-12A). Deletion of individual components of the Set1 complex cause varying degrees of silencing defects at telomeres (Nislow *et al.* 1997; Krogan *et al.* 2002). In order to study the genetic interaction between *GDH1* and the Set1 complex, the *gdh1Δ set1Δ* double mutant strain was generated. This double mutant exacerbated the telomeric silencing defect of each single mutant, indicating that the two gene products may regulate telomeric silencing through distinct pathways (Fig. A-12B). Further, it was reported that histone H3 Lys4 tri-methylation

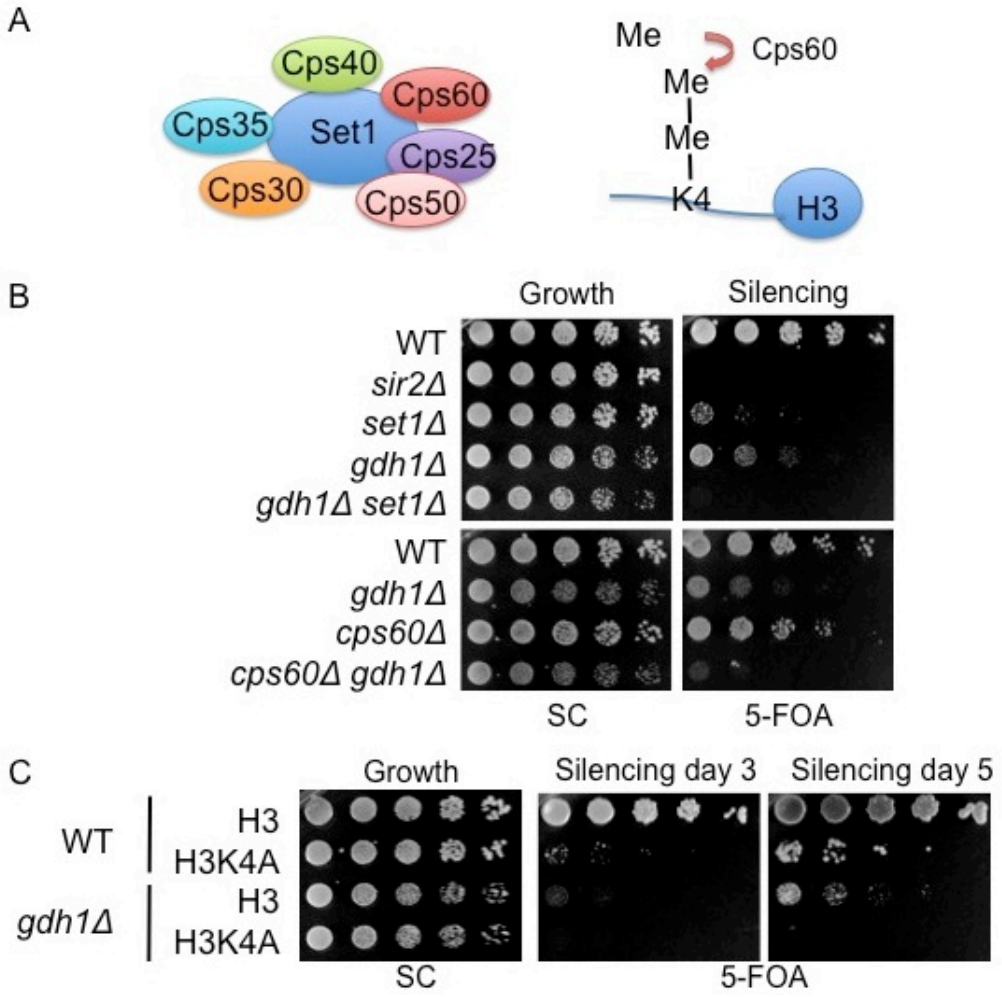

Figure A-12. Gdh1 and the Set1 complex do not regulate telomeric silencing through the same pathway. (*A*) Schematics depicting the components of the Set1 complex. The Cps60 subunit facilitates Set1 mediated methylation of di-methylated H3 Lys4. (*B*) Deletion of *SET1* or *CPS60* exacerbated the telomeric silencing phenotype of the *gdh1Δ* mutant. WT (LPY4916), *sir2Δ* (LPY4979), *gdh1Δ* (LPY16033), *set1Δ* (LPY6928), *cps60Δ* (LPY20703), *gdh1Δ set1Δ* (LPY20376), *gdh1Δ cps60Δ* (LPY20697) strains were plated on 5-FOA to assess telomeric silencing. (*C*) The H3K4A mutation exacerbated the telomeric silencing defect of the *gdh1Δ* mutant. The following histone shuffle strains were plated on 5-FOA to assess silencing: WT strains with WT histone H3 (LPY20469) or H3K4A (LPY20621); *gdh1Δ* strains with WT histone H3 (LPY20623) or H3K4A(LPY20473). Of note, the *gdh1Δ* histone shuffle strain exhibited a stronger silencing phenotype than a non-shuffle strain.

regulates silencing by facilitating the establishment of the boundaries between heterochromatin and euchromatin (Santos-Rosa *et al.* 2004), and the Cps60 subunit of the Set1 complex was shown to specifically facilitate Set1-mediated methylation of di-methylated H3K4 (Schneider *et al.* 2005; Fig. A12-A). Deletion of *GDH1* and *CPS60* had an additive effect on telomeric silencing (Fig. A12-B), confirming that Gdh1 and the H3K4 methylation machinery regulate silencing through distinct pathways. In support of the same conclusion, the H3K4A mutation exacerbated the silencing defect of the *gdh1Δ* mutant (Fig. A12-C). Taken together, Gdh1 is unlikely to regulate telomeric silencing by modulating the activity of the Set1 complex.

The Prb1 protease regulates telomeric silencing

In budding yeast, a vacuolar protease encoded by *PRB1* has histone H3 protease activity both *in vitro* and *in vivo* (Xue *et al.* 2014). Because H3 clipping is upregulated in *gdh1Δ* cells, the genetic interaction between *PRB1* and *GDH1* was evaluated. Increased dosage of *PRB1* reduced telomeric silencing both in the WT and in the *GDH* mutants (Fig. A-13A), consistent with the idea that increased H3 protease activity has a negative impact on telomeric silencing. Deletion of *PRB1*, on the other hand, modestly improved telomeric silencing in both the WT and *gdh1Δ* strains (Fig. A-13B). These mild interactions between *GDH1* and *PRB1* suggest that Prb1 plays a partial role in mediating Gdh1's effect on telomeric silencing. Future work is needed to further test this hypothesis, to assess the levels of H3 clipping in the *prb1*Δ *gdh1*Δ and *PRB1* over-expressing strains, and to establish the molecular pathway linking Gdh1 to Prb1.

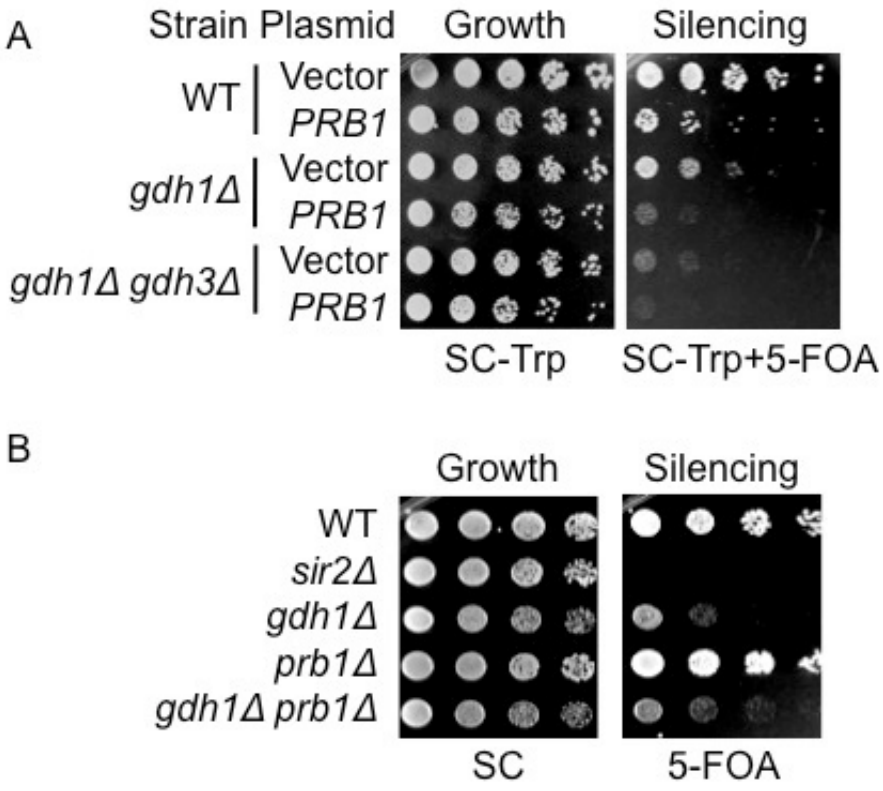

Figure A-13. Prb1 regulates telomeric silencing *in vivo*. (*A*) Increased dosage of *PRB1* reduced telomeric silencing in both the WT and the *GDH* deletion strains. WT (LPY4916), *gdh1Δ* (LPY16033), *gdh1Δ gdh3Δ* (LPY17916) strains were transformed with empty vector (pRS315) or *PRB1* (pLP3303) and plated on SC-Trp+5-FOA to assess silencing. (*B*) Deletion of *PRB1* weakly suppressed the silencing phenotype of the *gdh1Δ* mutant. WT (LPY4916), *sir2Δ* (LPY4979), *gdh1Δ* (LPY16033), *prb1Δ* (LPY16143), *gdh1Δ prb1Δ* (LPY16150) were plated on 5-FOA to assess silencing.

Gdh1 might regulate telomeric silencing through the same pathway as the histone chaperone Asf1

Although global H3 levels did not show changes in the *gdh1Δ* mutant (Fig. A-14A), ChIP experiments showed that total histone H3 levels changed at *TELVI-R* (Fig. A-14B). Sir2 binding was restored in the *gdh1Δ* histone shuffle strain for *TELVI-R* (Figure 2-S6C-D) and it was hypothesized this is due to altered histone dosage in the shuffle strain. Therefore, it is possible that Gdh1 also regulates telomeric silencing through modulating histone H3 levels at telomeres such as *TELVI-R*.

Histone chaperones such as Asf1 and Cac1 are known to regulate telomeric silencing by controlling subtelomeric H3 levels (Tamburini *et al.* 2006). Therefore, the genetic interactions between *GDH1* and *ASF1* or *CAC1* were tested. First, increased dosage of *ASF1* worsened telomeric silencing in both the WT and the *gdh1Δ* strains, consistent with the reported anti-silencing role of Asf1 (Fig. A-14C). Further, the *asf1Δ* mutant had a similar silencing defect as the *gdh1Δ* mutant and the double mutant showed no additive effect (Fig. A-14D). Similar results were observed with *CAC1*, although the *cac1Δ* mutant had a severe silencing defect for *TELVI-R* and so it was unclear whether the double mutant had additive effects (Fig. A-14E; Fig. A-14F). These results suggest that Gdh1 and Asf1/Cac1 may regulate telomeric silencing through a common pathway. Interestingly, the *asf1Δ* mutant also exhibited moderately increased clipping (Feser *et al.* 2010), although this result was not discussed in that study. Future work is required to ask whether Gdh1 and Asf1 work together to regulate SIR recruitment at *TELVI-R*.

Figure A-14. *GDH1* has genetic interactions with histone chaperones. (*A*) Global H3 levels did not change in the *GDH* mutants. Whole cell extract of WT (LPY4916), *gdh1Δ* (LPY16033) and *gdh1Δ gdh3Δ* (LPY17916) strains grown in SC medium were immunoblotted with anti-H3-CT or anti-Tub1 (loading control). (*B*) Deletion of *GDH1* changed H3-CT levels at *TELVI-R*. Sheared chromatin from WT (LPY5) and *gdh1Δ* (LPY16026) strains was IPed with anti-H3-CT antibody. Enrichment of H3-CT at each locus was normalized to that at the *ACT1* control locus. (*C*) Increased dosage of *ASF1* reduced telomeric silencing in both the WT and the *gdh1Δ* mutant. WT (LPY4916) and *gdh1Δ* (LPY16033) cells were transformed with empty vector (pRS314) or *ASF1* (pLP3138). Transformants were plated at 2.5-fold dilutions, starting with A_{600} of 0.5. (*D*) Deletion of *ASF1* and *GDH1* had no additive effect on telomeric silencing. WT (LPY4916), *sir2Δ* (LPY4979), *gdh1Δ* (LPY16033), *asf1Δ* (LPY19898), *asf1Δ gdh1Δ* (LPY19901), *asf1Δ* (LPY19900) and *asf1Δ gdh1Δ* (LPY19902) strains were plated on 5-FOA to assess telomeric silencing. (*E*) Increased dosage of *CAC1* exacerbated silencing in the *gdh1Δ* mutant. WT and *gdh1Δ* cells were transformed with empty vector (pRS314) or *CAC1* (pLP3073). (*F*) The *cac1Δ* and *cac1Δ gdh1Δ* mutants showed severe telomeric silencing defect. WT, *sir2Δ, gdh1Δ, cac1Δ* (LPY19928)*, gdh1Δ cac1Δ* (LPY19929 and LPY19930) mutants were plated on 5-FOA to assess telomeric silencing.

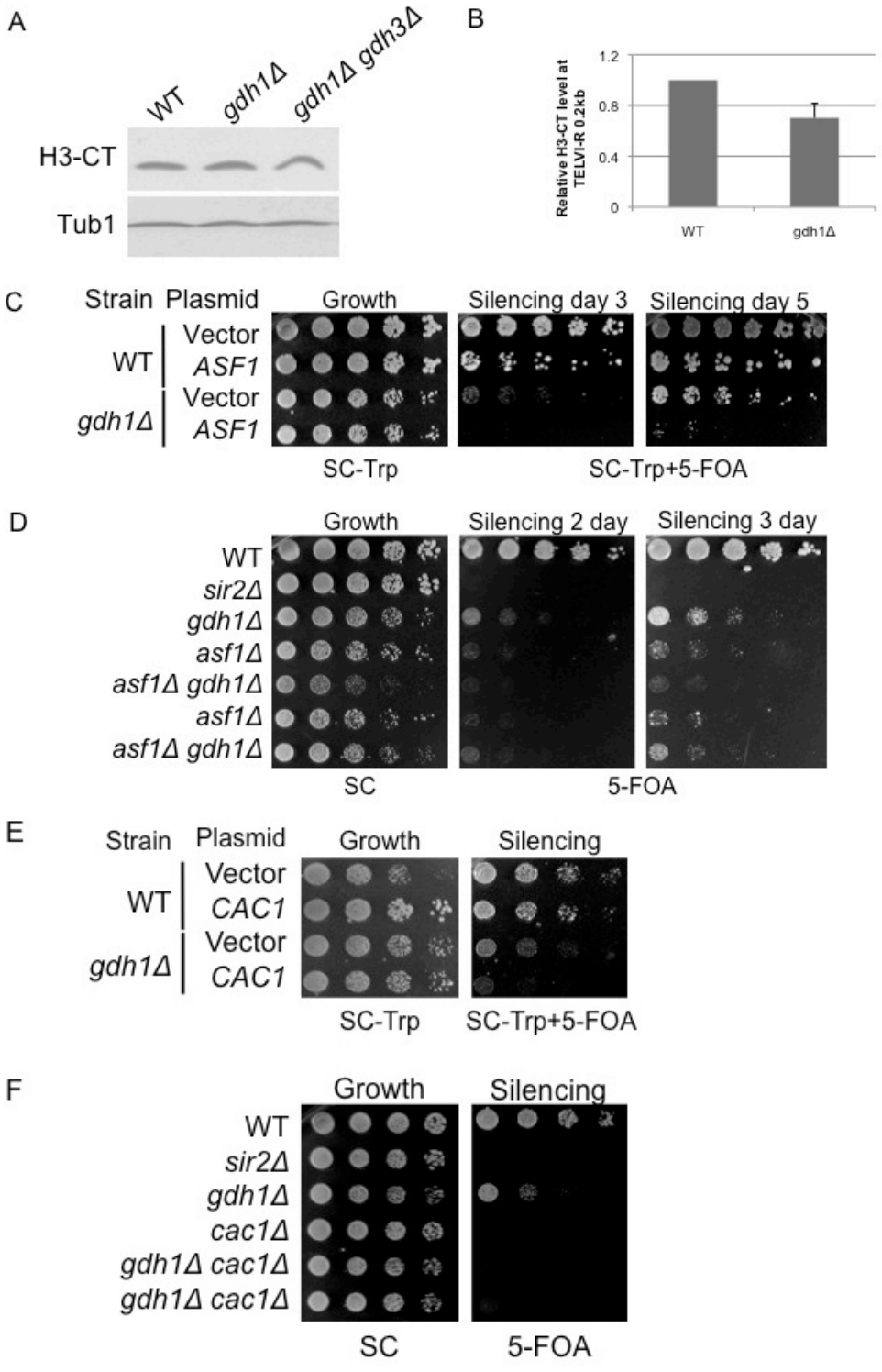
A
WT
gdh1Δ
gdh1Δ gdh3Δ
H3-CT
Tub1
B
Relative H3-CT level at TELVI-R 0.2kb
1.2
0.8
0.4
0
WT
gdh1Δ
C
Strain
Plasmid
Growth
Silencing day 3
Silencing day 5
WT
Vector
ASF1
gdh1Δ
Vector
ASF1
SC-Trp
SC-Trp+5-FOA
D
Growth
Silencing 2 day
Silencing 3 day
WT
sir2Δ
gdh1Δ
asf1Δ
asf1Δ gdh1Δ
asf1Δ
asf1Δ gdh1Δ
SC
5-FOA
E
Strain
Plasmid
Growth
Silencing
WT
Vector
CAC1
gdh1Δ
Vector
CAC1
SC-Trp
SC-Trp+5-FOA
F
Growth
Silencing
WT
sir2Δ
gdh1Δ
cac1Δ
gdh1Δ cac1Δ
gdh1Δ cac1Δ
SC
5-FOA

Increased dosage of *HTL1* suppresses the silencing phenotype of the *gdh1Δ* mutant

The RSC chromatin remodeling complex is a highly abundant complex that is known to regulate the deposition and the removal of histones (reviewed in Rando and Winston 2012). A small protein encoded by *HTL1* was found to be a component of the RSC complex (Romeo *et al.* 2002). Interestingly, a high throughput screen revealed a physical interaction between Htl1 and Gdh3 (Krogan *et al.* 2006). When *HTL1* was expressed on a high copy 2-micron plasmid, it suppressed the telomeric silencing defect of the *gdh1Δ* mutant (Fig. A-15). This result suggests that higher dosage of a RSC complex component rescued the effect of deleting *GDH1*, either by directly acting at the telomeres, or indirectly by regulating expression of other chromatin modifiers. Future experiments are needed to test if *GDH1* also interacts with other components of the RSC complex, and whether *HTL1* suppresses the telomeric silencing defect of the *gdh1Δ* mutant directly at the telomeres.

Gdh1 regulates Sas2 levels but works independently of Sas2

Sas2 is a HAT that carries out acetylation on histone H4 Lys16 (Suka *et al.* 2002). Sas2 is required for the correct establishment of the boundaries between euchromatin and heterochromatin (Shia *et al.* 2006). To assess the interaction between Gdh1 and Sas2, HA-tagged Sas2 protein levels were measured in the *sas2Δ* or *gdh1Δ sas2Δ* mutants. Reduced HA signals were observed in the *gdh1Δ sas2Δ* mutant (Fig. A-16A), suggesting that Sas2 protein levels were reduced in the *gdh1Δ* background. To assess whether this contributes to the silencing defect of the *gdh1Δ* mutant, the strain was transformed with a CEN plasmid carrying *SAS2*. Increased dosage of *SAS2* did not suppress the silencing

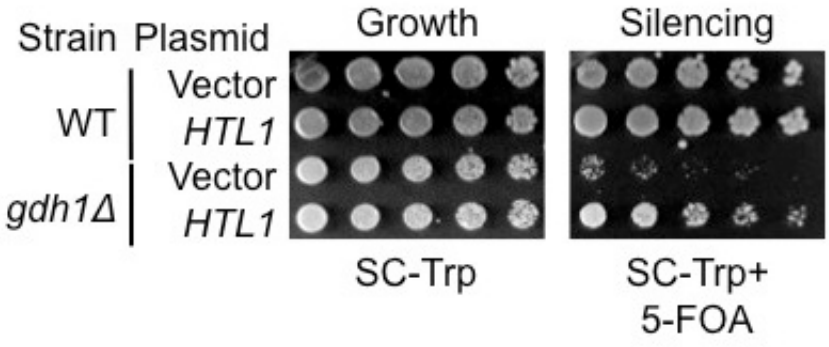

Figure A-15. *HTL1* is a high copy suppressor of *gdh1Δ* mutant's telomeric silencing phenotype. Increased dosage of *HTL1* suppressed the telomeric silencing phenotype of the *gdh1Δ* mutant. WT (LPY4916) and *gdh1Δ* (LPY16033) cells were transformed with empty vector (pRS424) or *HTL1* (pLP3084). A_{600} of 0.5 of transformants were plated at 2.5-fold serial dilutions on the indicated media.

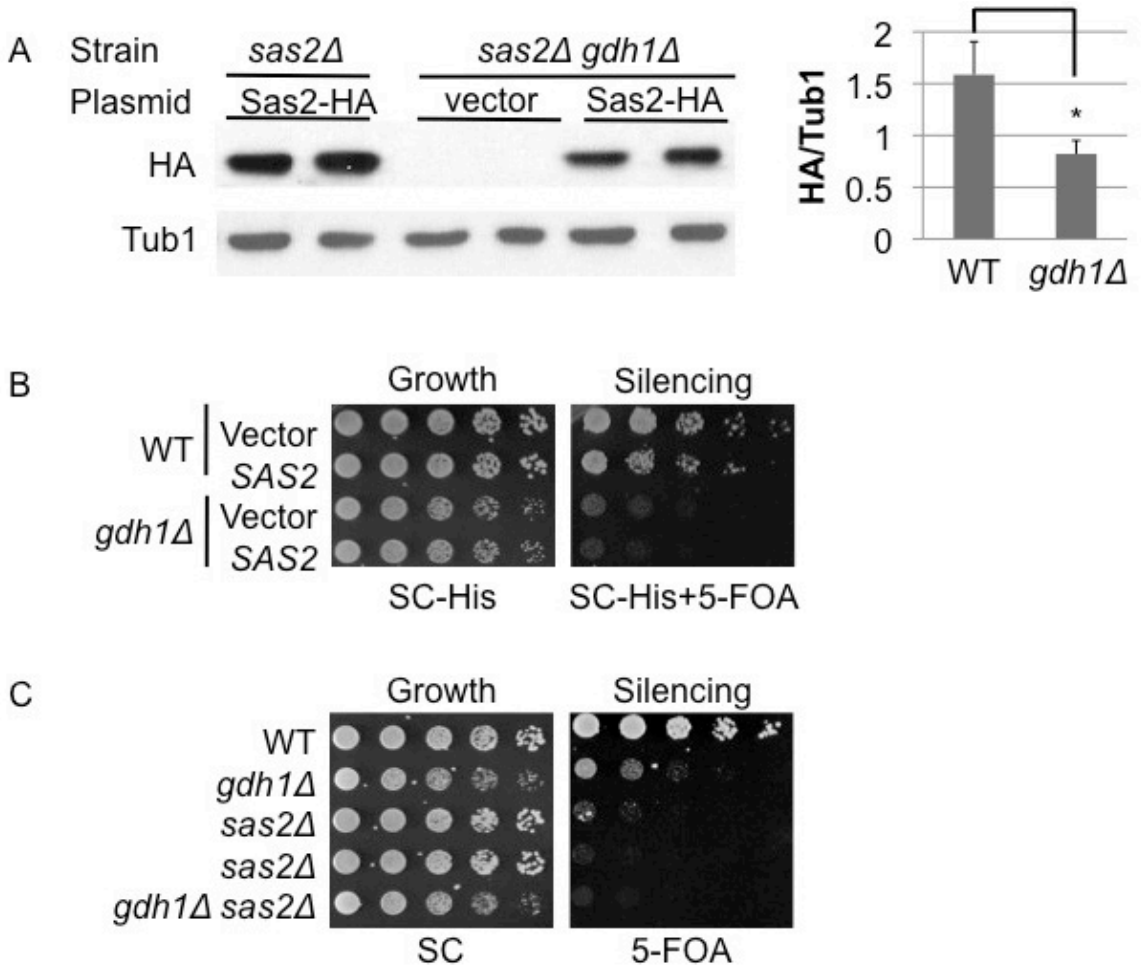

Figure A-16. Gdh1 regulates Sas2 levels but works independently of Sas2 at the telomeres. (*A*) Sas2 levels were reduced in the *gdh1Δ* mutant. The *sas2Δ* (LPY1589) and *gdh1Δ sas2Δ* (LPY21352) mutants were transformed with empty vector (pMA424) or *SAS2-HA* (pLP646). Whole cell extracts of the transformants were immunoblotted with anti-HA or anti-Tub1 (loading control). (*B*) Increased dosage of *SAS2* did not suppress the telomeric silencing defect of the *gdh1Δ* mutant. WT (LPY4916) and *gdh1Δ* (LPY16033) cells were transformed with empty vector (pRS313) or *SAS2* (pLP425) and plated on SC-His+5-FOA to assess telomeric silencing. (*C*) The *gdh1Δ sas2Δ* double mutant showed worse silencing defect than each single mutant. WT (LPY4916), *gdh1Δ* (LPY16033), independent spores of *sas2Δ* and *gdh1Δ sas2Δ* (LPY21354) were plated on 5-FOA to assess telomeric silencing.

phenotype of the *gdh1Δ* mutant (Fig. A-16B), indicating that lowered Sas2 protein levels are unlikely to explain *gdh1Δ*'s silencing defect. Also, the *gdh1Δ sas2Δ* mutant exhibited worse telomeric silencing than each single mutant, supporting the conclusion that Gdh1 and Sas2 regulate telomeric silencing through independent pathways.

Gdh1's role in telomeric silencing is independent of Rpd3

Rpd3 is the catalytic subunit of both the Rpd3L and Rpd3S histone deacetylase complexes (reviewed in Rando and Winston 2012). Rpd3 was reported to regulate the boundary formation between euchromatin and heterochromatin, through removing a substrate for Sir2 (Ehrentraut *et al.* 2010). The genetic interaction between Rpd3 and Gdh1 was assessed. Rpd3 protein levels in the *gdh1Δ* mutant did not change (Fig. A-17B). Further, deletion of *RPD3* partially suppressed the silencing defect of the *gdh1Δ* mutant (Fig. A-17C), suggesting that the Rpd3 pathway was functional in the *gdh1Δ* mutant yeast. Therefore, it seems unlikely that Gdh1 regulates telomeric silencing through an Rpd3-dependent pathway.

Discussion

Appendix A presented many experiments that were excluded from Chapter 2 due to length constraints. Briefly, this Appendix contains further information on two general aspects of Gdh1's function. The first aspect relates to the connection between metabolism and silencing, while the second aspect relates to Gdh1's genetic interactions with known chromatin regulators.

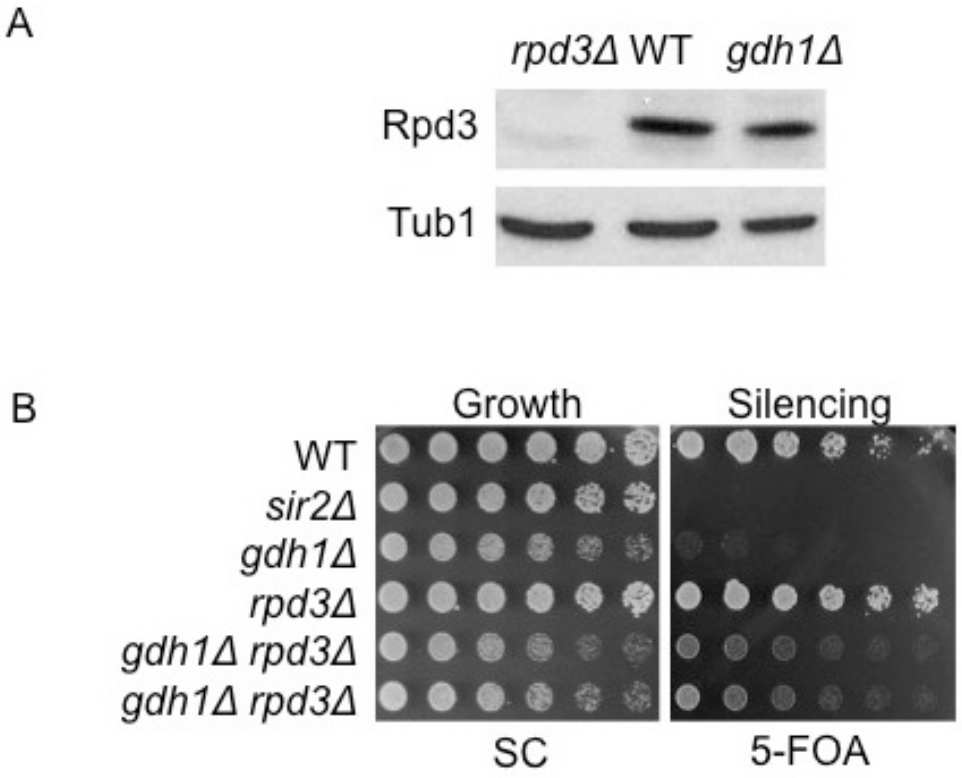

Figure A-17. Gdh1 and Rpd3 regulate telomeric silencing through independent pathways. (*A*) Deletion of *GDH1* did not affect Rpd3 protein levels. Whole cell extracts of *rpd3Δ* (LPY12093), WT (LPY5) and *gdh1Δ* (LPY16026) were immunoblotted with anti-Rpd3 or anti-Tub1 (loading control). (*B*) Deletion of *RPD3* partially suppressed the silencing defect of the *gdh1Δ* mutant. WT (LPY4916), *sir2Δ* (LPY4979), *gdh1Δ* (LPY16033), *rpd3Δ* (LPY12093), *gdh1Δ rpd3Δ* (LPY18970 and LPY18971) strains were plated on 5-FOA to assess telomeric silencing.

Gdh1's metabolic activity and silencing

In the first half of Appendix A, a number of experiments were undertaken to further dissect the relationship between the metabolic function of the Gdh proteins and their telomeric silencing activities. Mutational studies in the predicted catalytic domains were performed for both Gdh1 and Gdh3, and the results strengthened the idea presented in Chapter 2 that their metabolic activities were required for their silencing function.

Since Gdh1's metabolic activity determines its function in silencing, Chapter 2 explored Gdh1's impact on nuclear NAD^+ levels and the role of α-ketoglutarate in telomeric silencing. Appendix A evaluated whether other aspects of Gdh's metabolic activity participate in the regulation of telomeric silencing. First, two independent approaches were taken to assess the role of glutamate biosynthesis in telomeric silencing. Disrupting the alternative glutamate biosynthesis pathway had only a minor impact on telomeric silencing. Also, exogenously supplementing glutamate did not fully suppress the silencing defect of the *GDH* mutants. Therefore, it is unlikely that the levels of glutamate regulate telomeric silencing directly. Second, the role of catabolite repression in silencing was assessed using two independent genetic experiments. Neither the deletion of *URE2* nor the use of alternative nitrogen sources altered telomeric silencing. Hence, upregulation of genes involved in the use of alternative nitrogen sources is unlikely to be a cause of the silencing defect of the *gdh1Δ* mutant.

Lastly, the effect of the *GDH* mutants on H3 clipping was examined under nitrogen starvation conditions. It was found that the double mutant elevated both H3 clipping and H3 levels when cells were starved for nitrogen. Quantification of

independent experiments will determine whether the percentage of clipped H3 increases in the *GDH* mutants under nitrogen starvation conditions.

As a continuation of Chapter 2 and Appendix A, a number of general questions are worthy of future exploration. First, although it is known that the D150S mutant of Gdh1 fails to silence the reporter gene or to remove the inhibitory effect on H3 clipping, chromatin IP experiments are needed to unequivocally establish whether the D150S mutant loses the regulatory role in SIR binding or H3 clipping at the telomeres. Also, the role of Gdh3 in SIR binding or H3 clipping at the telomeres needs to be established by chromatin IP experiments. These results will reveal whether Gdh3 simply works redundantly to Gdh1 or if it has a more complex role in telomeric silencing. Further immunofluorescence experiments are needed to validate the finding that Gdh1 increases nuclear localization under nitrogen starvation conditions. If this is the case, it will be worthwhile to study the general impact of nitrogen starvation on SIR binding and H3 clipping at the telomeres.

Gdh1's genetic interaction with established regulators of telomeric silencing

The second half of Appendix A surveyed Gdh1's genetic interactions with a number of known regulators of telomeric silencing. Gdh1 was found to have complex genetic interactions with the JMJC-domain containing demethylases. Also, Gdh1 appears to regulate telomeric silencing through a different pathway than the Set1 complex, Sas2 or Rpd3. In contrast, Gdh1 likely functions in the same pathway as the histone chaperone Asf1. Gdh1 might also mediate the effect of Prb1 on telomeric silencing. And lastly, the RSC complex might also be involved in Gdh1's function in telomeric silencing.

A number of directions could be pursued based on the abovementioned results. First, the *gdh1Δ gis1Δ* mutant was not constructed. Gis1 is an interesting protein, because it was first implicated in controlling gene expression during nutrient limitation (Pedruzzi *et al.* 2002) and later found to be a JMJC-domain containing protein (Tu *et al.* 2007). Also, Gis1 was reported to translocate from the nucleus to the cytosol in response to hypoxia (Dastidar *et al.* 2012). Therefore, the genetic interaction between Gdh1 and Gis1 is worth exploring. For example, it could be asked whether Gdh1's metabolic activity influences Gis1 subcellular localization and whether Gdh1 influences H3K36 methylation marks at different genomic loci.

A second area worthy of exploration is the genetic interaction between Gdh1 and the histone chaperone Asf1. For instance, telomeric SIR complex binding and H3 clipping should be examined and compared in the *ASF1* and *GDH1* single and double mutants.

A number of questions could also address the interaction between Gdh1 and Prb1. H3 clipping should be assessed in the *gdh1Δ prb1Δ* double mutant, to determine whether Gdh1 inhibits Prb1's clipping activity *in vivo.* If this is the case, Gdh1's biochemical interaction with Prb1 should be dissected. Also, Prb1 was previously characterized as a vacuolar protease, and it remains unclear whether there is a nuclear pool of Prb1, since H3 clipping would presumably occur in the nucleus or cytoplasm, but not within the vacuole. Therefore, Prb1's subcellular localization should be studied under different growth conditions and in strains deleted for the *GDH* homologs.

Since *HTL1* acted as a high dosage suppressor of the *gdh1Δ* mutant's silencing defect, it will be interesting to examine if the suppression occurs directly at the telomeres.

To address this question, the *gdh1Δ* mutant transformed with *HTL1* should be analyzed with chromatin IP to determine the levels of SIR protein and histone H3 at the telomeres.

Materials and Methods

Yeast strains

All strains used in this study were listed in Table A-1. The W303 null mutant strains were constructed by amplification of the *kanMX* cassette from *Saccharomyces* Genome Deletion Project strains using oligos listed in Table A-2 and transformed into W303-1a (LPY5). Correct deletion was confirmed by molecular genotyping. The double and triple mutants were constructed by standard genetic crosses.

Plasmids

All plasmids used in this study are listed in Table A-3. A 2.8kb SacII-NheI fragment of *GDH3* was digested from yeast tiling library plasmid, and ligated with SacII-SpeI digested pbluescript to make pbluescript-*GDH3* (pLP2643). The D151S mutation was introduced into pLP2643 by site-directed mutagenesis with oLP1600 and oLP1601. SacII-HindIII fragments of WT *GDH3* and *gdh3-D151S* were subcloned into pRS425 to make pLP2662 and pLP2661, respectively.

The K74A mutation and the D248L, S249A mutations were introduced into pbluescript-*GDH1* (pLP2631; Table B-1) or pbluescript-*GDH1-Myc* (pLP2803; Table B-1) by site-directed mutagenesis, using oligos oLP1874+oLP1875 and oLP1866+oLP1867 respectively. SacI-XhoI digested fragments containing the *GDH1* point mutants were ligated into pRS315 to make pLP2939 and pLP2970. SacI-XhoI digested fragments

containing the Myc-tagged *GDH1* point mutants were ligated into pRS316 to make pLP2987 and pLP2989.

A 2.3kb BglII-BglII fragment containing *JHD1* was digested from the yeast tiling library plasmid and ligated into BamHI-digested pRS315 to make pLP2942. A 3.1kb MfeI-SacI fragment containing *JHD2* was digested from the yeast tiling library plasmid and subcloned into EcoRI-SacI digested pRS314 to make pLP2928. A 3.9kb HindIII-HindIII fragment containing *RPH1* was digested from the yeast tiling library plasmid and ligated into HindIII-digested pRS315 to make pLP2930. A 4.3kb MfeI-NarI fragment containing *GIS1* was digested from the yeast tiling library plasmid and cloned into EcoRI-ClaI digested pRS314 to make pLP2929.

A 3.7kb MscI-MscI fragment containing *PRB1* was digested from the yeast tiling library plasmid and ligated into SmaI-digested pRS314 to construct pLP3303.

A 2.4kb BamHI-NheI fragment containing *ASF1* was digested from the yeast tiling library plasmid and ligated into BamHI-SpeI digested pRS314 to construct pLP3138. A 2.9kb EcoRI-BamHI fragment of *CAC1* was digested from the yeast tiling library plasmid and ligated into pRS314 to make pLP3073.

A 0.6 kb HindIII-HindIII fragment containing *HTL1* was first subcloned into pRS425 to make pLP2659. XhoI-BamHI fragment of *HTL1* was digested from pLP2659 and ligated with XhoI-BamHI digested pRS424 to make pLP3084.

Growth and silencing assays

All starter cultures were prepared from cells grown in 3mL SC or SC-dropout medium for 2 days at 30°. Unless otherwise stated, cells equivalent to A_{600} of 1.0 were

pelleted, washed once with sterile water and plated in five-fold serial dilutions. A few dilution assays had adjusted starting OD and dilution folds, which are indicated in the figure legends. Silencing reporter assays were plated on SC medium with 1 g/L 5-FOA (US Biological).

Protein immunoblots

Whole cell lysates were prepared from cells grown to A_{600} of 0.6-1.0. Lysates were prepared by bead-beating as described previously (Clarke *et al.* 1999). For the nuclear extracts, cells were grown in 100mL SC medium to A_{600} of 0.4, centrifuged, washed with phosphate buffered saline and resuspended in 100mL yeast nitrogen base without ammonium sulfate or amino acid supplemented with 2% glucose. Cells were grown under nitrogen starvation condition overnight (~18 hrs) and subject to the nuclear preparation protocol as described (Kizer *et al.* 2006). For histone immunoblots, proteins were separated on 18% SDS-polyacrylamide gels and for all the other immunoblots, proteins were separated on 8% SDS-polyacrylamide gels. Separated proteins were transferred to nitrocellulose membrane (0.2μm). Primary antisera used were anti-Myc (1:10000, Evan *et al.* 1985), anti-Sir2 (1:10000, Garcia *et al.* 2002), anti-H3-CT (1:10000, Millipore), anti-HA (1:5000, Covance), anti-Tub1 (1:20000, Bond *et al.* 1986) and anti-Rpd3 (1:5000, Rundelett *et al.* 1996). Quantification was done using ImageJ.

Acknowledgements

The Rpd3 antibody was a gift from the Grunstein lab.

Table A-1. Yeast strains used in Appendix A

Strain	Genotype	Source /Reference
LPY5 (W303-1a)	*MATa ade2-1 can1-100 his3-11,15 leu2-3,112 trp1-1 ura3-1*	R. Rothstein
LPY1589	W303 *MATa sas2Δ::TRP1*	
LPY4916	W303 *MATa TELV-R::URA3*	
LPY4979	W303 *MATα TELV-R::URA3 sir2Δ::HIS3*	
LPY6928	W303 *MATa TELV-R::URA3 set1Δ::HIS3*	
LPY12093	W303 *MATα TELV-R::URA3 rpd3Δ::kanMX*	Chang and Pillus 2009
LPY16026	W303 *MATa gdh1Δ::kanMX*	
LPY16033	W303 *MATα TELV-R::URA3 gdh1Δ::kanMX*	
LPY16143	W303 *MATa TELV-R::URA3 prb1Δ::LEU2*	
LPT16150	W303 *MATa TELV-R::URA3 gdh1Δ::kanMX prb1Δ::LEU2*	
LPY16785	W303 *MATa TELV-R::URA3 gdh3Δ::kanMX*	
LPY16796	W303 *MATα TELV-R::URA3 mks1Δ::kanMX*	
LPY17916	W303 *MATα TELV-R::URA3 gdh1Δ::kanMX gdh3Δ::kanMX*	
LPY18316	W303 *MATa TELV-R::URA3 glt1Δ::kanMX*	
LPY18414	W303 *MATa TELV-R::URA3 gdh1Δ::kanMX jhd2Δ::kanMX*	
LPY18501	W303 *MATa TELV-R::URA3 rph1Δ::kanMX*	
LPY18576	W303 *MATα TELV-R::URA3 hmrΔE::TRP1 gdh1Δ::kanMX gdh3Δ::kanMX glt1Δ::kanMX*	
LPY18600	W303 *MATa TELV-R::URA3 gdh1Δ::kanMX rph1Δ::kanMX*	
LPY18673	W303 *MATα TELV-R::URA3 gdh1Δ::kanMX jhd1Δ::kanMX*	
LPY18873	W303 *MATα TELV-R::URA3 jhd1Δ::kanMX*	
LPY18880	W303 *MATa TELV-R::URA3 jhd2Δ::kanMX*	
LPT18970	W303 *MATa TELV-R::URA3 gdh1Δ::kanMX rpd3Δ::LEU2*	
LPT18971	W303 *MATα TELV-R::URA3 gdh1Δ::kanMX rpd3Δ::LEU2*	
LPY19570	W303 *MATa TELV-R::URA3 ure2Δ::kanMX*	
LPY19898	W303 *MATα TELV-R::URA3 asf1Δ::kanMX*	
LPY19900	W303 *MATa TELV-R::URA3 asf1Δ::kanMX*	

Table A-1. Yeast strains used in Appendix A, continued

Strains	Genotype	Source/ Reference
LPY19901	W303 *MATa TELV-R::URA3 asf1Δ::kanMX gdh1Δ::kanMX*	
LPY19902	W303 *MATa TELV-R::URA3 asf1Δ::kanMX gdh1Δ::kanMX*	
LPY19928	W303 *MATα TELV-R::URA3 cac1Δ::kanMX*	
LPY19929	W303 *MATα TELV-R::URA3 cac1Δ::kanMX gdh1Δ::kanMX*	
LPY19930	W303 *MATa TELV-R::URA3 cac1Δ::kanMX gdh1Δ::kanMX*	
LPY20376	W303 *MATα TELV-R::URA3 gdh1Δ::kanMX set1Δ::HIS3*	
LPY20469	W303 *MATα hht1-hhf1Δ::kanMX hht2-hhf2Δ::kanMX hta2-htb2Δ::HPH TELV-R::URA3*+ pLP1775	
LPY20473	W303 *MATα hht1-hhf1Δ::kanMX hht2-hhf2Δ::kanMX hta2-htb2Δ::HPH gdh1Δ::kanMX TELV-R::URA3* + pRS314-*hht2-K4A-HHF2*	
LPY20621	W303 *MATα hht1-hhf1Δ::kanMX hht2-hhf2Δ::kanMX hta2-htb2Δ::HPH TELV-R::URA3*+ pRS314-*hht2-K4A-HHF2*	
LPY20623	W303 *MATα hht1-hhf1Δ::kanMX hht2-hhf2Δ::kanMX hta2-htb2Δ::HPH gdh1Δ::kanMX TELV-R::URA3* + pLP1775	
LPY20697	W303 *MATa TELV-R::URA3 cps60Δ::kanMX gdh1Δ::kanMX*	
LPY20703	W303 *MATa TELV-R::URA3 cps60Δ::kanMX*	
LPY21352	W303 *MATa gdh1Δ::kanMX sas2Δ::TRP1*	
LPY21354	W303 *MATa TELV-R::URA3 gdh1Δ::kanMX sas2Δ::TRP1*	

Note: Unless otherwise stated, yeast strains were constructed during the course of this study or are part of the standard lab collection.

Table A-2. Oligonucleotides used in Appendix A

Oligo #	Name	Sequence
1592	*GLT1* KO forward	GCTCCGATAAGCTTTTGCAC
1593	*GLT1* KO reverse	GGCAATATCGAGGATGAGG
1600	*gdh3-D151S* forward	GACGTGCCCGCAGGATCTATTGGTGTC GGTGGC
1601	*gdh3-D151S* reverse	GCCACCGACACCAATAGATCCTGCGG GCACGTC
1860	*JHD1* KO forward	CTAGTGGATTTGCACCGG
1861	*JHD1* KO reverse	CTTGCTGAAGAAGGCATC
1866	*gdh1-D248L, S249A* forward	GTCGTTTCCCTATCTTTGGCTAAGGGTT GTATCATC
1867	*gdh1-D248L, S249A* reverse	GATGATACAACCCTTAGCCAAAGATA GGGAAACGAC
1868	*JHD2* KO forward	CAAGGGCTTCGGACTTACTG
1869	*JHD2* KO reverse	AACAAAAGAAGGCGATCGTG
1874	*gdh1-K74A* forward	GCCAAGGGTCCATACGCTGGTGGTCTA CGTTTC
1875	*gdh1-K74A* reverse	GAAACGTAGACCACCAGCGTATGGAC CCTTGGC
1894	*RPH1* KO forward	CAAGCGGCCAATTTAATCA
1895	*RPH1* KO reverse	GCTTGCTAACCCTGTTCCT
1898	*URE2* KO forward	GGATTGATGAGCTGCCACT
1899	*URE2* KO reverse	GCTTTATTGAAAGCGCCAG
1990	*CAC1* KO forward	CCTGGCGCGATCTATAGTGT
1991	*CAC1* KO reverse	GCGAAGTTGCTCTTCTGGTC
2076	*CPS60* KO forward	GGGTCCAAAGAAACACATGG
2077	*CPS60* KO reverse	CAAGGATAAAGGACCGTGGA

Note: All oligonucleotides listed in Table A-2 were designed during the course of this study.

Table A-3. Plasmids used in Appendix A

Plasmid (alias)	Description	Source/Reference
pLP60 (pRS313)	Vector *HIS3* CEN	Sikorski and Heiter 1989
pLP61 (pRS314)	Vector *TRP1* CEN	Sikorski and Heiter 1989
pLP62 (pRS315)	Vector *LEU2* CEN	Sikorski and Heiter 1989
pLP126 (pRS316)	Vector *URA3* CEN	Sikorski and Heiter 1989
pLP190	pRS315-*SIR3*	Stone *et al.* 2000
pLP360 (pRS424)	Vector *TRP1* 2 micron	
pLP425	pRS313-*SAS2*	
pLP493 (pMA424)	Vector *HIS3 GBD*	G. Chinnadurai
pLP646	pMA424-*SAS2*	Jacobson and Pillus 2004
pLP1237	pRS315-*SIR2*	Garcia *et al.* 2002
pLP1623 (pRS425)	Vector *LEU2* 2μ	Christianson *et al.* 1992
pLP1775	pRS314-*HHT2-HHF2*	S. Berger
N/A	pRS314-*hht2-K4A-HHF2*	Nakanishi *et. al* 2006
pLP2637	pRS315-*GDH1*	
pLP2643	pbluescript-*GDH3*	
pLP2659	pRS425-*HTL1*	
pLP2661	pRS425-*gdh3-D151S*	
pLP2662	pRS425-*GDH3*	
pLP2928	pRS314-*JHD2*	
pLP2929	pRS314-*GIS1*	
pLP2930	pRS315-*RPH1*	
pLP2939	pRS315-*gdh1-D248L, S249A*	
pLP2942	pRS315-*JHD1*	
pLP2970	pRS315-*gdh1-K74A*	
pLP2987	pRS316-*gdh1-K74A-Myc*	
pLP2989	pRS316-*gdh1-D248L, S249A-Myc*	
pLP3073	pRS314-*CAC1*	
pLP3084	pRS424-*HTL1*	
pLP3138	pRS314-*ASF1*	
pLP3303	pRS314-*PRB1*	

Note: Unless otherwise stated, all strains used were constructed during this study or are part of the standard lab collection.

References

Bond JF, Fridovich-Keil JL, Pillus L, Mulligan RC, Solomon F. 1986. A chicken-yeast chimeric beta-tubulin protein is incorporated into mouse microtubules in vivo. *Cell* **44**: 461-468.

Breker M, Gymrek M, Moldavski O, Schuldiner M. 2014. LoQAtE--Localization and Quantitation ATlas of the yeast proteomE. A new tool for multiparametric dissection of single-protein behavior in response to biological perturbations in yeast. *Nucleic Acids Res* **42**: D726-30.

Chang CS, Pillus L. 2009. Collaboration between the essential Esa1 acetyltransferase and the Rpd3 deacetylase is mediated by H4K12 histone acetylation in Saccharomyces cerevisiae. *Genetics* **183**: 149-160.

Cho SW, Yoon HY, Ahn JY, Choi SY, Kim TU. 1998. Identification of an NAD+ binding site of brain glutamate dehydrogenase isoproteins by photoaffinity labeling. *J Biol Chem* **273**: 31125-31130.

Clarke AS, Lowell JE, Jacobson SJ, Pillus L. 1999. Esa1p is an essential histone acetyltransferase required for cell cycle progression. *Mol Cell Biol* **19**: 2515-2526.

Dastidar RG, Hooda J, Shah A, Cao TM, Henke RM, Zhang L. 2012. The nuclear localization of SWI/SNF proteins is subjected to oxygen regulation. *Cell Biosci* **2**: 30-3701-2-30.

Ehrentraut S, Weber JM, Dybowski JN, Hoffmann D, Ehrenhofer-Murray AE. 2010. Rpd3-dependent boundary formation at telomeres by removal of Sir2 substrate. *Proc Natl Acad Sci U S A* **107**: 5522-5527.

Evan GI, Lewis GK, Ramsay G, Bishop JM. 1985. Isolation of monoclonal antibodies specific for human c-myc proto-oncogene product. *Mol Cell Biol* **5**: 3610-3616.

Feser J, Truong D, Das C, Carson JJ, Kieft J, Harkness T, Tyler JK. 2010. Elevated histone expression promotes life span extension. *Mol Cell* **39**: 724-735.

Garcia SN, Pillus L. 2002. A unique class of conditional sir2 mutants displays distinct silencing defects in Saccharomyces cerevisiae. *Genetics* **162**: 721-736.

Jacobson S, Pillus L. 2004. Molecular requirements for gene expression mediated by targeted histone acetyltransferases. *Mol Cell Biol* **24**: 6029-6039.

Kim T, Buratowski S. 2007. Two *Saccharomyces cerevisiae* JmjC domain proteins demethylate histone H3 Lys36 in transcribed regions to promote elongation. *J Biol Chem* **282**: 20827-20835.

Krogan NJ, Cagney G, Yu H, Zhong G, Guo X, Ignatchenko A, Li J, Pu S, Datta N, Tikuisis AP et al. 2006. Global landscape of protein complexes in the yeast *Saccharomyces cerevisiae. Nature* **440**: 637-643.

Krogan NJ, Dover J, Khorrami S, Greenblatt JF, Schneider J, Johnston M, Shilatifard A. 2002. COMPASS, a histone H3 (Lysine 4) methyltransferase required for telomeric silencing of gene expression. *J Biol Chem* **277**: 10753-10755.

Liang G, Klose RJ, Gardner KE, Zhang Y. 2007. Yeast Jhd2p is a histone H3 Lys4 trimethyl demethylase. *Nat Struct Mol Biol* **14**: 243-245.

Ljungdahl PO, Daignan-Fornier B. 2012. Regulation of amino acid, nucleotide, and phosphate metabolism in *Saccharomyces cerevisiae. Genetics* **190**: 885-929.

Nakanishi S, Sanderson BW, Delventhal KM, Bradford WD, Staehling-Hampton K, Shilatifard A. 2008. A comprehensive library of histone mutants identifies nucleosomal residues required for H3K4 methylation. *Nat Struct Mol Biol* **15**: 881-888.

Nislow C, Ray E, Pillus L. 1997. *SET1*, a yeast member of the trithorax family, functions in transcriptional silencing and diverse cellular processes. *Mol Biol Cell* **8**: 2421-2436.

Pedruzzi I, Burckert N, Egger P, De Virgilio C. 2000. *Saccharomyces cerevisiae* Ras/cAMP pathway controls post-diauxic shift element-dependent transcription through the zinc finger protein Gis1. *EMBO J* **19**: 2569-2579.

Rando OJ, Winston F. 2012. Chromatin and transcription in yeast. *Genetics* **190**: 351-387.

Romeo MJ, Angus-Hill ML, Sobering AK, Kamada Y, Cairns BR, Levin DE. 2002. *HTL1* encodes a novel factor that interacts with the RSC chromatin remodeling complex in Saccharomyces cerevisiae. *Mol Cell Biol* **22**: 8165-8174.

Rundlett SE, Carmen AA, Kobayashi R, Bavykin S, Turner BM, Grunstein M. 1996. HDA1 and RPD3 are members of distinct yeast histone deacetylase complexes that regulate silencing and transcription. *Proc Natl Acad Sci U S A* **93**: 14503-14508.

Santos-Rosa H, Bannister AJ, Dehe PM, Geli V, Kouzarides T. 2004. Methylation of H3 lysine 4 at euchromatin promotes Sir3p association with heterochromatin. *J Biol Chem* **279**: 47506-47512.

Schneider J, Shilatifard A. 2006. Histone demethylation by hydroxylation: chemistry in action. *ACS Chem Biol* **1**: 75-81.

Schneider J, Wood A, Lee JS, Schuster R, Dueker J, Maguire C, Swanson SK, Florens L, Washburn MP, Shilatifard A. 2005. Molecular regulation of histone H3 trimethylation by COMPASS and the regulation of gene expression. *Mol Cell* **19**: 849-856.

Shia WJ, Li B, Workman JL. 2006. SAS-mediated acetylation of histone H4 Lys 16 is required for H2A.Z incorporation at subtelomeric regions in Saccharomyces cerevisiae. *Genes Dev* **20**: 2507-2512.

Sikorski RS, Hieter P. 1989. A system of shuttle vectors and yeast host strains designed for efficient manipulation of DNA in *Saccharomyces cerevisiae*. *Genetics* **122**: 19-27.

Smith TJ, Peterson PE, Schmidt T, Fang J, Stanley CA. 2001. Structures of bovine glutamate dehydrogenase complexes elucidate the mechanism of purine regulation. *J Mol Biol* **307**: 707-720.

Stone EM, Reifsnyder C, McVey M, Gazo B, Pillus L. 2000. Two classes of *sir3* mutants enhance *the sir1* mutant mating defect and abolish telomeric silencing in *Saccharomyces cerevisiae. Genetics* **155**: 509-522.

Suka N, Luo K, Grunstein M. 2002. Sir2p and Sas2p opposingly regulate acetylation of yeast histone H4 lysine16 and spreading of heterochromatin. *Nat Genet* **32**: 378-383.

Szklarczyk R, Huynen MA, Snel B. 2008. Complex fate of paralogs. *BMC Evol Biol* **8**: 337-2148-8-337.

Tamburini BA, Carson JJ, Linger JG, Tyler JK. 2006. Dominant mutants of the *Saccharomyces cerevisiae* ASF1 histone chaperone bypass the need for CAF-1 in transcriptional silencing by altering histone and Sir protein recruitment. *Genetics* **173**: 599-610.

Tu S, Bulloch EM, Yang L, Ren C, Huang WC, Hsu PH, Chen CH, Liao CL, Yu HM, Lo WS et al. 2007. Identification of histone demethylases in *Saccharomyces cerevisiae. J Biol Chem* **282**: 14262-14271.

Appendix B. Details of cloning strategies used for Chapter 2

Construction of plasmids carrying WT *GDH1*

pRS315-*GDH1* (pLP2627): WT *GDH1* was originally sublconed from yeast tiling library plasmid. A 4kb Xho-XbaI fragment of YGpM26a16 was ligated into SpeI-SalI digested pRS315 vector, to generate pRS315-*GDH1* (pLP2627).

pbluescript-*GDH1* (pLP2631): pLP2631 was made by digesting pLP2627 with SacI and ClaI to obtain a 2.9 kb fragment containing *GDH1* and ligating into SacI-ClaI digested pbluescript KS+ vector. pLP2631 was the founding plasmid for additional cloning and mutagenesis experiments. Note that the *GDH1* fragment in pLP2631 was shorter than that in pLP2627, because it contained a shorter 3'UTR (approximately 290bp).

pRS315-*GDH1* (pLP2637), pRS425-*GDH1* (pLP2764), pRS314-*GDH1* (pLP3082): The SacI-ApaI fragment containing *GDH1* was digested from pLP2627 and subcloned into the corresponding vectors to generate pLP2637, pLP2764 and pLP3082.

Construction of *gdh1-D150S* mutant

The pbluescript-*GDH1* (pLP2631) plasmid was mutated with primers oLP1556 and oLP1557 (Table 2-S4) to generate pbluescript-*gdh1-D150S* (pLP2632). SacI-ApaI fragment of pLP2632 was ligated into similarly digested vectors to generate

pRS315-*gdh1-D150S* (pLP2638), pRS425-*gdh1-D150S* (pLP2698), or pRS314-*gdh1-D150S* (pLP3083).

Construction of plasmid-borne *GDH1-13Myc*

pbluescript- *GDH1-13Myc* (pLP2803): In order to add 13Myc tag to the C terminus of Gdh1, the stop codon of the *GDH1* gene was removed and replaced with an XmaI site. This was done by site-directed mutagenesis using primers oLP1598 and OLP1599 (Table B-2), using pbluescript-*GDH1* (pLP2631) as a template. The resulting plasmid was pbluescript-*gdh1-stop::XmaI* (pLP2648). A 0.8kb PCR fragment containing the 13Myc tag and the terminator sequence was amplified from pFA6a-13Myc plasmid (pLP1651) using primers oLP1753 and pLP1629 (Table B-2). This PCR fragment carried XmaI sites at both ends, and therefore was digested and ligated into XmaI-digested pLP2648. The resulting plasmid was pbluescript- *GDH1-13Myc* (pLP2803).

pRS316-*GDH1*-13Myc (pLP2833): A 3.7kb SacI-ClaI fragment containing Gdh1-13Myc-3'UTR was digested from pLP2803 and was ligated into pRS316 to make pRS316-*GDH1*-13Myc (pLP2833).

pRS316-*gdh1-D150S-13Myc* (pLP2834): pbluescript-*GDH1-13Myc* (pLP2803) was mutated with oLP1556 and oLP1557 (Table B-2) to introduce the D150S mutation. The resulting plasmid was pbluescript-*gdh1-D150S-13Myc* (pLP2821). SacI-ClaI fragment of pLP2821 was subcloned into pRS316 to make pRS316-*gdh1-D150S-13Myc* (pLP2834).

Construction of pFA6a-13Myc-NES-kanMX

To insert the NES sequence, an XbaI site was first introduced to replace the stop codon after the 13Myc sequence in pFA6a-13Myc-kanMX (pLP1650), using oligos oLP1785 and oLP1786 (Table B-2). The resulting plasmid was pFA6a-13Myc-stop::XbaI (pLP2819). This provided the backbone for NES insertion.

The NES sequence was amplified from the Lys20-NES plasmid (pLP2402), using primers oLP1791 and oLP1792 (Table B-2). Of note, oLP1791 contained the coding sequence for two glycine linker amino acids. In addition, both primers carried XbaI sites at their 5' ends. The PCR product (<100bp) was separated on a 10% PAGE gel, excised, eluted and digested with XbaI. The resulting fragment was ligated with XbaI-digested pLP2819 and the correct directionality of insertion was confirmed by sequencing.

Construction of plasmid-borne *JHD2*

A 3.1 kb MfeI-SacI fragment containing *JHD2* was digested from the yeast tiling library plasmid and ligated into EcoRI-SacI digested pRS314 to generate pRS314-*JHD2* (pLP2928). To subclone *JHD2* into pRS315, SalI-SacI (HF) digested pLP2928 was ligated with similarly digested pRS315, generating pRS315-*JHD2* (pLP3181).

Construction of plasmid-borne *IDP1*

A 3.3 kb NheI-Bstz171 fragment containing *IDP1* was digested from the yeast tiling library plasmid, and ligated into SpeI-SmaI digested pRS314, to generate pRS314-*IDP1* (pLP3238).

Table B-1. Intermediary plasmids used for the Gdh1 study

Plasmid (alias)	Description
pLP2627	pRS315-*GDH1* (4kb fragment)
pLP2631	pbluescript-*GDH1* (2.2kb fragment)
pLP2632	pbluescript-*gdh1-D150S*
pLP2643	pbluescript-*GDH3*
pLP2644	pRS315-*GDH3*
pLP2648	pbluescript-*gdh1-stop::XmaI*
pLP2661	pRS425-*gdh3-D151S*
pLP2803	pbluescript-*GDH1-13Myc*
pLP2819	pFA6a-13Myc-stop::XbaI-kanMX
pLP2821	pbluescript-*gdh1-D150S-13Myc*
pLP2928	pRS314-*JHD2*

Table B-2. Oligonucleotides used for Appendix B

Oligo #	Oligo name	Sequence
1598	*GDH1* XmaI for	CCAAGGTGATGTATTTCCCGGGGTCTAAAA GAAAGAAAAGAGG
1599	*GDH1* XmaI rev	CCTCTTTTCTTTCTTTTAGACCCCGGGAAATA CATCACCTTGG
1629	*GDH1*_Cmyc for	CAAGTTTCATCAAGGTCTCTGATGCTATGTTT GACCAAGGTGATGTATTTCGGATCCCCGGGT TAATTAA
1753	XmaI_pFA6a_rev	TCCCCCCGGGGGACGAGGCAAGCTAAACAG
1785	Myc_XbaImutF	ATCAATCACTCTAGAGAATTCGCGC
1786	Myc_XbaImutR	GCGCGAATTCTCTAGAGTGATTGAT
1791	XbaI_GG_NES for	GCTCTAGAGGTGGTCAAGGATCCGAGCTAGC
1792	XbaI_NES rev	CGTCTAGATTAGTTGATGTCCAGAC